

The role and regulation of the p84 adaptor subunit in phosphatidylinositol 3-kinase γ lipid-kinase signalling and the control of PI3K γ -dependent cell migration

Michelle Elizabeth Turvey, B.Sc. (Biotech) (Hons)

Discipline of Microbiology and Immunology
Department of Molecular and Cellular Biology
School of Biological Sciences
The University of Adelaide

A thesis submitted to The University of Adelaide in fulfilment of
the requirements for the degree of Doctor of Philosophy

2015



Declaration

I, Michelle Turvey certify that this work contains no material which has been accepted for the award of any other degree or diploma in any university or other tertiary institution and, to the best of my knowledge and belief, contains no material previously published or written by another person, except where due reference has been made in the text.

I give consent to this copy of my thesis, when deposited in the University Library, being made available for loan and photocopying, subject to the provisions of the Copyright Act 1968.

I also give permission for the digital version of my thesis to be made available on the web, via the University's digital research repository, the Library catalogue and also through web search engines, unless permission has been granted by the University to restrict access for a period of time.

Michelle Elizabeth Turvey, B. Sc. (Biotech) (Hons)

May 2015

Acknowledgements

A PhD research project and thesis would be a daunting and near impossible task without the guidance and support of many people along the way. I have been fortunate enough to be surrounded by enthusiastic, determined and knowledgeable work colleagues and a loving and supportive network of family and friends who have made my PhD experience such a rewarding time.

Firstly, I would like to extend a huge thank you to Professor Shaun McColl for accepting me into his lab for Summer Vac, Honours, RA and PhD positions over the many years. On a professional level, you have provided me with valuable lessons in manuscript preparation and grant writing, but above all, your willingness to trust and allow me to work independently through the design and experimentation of my PhD and RA projects taught me so much about the up's, down's and challenges of scientific research. I must also thank you for your acceptance and support of my incessant need to travel and see the world, and for the invaluable work opportunities you provided me with in Canada.

Next I must thank Manuela as my co-supervisor and signal transduction guru. I have learnt so much from you during my PhD and you've been instrumental in keeping me, and my word counts, grounded. The insights and feedback you provided regarding the biochemistry of my work challenged me to extend my conceptualisation of protein signalling. Despite moving on from the lab, you were easily able to continue your support and guidance of my project and made every effort to be available when I needed your help, which I appreciate immensely. Thank you must also go to Peter as my second co-supervisor and his team at the Adelaide Proteomics Centre, who provided me with valuable technical support and endless problem solving help for the challenging phospho-proteomics aspects of my project.

I would also like to thank everyone, both past and present, which I have worked with at the chemokine biology lab. The environment has always been stimulating and supportive, and I have enjoyed learning from so many people with such diverse expertise. Adriana, your lab management skills are unchallenged and I have loved having a bench close to yours to chat about walking tracks, travel destinations and food (and science). To Yuka, Iain and Marina, thank you for offering your help and perspectives on my work, each of you has

supported me both intellectually and creatively during my time in the lab. Next, thanks and a big shout out to the rest of the McColl team; Carly, Kevin, Sarah, Ervin, Cameron, Duncan, Kerrie, Jess, Jasmine, Jade and to past players, Oli, Sarah HJ, Wendel, Julie, Mark, Matt, Brock, Meizhi and Valentina who have all contributed to a lively and enjoyable work environment.

Lastly, a tremendous thank you must go to my family and friends for their continual support during my PhD. To the girls, thanks for the walks, girls' dinners, shared bottles of wine, and adventures around Australia and overseas, you're friendship means the world to me. To Andrew, thank you for your constant love and encouragement, I've had so much fun in all that we've shared so far and can't wait to take on the world with you. Finally, to Mum, Dad and Pip, I could not ask for a more supportive and loving family, so thank you for everything over the last few years, I could not have survived this PhD without you.

Table of contents

Declaration.....	i
Acknowledgements	ii
Table of contents	iv
List of tables.....	xii
Abbreviations	xiii
Publications arising from this work	xvi
Abstract.....	xvii
Chapter 1: Introduction	3
1.1 Overview	3
1.2 Lipid signal transduction.....	4
1.3 The phosphatidylinositol 3-kinase family	6
1.4 Class I PI3Ks	11
1.4.1 The structure of Class I PI3K subunits	11
1.4.2 Regulating the lipid-kinase activity of Class I PI3K enzymes.....	14
1.4.3 Determining the tissue-specific functions of Class I PI3K enzymes	18
1.5 The PI3K Class IB enzyme, PI3Kγ	23
1.5.1 PI3K γ subunits: expression, stability and localisation	24
1.5.2 The interaction between p110 γ and an adaptor subunit	28
1.5.3 Activation of PI3K γ lipid-kinase activity at the plasma membrane	30
1.5.4 Mechanisms of PI3K γ signal regulation	33
1.6 Functional roles for PI3Kγ	35
1.6.1 PI3K γ in cardiac function.....	37
1.6.2 PI3K γ in haematopoietic cell development and function	38
1.6.3 PI3K γ in autoimmunity	41
1.6.4 Roles for Class I PI3K enzymes in cancer initiation and progression	46
1.7 Advances in genome-editing technologies.....	51
1.8 The research project	54
Chapter 2: Methods and materials.....	63
2.1 Mice	63

2.1.1	Housing and maintenance	63
2.1.2	CRISPR gRNA construct design and injection	63
2.1.3	TALEN design and injection	63
2.2	Expression construct design and DNA cloning	64
2.2.1	Cloning p84 expression constructs	64
2.2.2	Site-directed mutagenesis of p84 expression constructs.....	64
2.2.3	Transfection and retroviral transduction of p84 expression vectors.....	65
2.2.4	DNA sequencing.....	65
2.3	Cell lines and <i>ex vivo</i> cell culture	66
2.3.1	MDA.MB.231 and HEK293FT cell culture	66
2.3.2	BMMC culture from total bone marrow isolates.....	66
2.4	<i>In silico</i> analyses.....	67
2.4.1	<i>In silico</i> phospho-prediction database analyses	67
2.4.2	Database mining	67
2.5	<i>In vitro</i> techniques.....	68
2.5.1	Immunoprecipitation and LDS-PAGE.....	68
2.5.2	Coomassie Brilliant Blue staining	69
2.5.3	Western blot analysis	69
2.5.4	Enzyme-linked immunosorbent assay (ELISA)	69
2.5.5	XTT/PMS proliferation assay	70
2.5.6	Soft agar 3D attachment-independent growth assay.....	70
2.5.7	Membrane fractionation.....	70
2.5.8	Incucyte migration assay	71
2.5.9	PCR.....	71
2.5.10	Flow cytometry	72
2.5.11	BMMC β -hexaminidase release assay.....	73
2.5.12	BMMC cytokine release assay	74
2.5.13	<i>In vitro</i> transwell chemotaxis assay	74
2.5.14	<i>In vitro</i> Akt phosphorylation in bone marrow cells.....	74
2.6	<i>In vivo</i> techniques.....	75
2.6.1	Phospho-specific antibody production	75
2.6.2	Experimental haematogenous metastasis.....	75

2.6.3	Induction of chronic MOG ₃₅₋₅₅ -induced EAE.....	76
2.6.4	Induction of relapsing-remitting PLP ₁₃₉₋₁₅₁ -induced EAE.....	76
2.7	Proteomics.....	77
2.7.1	Orbitrap LTQ XL ETD LC-MS for p84 phosphorylation studies	77
2.7.2	<i>In vitro</i> Akt kinase assay	79
2.7.3	Parallel reaction monitoring (PRM).....	79
2.7.4	Isotope-Coded Protein Labelling (ICPL) analyses: Sample preparation	80
2.7.5	ICPL analyses: Labelling, LDS-PAGE and peptide isolation	81
2.7.6	ICPL triplex: HPLC, fraction collection and mass spectrometry	81
2.7.7	ICPL quadruplex: HPLC, fraction collection and mass spectrometry.....	82
2.7.8	ICPL analyses: Determination of peptide and protein ratios	84
2.8	Antibodies and General Reagents	85
2.8.1	Primers and antibodies	85
2.8.2	Phosphate buffered saline (PBS) / Tris buffered saline (TBS)	85
2.8.3	Diethyl Pyrocarbonate (DEPC) reagents for RNA isolation	85
2.8.4	Murine Red Cell Removal Buffer (MRCRB).....	85
2.8.5	PBS/BSA/Azide	86
2.8.6	PBS/Azide	86
2.8.7	Paraformaldehyde solutions (PFA).....	86
2.8.8	NP-40 lysis buffer	86
2.8.9	Tyrodes buffer.....	86
2.8.10	Coomassie Brilliant Blue G-250 (CBB)	86
2.9	Statistical analyses.....	87
 Chapter 3: Identification and characterisation of regulatory phosphorylation sites within p84 in the context of PI3Kγ signalling and implications for cell migration..... 95		
3.1	Introduction.....	95
3.2	Results	95
3.2.1	<i>In silico</i> prediction of phosphorylation sites within p84.....	95
3.2.2	Identifying phosphorylation sites within p84.....	96
3.2.3	Development of an expression system to detect and immunoprecipitate wildtype and mutant p84 proteins.....	100

3.2.4	Investigating the tumour suppressor function of p84 and the role of Ser358 and Thr607 phosphorylation sites.....	101
3.2.5	The effect of wildtype and mutant p84 protein expression on PI3K γ signal activation	102
3.2.6	The effect of wildtype and mutant p84 protein expression on MDA.MB.231 cell proliferation and 3D growth.....	103
3.2.7	Assessing the formation of p84/p110 γ heterodimers and their translocation to the membrane	104
3.2.8	Implications of p84 expression on MDA.MB.231 cell migration	106
3.3	Summary.....	107
Chapter 4: Generation, screening and characterisation of a novel p84-deficient mouse (C57Bl/6 <i>Pik3r6</i>^{-/-})		141
4.1	Introduction.....	141
4.2	Results	142
4.2.1	Targeting <i>Pik3r6</i> using CRISPR gene-editing technology.....	142
4.2.2	Screening CRISPR-induced mutations within <i>Pik3r6</i> exon 1	143
4.2.3	Targeting <i>Pik3r6</i> with TALEN gene-editing technology and screening of TALEN-induced mutations	145
4.2.4	Characterising large CRISPR-induced deletions flanking the target site..	146
4.2.5	PI3K γ subunit expression in <i>Pik3r6</i> ^{-/-} tissues	147
4.2.6	Lymphoid organ development in <i>Pik3r6</i> ^{-/-} mice.....	149
4.2.7	Reduced PI3K γ signal activation in <i>Pik3r6</i> ^{-/-} bone marrow-derived cells.	150
4.2.8	The effect of p84 deletion on bone marrow-derived mast cell maturation and function	151
4.2.9	Thymocyte development is unaltered in <i>Pik3r6</i> ^{-/-} mice.....	155
4.2.10	Neutrophil migration is inhibited by the loss of p84 in <i>Pik3r6</i> ^{-/-} mice	155
4.2.11	<i>Pik3r6</i> ^{-/-} mice are protected from EAE disease.....	156
4.3	Summary.....	159
Chapter 5: Quantitative proteome profiling of CNS-infiltrating CD4⁺ Th cells reveals selective changes during experimental autoimmune encephalomyelitis		207

5.1 Introduction.....	207
5.2 Results	210
5.2.1 Isolating CD4 ⁺ cells during EAE disease progression for ICPL labelling	210
5.2.2 ICPL labelling and triplex/quadruplex analyses	211
5.2.3 Validating protein candidates identified to be up-regulated during EAE..	214
5.3 Summary.....	216
Chapter 6: Discussion	235
6.1 The induction of Thr607-dependent p84/p110γ heterodimers represents a regulatory mechanism of PI3Kγ signalling that is required for the tumour suppressor function of p84	238
6.2 Generation of a Pik3r6^{-/-} mouse and characterisation of p84-dependent processes in haematopoietic cell function	251
6.3 Proteomic analyses of CNS-infiltrating CD4⁺ cells during EAE disease	261
6.4 Summary and outlook	263
Appendix A1:.....	271
Appendix A2:.....	273
Appendix A3:.....	275
Appendix A4:.....	277
References:.....	281

List of figures

Figure 1.1: The lipid signalling network.	4
Figure 1.2: Signalling substrates and effectors of Class I, II and III PI3K lipid kinases.....	9
Figure 1.3: Domain structures of Class I, II and III PI3K enzymes.	10
Figure 1.4: Variants of the p85 Class IA PI3K adaptor subunit.	13
Figure 1.5: Proposed structure of Class IB PI3K γ adaptor subunits.....	14
Figure 1.6: Dynamic regulation of PIP ₃ levels	16
Figure 1.7: Crystal structure of the p110 γ catalytic subunit complexed with AS605240. ...	19
Figure 1.8: The p101 and p84 gene locus.....	24
Figure 1.9: The conformation of p110 γ modulates its lipid-kinase activity.....	34
Figure 1.10: CRISPR-Cas targeted gene-editing.....	52
Figure 1.11: TALEN gene-targeting.....	54
Figure 3.1: Assessing p84-specific antibodies.....	111
Figure 3.2: Generating a p84 expression construct with an HA fusion tag.....	113
Figure 3.3: Transient expression of p84-HA in transfected MDA.MB.231 cells.....	115
Figure 3.4: Proteomic analysis of p84-HA precipitated from stimulated MDA.MB.231 cell lysates.	116
Figure 3.5: p84 is constitutively phosphorylated at Serine 358 (Ser358).....	121
Figure 3.6: Identifying Thr607 phosphorylation within p84 <i>in vitro</i>	122
Figure 3.7: Thr607 is part of an Akt phosphorylation consensus site and can be phosphorylated by Akt kinase <i>in vitro</i>	124
Figure 3.8: Akt interacts with p84.	125
Figure 3.9: Generation of a phospho-specific p84 antibody (anti-p84-pThr607).....	126
Figure 3.10: Site-directed mutagenesis of Ser358 and Thr607 residues.	127
Figure 3.11: Validation of S358A and T607A mutations.....	128
Figure 3.12: Stable transduction of MDA.MB.231 cells with p84 retroviral vectors.	130
Figure 3.13: p84 expression limits the metastatic capability of MDA.MB.231 cells in a model of experimental haematogenous metastasis.....	131
Figure 3.14: Expression of wildtype or mutant p84 proteins does not alter PI3K γ signal activation.....	132
Figure 3.15: Expression of p84 does not alter cell proliferation but affects attachment-independent colony formation of MDA.MB.231 cells <i>in vitro</i>	133

Figure 3.16: p84 forms an inducible heterodimer with p110 γ upon CXCL12 stimulation that is dependent on Thr607.....	134
Figure 3.17: Recruitment of p110 γ to the membrane is transient and is not affected by the expression of wildtype p84.	135
Figure 3.18: MDA.MB.231 cells transduced to express mutant p84-T607A are functionally similar to p84 knockdown cells in a model of PI3K γ -dependent migration.....	136
Figure 4.1: CRISPR target design for murine <i>Pik3r6</i> (p84).	162
Figure 4.2: Strategy workflow of CRISPR component injection into C57Bl/6n zygotes.	164
Figure 4.3: Screening for <i>Pik3r6</i> CRISPR-induced mutations within exon 1.....	165
Figure 4.4: Screening CRISPR-induced mutations within exon 1 from <i>Pik3r6</i> CRISPR pups.....	173
Figure 4.5: TALEN design to target murine <i>Pik3r6</i> (p84).	174
Figure 4.6: Screening TALEN-induced mutations within exon 1 from <i>Pik3r6</i> TALEN pups.	177
Figure 4.7: CRISPR-based gene-targeting can induce large deletions to regions immediately flanking the CRISPR target site.	178
Figure 4.8: Sequencing PCR of <i>Pik3r6</i> CRISPR pups #1, #5, #7, #16 and #20 confirms large deletions to regions flanking the CRISPR target site.....	181
Figure 4.9: Genomic CRISPR-induced deletion (Δ -10bp) within <i>Pik3r6</i> does not alter the transcript expression of PI3K γ subunits.....	183
Figure 4.10: Genetic mutation of <i>Pik3r6</i> does not destabilise the protein expression of p101 and p110 γ PI3K γ subunits.....	184
Figure 4.11: The weights of lymphoid organs of <i>Pik3r6</i> ^{-/-} mice are comparable to wildtype C57Bl/6n mice.	187
Figure 4.12: Immune cell subsets within lymphoid compartments and the blood of <i>Pik3r6</i> ^{-/-} mice are consistent with wildtype mice.	188
Figure 4.13: <i>Pik3r6</i> ^{-/-} bone marrow cells display inhibited induction of phosphorylated Akt in response to GPCR stimulation.	191
Figure 4.14: p84-deficient bone marrow-derived mast cells are phenotypically similar to wildtype cells and express maturity markers.	192
Figure 4.15: <i>Pik3r6</i> ^{-/-} BMDCs maintain adenosine-mediated potentiation of degranulation and IL-6 cytokine production.....	194

Figure 4.16: <i>Pik3r6</i> ^{-/-} BMMCs display redundancy between p84 and p101 adaptor subunits.	195
Figure 4.17: Thymocyte development is unaffected in <i>Pik3r6</i> ^{-/-} mice.	196
Figure 4.18: <i>Pik3r6</i> ^{-/-} bone marrow-derived neutrophils display reduced migration <i>in vitro</i>	197
Figure 4.19: <i>Pik3r6</i> ^{-/-} mice display attenuated disease upon induction of MOG ₃₅₋₅₅ -induced chronic experimental autoimmune encephalomyelitis.	199
Figure 4.20: Dampened EAE disease severity in <i>Pik3r6</i> ^{-/-} mice is coupled with reduced infiltration of Th cells into the CNS.	201
Figure 4.21: Generation of Th1 and Th17 effector cells is unaffected in <i>Pik3r6</i> ^{-/-} mice during early stage EAE disease compared with wildtype controls.....	202
Figure 5.1: CD4 ⁺ cell sample preparation and ICPL proteomic workflow.	218
Figure 5.2: CD4 ⁺ cell isolation from the CNS during EAE disease progression.	220
Figure 5.3: Examining two EAE disease models: ICPL analysis of CD4 ⁺ cells isolated from the CNS during relapsing-remitting and chronic EAE disease progression.	222
Figure 5.4: Analyses of CNS-infiltrating CD4 ⁺ cells isolated during relapsing-remitting and chronic EAE disease progression identified a broad coverage of regulated proteins.	224
Figure 5.5: Candidate validation by quantitative PCR of mRNA transcript levels.....	231
Figure 6.1: Proposed mechanism of PI3Kγ signalling in MDA.MB.231 cells in response to CXCL12 stimulation.....	250

List of tables

Table 1.1: Common Experimental Inhibitors of Class I PI3Ks	20
Table 1.2: Class I PI3K subunit-deficient genetically-modified mouse strains.	21
Table 1.3: Expression of p84 and p101 subunits in human tissues measured by RT-PCR.	25
Table 2.1: Primers used in this study	88
Table 2.2: Antibodies used in this study	89
Table 2.3: Clinical disease scoring of murine experimental autoimmune encephalomyelitis	91
Table 3.1: Predicted phosphorylation sites within p84.	109
Table 3.2: Summary of post-translational modifications identified within p84.....	118
Table 5.1: Proteins up-regulated by CNS-infiltrating CD4 ⁺ cells during both relapsing- remitting and chronic EAE progression.....	226
Table 5.2: Proteins down-regulated by CNS-infiltrating CD4 ⁺ cells during both relapsing- remitting and chronic EAE progression.....	228
Table 5.3: Established cellular functions of identified regulated proteins.	230

Abbreviations

A2AR	A2A adenosine receptor
A3AR	A3 adenosine receptor
Ab	Antibody
ABD	Adaptor-binding domain
ACN	Acetonitrile
AnxA1/A2	Annexin A1/A2
Arg	Arginine
ATP	Adenosine triphosphate
β -AR	Beta adrenergic receptor
BAD	BCL-2 antagonist of cell death
BCR	B cell receptor
BH	Breakpoint-cluster-region homology
BMMC	Bone marrow-derived mast cell
bp	Base pair
BSA	Bovine serum albumin
C2	Protein-kinase C homology-2 domain
cAMP	Cyclic adenosine monophosphate
CBB	Coomassie Brilliant Blue stain
CCL	CC chemokine ligand
CCR	CC chemokine receptor
CD	Cluster of differentiation
CFA	Complete Freund's adjuvant
CIA	Collagen-induced arthritis
CNA	Copy number alteration
CNS	Central nervous system
ConA	Concanavalin A
CRISPR	Clustered regularly interspaced short palindromic repeat
CXCL	CXC chemokine ligand
CXCR	CXC chemokine receptor
DAG	Diacyl-glycerol
DAVID	Database for Annotation, Visualisation and Integrated Discovery
DEPC	Diethylpyrocarbonate
DN	Double negative (thymocytes)
DP	Double positive (thymocytes)
DTT	Dithiothreitol
EAE	Experimental autoimmune encephalomyelitis
EDTA	Ethylenediaminetetraacetic acid
ELISA	Enzyme-linked immunosorbent assay
ERK1/2	Extracellular signal-related kinases 1/2
ES cell	Embryonic stem cell
EUCOMM	European Conditional Mouse Mutagenesis Program
FA	Formic acid
Fc ϵ RI	Fc epsilon receptor 1
fMLP	Formyl-methionyl-leucyl-phenylalanine
FOXO	Forkhead box O
FRET	Fluorescent resonance energy transfer
GFP	Green fluorescent protein
GPCR	G protein-coupled receptor

gRNA	Guide RNA
GSK-3	Glycogen synthase kinase 3
GTP	Guanosine triphosphate
HA	Haemagglutinin
HBSS	Hank's Balanced Salt Solution
HDX-MS	Hydrogen-deuterium exchange mass spectrometry
HPLC	High-performance liquid chromatography
HRP	Horseradish peroxidase
ICPL	Isotope-coded protein labelling
IFN	Interferon
Ig	Immunoglobulin
IGF-1	Insulin-like growth factor-1
IL	Interleukin
IMVS	Institute of Medical and Veterinary Science
INPP5	Inositol polyphosphate-5-phosphatase
InsP3	Inositol triphosphate
IP	Immunoprecipitation
iSH2	Inter-SH2
KD	Knockdown
kDa	Kilodalton
LCMV	Lymphocytic choriomeningitis virus
LDS-PAGE	Lithium dodecyl sulphate polyacrylamide gel electrophoresis
LPA	Lysophosphatidic acid
Lys	Lysine
mAb	Monoclonal antibody
MALDI-TOF/TOF	Matrix-assisted laser desorption/ionisation time-of-flight MS
MSCV	Murine stem cell virus
MS/MS	Tandem mass spectrometry
Met	Methionine
MOG	Myelin oligodendrocyte glycoprotein
miRNA	Micro RNA
MRCRB	Mouse red cell removal buffer
mRNA	Messenger RNA
MS	Multiple Sclerosis
mTOR	Mammalian target of rapamycin
mTORC1	Mammalian target of rapamycin complex 1
NIP-OVA	Nitroiodophenylacetic acid conjugated to ovalbumin
NLS	Nuclear localisation sequence
NMR	Nuclear magnetic resonance
p-Akt	Phosphorylated Akt
PBS	Phosphate-buffered saline
PCR	Polymerase chain reaction
PDE3B	Phosphodiesterase 3B
PDK-1	Phosphoinositide-dependent kinase 1
PFA	Paraformaldehyde
PH	Pleckstrin homology
PI3K	Phosphatidylinositol 3-kinase
PIP	PtdIns(4)P; PtdIns-4-phosphate
PIP ₂	PtdIns(4,5)P ₂ ; PtdIns-4,5-bisphosphate
PIP ₃	PtdIns(3,4,5)P ₃ ; PtdIns-3,4,5-triphosphate

PKA	Protein kinase A
PKC	Protein kinase C
PKD	Protein kinase D
PLC	Phospholipase C
PLP	Myelin proteolipid protein
PMS	N-methyl dibenzopyrazine methyl sulphate
PMSG	Pregnant mare's serum gonadotropin
PP2A	Protein phosphatase 2
PPMT-1	PP2A methyltransferase-1
PRM	Parallel Reaction Monitoring
PtdIns	Phosphatidyl inositol
PTEN	Phosphatase and tensin homologue
PVDF	Polyvinylidene fluoride (membrane)
PX	Phox homology
qPCR	quantitative PCR
RA	Rheumatoid arthritis
RBD	Ras-binding domain
ROS	Reactive oxygen species
RTK	Receptor tyrosine kinase
RVD	Repeat-variable diresidue
SAGE	South Australian Genome-Editing facility
SCID	Severe Combined Immunodeficient
SDS-PAGE	Sodium dodecyl sulphate polyacrylamide gel electrophoresis
Ser	Serine
SH2	Src homology 2 domain
SH3	Src homology 3 domain
Shh	Sonic hedgehog
SHIP	Src homology 2 domain-containing inositol phosphatase
siRNA	Small interfering RNA
SLE	Systemic lupus erythematosus
SP	Single positive (thymocytes)
S/T	Serine/Threonine
STRING	Search Tool for the Retrieval of Interacting Genes
TALEN	Transactivator-like effector nuclease
T-ALL	T-cell acute lymphoblastic leukemia
TCR	T cell receptor
TBS	Tris-buffered saline
TFA	Trifluoroacetic acid
Th	T helper lymphocyte
Thr	Threonine
TNF	Tumour necrosis factor
Tyr	Tyrosine
VEGF-A	Vascular endothelial growth factor-A
VEGFR1	Vascular endothelial growth factor receptor 1
WB	Western blot
WEHI	Walter and Eliza Hall Institute
WT	Wildtype
XTT	2,3-Bis(2-methoxy-4-nitro-5-sulphophenyl)-2H-tetrazolium-5-carboxanilide

Publications arising from this work

Manuscripts

Turvey ME, Klingler-Hoffmann M, Hoffmann P, McColl SR. p84 forms a negative regulatory complex with p110 γ to control PI3K γ signalling during cell migration. *Immunol Cell Biol.* 2015 Mar. doi; 10.1038/icb.2015.35. (Epub ahead of print).

Refer to **Appendix A1**.

Turvey ME, Koudelka T, Comerford I, Greer JM, Carroll W, Bernard CC, Hoffmann P, McColl SR. Quantitative proteome profiling of CNS-infiltrating autoreactive CD4⁺ cells reveals selective changes during experimental autoimmune encephalomyelitis. *J Proteome Res.* 2014 Aug 1;13(8):3655-70.

Refer to **Appendix A2**.

Conference proceedings

Australian Society for Immunology Annual Scientific Meeting (2013): Poster entitled 'Quantitative proteome profiling of CNS-infiltrating autoreactive CD4⁺ cells reveals selective changes during experimental autoimmune encephalomyelitis'

Australian Society for Immunology (SA / NT Branch) 9th Adelaide Immunology Retreat (2013): Oral Presentation entitled 'The role and regulation of the adaptor subunit p84 in phosphatidylinositol 3-kinase γ signalling and implications for cancer metastasis'

Abstract

The Class IB phosphatidylinositol 3-kinase (PI3K) enzyme, PI3K γ , is activated and recruited to the plasma membrane in response to G protein-coupled receptor stimulation. Upon activation, the lipid-kinase activity and downstream signalling cascades initiated by PI3K γ lead to cytoskeletal rearrangements and the formation of a leading edge for the induction of directed cell migration. PI3K γ consists of the catalytic subunit p110 γ , which forms a mutually exclusive heterodimer with one of two regulatory adaptor subunits, p84 or p101. Although expressed by most cells in the organism, PI3K γ subunits are expressed at highest levels in motile haematopoietic cells, where the regulation of PI3K γ signalling is critical to controlling and maintaining coordinated cell migration during immune responses. Consistent with a central role in leukocyte chemotaxis, innate and adaptive immune cell subsets from p110 γ -deficient mice have been shown to exhibit migration defects *in vitro* and *in vivo*. Furthermore, the aberrant expression of PI3K γ subunits and dysregulation of PI3K γ signalling pathways has been shown to contribute to pathologies such as cancer and autoimmunity where enhanced cell migration promotes disease progression. Despite this, the mechanistic basis for PI3K γ signal regulation is not well understood, particularly with respect to the distinct contributions of the individual regulatory adaptor subunits, p84 and p101. Many PI3K γ -dependent cell functions have been elucidated experimentally using p110 γ - and p101-deficient genetically-modified mouse strains and the PI3K γ -selective inhibitor, AS605240. However, detailed functional data regarding p84 is lacking due to the absence of a p84-deficient mouse strain and limited availability of high quality p84-specific reagents. Three major research goals were addressed in the present study to improve our understanding of the role of p84 in PI3K γ lipid-kinase signalling and its implication in PI3K γ -dependent cell migration.

The first goal was to examine the phosphorylation status of p84 during PI3K γ signalling and assess the role of identified regulatory phosphorylation sites for p84 function using the mammary epithelial carcinoma model cell line, MDA.MB.231. Data presented in this thesis demonstrate that in contrast to the p110 γ and p101 subunits that promote the migration and metastasis of carcinoma cells, the p84 adaptor protein has tumour suppressor function *in vitro* and *in vivo*, which was determined to be dependent on a potential phosphorylation site within p84, Thr607. It was found that Thr607 was required for p84 to form an inducible heterodimer with p110 γ (after initial PI3K γ signal activation) in a

complex sequestered from active signalling at the membrane. This Thr607-dependent p84/p110 γ dimerisation may therefore represent a novel mechanism of negative PI3K γ signal regulation that limits the migration and metastasis of cancer cells.

Next, the contribution of p84 to PI3K γ -dependent immune cell function was determined through the generation and characterisation of a novel p84-deficient mouse (Pik3r6^{-/-}) using CRISPR gene-editing technology. Pik3r6^{-/-} mice were characterised in the context of immune cell development, activation and migration in a variety of haematopoietic cell subsets. It was shown that Pik3r6^{-/-} mice develop normally with respect to lymphoid organ and circulating leukocyte populations at homeostasis. However upon stimulation, neutrophils from Pik3r6^{-/-} mice display reduced migration in response to GPCR agonists *in vitro* and in a murine model of inflammatory autoimmunity (experimental autoimmune encephalomyelitis; EAE), it was found that activated Th lymphocytes display impaired trafficking and reduced infiltration to inflammatory sites.

The final goal was to develop and optimise a proteomic platform to investigate and compare the proteomes of migratory CD4⁺ lymphocytes isolated from tissues at different stages of inflammatory disease progression using experimental autoimmune encephalomyelitis as a model. An isotope-coded protein-labelling (ICPL) approach was developed and optimised to assess the proteomes of CNS-infiltrating CD4⁺ lymphocytes during disease progression in two models of EAE; chronic MOG₃₅₋₅₅-induced EAE and relapsing-remitting PLP₁₃₉₋₁₅₁-induced EAE. This study identified differentially regulated proteins related to immune cell function and represented a initial feasibility study to verify the validity of ICPL as an approach to examine the differential proteomes of wildtype and p84-deficient migratory CD4⁺ lymphocytes during inflammatory disease.

Collectively, the data presented in this thesis represent the identification and characterisation of novel roles for p84 within PI3K γ lipid-kinase signalling during both the regulation of cell migration in carcinoma cells and in haematopoietic cells during immune responses. In addition to furthering the understanding of the unique roles for p84 within PI3K γ signal regulation, the generation of a p84-deficient mouse strain constitutes an important tool to further experimental research in this area.

Chapter 1: Introduction

Chapter 1: Introduction

1.1 Overview

Phosphatidylinositol 3-kinases (PI3K) are a family of dual specificity protein- and lipid-kinases that represent major contributors to lipid signal transduction downstream of transmembrane receptors. Within the PI3K family, Class I heterodimeric enzymes activated downstream of receptor tyrosine kinases and G protein-coupled receptors (GPCRs) are responsible for the catalysis of PtdIns(3,4,5)P₃ (PIP₃) lipid species¹⁻³. PIP₃ derived from Class I PI3K activity is involved in the induction of phosphorylation-dependent signalling cascades within the cell that are required for the regulation of fundamental cellular processes such as growth, survival, migration and metabolism³. Class I PI3Ks are further segregated into two subclasses, Class IA enzymes (PI3K α , PI3K β and PI3K δ) and a sole Class IB enzyme named PI3K γ , based on coupling to upstream activating receptors and dimerisation of the p110 catalytic subunit to distinct adaptor proteins. Whilst the regulation of Class IA enzymes has been well characterised due to the availability of enzyme crystal structures, isoform-selective inhibitors and subunit-deficient genetically-modified mouse strains, in contrast, there is very little known about the regulation of the Class IB enzyme PI3K γ . PI3K γ consists of the catalytic subunit p110 γ , which forms a mutually exclusive heterodimer with one of two adaptor subunits, p84 or p101⁴⁻⁶. Regulation of PI3K γ signal activation and duration is critical to controlling and maintaining coordinated cell migration, principally within highly motile cells of the haematopoietic system during the induction of immune responses⁷⁻⁹. However the mechanistic basis for PI3K γ signal regulation is poorly understood, particularly with respect to the distinct contributions of the individual adaptor subunits. Recent data has suggested that relative to p101, p84 is less adept at transducing robust PI3K γ activity^{6, 10-12} and may therefore have additional, alternative roles in the regulation of PI3K γ signalling. The data and discussion presented in this thesis are focused on the role and regulation of the p84 PI3K γ adaptor subunit, in the context of PI3K γ signal activation/termination and the control of PI3K γ -dependent cell functions such as directed migration.

1.2 Lipid signal transduction

Lipid signalling at the plasma membrane serves as a mode of membrane-to-cytosol communication, propagated through the simultaneous activation of intracellular phosphorylation cascades that ultimately result in transcriptional changes within the cell. Signalling through lipid mediators is therefore an integral process required for the maintenance of fundamental cellular functions such as growth and survival (reviewed in ¹³⁻¹⁵). The activation of transmembrane receptors through engagement with extracellular protein ligands leads to the selective recruitment of lipid kinase effectors to the intracellular portion of the activated receptor. Here, the kinase is proximal to lipid substrates embedded or docked at the lipid membrane bilayer and can facilitate the phosphorylation of specific lipid species^{3, 13}. A summary of major lipid signalling pathways and associated effectors is presented in **Figure 1.1**. These signalling mediators include phosphatidylinositol species and DAG/InsP3, which become activated downstream of chemokines, cytokines, growth factors, hormones and neurotransmitters¹, in addition to ceramides, sphingosines^{16, 17} and serum components such as lysophosphatidic acid (LPA)^{18, 19} that have been shown to act in autocrine and paracrine manners through direct interactions with GPCRs. Collectively, these lipid pathways contribute to the dynamic network of signalling lipids required for cellular communication.

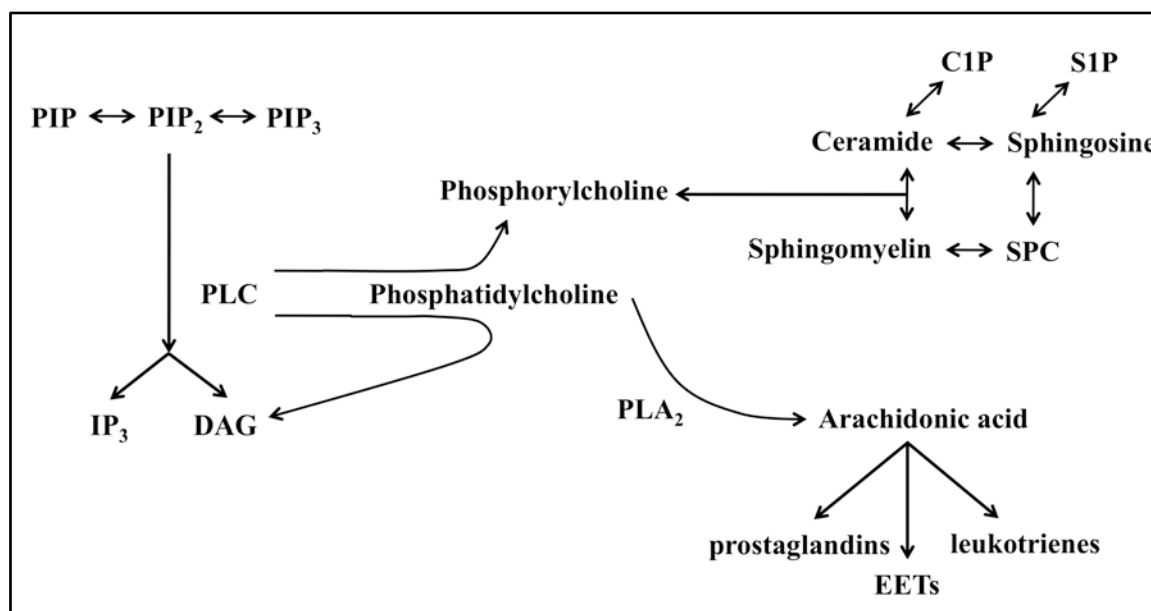


Figure 1.1: The lipid signalling network.

PIP, Phosphatidylinositol-phosphate; PLC, Phospholipase C; IP₃, inositol triphosphate; DAG, Diacylglycerol; PLA₂, Phospholipase A₂; C1P, Ceramide-1-phosphate; S1P, Sphingosine-1-phosphate; SPC, Sphingosylphosphorylcholine; EETs, Epoxyeicosatrienoic acids.

Signal specificity is believed to be, at least in part, controlled by the expression and subcellular localisation of lipid-kinases and their spatial regulation by opposing phosphatases. Within the cell, kinases and their lipid substrates are restricted to distinct subcellular locations through the assembly and congregation of lipid rafts, to which opposing phosphatases are actively excluded^{20, 21}. This spatial organisation has been shown to be essential for the transmission of effective cellular communication. For example, the initiation of cell migration requires the organisation and regulation of PI3K lipid signalling in order to promote the formation of leading and trailing cell edges that are necessary for the cell to respond to directional cues²²⁻²⁴. Firstly, signalling is regulated by the chemoattractant signal and cognate receptor, which dictates the PI3K isoform recruited to the membrane²⁵. Then, cell polarisation requires the clustering of PI3K-rich lipid rafts that leads to the accumulation of PI3K-derived PIP₃ at the leading edge membrane of the migrating cell^{20, 23, 24}. This is coupled with the simultaneous exclusion of phosphatase and tensin homolog (PTEN) and Src homology domain 2 (SH2)-containing inositol phosphatase (SHIP) enzymes that counteract PI3K-activity, which are instead targeted to the trailing edge of the polarised cell. Polarisation induced by PI3K signalling at the leading edge is essential for the cell to migrate directionally toward the chemoattractant signal. However, whilst the events that define the formation of leading and trailing cell edges have been established, the molecular mechanisms that control PI3K activation and signal termination at the leading edge are not well understood. Furthermore, while initially conceptualised as linear pathways leading to a single outcome, it is now apparent that intracellular lipid signalling pathways exists as an integrated network of kinases and phosphatases that require complex regulation dependent on the cellular context and activating signal.

The dysregulation of major lipid signal transduction pathways has been linked to diseases such as chronic inflammation²⁶, autoimmunity^{8, 9, 27}, allergy²⁸⁻³⁰, cancer³¹⁻³⁵, atherosclerosis³⁶⁻³⁸, hypertension^{39, 40}, heart hypertrophy^{41, 42} and metabolic diseases⁴³. Disease development in these conditions is often attributed to mutational activation (such as cancer) or deactivation (such as myopathies, neuropathies or ciliopathies) of lipid-signalling kinases (reviewed in ¹³). However, targeting signalling lipids and downstream kinase effectors in the treatment of such diseases is complicated since these effectors are rarely unique to a single pathway. For instance, many pathways converge on phosphatidyl inositols, PLC or Ca²⁺ mediators and their effectors (refer to **Figure 1.1**) and as such, their

inhibition will impact several pathways. Therefore, a robust understanding of lipid signalling pathways and networks, particularly with respect to their regulation, is key to comprehending their role in normal cellular function and their contribution to disease when pathways become deregulated.

The following sections will introduce the PI3K family, outline what is known about the regulation of Class I PI3K enzymes and then highlight the significant gaps in knowledge regarding the regulation of PI3K γ signal activation and the challenges facing PI3K γ research to this point.

1.3 The phosphatidylinositol 3-kinase family

Phosphatidylinositol 3-kinases (PI3Ks) are a highly conserved family of dual-specificity lipid and protein kinases divided into Class I (Class IA and IB), Class II and Class III enzymes based on their substrate specificity, modular structure and regulation. Through their lipid-kinase activity, PI3K enzymes catalyse the transfer of the γ -phosphate group of ATP to the 3-hydroxyl group of the inositol ring of three species of phosphatidylinositol (PtdIns) lipid substrates; namely PtdIns, PtdIns-4-phosphate (PtdIns(4)P) and PtdIns-4,5-bisphosphate (PtdIns(4,5)P₂)¹. The 3' phosphorylated lipid species produced by PI3K activity (PtdIns(3)P (PIP), PtdIns(3,4)P₂ (PIP₂) and PtdIns(3,4,5)P₃ (PIP₃)) at the plasma membrane induce the recruitment of protein effectors comprising pleckstrin homology (PH), phox homology (PX) and FYVE lipid-binding domains. Upon docking to lipid species at the membrane, protein effectors become activated and perpetuate phosphorylation-dependent signalling cascades that ultimately lead to the regulation of transcription for cellular processes such as growth, proliferation, survival, vesicular transport, differentiation and migration^{2,3}.

PI3Ks have been identified in algae, *Dictyostelium discoideum* (slime mould), plants, *Saccharomyces cerevisiae* (yeast), diptera (fly) and mammals. After the initial discovery of enzymatic PtdIns-kinase activity in 1988 by Cantley *et al.*, numerous isoforms of PI3Ks were identified predominantly through sequence homology analyses and *in vitro* lipid-kinase activity screening methods^{2,44}. In mammals, there are eight known isoforms of PI3Ks; four Class I isoforms, three Class II isoforms and a single Class III isoform. A

schematic of mammalian PI3K isoforms and signalling effectors is depicted in **Figure 1.2** and the domain structures for Class I, II and III PI3K enzymes are presented in **Figure 1.3**.

Class I PI3Ks are receptor-regulated PtdIns(4,5)P₂ kinases that generate intracellular PtdIns(3,4,5)P₃ (PIP₃) in response to extracellular stimuli such as growth factors and chemokines. They are activated downstream of cell surface receptor tyrosine kinases and G protein-coupled receptors and exist as obligate heterodimeric enzymes composed of a catalytic subunit coupled with a regulatory adaptor protein. Upon recruitment of Class I PI3K heterodimers to the membrane receptor, the lipid-kinase activity of the enzyme results in the accumulation of PIP₃ lipids and the selective recruitment of PH-domain containing effector proteins. Collectively, the coordinated receptor engagement and lipid kinase activity of Class I PI3Ks potentiates multi-step signalling cascades involved in the regulation of essential cellular functions. Class I PI3Ks are further divided into subclasses IA (PI3K α , PI3K β and PI3K δ) and IB (PI3K γ) based on structural differences between adaptor proteins. This study is focused on the role and regulation of the Class IB PI3K γ enzyme system and therefore, the expression, function and regulation of Class I enzymes will be discussed in detail in later sections.

Class II PI3Ks are large 170-210 kDa monomeric enzymes with a characteristic C-terminal C2 homology domain (namely PI3K-C2 α , PI3KC2 β and PI3KC2 γ kinases). Whilst the *in vitro* lipid substrate targets of these enzymes are restricted to PtdIns and PtdIns(4)P, the activating signals and lipid substrates *in vivo* are not yet fully characterised⁴⁵⁻⁴⁸. However, it has been proposed that PtdIns(3)P produced by mammalian Class II enzymes is involved in intracellular membrane trafficking, endocytosis, exocytosis and autophagy⁴⁹⁻⁵¹. Specifically, PI3K-C2 α has been linked to endosomal trafficking via RhoA activation and regulation of PtdIns(3)P levels in endothelial cells, where these processes are required for endothelial cell maturation and vessel integrity during vasculogenesis⁵²⁻⁵⁴. The control of PtdIns(3)P production by PI3K-C2 α has also been shown to be crucial at the endocytic recycling compartment located at the base of the cilium⁵⁴. Here, PI3K-C2 α was identified to regulate Sonic Hedgehog (Shh) signalling and contribute to the structural organisation of the primary cilium⁵³. In addition to the regulation of PtdIns(3)P levels within cells, PtdIns(3,4)P₂ generated by PI3K-C2 α at the plasma membrane has been shown to be critical for clathrin-coated pit maturation during endocytosis. Therefore, consistent with

these major roles in intracellular membrane trafficking, the targeted knockout of the PI3K-C2 α gene has been shown to be embryonically lethal in mice (*Pik3c2a*^{-/-})⁵⁴.

The single Class III PI3K is the PtdIns-specific enzyme, Vps34, which is responsible for the generation of the major fraction of PtdIns(3)P generated on endocytic vesicles⁵⁵⁻⁵⁷. Accumulation of PtdIns(3)P induces the recruitment of FYVE- and PX-domain containing proteins that directly bind PtdIns(3)P lipids, thereby linking PI3K lipid signalling to endosomal and vesicular transport through the docking and fusion of endosomes and the generation of autophagosomes⁵⁸⁻⁶⁰. In fact, the first identification of PI3K cellular function was of the Class III enzyme of *S. cerevisiae*, Vps34p⁶¹. Initially identified to be essential for vacuolar segregation and protein sorting, the further characterisation of Vps34p revealed PI3K lipid-kinase activity, where the function of the enzyme was dependent on the Vps15p adaptor protein that was required for the recruitment of the enzyme to the late Golgi compartments⁶². Since the characterisation of Vps34p in *S. cerevisiae*, many homologues have since been identified including Vps34 in mammals.

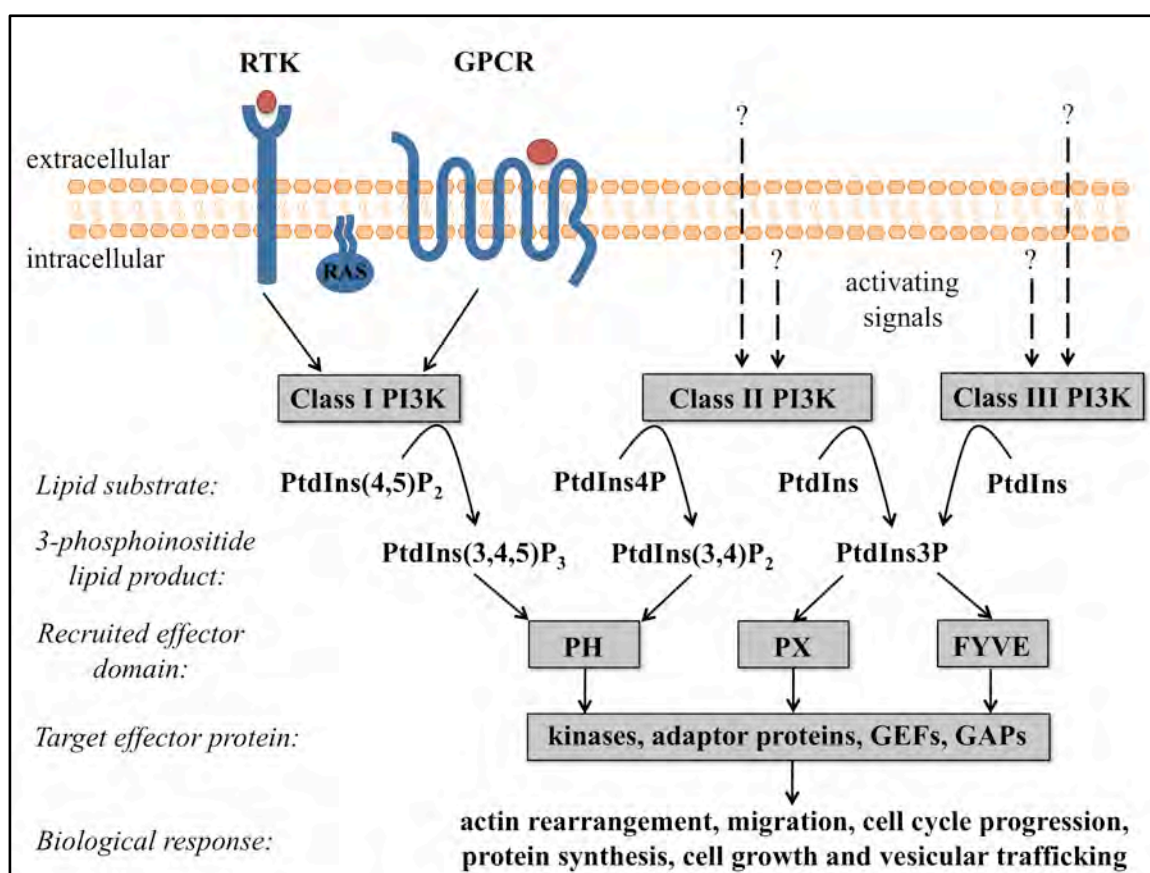


Figure 1.2: Signalling substrates and effectors of Class I, II and III PI3K lipid kinases.

PH, Pleckstrin homology domain; PX, Phox homology domain; FYVE, FYVE lipid-binding domain; GEFs, Guanine nucleotide exchange factors; GAPs, GTPase-activating proteins.

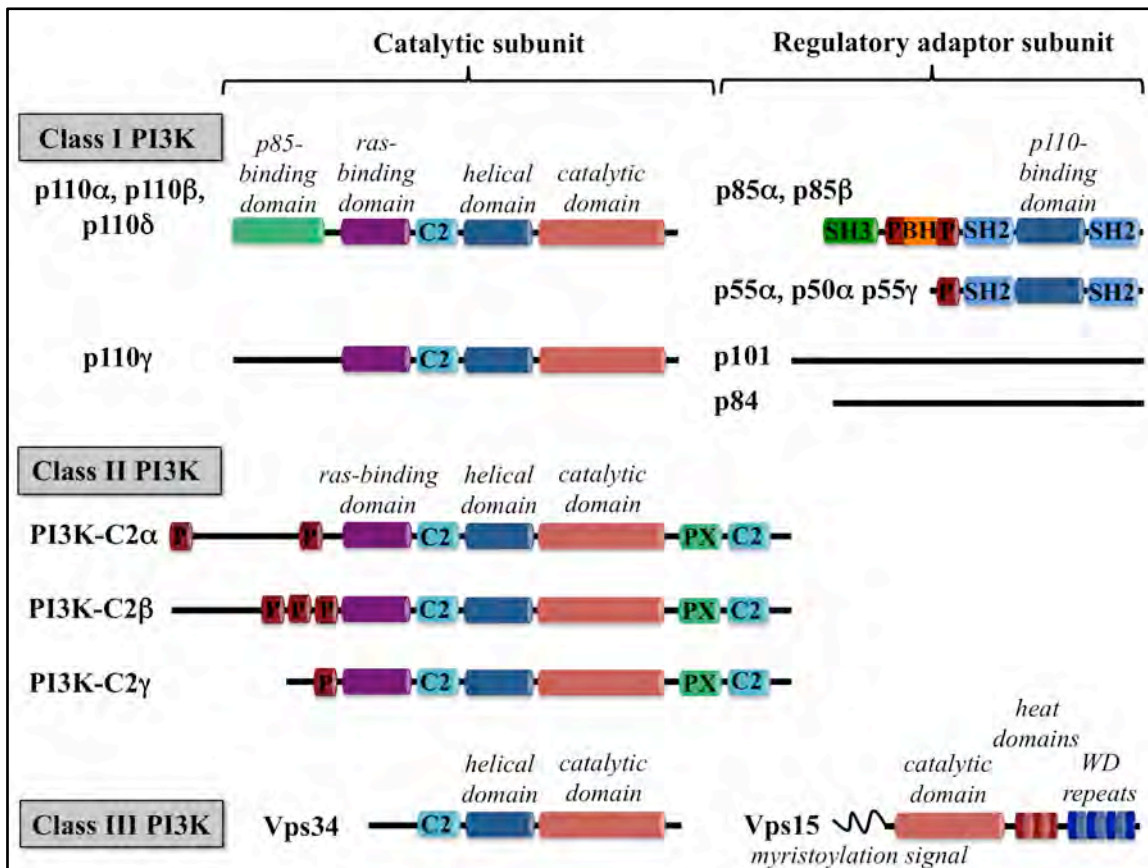


Figure 1.3: Domain structures of Class I, II and III PI3K enzymes.

SH3, SRC homology 3 domain; P, Proline-rich regions; BH, Breakpoint-cluster-region homology domain; NSH2, N-terminal SRC homology 2 domain; iSH2, inter-SH2 region; CSH2, C-terminal SRC homology 2 domain.

1.4 Class I PI3Ks

1.4.1 The structure of Class I PI3K subunits

All Class I PI3Ks are obligate heterodimeric enzymes composed of a p110 catalytic subunit (α , β , γ , δ isoforms) that are highly conserved amongst the family, bound to a regulatory adaptor subunit (see representative diagram; **Figure 1.3**)³. Within Class IA PI3Ks there are three p110 catalytic subunit isoforms; α , β and δ which bind to the adaptor subunit p85 (or p85-related subunits, p50 and p55)⁶³. The activation of PI3K α , PI3K β and PI3K δ enzymes is predominantly downstream of receptor tyrosine kinases (RTKs) stimulated by exogenous growth factor and hormone ligands^{26, 64-66}. In contrast, the lone Class IB kinase PI3K γ consists of the p110 γ catalytic subunit that associates with one of two regulatory adaptor subunits, p101 or p84 (also called p87^{PIKAP}), and is activated primarily downstream of G protein-coupled receptors⁴⁻⁶.

Unlike the p110 catalytic subunits that share extensive sequence homology and a common domain structure between isoforms, the Class IA and IB regulatory subunits share minimal homology between subclasses, despite common functions as adaptor proteins responsible for the translocation of the catalytic subunit to the plasma membrane. The modular structure and domain function of the Class IA PI3K α , PI3K β and PI3K δ enzymes has been well characterised for both the p110 catalytic and p85, p55 and p50 adaptor subunits⁶⁷⁻⁷². Whereas in comparison, far less has been established regarding the structure and function of PI3K γ , particularly with respect to the regulatory subunits p101 and p84, of which there is no structural information or domain data to this point.

The p110 catalytic subunits

The p110 subunits of all Class I PI3Ks consist of an N-terminal adaptor-binding domain (ABD) that facilitates interactions with p85 or p101/p84 regulatory subunits, a ras-binding domain (RBD), C2 domain, helical domain and a C-terminal kinase domain (refer to **Figure 1.3**). As the name suggests, the Ras-binding domain mediates the direct interaction of p110 with ras-GTPase and other small, related GTPases that allows the stimulation of both PI3K- and ras-driven signalling pathways¹¹. The C2 (protein-kinase-C homology-2) domain has high affinity for lipids and is proposed to facilitate the partial integration of PI3K complexes into the plasma membrane upon activation. The helical domain of p110 subunits possesses scaffolding function and contributes to the conformation of PI3K

complexes^{12, 72, 73}, in addition to acting as a docking site for further protein-protein interactions. As expected, the kinase domain is highly conserved between Class I PI3K isoforms, where extensive homology is observed within the ATP-binding site of the enzyme and mapping of this region has led to the development of both pan- and isoform-selective Class I PI3K inhibitors^{25, 69, 74-77}. Specifically, Lys802 within the ATP-binding site of p110 α has been identified as required for phosphate transfer and the site-directed mutagenesis of this lysine residue has been shown to completely abolish protein- and lipid-kinase activity of PI3K α ^{75, 78}. Analogous residues have been mapped in p110 β , p110 δ and p110 γ isoforms in addition to other related enzymes^{75, 79}. As the domain structures of p110 kinases are highly conserved between isoforms and PI3K α , β , δ and γ each catalyse the generation of PIP₃ lipids, signal specificity is achieved through varied tissue and cellular distributions of the isoforms and specific activating signals²⁵.

Class I PI3K adaptor subunits

Class IA and IB catalytic subunits associate with unique regulatory adaptor subunits that share minimal homology between subclasses. The Class IA adaptor subunit, p85, consists of an N-terminal Src homology 3 (SH3) domain, a breakpoint-cluster-region homology (BH) domain flanked by two proline-rich regions, followed by two C-terminal SH2 domains separated by an inter-SH2 (iSH2) region (refer to **Figure 1.3**). In addition to p85, which represents the major Class IA adaptor protein, there also exist truncation variants of the p85 subunit, termed p55 and p50, which are described below and depicted in **Figure 1.4**. The heterodimerisation of the p85 adaptor with the p110 catalytic subunit is mediated through the iSH2 domain^{66, 71, 74, 80}. The N- and C-terminal SH2 domains recognise and bind the canonical phosphotyrosine motif (pYXXM) found on the intracellular portion of autophosphorylated activated receptor tyrosine kinases. This interaction between the SH2 domains of p85 and the activated receptor facilitates the translocation of p85/p110 complexes to the plasma membrane. Furthermore, the structural requirements of p85 to bind RTK phosphotyrosine residues have been elucidated by nuclear magnetic resonance (NMR) and X-ray diffraction methods in conjunction with crystal structure mapping. These analyses have revealed that conserved residues within p85, Arg340, Arg358 and Thr369, encase the phosphate group of phosphotyrosine (pYXXM) and that Tyr416 is displaced in order to accommodate the Met residue (pYXXM) in a hydrophobic binding pocket^{71, 72, 81}.

The complexity and versatility of adaptor/catalytic subunit interactions for Class IA PI3Ks is increased through the number of adaptor subunit isoforms, shown in **Figure 1.4**. There are three genes that code for Class IA adaptors, namely p85 α , p85 β and p55 γ . Furthermore, alternative splicing of p85 α leads to the translation of an additional 53-55 kDa variant, called p55 α , or a 50 kDa product called p50 α ⁸²⁻⁸⁵. In these truncated variants, the N-terminal SH3 and BH domains are replaced with either a unique 34 amino acid stretch or a shorter 6 amino acid stretch of yet unknown function. In addition, both p85 α and p55 α isoforms have been identified with an 8-amino acid insertion that results in the inclusion of two potential serine phosphorylation sites. Tissue-specific expression of these subunit variants has been shown to contribute to Class IA signal specificity, where p85 α is the predominant subunit expressed in the brain, adipose tissue, heart, kidney, lung and spleen, whereas p55 α variants are expressed in the muscle and p85 β and p55 γ variants are preferentially expressed in the testis^{85, 86}.

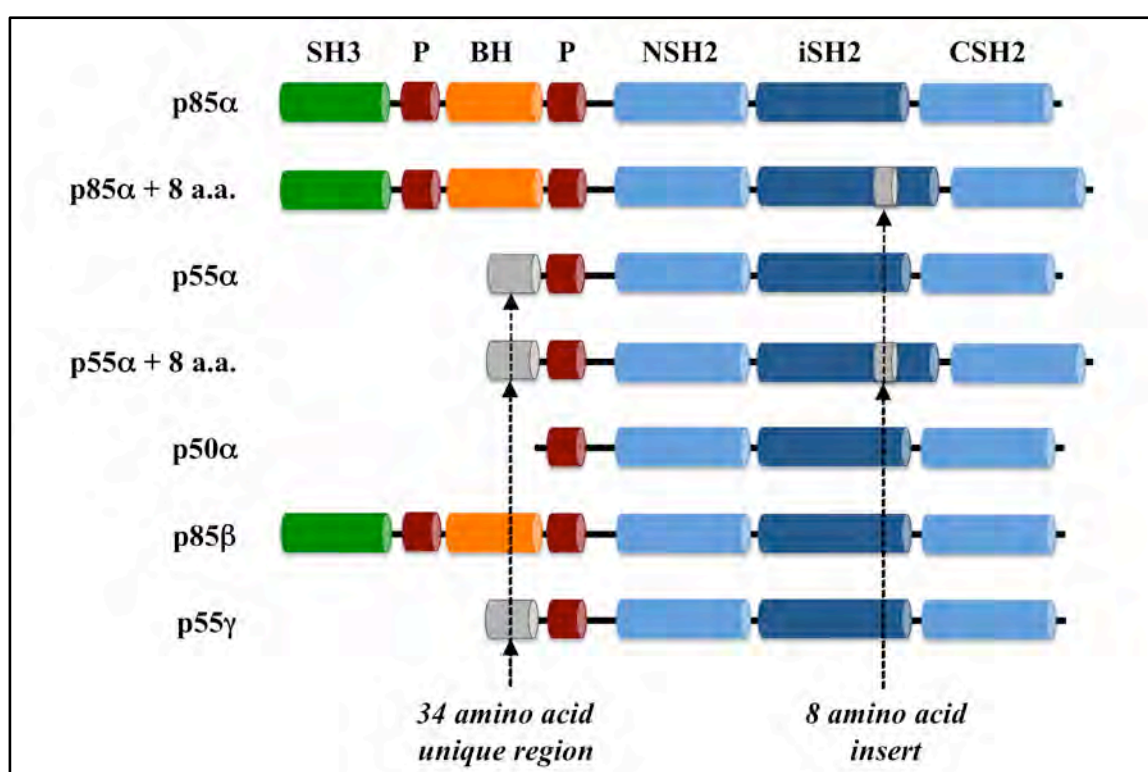


Figure 1.4: Variants of the p85 Class IA PI3K adaptor subunit.

SH3, SRC homology 3 domain; P, Proline-rich regions; BH, Breakpoint-cluster-region homology domain; NSH2, N-terminal SRC homology 2 domain; iSH2, inter-SH2 region; CSH2, C-terminal SRC homology 2 domain.

In contrast to the Class IA adaptor subunits described above that are well characterised in terms of defined functional domains, the modular structures of the p84 and p101 adaptor subunits that bind and regulate the lone Class IB PI3K γ enzyme have not yet been resolved. In fact, p84 and p101 share surprisingly little homology with other regulatory subunits within the PI3K family, despite sharing common functions. The *Pik3r5* and *Pik3r6* gene loci, which encode p101 and p84 respectively, are present immediately downstream of one another and are located on chromosome 17 in humans and chromosome 11 in mice (NCBI gene ID: *Pik3r5*: 23533 (*homo sapiens*) / 320207 (*mus musculus*); *Pik3r6*: 146850 (*homo sapiens*) / 104709 (*mus musculus*)). Human p101 and p84 proteins share approximately 37% sequence similarity and 30% amino acid sequence identity. This homology exists predominantly within N- and C-terminal portions of the proteins, which have been shown in p101 at least, to be required for adaptor binding to p110 γ and G $\beta\gamma$, respectively^{5, 6, 87}. These proposed association domains within p101 were determined by fluorescent resonance energy transfer (FRET), co-immunoprecipitation and localisation studies using p101 truncation and deletion mutants⁵. By comparison, the structural organisation of p84 is unknown and no crystal structure has been resolved. However due to the similarity with p101 within the N- and C-termini, it has been hypothesised that these regions within p84 are similarly required for p110 γ - and G $\beta\gamma$ -binding. The proposed modular structures of p84 and p101 adaptor subunits are outlined in **Figure 1.5**.

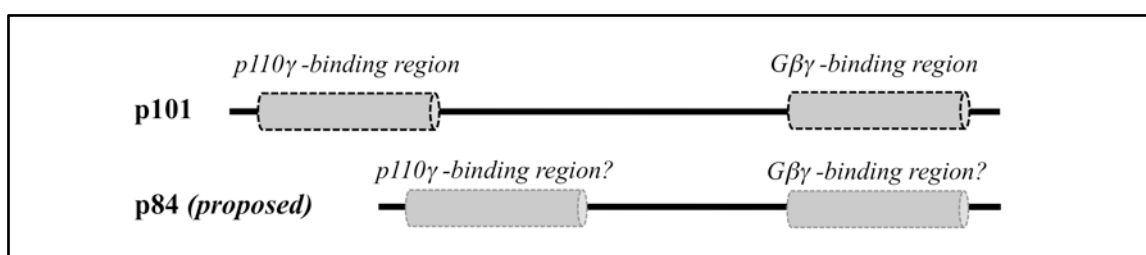


Figure 1.5: Proposed structure of Class IB PI3K γ adaptor subunits

1.4.2 Regulating the lipid-kinase activity of Class I PI3K enzymes

The exclusive lipid substrate of Class I PI3K enzymes, PtdIns(4,5)P₂ (PIP₂), is produced at the membrane where it is localised for phosphorylation at the D-3 position of the inositol lipid head group by the lipid-kinase activity of PI3K α , β , δ and γ enzymes, thereby producing the principal second messenger molecule PtdIns(3,4,5)P₃ (PIP₃). Tracking of

lipid species within cells has revealed that in a basal state, there is substantial PIP relative to low levels of PIP₂ and PIP₃. However upon activation of RTKs and GPCRs in response to extracellular stimuli, PIP₃ is rapidly generated at the plasma membrane⁸⁸⁻⁹⁰. One of the major effectors of Class I PI3K signalling is Akt kinase (PKB), which is recruited to PIP₃ accumulated at the membrane through its PH-lipid-binding domain. Membrane localisation of Akt positions it for activation by enzymes PDK1 and mTORC1 that phosphorylate Akt at residues Thr308 and Ser473 (p-Akt), respectively^{91, 92}. The induction of p-Akt is therefore an established experimental readout of Class I PI3K lipid-kinase activity. Upon activation, p-Akt potentiates further signalling events through the phosphorylation of protein substrates such as the cell cycle regulators p21 and p27, glycogen synthase kinase 3 (GSK-3) in the insulin signalling pathway, the pro-apoptotic protein BCL-2 antagonist of cell death (BAD), and forkhead box O (FOXO) transcription factors⁹³⁻⁹⁵.

These events, initially driven by PI3K-dependent PIP₃ accumulation, culminate in the regulation of cellular processes such as chemotaxis, differentiation, proliferation and survival. Considering the role of PI3K signalling in these fundamental cell functions, it is not surprising that the dysregulation of Class I PI3K lipid-kinase activity has been linked to pathologies such as cancer and autoimmune conditions where aberrant cellular migration and survival contributes to disease^{8, 9, 31, 76, 96}. The regulation of Class I PI3K lipid-kinase activity is therefore key to maintaining normal cell function, which is controlled by both extrinsic and intrinsic regulatory mechanisms, described hereafter.

Extrinsic regulation of PIP₃ levels by phosphatase-dependent hydrolysis

The actions of Class I PI3Ks are counteracted by three lipid-phosphatases that catalyse the conversion of PIP₃ to PIP₂, namely phosphatase and tensin homolog (PTEN), Src homology domain 2 (SH2)-containing inositol phosphatase (SHIP) and inositol polyphosphate-5-phosphatase (INPP5), as shown in **Figure 1.6**^{20, 22, 23, 97}. PTEN is the major negative regulator of Class I enzymes and is responsible for the hydrolysis of phosphates from the 3' position of phosphoinositides, thereby controlling the level and spatial distribution of PIP₃ within cells. The balance and coordination between the kinase activity of PI3Ks and the phosphatase activity of PTEN is important to ensure that lipid signal transduction is both transient and spatially regulated. As described previously, the spatial organisation of enzymes within cells is particularly relevant during migratory responses. During migration, the accumulation and restriction of PIP₃ at the leading edge

of the polarised cell is achieved through the targeting of PI3Ks to the leading edge and the parallel hydrolysis of phospho-lipids by PTEN at the trailing edge²⁰. Furthermore, the hydrolysis of PI3K-derived PIP₃ is necessary to control proliferation and prevent cell transformation. In keeping with this, the mutation or loss of PTEN is associated with many cancer types and leads to the hyperactivation of PI3K signalling through sustained recruitment and activation of downstream effectors. Specifically, mutations in the catalytic or membrane localisation-domains of the enzyme lead to loss of PTEN tumour suppressor activity⁹⁸⁻¹⁰².

Like PTEN, SHIP (SHIP1) phosphatase also catalyses the conversion of PIP₃ lipids to PIP₂, though in contrast, hydrolysis occurs exclusively from the 5' position. SHIP is ubiquitously expressed in differentiated haematopoietic cells, endothelial cells and some stem cells where it is involved in the control of cell growth and proliferation²². Recently, mutation of another inositol phosphatase, INPP5, has been linked to ciliopathies. This has revealed a role for INPP5 in the regulation of primary cilia function through the hydrolysis of PIP₃ at the primary cilia membrane during protein trafficking^{103, 104}.

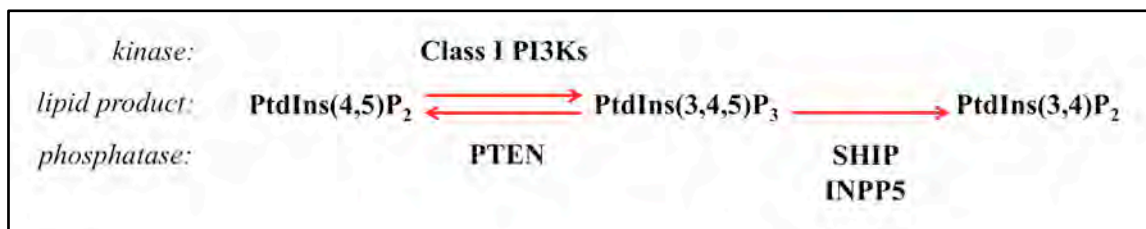


Figure 1.6: Dynamic regulation of PIP₃ levels

Further regulation of PI3K lipid-kinase signalling is achieved through auxiliary phosphatase activity that directly inhibits Akt kinase, the major effector of Class I signalling. Protein phosphatase 2 (PP2A) is a serine/threonine phosphatase that is abundantly and ubiquitously expressed and contributes to the major fraction of S/T phosphatase activity within the cell^{105, 106}. It is therefore integral in the regulation of multiple signal transduction pathways. PP2A is capable of hydrolysing Akt at both Ser473 and Thr308 phosphorylation sites and is the only phosphatase that regulates phosphorylation of Thr308¹⁰⁷. In summary, the culmination of PTEN, SHIP, INPP5 and PP2A phosphatase activities are required for the effective regulation of PI3K signalling in

order to ensure the appropriate signal intensity and duration is achieved downstream of receptor stimulation.

Intrinsic regulation of Class I lipid-kinases

The lipid-kinase activities of Class IA PI3K α , β and δ enzymes are also regulated by intrinsic conformation- and phosphorylation-dependent mechanisms, where the interaction between catalytic and adaptor subunits or the interaction between PI3K complexes and the activated RTK are either promoted or negated^{67, 72}. These mechanisms rely on two functions of the p85 subunit as an adaptor protein. Firstly, p85 acts as a stabilising/inhibitory binding-partner that holds p110 in a conformationally inactive state until RTK-induced activation, then secondly, upon receptor stimulation, the p85 adaptor protein is responsible for the translocation of p110 to the plasma membrane through direct interactions with RTK phosphotyrosine motifs. The inhibitory role of p85 occurs in the absence of receptor stimulation when the p110/p85 complex is located in the cytosol. Hydrogen-deuterium exchange mass spectrometry (HDX-MS) has been used to show that in the absence of stimulation, the SH2 domains within p85 provide a structural constraint on the proximal iSH2 domain (inter-SH2; involved in p110-binding)^{64, 71, 74, 80}. This results in a p85/p110 heterodimer conformation that is stable, but inactive due to the conformational suppression of the p110 kinase domain.

In addition to structural repression of p85/p110 heterodimers, the lipid-kinase activity of Class IA enzymes can be further regulated by phosphorylation-dependent mechanisms, where the phosphorylation of p85 by p110 α and p110 β protein-kinase activity has been shown to modulate lipid signalling^{66, 74, 108}. Specifically, p85 α can be phosphorylated by p110 α on Ser608, which has been shown to reduce the lipid-kinase activity of heterodimeric PI3K α by 3- to 7-fold¹⁰⁸. Ser608 lies within the iSH2 domain of p85 and the incorporation of the negatively charged phosphate group at this site has been proposed to inhibit a nearby region required for the presentation of lipid substrates to the catalytic subunit of p110¹⁰⁸.

There is also evidence to suggest that Class IA PI3K signalling can be regulated by the activity of other signalling kinases through the phosphorylation of the p85 adaptor subunit. For instance, the membrane translocation of PI3K α can be negatively regulated by the

parallel activation of the PKC signalling pathway, representing crosstalk between the two signalling networks. In this case, persistent PKC signalling leads to the phosphorylation of two analogous serine residues, Ser361 and Ser652, within the SH2 pTyr-binding pockets of p85 α ⁶⁶. Phosphorylation at these residues was determined to be mediated by PKD activated downstream of PKC activation and was shown to block the recruitment of PI3K α to the activating receptor⁶⁶. Inhibition of adaptor-mediated membrane translocation is an efficient means of regulating PI3K activity, as the proximity of the kinase to lipid substrates is essential to its function.

To summarise, in addition to the regulation of Class I PI3K signalling by opposing phosphatases that hydrolyse PIP₃, many regulatory mechanisms that exist to control PI3K heterodimer interactions and lipid-kinase activity involve transient phosphorylation of the adaptor subunit. However, whilst regulatory phosphorylation events such as these have been demonstrated for Class IA enzymes, the phosphorylation status of the Class IB adaptor subunits p84 and p101 during rest and upon PI3K γ signal activation remain unknown.

1.4.3 Determining the tissue-specific functions of Class I PI3K enzymes

Since the initial characterisation of lipid-kinase activity *in vitro*, functional analyses of Class I PI3K enzymes have rapidly advanced with the resolution of crystal structures for the complexes, which have allowed detailed structural mapping and the generation of isoform-selective small molecule inhibitors. Crystal structures have now been resolved for all of the Class I catalytic p110 α , β , δ and γ subunits, beginning with the successful crystallisation and modelling of p110 γ in 1999^{69, 78, 80, 109}. The report by Walker *et al.* (1999) of the 2.2 Å X-ray crystallographic structure of p110 γ revealed a modular organisation based around a helical domain spine, which was surrounded by C2 and kinase domains positioned to allow interactions with membrane lipids and a ras-binding domain positioned proximal to the kinase domain in order to facilitate allosteric activation of the enzyme⁷⁸. The crystal structure of the Class IB catalytic subunit, p110 γ complexed with the isoform-selective PI3K γ inhibitor AS605240 is presented in **Figure 1.7**.

Structural mapping of the ATP-binding pocket within the kinase domain of p110 subunits has enabled the discovery and/or generation of small molecule inhibitors that non-

discriminately target Class I PI3K enzymes by preventing ATP hydrolysis. There are two widely-used pan-PI3K inhibitors that bind within the ATP-binding pocket. These are wortmannin, a mould metabolite originally described in 1974 as possessing anti-inflammatory properties and later characterised as being a highly potent, selective and cell-permeable PI3K inhibitor, and LY294002, the first synthetic inhibitor of PI3Ks^{77, 110, 111}. The introduction of these tools accelerated research in this area and allowed the rapid identification of many PI3K-dependent cellular responses including mitogenesis, glucose uptake, chemotaxis and respiratory burst. In addition to these pan-PI3K inhibitors, isoform-selective small molecule inhibitors have been synthesised to inhibit the kinase activity of p110 isoforms with varied specificity. The structures of Class I PI3K inhibitors are presented in **Table 1.1**.

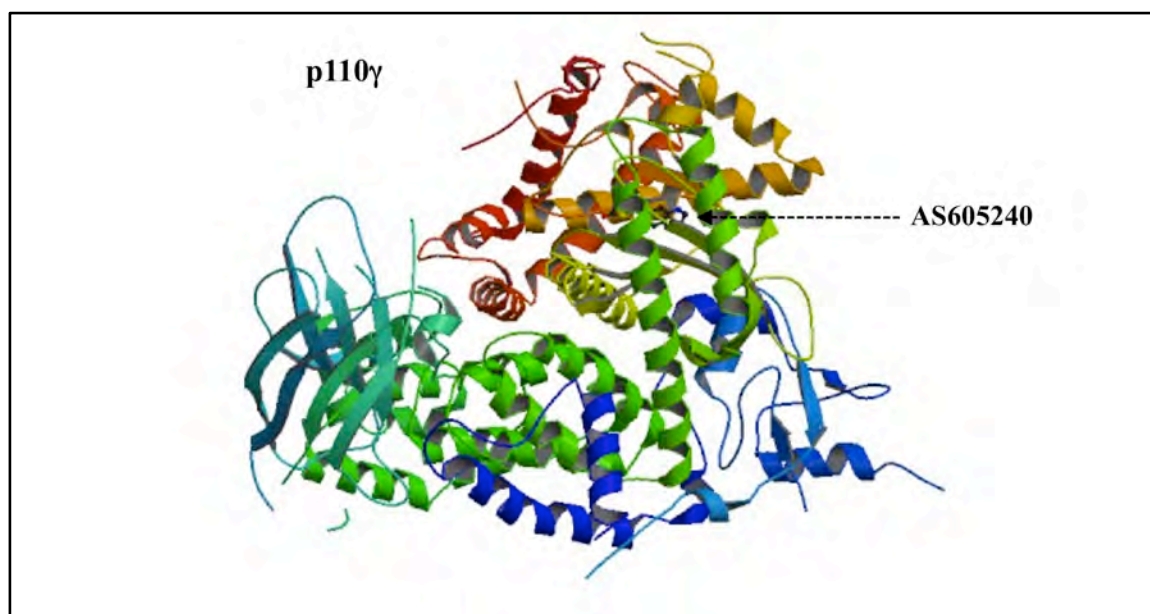
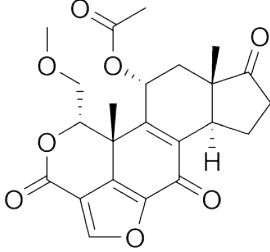
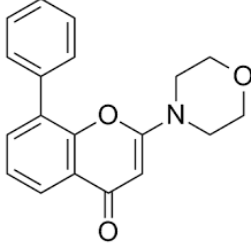
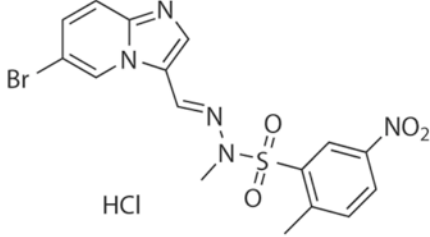
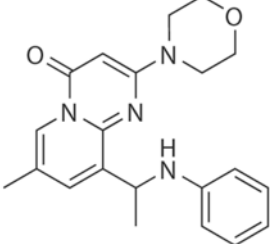
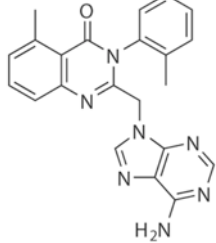
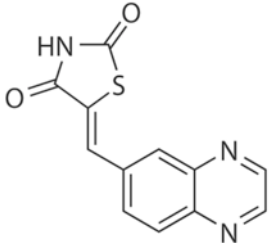


Figure 1.7: Crystal structure of the p110 γ catalytic subunit complexed with AS605240.

Sourced from: Camps *et al.* (2005) *Nature Medicine* doi: 10.1038/nm1284. Protein structure resolved to 2.70 Å by X-ray diffraction.

Table 1.1: Common Experimental Inhibitors of Class I PI3Ks

Name	Isoform Selectivity	Chemical Structure
Wortmannin	Pan-inhibitor	
LY294002	Pan-inhibitor	
PIK-75	Isoform-selective p110 α inhibitor	
TGX221	Isoform-selective p110 β inhibitor	
IC87114	Isoform-selective p110 δ inhibitor	
AS605240	Isoform-selective p110 γ inhibitor	

Genetically-modified mouse strains are also an invaluable tool to study the function of individual proteins through the specific deletion of one or more gene products. Within the Class I PI3K family, genetic deletion of p110 α or p110 β isoforms results in an embryonically lethal phenotype, which reflects their ubiquitous tissue expression and central roles in cell growth and survival signalling^{112, 113}. This is in contrast to p110 δ and p110 γ isoforms, which display restricted tissue expression and their genetic deletion results in viable offspring that display mild phenotypes at homeostasis, although significant immune defects are apparent upon the induction of inflammation^{7, 9, 114}. There are a number of genetically-modified strains available with PI3K deletions including broad germline deletions of catalytic and adaptor subunits, germline p110 knockout/kinase-dead p110 knock-in mutations, tissue-specific conditional knockouts and double/triple gene knockouts. The generation of tissue-specific knockout strains has allowed the roles of PI3K α and PI3K β to be assessed in more detail, which has elucidated further functions for PI3K α as a mediator of insulin signalling and PI3K β in platelet biology, respectively¹¹⁵⁻¹¹⁸. The knockout strains available for Class I PI3K isoforms and the functional roles that have been characterised based on the phenotypes displayed are summarised in **Table 1.2**.

Table 1.2: Class I PI3K subunit-deficient genetically-modified mouse strains.

Adapted from Liu *et al.* (2009) *Nature Reviews Drug Discovery* doi: 10.1038/nrd2926.

Subunit	Genotype	Phenotypes
p110α	p110 α ^{-/-}	Embryonic lethality (E10.5)
	p110 α ^{D933A/D933A}	Embryonic lethality (E10.5) E10-11; severe vascular abnormalities at E10.5
	p110 α ^{+D933A}	Defective in growth and metabolic regulation associated with hyperinsulinemia and glucose intolerance
	p110 α ^{RBD/RBD}	Defective lymphatic development; a small fraction survived to adult, associated with proliferative defects and altered growth factor signalling to PI3K; protected from Kras-driven tumourigenesis in a lung cancer model
	Endothelial p110 α ^{-/-}	Severe vascular abnormalities at E10.5 and died before E12.5
	Prostate p110 α ^{-/-}	Normal for prostate development; not protected from PTEN-loss-induced high-grade prostatic intraepithelial neoplasia
p110β	p110 β ^{-/-}	Embryonic lethality (E3.5)
	p110 β ^{K805R/K805R}	Some survived to adult, associated with retarded growth and mild insulin resistance with age; attenuated Erbb2-driven mammary tumour development

	Liver p110 β ^{-/-}	Impaired insulin sensitivity and glucose homeostasis
	Prostate p110 β ^{-/-}	Normal for prostate development; protected from PTEN-loss-induced high-grade prostatic intraepithelial neoplasia
p110δ	p110 δ ^{-/-}	Viable; impaired B, NK cell development and functions; decreased immunoglobulin levels and defective humoral response; impaired neutrophil chemotaxis
	p110 δ ^{D910A/D910A}	Viable; defective B, NK and mast cell development and function; impaired antigen receptor signalling in B and T cells, attenuated immune and allergic response
p110γ	p110 γ ^{-/-}	Viable; reduced insulin secretion; increased insulin sensitivity and β -cell mass; impaired mast cell functions and inflammatory response; reduced neutrophil and macrophage migration and oxidative burst; increased heart contractility
	p110 γ ^{KD/KD}	Viable; reduced inflammatory reactions with no alterations in cardiac contractility
	p110 δ ^{-/-} / p110 γ ^{-/-}	Viable; severe defects in T and NK cell development and functions
p85	p85 α ^{-/-}	Hypoglycemia and hypoinsulinemia; impaired B cell development and function; normal T cell activation
	p55 α ^{-/-} / p50 α ^{-/-}	Viable; enhanced insulin sensitivity
	p85 α ^{-/-} / p55 α ^{-/-} / p50 α ^{-/-}	Perinatal death; liver necrosis and hypoglycemia; increased insulin sensitivity; impaired B cell development and function
	p85 β ^{-/-}	Improved insulin sensitivity; increased T cell proliferation and accumulation in response to various stimuli
	Liver p85 α ^{-/-} / p55 α ^{-/-} / p50 α ^{-/-} / p85 β ^{-/-}	Defects in glucose and lipid homeostasis; hyperinsulinemia and hypolipidemia
	Muscle p85 α ^{-/-} / p55 α ^{-/-} / p50 α ^{-/-} / p85 β ^{-/-}	Viable; reduced muscle growth, insulin response, and hyperlipidemia
	Endothelial p85 α ^{-/-} / p55 α ^{-/-} / p50 α ^{-/-} / p85 β ^{-/-}	Acute embryonic lethality at E11.5 due to haemorrhaging
	Endothelial p85 α ^{+/-} / p55 α ^{-/-} / p50 α ^{-/-} / p85 β ^{-/-}	Viable but with localised vascular abnormalities when challenged with pathological insults
p101	p101 ^{-/-}	Viable; reduced neutrophil migration and inflammatory response; impaired thymocyte development.

1.5 The PI3K Class IB enzyme, PI3K γ

Whilst the structure, functions and regulation of Class IA enzymes have been extensively examined, there is far less information regarding the lone Class IB enzyme PI3K γ , particularly with respect to the regulation of the heterodimeric complex and the distinct roles of the individual adaptor subunits. PI3K γ consists of the p110 γ catalytic subunit bound to one of two putative adaptor subunits, p101 or p84 (also called p87^{PIKAP}), which are unique to the IB subclass⁴⁻⁶. Compared with Class IA enzymes that are activated primarily downstream of receptor tyrosine kinases, PI3K γ is predominantly activated downstream of G protein-coupled receptor (GPCR) stimulation. Ligand binding to the 7-transmembrane GPCR induces the dissociation of coupled G-proteins to G α and G $\beta\gamma$ subunits, where G $\beta\gamma$ contributes to the activation of PI3K γ that has translocated from the cytosol to the plasma membrane⁸⁷. The membrane recruitment of PI3K γ heterodimers is dependent on the adaptor protein interaction with G $\beta\gamma$, whereby the maximal activation of PI3K γ is achieved with the additional association of the complex with membrane-localised ras-GTPase^{11, 12}. PI3K γ subunits are expressed at highest levels in cells of the haematopoietic system where roles for PI3K γ have been demonstrated during development, homeostasis and during immune responses. In these contexts, PI3K γ is involved in signalling downstream of chemokine receptors for the induction of immune cell chemotaxis towards extracellular chemokine stimuli⁷.

While it is known that p84 and p101 PI3K γ adaptor subunits are imperative for interactions with G $\beta\gamma$ and the translocation of p110 γ to the plasma membrane, the precise roles of the distinct subunits in PI3K γ regulation and signal specificity are not yet clear. The initial characterisation of PI3K γ signalling was conducted at a time when p101 was believed to be the sole adaptor subunit for p110 γ , which alone contributed to the protein- and lipid-kinase activity of the enzyme. It was not until the cloning and characterisation of p84 as a second p110 γ adaptor in 2005⁽⁶⁾ that the regulation of this system by dual adaptors was considered. The gene encoding p84 (*Pik3r6*) is present in *Homo sapiens*, *Mus musculus*, *Canis lupus familiaris* (dog), *Gallus gallus domesticus* (chicken) and *Anura* (frog) genomes and is always located immediately downstream of the p101 locus^{6, 119}. The gene region surrounding *Pik3r5* (p101) and *Pik3r6* (p84) loci is outlined in **Figure 1.8**.

Although originally proposed to have redundant roles, solely as G $\beta\gamma$ -adaptors, recent data have contributed to an increasing body of evidence suggesting that p101 and p84 differ both in their tissue expression patterns^{4, 6, 119, 120}, their ability to coordinate p110 γ activity in separate signalling cascades¹²¹⁻¹²³ and their coupling to upstream inputs in a variety of different cellular systems^{11, 122, 124}. It is becoming clear that p84 is less able to transduce robust PI3K γ signalling relative to its p101 counterpart, suggesting that p84 may play an, as yet, undefined role in PI3K γ regulation. The remainder of this literature review will focus on what is known about the activation of PI3K γ , with particular respect to the regulation of lipid-kinase signalling by p84 and p101 adaptor subunits. The research presented in this thesis concentrates on the distinct role of p84 in PI3K γ signal regulation and the investigation of tissue-specific functions of p84 in the context of immune cell development and migration during inflammation.

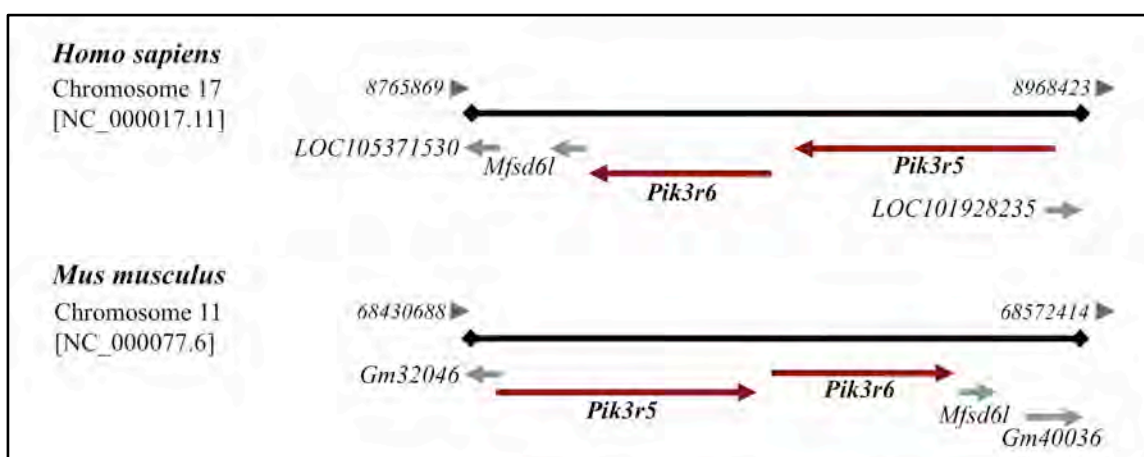


Figure 1.8: The p101 and p84 gene locus

1.5.1 PI3K γ subunits: expression, stability and localisation

The expression of the PI3K γ catalytic subunit p110 γ is exclusively coupled with the expression of one or both regulatory adaptor proteins. A recent mRNA array of human tissues by Shymanets *et al.* (2013) revealed that whilst p101 is expressed at high levels in restricted cell types, p84 is more widely expressed but generally at a low level when expressed as the sole adaptor (refer to **Table 1.3**)⁴. The highest expression of PI3K γ subunits was observed for cells of the immune system where it has been shown that PI3K γ signalling is required for haematopoietic cell migration in response to chemokines⁷, in

addition to maturation and differentiation processes downstream of cell surface antigen receptors¹¹⁴. In immune compartments such as the bone marrow, spleen and lymph nodes, highly motile cells were identified to co-express p101 and p84 at high levels⁴. Although both adaptors can facilitate lipid-kinase activity of PI3K γ complexes, the level of functional redundancy, if any, that exists between the two adaptors is not yet apparent.

Table 1.3: Expression of p84 and p101 subunits in human tissues measured by RT-PCR

Human tissue	p84 adaptor expression	p101 adaptor expression
Adrenal gland	+	+
Bone marrow	+++	+++
Brain	+	+
Cervix	++	ND
Colon	+	+
Duodenum	+	+
Epididymis	+	ND
Esophagus	+	ND
Fat	++	+
Heart *	+	ND
Intestine	++	+
Intracranial artery	+	ND
Liver	ND	+
Lung	++	+++
Lymph node	+++	+++
Mammary gland	+	ND
Optic nerve	+	ND
Ovary	+	ND
Oviduct	+	ND
Pancreas	+	ND
Pituitary gland	+	+
Placenta	+	+
Plasma blood leukocytes	+++	+++
Prostate	++	++
Rectum	+++	ND
Retina	+	+
Seminal vesicles	+	ND
Skin	++	+
Spinal cord	+	+
Spleen	+++	+++
Stomach	++	++
Testis	+	ND
Thymus	++	+++
Tonsil	++	+
Trachea	+	+
Urethra	++	ND

Urinary bladder	+	ND
Uterus	+	+
Uvula	+	ND
Vagina	+	ND
Vena Cava	+	ND

Sourced from Shymanet *et al.* (2013) *J Biol Chem* doi: 10.1074/jbc.M113.508234.

* *more recent data has shown p101 expression in the heart*^{120, 125}.

The stability and localisation of PI3K γ subunits has been elucidated using subunit reconstitution experiments, where cells lacking PI3K γ are complemented with p110 γ , p101 or p84 subunits alone or in combination. These experiments have been conducted in mast cells, an innate granulocytic leukocyte subset responsible for IgE-mediated allergic responses, which activate PI3K γ downstream of both antigen/IgE-induced Fc ϵ RI-clustering and GPCR stimulation through adenosine receptors^{28, 29, 126}. Unlike other haematopoietic cell subsets, mast cells have been reported not to express detectable levels of p101, rather they express only the p84 regulatory subunit in conjunction with p110 γ ^{121, 124}. However, it was observed that bone marrow-derived mast cells (BMMCs) isolated from p110 γ -deficient (p110 γ ^{-/-}) mice also completely lack the expression of p84¹²¹. This suggested that the expression and/or stability of PI3K γ adaptor proteins may be dependent on the p110 γ catalytic subunit, at least in mast cells, although the mechanism by which p84 expression was lost in this instance was not investigated. Mechanism aside, p110 γ ^{-/-} BMMCs that lack expression of p110 γ , p84 and p101 subunits have allowed these cells to be utilised for subunit complementation experiments, where the expression of one or a combination of PI3K γ subunits can be re-introduced by nucleofection in order to study monomeric and dimeric interactions^{11, 121}. Although PI3K γ is functional only as a heterodimeric enzyme, using subunit reconstituted p110 γ ^{-/-} BMMCs as a model system; the stability of monomeric p110 γ , p101 and p84 subunits have been shown to differ under resting conditions. Both p110 γ and p84 were shown to be stable as monomers, whereas p101 has little stability in the absence of p110 γ ^{4, 119}. The relative stability of monomeric p84 in the absence of p110 γ in these experiments indicates that the loss of p84 expression in p110 γ ^{-/-} BMMCs occurs through an alternate mechanism.

When assessing the subcellular localisation of reconstituted PI3K γ subunits, it was found that monomeric p110 γ and p101 localised to the nucleus of cells whilst p84 displayed primarily cytosolic expression^{5, 119}. This can be attributed to the presence of nuclear localisation sequences (NLS) within the C2 domain of p110 γ and the central region of p101, but which is lacking from p84. Under resting conditions, constitutive p101/p110 γ and p84/p110 γ heterodimer complexes have been identified, which are localised primarily in the cytosol^{5, 119}. In spite of these observations, it should be noted that the expression of PI3K γ subunits induced by nucleofection of p110 $\gamma^{-/-}$ BMMCs does not represent endogenous proteins and therefore may not completely reflect the situation in unmodified cells.

The analysis of endogenous protein levels in primary cells has revealed that the expression of p110 γ remains constant during both resting conditions and upon stimulation, whereas the expression of p101 and p84 adaptor subunits have been found to be differentially regulated upon stimulation^{4, 120}. In peripheral blood mononuclear cells, it has been shown that the expression of p101, but not p84, can be induced by persistent GPCR stimulation over 24 hours. The induction of p101 in this context also correlated with increased p101/p110 γ heterodimerisation compared with that of p84/p110 γ ⁴. A similar effect was observed in cardiomyocytes, where the tissue expression of p101 could be increased with persistent heart stress, whereas the expression of p84 remained unchanged¹²⁰. However, in relation to these experiments and as discussed in earlier sections, the molecular mechanism by which protein levels of p101 are increased remains unknown. Furthermore, the biological relevance of induced expression of PI3K γ subunits and heterodimerisation with p110 γ is unclear, as to date there are no data to suggest that p101 and p84 directly compete for p110 γ binding in an endogenous system.

At this point, the only description of direct regulation of PI3K γ gene expression is of the *Pik3r5* (p101) and *Pik3r6* (p84) genes in BMMCs, where miRNA-155 was found to specifically suppress the expression of p101 and p84¹²⁷. Down-regulation of PI3K γ adaptor subunits in mast cells was shown to inhibit the induction of phosphorylated Akt upstream of degranulation, cytokine secretion and migration¹²⁷. miRNA-155 has also been shown to suppress the expression of other PI3K isoforms (specifically p85 α) and regulate signalling downstream of B- and T-cell receptors in mature lymphocytes¹²⁸. Consistent with

heightened PI3K subunit expression and activation, the miR-155-deficient mouse (miRNA-155^{-/-}) displays an enhanced anaphylaxis response perpetuated by increased FcεRI-mediated degranulation and release of TNF-α, IL-13 and IL-6 from mast cells¹²⁷.

Together, the studies described above regarding the expression and stability of PI3Kγ subunits showed that whilst p110γ is invariably expressed in conjunction with one or both adaptor subunits, the adaptor subunits themselves display cell-type specific expression patterns and can be differentially regulated. It is also important to consider that although both p84 and p101 adaptor proteins may be expressed in the same cell, it has not yet been established whether functional redundancy exists between the subunits and to what degree, or whether p84/p110γ and p101/p110γ heterodimers mediate distinct functions defined by the activating signal.

1.5.2 The interaction between p110γ and an adaptor subunit

PI3Kγ functions as an obligate heterodimeric enzyme composed of p110γ and an adaptor subunit. However, the heterodimers formed by p84 and p101 regulatory subunits are not equal in their capacity to transduce lipid-kinase signalling. At a basic level, the p101/p110γ heterodimer maintains a stronger interaction than p84/p110γ^{4, 11}, as demonstrated by the inability of increasing concentrations of p84 to outcompete p101 for p110γ-binding *in vitro*, whereas increasing amounts of p101 were shown to readily displace p84 from p110γ⁴. Although, these data are contrary to earlier reports generated during the characterisation of p84¹¹⁹, which showed using Fluorescent Resonance Energy Transfer (FRET) that p84 and p101 subunits expressed in HEK cells were similarly capable of displacing one another from p110γ. Moreover, while it is known that binding of p101 or p84 adaptors to p110γ is a mutually exclusive interaction^{6, 12}, whether distinct pools of p84/p110γ and p101/p110γ heterodimers participate in separate signalling cascades or whether a single p110γ molecule is capable of exchanging adaptor proteins depending on the cellular context is yet to be elucidated.

The regions within PI3Kγ heterodimers that form the interface between the interacting proteins have been partially resolved using hydrogen-deuterium exchange mass spectrometry (HDX-MS). HDX-MS methods have been successfully employed to generate

complete data relating to the p101/p110 γ interaction, though unfortunately the interaction domains within p84 remain unknown due to an inability to crystallise the protein. Analysis of the p101/p110 γ heterodimer confirmed firstly that p101 interacts predominantly with the helical domain of p110 γ , as previously described for other p110 isoforms with their cognate adaptors, and secondly, that the complex is stabilised through further interactions of p101 with the RBD-linker domain of p110 γ , a mechanism that is unique to PI3K γ ¹². Upon exposure of p101/p110 γ to membrane lipids, HDX-MS analyses revealed two protected regions within the kinase domain of p110 γ , namely the K α 2 N-lobe helix and the K α 12 C-terminal helix¹². This demonstrates that portions of the kinase domain partially insert into the membrane upon translocation. Further analysis showed that the direct interaction of p110 γ with membrane lipids changed the conformation of the helical domain so that regions involved in G $\beta\gamma$ -binding were exposed. When G $\beta\gamma$ was subsequently introduced to membrane-bound p101/p110 γ , it was found that G $\beta\gamma$ bound p110 γ within the exposed helical domain regions proximal to p101 and also interacted with residues R552 and K553 within the C2-helical linker¹². Interactions between the C2-helical linker (K532 and K533) and G $\beta\gamma$ have also been described for p110 β ¹²⁹, which suggests that this interface is common amongst G $\beta\gamma$ -sensitive enzymes, since analogous residues are absent from p110 α and p110 δ isoforms^{71, 72}. Conversely, two key binding regions surrounding C-terminal residues 777 and 821 within p101 were identified to mediate G $\beta\gamma$ -binding, in addition to further residues within the C-terminus of p101 that have been shown to stabilise the protein complex¹².

In comparison, HDX-MS interaction studies for p84/p110 γ heterodimers have been largely ineffective due to the inability to form sufficient crystals for monomeric p84 or p84/p110 γ heterodimers. As such, the only interface resolved by HDX-MS to this point is the p110 γ interface involved in binding to p84, which involved the expression and purification of p110 γ and p84 from baculovirus-transduced Sf9 insect cells. As previously proposed based on the interaction of the p101 adaptor protein with p110 γ , p84 was also identified to bind within the helical domain of p110 γ in addition to smaller interaction interfaces within the N-terminal region that were shown to stabilise the complex¹²⁴.

Mechanisms that regulate the formation of p84/p110 γ and p101/p110 γ heterodimeric PI3K γ complexes are not well understood. An interesting mechanism controlling the

heterodimerisation interaction between p84 and p110 γ has been described recently in BMMCs. In this study by Walser *et al.* (2013), the p84/p110 γ heterodimer was shown to be regulated through the transient phosphorylation of p110 γ within the helical domain, to which p84 has been shown to bind¹²⁴. This represents yet another instance where transient phosphorylation events within PI3K complexes exist as a mode of enzyme regulation^{66, 108}, as previously discussed in section 1.4.2. In response to intracellular calcium mobilisation and Fc ϵ RI clustering, activated PKC β was found to phosphorylate p110 γ on Ser582 leading to a conformational change within the helical domain (to accept the phosphate group)¹²⁴. This phosphorylation-dependent structural change resulted in the displacement of p84. A simultaneous conformational change was observed in the catalytic pocket of p110 γ , thereby inactivating PI3K γ lipid-kinase activity and allowing p110 γ to uncouple from GPCR-inputs. It was proposed that p110 γ subsequently participated in alternate roles downstream of calcium signalling in mast cells, however whether any catalytic activity of monomeric p110 γ was maintained was not investigated¹²⁴. Despite this, the phosphorylation-dependent uncoupling of p110 γ from p84 in BMMCs represents the first description of p110 γ acting independently of an adaptor subunit and is therefore a significant finding.

To summarise, HDX-MS has been a useful tool to elucidate the molecular events that occur during the dimerisation of p110 γ with p101 and p84 adaptors and the interaction of PI3K γ heterodimers with G $\beta\gamma$ and lipid components. Though these events have only been partially mapped and the crystallisation of p84 and p84/p110 γ complexes still remain elusive, the aforementioned data has resolved structural aspects related to PI3K γ kinase activity at the plasma membrane. To further understand the regulation of PI3K γ complexes, detailed information regarding adaptor-mediated intrinsic regulatory mechanisms controlling the enzymatic activity of PI3K γ (such as has been described for p85-dependent regulation of PI3K α activity in section 1.3.2) must be attained.

1.5.3 Activation of PI3K γ lipid-kinase activity at the plasma membrane

In response to GPCR activation, PI3K γ heterodimers translocate from the cytosol to the plasma membrane where the enzyme binds the dissociated G-protein subunit, G $\beta\gamma$, that has been released from the activated receptor. The translocation of the catalytic subunit to the

membrane and the activation of p110 γ lipid-kinase activity towards proximal lipid substrates are mediated by the adaptor subunit. However, p101 and p84 regulatory subunits display disparate abilities as G $\beta\gamma$ -adaptors. Firstly, it has been shown that p101 displays 4-fold higher affinity to G $\beta\gamma$ -binding than p84⁽¹¹⁾, and that as a consequence; p101/p110 γ heterodimers are more readily recruited to the membrane upon receptor stimulation^{6, 10, 11, 130}. Secondly, by measuring the kinase activity of membrane-tethered myristoylated or prenylated p110 γ , it was shown that partial activation of kinase activity could be mediated by G $\beta\gamma$ alone, p101 alone or by lipid exposure alone, albeit at a sub-maximal level¹⁰. Maximum stimulation of PI3K γ required the interaction of p110 γ with G $\beta\gamma$, p101 and lipid components in combination¹⁰. These data suggest that p101 possesses an intrinsic capacity to stimulate the lipid-kinase activity of p110 γ . In comparison to p101/p110 γ heterodimers, p84/p110 γ heterodimers display less efficient translocation to the membrane and p84 is incapable of directly stimulating membrane-tethered p110 γ in the absence of G $\beta\gamma$ ^{4, 10}. Furthermore, p84-mediated PI3K γ requires the action of ras-GTPase, which directly binds p110 γ as a co-factor and promotes its kinase activity¹¹.

Consistent with enhanced membrane translocation, p101/p110 γ heterodimers have been shown to produce a more robust PI3K γ signal than p84/p110 γ heterodimers as determined by the lipid-kinase activity of p110 γ , which can be visualised by PIP₃ accumulation at the membrane and the recruitment of PH-domain containing effectors^{4, 12}. The kinetics of PI3K γ -dependent PIP₃ production has been found to vary based on the receptor/stimulus and the cell type interrogated, although in general, transient generation of PIP₃ can be observed at the plasma membrane within minutes of GPCR stimulation. For example, in human embryonic kidney cells transfected with p110 γ and p101 in conjunction with a PH-domain/GFP fusion-tagged protein, PIP₃ accumulation was shown to occur by 5-10 seconds of fMLP receptor stimulation where recruitment of PH-GFP to the membrane was visualised by live-cell microscopy¹². In the case of bone marrow-derived mast cells that express p84 as the sole adaptor protein, p84/p110 γ has been shown to readily translocate to the membrane within 15 seconds of GPCR stimulation¹²¹. In contrast, a more delayed recruitment and activation of PI3K γ has been observed in MDA.MB.231 mammary carcinoma cells where PIP₃ accumulation at the membrane and the induction of phosphorylated Akt occurs within 5 minutes of CXCL12 stimulation through CXCR4¹²³.

Contrary to the established dogma that Class IB PI3K γ is activated solely downstream of GPCRs, recent data generated in tumour-infiltrating myeloid cells has challenged this concept, where PI3K γ was identified to be activated downstream of the VEGFR1 receptor, an RTK previously thought to activate only Class IA kinases¹²². This report by Schmid *et al.* (2011) found that in tumour-infiltrating myeloid cells, p84-mediated PI3K γ was activated exclusively downstream of RTKs whilst p101-mediated PI3K γ complexes exclusively coupled to GPCRs. Both signalling pathways in this context were found to require ras-GTPase as a co-factor. In this study, p84/p110 γ -induced PIP₃ accumulation at the plasma membrane was shown to occur within 15 seconds of VEGF-A stimulation in a PI3K γ -dependent manner, as determined by sensitivity to AS605240 inhibition¹²². p110 γ could also be co-precipitated with VEGFR1 upon stimulation¹²². However, the mechanism by which p84/p110 γ was recruited to VEGFR1 and interacted with the phosphotyrosine residues of activated receptor is not clear, since p84 has not been predicted to contain SH2 domains that facilitate the interaction of p85 with cognate RTKs. An alternate explanation is that cross-activation of p84/p110 γ may occur through an interaction between VEGFR1 and a GPCR, as has been described for IGF1/CXCR4¹³¹. VEGF-A stimulation of myeloid cells resulted in the activation of integrin $\alpha 4\beta 1$, which facilitated cell adhesion to endothelial vessels, extravasation and infiltration of myeloid cells into the tumour mass¹²². Similar to the ability of PI3K γ to signal downstream of RTKs, it has also been shown that Class IA PI3K β can be activated downstream of both RTK and GPCR stimulation, whereas PI3K α and PI3K δ are exclusively activated downstream of RTKs^{132, 133}.

Collectively, studies concerning the actions of p84 and p101 as adaptor subunits have demonstrated that p101 is more effective than p84 at facilitating the rapid translocation of PI3K γ enzyme complexes to the activating receptor and G $\beta\gamma$ at the plasma membrane. However, a novel function of p84-mediated PI3K γ heterodimers has recently been identified in myeloid cells where p84/p110 γ was found to be activated downstream of receptor tyrosine kinases, challenging the previously accepted dogma that PI3K γ coupled exclusively to GPCR signalling.

1.5.4 Mechanisms of PI3K γ signal regulation

As described in section 1.4.2, PI3K family complexes are commonly regulated by both conformation- and phosphorylation-dependent mechanisms, although in contrast to Class IA PI3K enzymes, there is considerably less known about the regulation of PI3K γ . Unlike the Class IA regulatory subunit, p85, which inhibits the lipid-kinase activity of p110 α , p110 β and p110 δ subunits through conformational restraints whilst inactive in the cytoplasm⁷⁴, the Class IB regulatory subunits p101 and p84 have not been shown to directly suppress the enzymatic activity of p110 γ . However, structural modelling and comparisons between inactive p110/p85 and p110 γ have led to the proposal of a negative regulatory mechanism where the tertiary conformation of p110 γ inhibits its own kinase activity rather than an interaction with an inhibitory adaptor¹².

For Class IA enzymes, inactive p85/p110 heterodimers adopt a conformation of p110 where the last two helices of the kinase domain, together with proximal loops, form an arch critical for PI3K regulation^{72, 74, 80}. The elbow region within this regulatory arch provides the interface to which p85 binds and inhibits the kinase activity of p110 until the complex is translocated to the membrane. In contrast, p110 γ does not maintain this inhibitory interaction with an adaptor protein through its kinase domain. Instead, it has been found that when p110 γ is not associated with membrane lipids, the K α 12 helix functions as an autoinhibitory region by forming inhibitory contacts with the elbow and activation loops underneath it¹². This results in a kinase-inactive conformation of p110 γ . Upon translocation of PI3K γ to the membrane and interaction with membrane lipids, the K α 12 helix partially inserts into the membrane, thereby opening the conformation of p110 γ and leaving the elbow region of the kinase domain and activation loops exposed. The disruption of autoinhibitory contacts between the K α 12 helix and elbow/activation loop regions allows the induction of p110 γ kinase activity¹². A similar mechanism of intrinsic structural regulation has also been described for the Class III PI3K, Vps34^{59, 134}.

The autoinhibited state of p110 γ and the conformational changes induced upon lipid exposure, p101-binding and G β γ -binding are illustrated in **Figure 1.9**.

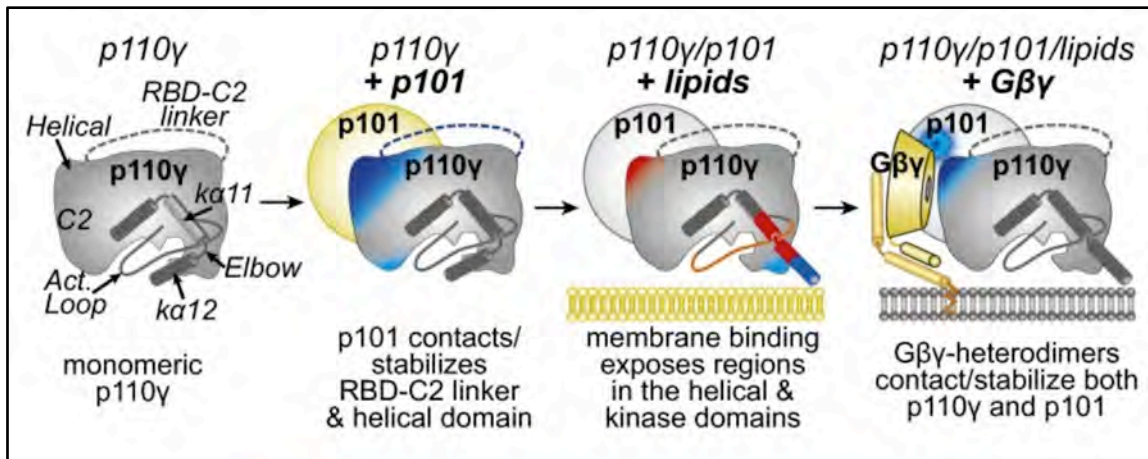


Figure 1.9: The conformation of p110 γ modulates its lipid-kinase activity.

Sourced from Vadas *et al.* (2013) *PNAS* doi: 10.1073/pnas.1304801110.

To date, there has been no description of regulatory phosphorylation events for p84 and p101 adaptor subunits in the control of PI3K γ signal regulation. This is in comparison to what has been established for the phosphorylation-dependent regulation of Class IA enzymes by p85^(66, 108) (refer to section 1.4.2).

However, there are two studies to propose that PI3K γ signalling may be negatively regulated through the control of p101 expression and subcellular localisation^{121, 135}. These studies by Johnson *et al.* (2011) and Bohnacker *et al.* (2009) involved the over-expression of p101 in either primary haematopoietic T lymphocytes or mast cells, respectively. In T lymphocytes, it was found that although high p101 expression correlated with increased PIP₃ levels, the excessive signalling produced by p101/p110 γ heterodimers ultimately resulted in cell death through the activation of apoptotic pathways¹³⁵. Since moderate over-expression of p101 in these experiments instead resulted in the oncogenic transformation of T lymphocytes¹³⁵, it suggests that the activation of death pathways is a mechanism to prevent aberrant over-activity of PI3K γ signalling and subsequent oncogenesis.

In comparison, in mast cells, the subcellular localisation of PI3K γ heterodimers was shown to correlate with distinct signalling outcomes (refer to section 1.5.2). In subunit-reconstituted p110 γ ^{-/-} BMDCs (described in Section 1.5.1), it was shown that p84/p110 γ and p101/p110 γ heterodimers formed separate pools of PI3K γ in distinct subcellular localisations¹²¹. Here, p110 γ ^{-/-} BMDCs (lacking expression of p110 γ , p84 and p101) were

reconstituted with p110 γ alone or p110 γ in combination with a single adaptor or both adaptors. Whilst both p84/p110 γ and p101/p110 γ complexes were capable of contributing to PIP₃ accumulation and the induction of phosphorylated Akt, indicative of active PI3K γ signalling, only the activation of p84/p110 γ resulted in full-scale degranulation of mast cells¹²¹. This discrepancy was attributed to the subcellular localisation of PIP₃ generated by the distinct dimers, where p84/p110 γ activity was shown to readily generate plasma membrane-associated PIP₃, whereas p101/p110 γ dimers were rapidly endocytosed and signalling occurred at intracellular endosome membranes¹²¹. However, it should be noted that the biological relevance of activation-induced endocytosis of p101/p110 γ complexes and PI3K γ signalling at distinct membrane compartments is still to be confirmed in further cell types since mast cells do not endogenously express p101.

To summarise, in comparison to the regulation of Class IA PI3K enzymes, the regulatory mechanisms that control PI3K γ signalling are not well understood. Furthermore, phosphorylation-dependent control of PI3K γ lipid-kinase activity is yet to be investigated or described.

1.6 Functional roles for PI3K γ

PI3K γ has been identified to possess cell type-specific functions that are both kinase-dependent and kinase-independent depending on the tissue context and activating signal. For instance within cardiomyocytes, the lipid-kinase activity of p101-mediated PI3K γ controls β -adrenergic receptor density and the regulation of the cardiac response to adrenalin, whilst p84-mediated PI3K γ facilitates a unique kinase-independent scaffolding function during the regulation of cellular cAMP levels and heart contractility (described further in section 1.6.1)^{120, 125}.

In contrast, PI3K γ signalling in haematopoietic cells is activated for the induction of chemotaxis and is required for both the homeostatic trafficking of naïve and memory cells through secondary lymphoid organs and during immune responses^{7, 114, 136, 137}. The chemokine receptor profile of a cell population in conjunction with the surrounding inflammatory milieu dictates their migratory phenotype. For instance, the temporal expression of CCR7 on activated Langerhan dendritic cells allows them to respond to

chemotactic gradients of CCL19 and CCL21 within the skin¹³⁷⁻¹³⁹. This facilitates their directed migration into the lymphatics to draining lymph nodes where they present processed antigen to T lymphocytes and initiate the adaptive immune response¹³⁸. Upon PI3K γ signalling downstream of chemokine receptors such as CCR7, the cell becomes polarised through the rearrangement of the actin cytoskeleton to form a 'leading' and a 'trailing' edge (described in section 1.4.2). The leading edge is formed by the spatially restricted localisation of PI3K γ -dependent PIP₃ within lipid rafts at the plasma membrane in the direction of the increasing chemokine gradient^{20, 23, 24}. Protrusions at the leading edge propel the cell directionally towards the increasing chemotactic signal. PTEN and SHIP phosphatases that counteract PIP₃ accumulation are excluded from these lipid rafts and are instead targeted to the trailing edge of the cell²³. This polarisation ensures tightly localised signalling that is restricted to the leading edge. In fact the breakdown of this subcellular organisation and kinase/phosphatase distribution, through either the disruption of lipid rafts and/or the loss of PTEN or SHIP phosphatase activity has been shown to completely inhibit directed cell migration^{20, 97}.

The temporal and spatial regulation of PI3K γ signalling must therefore be tightly controlled to maintain normal cellular functions. Aberrant signalling through PI3K γ pathways has been shown to result in cardiac dysfunction and also lead to pathologies such as autoimmunity and cancer metastasis, which can be attributed to enhanced migration of autoreactive or oncogenic cells, respectively. The following sections outline the established functional roles for PI3K γ in normal cell function and during disease when PI3K γ signalling becomes dysregulated. Many of these roles have been elucidated using the PI3K γ -selective inhibitor, AS605240, and disease models in PI3K γ -deficient mice (refer to section 1.3.3 and Tables 1.1 and 1.2). AS605240 is the most robustly characterised selective PI3K γ -inhibitor, which was developed by Camps *et al.* in 2005⁽⁸⁾ and freely distributed to the research community. The small molecule inhibitor was strategically developed using low throughput enzyme screening and high content ATP-binding pocket cell-based screening, together with structural-based design and optimisation⁸. PI3K γ -deficient mice currently include broad p110 γ knockout (p110 γ ^{-/-}) and p110 γ kinase-dead (p110 γ ^{KD/KD}) strains and a p101 broad knockout strain. At the time of writing, no p84 knockout mouse was available, and as such, a novel p84 knockout mouse was developed in the present study to elucidate p84-dependent roles for PI3K γ . However during final thesis

preparation, another p84 knockout mouse was published. This will be discussed in detail in Results and Discussion Chapters.

1.6.1 PI3K γ in cardiac function

Cardiomyocytes express p110 γ in conjunction with both p101 and p84 adaptors, where the regulatory subunits have been found to execute distinct functions within separate subcellular compartments^{4, 125, 140, 141}. The kinase-dependent function of PI3K γ in cardiomyocytes is mediated by p101/p110 γ heterodimers activated downstream of cell surface β -adrenergic receptors (β -AR) in response to adrenalin. Lipid signalling driven downstream of PIP₃ at the plasma membrane promotes a transduction pathway resulting in β -AR internalisation^{120, 125, 140, 141}. This regulation of β -AR density mediated by PI3K γ signalling is critical to cardiac function. For instance, increased expression of p101 has been found to increase PI3K γ signalling activity and lead to enhanced receptor internalisation, which subsequently causes decreased β -AR density and ultimately causes heart failure¹²⁰.

In addition to the regulation of β -AR density, p110 γ present in the cytosol of cardiomyocytes has been found to regulate cardiac hypertrophy through the inhibition of GSK-3 signalling pathways¹⁴². GSK-3 is a protein kinase responsible for the phosphorylation and activation of numerous transcription factors involved in the regulation of hypertrophy, where the inhibition of GSK-3 promotes cardiac growth. In this context, p110 γ has been shown to directly bind and inhibit PPMT-1 in the cytosol thereby preventing the interaction of PPMT-1 with PP2A, a complex that is required for the activation of GSK-3¹⁴². The expression and localisation of p110 γ therefore indirectly affects GSK-3 activation and aberrant regulation of PI3K γ signalling can result in abnormal cardiac growth.

A unique kinase-independent role for p84-mediated PI3K γ has also been identified within the heart. In this capacity, the p84/p110 γ dimer acts as a scaffold to support a multimeric complex with protein kinase A (PKA) and phosphodiesterase 3B (PDE3B), which has been shown to negatively regulate cardiac contractility through the regulation of cAMP hydrolysis^{119, 120, 143}. Within the multimer, PKA is responsible for the phosphorylation of

PDE3B (required for PDE3B phosphodiesterase activity), whilst p110 γ anchors PKA through the N-terminal domains and p84 is necessary to link the complex through the binding of both PDE3B and p110 γ ¹²⁰. Whilst the disruption of this multimeric complex in p110 γ -deficient animals (p110 γ ^{-/-}) leads to cardiac failure in response to aortic compression, animals that express the kinase-dead p110 γ mutant protein (p110 γ ^{KD/KD}) display a phenotype comparable to wildtype animals¹²⁰. This confirms the necessity of p110 γ and p84 as structural components rather than a catalytic entity within this complex. Furthermore, in addition to protein-kinase activity towards PDE3B, PKA anchored by p110 γ , has also been found to phosphorylate p110 γ at Thr1024, inactivating PI3K γ kinase activity and thereby allowing p110 γ and p84 to act solely as scaffolding proteins¹²⁰. Of note, this inhibitory phosphorylation of p110 γ was also observed to result in the stabilisation of β -AR density, suggesting a degree of cross-talk between PI3K γ signal transduction pathways within cardiomyocytes and the regulation of β -AR/cAMP/PKA signalling^{120, 125}. Although the mechanisms regulating p110 γ in cardiomyocytes remain unclear with respect to the activation of PI3K γ by p101 or p84 and the alternate subcellular localisations occupied by each of these pathways, it does suggest a dynamic environment where p110 γ can participate in both kinase-dependent and -independent functions.

1.6.2 PI3K γ in haematopoietic cell development and function

Consistent with highest expression of PI3K γ subunits observed within haematopoietic compartments, PI3K γ signalling has been shown to be required for functions within both innate and adaptive immune cell subsets. The role of PI3K γ has been most extensively characterised in neutrophils and the propagation of inflammation, whereby neutrophils from p110 γ ^{-/-} mice display activation defects^{7, 136, 144}. Specifically, p110 γ -deficient neutrophils are incapable of generating PIP₃ downstream of GPCR stimulation, which correlates with decreased levels of phosphorylated Akt, ERK1 and ERK2 species, and results in reduced migration to chemokines (such as CCL3, CCL5, CXCL1 and CXCL8) and chemoattractants (such as C5a and the bacterial peptide fMLP) *in vitro* and *in vivo*^{7, 114, 145}. Impaired neutrophil recruitment in p110 γ ^{-/-} mice has been observed in models of casein-induced peritonitis, to sites of *Listeria monocytogenes* or *E.coli* infections when seeded to the peritoneal cavity and in models of neutrophil infiltration during lung sepsis^{8, 24, 114, 145-147}. Furthermore, PI3K α , PI3K β or PI3K δ isoforms cannot compensate for the

loss of PI3K γ activity required for neutrophil migration, indicating that PI3K γ is the sole isoform responsible for mediating neutrophil chemotaxis towards chemoattractants. In addition to migratory defects, cytokine-primed neutrophils from p110 γ ^{-/-} mice display reduced respiratory burst, characterised by decreased production of reactive oxygen species (ROS) in response to fMLP. ROS production is a biphasic process, and while multiple PI3K isoforms coordinate to produce the second phase of ROS, the first phase of ROS production is mediated by PI3K γ alone^{130, 136, 144, 148}.

Another cell type that has been extensively used to study PI3K γ interactions is the mast cell, the innate inflammatory mediator activated during allergic responses. In response to allergen exposure, mast cells become sensitised with surface-bound allergen-specific IgE then are activated to degranulate upon subsequent stimulation, where they release intracellular granule stores of inflammatory mediators such as histamine. Degranulation of mast cells occurs downstream of antigen/IgE and Fc ϵ RI clustering and involves the parallel activation of PI3K γ and Ca²⁺ signalling pathways²⁹. Unlike other immune cell subsets, mast cells have been reported to express only the p84 regulatory subunit in conjunction with p110 γ ^{121, 124}. Therefore in the context of mast cells, p84/p110 γ heterodimers are solely responsible for the activation of PI3K γ -dependent signalling cascades. Specifically, PI3K γ is activated downstream of adenosine A3 receptors (A3AR) during mast cell activation where stimulation with adenosine leads to the potentiation and amplification of the degranulation response^{29, 121, 126}. Consistent with this, and likewise with p110 γ -deficiency in neutrophils, bone marrow-derived mast cells from p110 γ ^{-/-} mice are similarly unable to generate PIP₃ at the plasma membrane and cannot stimulate Akt/ERK1/ERK2 signalling pathways¹²¹. Moreover, the loss of p110 γ expression in p110 γ ^{-/-} mast cells and neutrophils has also been shown to result in decreased adaptor subunit expression (as previously described in section 1.5.1), suggesting that the stability of the adaptor proteins is dependent on the catalytic subunit¹²¹. Collectively, the inability of p110 γ ^{-/-} bone marrow-derived mast cells to generate PIP₃ lipids results in the inhibition of adenosine-mediated potentiation of Fc ϵ RI-induced mast cell degranulation and protects p110 γ ^{-/-} mice from mast cell-mediated cutaneous anaphylaxis and passive systemic anaphylactic shock in the presence of intradermal adenosine^{29, 126}.

p110 γ -deficient mice also display migratory defects, where the recruitment of macrophages and dendritic cells to inflamed sites has been shown to be limited. For example, the migration of activated mature dendritic cells towards the draining lymphatics (but not their antigen-presentation capacity) has been shown to be impaired in p110 γ ^{-/-} mice in a model of contact hypersensitivity, thereby blocking the intermediary link between innate and adaptive immune responses and leading to decreased T cell activation¹³⁷.

Within the adaptive immune system, B and T lymphocytes vary in their expression of PI3K γ subunits and the involvement of PI3K γ signalling for their activation, differentiation and effector functions. PI3K γ is expressed at low levels in B lymphocytes and has not been found to play a major role in B cell differentiation or effector functions¹¹⁴. This is in contrast to the expression and requirement of PI3K δ , which has been found to be the predominant PI3K functional isoform in B cells, where PI3K δ lipid-kinase activity is required for B cell development, BCR signalling and the generation of T cell-dependent and -independent antibody responses after antigen stimulation *in vivo*¹⁴⁹⁻¹⁵³.

The role of PI3K γ is more prominent in T lymphocyte biology. Whilst p110 γ ^{-/-} T cells display normal TCR-dependent Ca²⁺ mobilisation upon antigen stimulation, these cells have been shown to proliferate at a lower rate after anti-CD3 or ConA treatment and display reduced cytokine production in response to TCR-dependent and -independent stimuli relative to wildtype counterparts¹¹⁴. This indicates that PI3K γ is not directly involved in signalling downstream of the TCR, but is instead required for the transduction of subsequent stimulatory signals downstream of GPCRs activated in parallel to the TCR. After activation, the differentiation of mature T lymphocytes, like B lymphocytes, is primarily driven by signalling through the PI3K δ isoform and is independent of PI3K γ ¹⁵⁴⁻¹⁵⁶.

However during the development of immature T cells in the thymus, PI3K γ has been shown to control immature thymocyte survival and differentiation. Relative to wildtype littermates, p110 γ ^{-/-} mice possess equivalent proportion and numbers of mature single positive CD4⁺ and CD8⁺ T lymphocytes, but display increased proportions of double negative cells and a reduction in the proportion of double positive cells in the thymus^{114, 157, 158}. The reduction at the double positive (CD4⁺CD8⁺) stage was determined to be as a

result of an inability of p110 γ ^{-/-} thymocytes to respond to adenosine stimulation through the A2A receptor expressed during this transitional stage, where a lack of stimulation through A2A results in the activation of apoptotic pathways and cell death^{114, 158}. This demonstrates the contribution of PI3K γ signalling to the control of thymic selection through pro-survival signalling.

During immune responses, PI3K γ signalling in mature T lymphocytes is required for activation and migration. Early phase pathogenesis in a model of lymphocytic choriomeningitis virus (LCMV) is mediated by cytotoxic CD8⁺ T cells and is characterised by a footpad swelling reaction¹⁵⁹. In this model, p110 γ ^{-/-} mice display reduced footpad swelling upon viral infection relative to wildtype mice¹¹⁴. Here, reduced inflammation was observed despite the equivalent ability of p110 γ ^{-/-} CD8⁺ cells (recovered ex-vivo from the site of infection) to elicit cytotoxic responses to viral peptides *in vitro* compared with CD8⁺ cells recovered from wildtype animals. Instead, it was found that protection of p110 γ ^{-/-} mice from LCMV infection was as a result of impaired migration of activated CD8⁺ cells to the inflamed footpad¹¹⁴. PI3K γ signalling is similarly required in mature CD4⁺ lymphocytes for their function as helper cells in models of T cell-dependent antibody production. In this context, CD4⁺ T follicular helper cells are required to help B cells during antibody responses to produce high-affinity class-switched antibodies within germinal centres. Upon immunisation of animals with the CD4⁺-dependent hapten, NIP-OVA, p110 γ ^{-/-} mice display reduced high-affinity antibody production *in vivo* relative to wildtype counterparts¹¹⁴. The migration of activated CD4⁺ cells is also significantly impaired in p110 γ ^{-/-} animals and is described in the following section 1.6.3. Collectively, these data indicate that PI3K γ is indispensable to lymphocyte migration.

1.6.3 PI3K γ in autoimmunity

The contribution of PI3K γ signalling to haematopoietic cell migration is essential to the maintenance of the immune system during homeostasis and the activation of inflammatory responses, where the coordinated migration of cell subsets to defined tissue locations is required for their activation and effector functions. As a result of this, PI3K γ has been identified as a promising therapeutic target for the treatment of acute and chronic autoimmune conditions through the selective blockade of PI3K γ -dependent migration^{8, 9, 28}.

The involvement of PI3K γ in the pathology of these diseases has been elucidated using both the p110 $\gamma^{-/-}$ (and kinase-inactive p110 $\gamma^{KD/KD}$) PI3K γ -deficient mice and the inhibition of PI3K γ in wildtype animals using the isoform-selective inhibitor, AS605240. PI3K γ -deficient animals are protected from several inflammatory pathologies such as asthma, allergic contact hypersensitivity, psoriasis, systemic lupus erythematosus (SLE), rheumatoid arthritis (RA), and experimental autoimmune encephalomyelitis (EAE) in which pathology is driven by the infiltration of one or more immune cell subsets to the site of inflammation where they potentiate tissue damage^{8, 9, 27-29, 137, 160}.

Systemic lupus erythematosus (SLE) is a chronic inflammatory condition characterised by the uncontrolled expansion of long-lived autoreactive CD4⁺ memory T cells that trigger polyclonal B cell activation. Broad activation of plasma cells during SLE leads to the formation of immune complexes from autoantibodies that aggregate in the kidneys, which results in the activation of complement pathways, the induction of a local inflammatory response and culminates in glomerulonephritis and renal failure (reviewed in¹⁶¹).

Current treatment regimes for SLE patients comprise broad immunosuppressant and cytostatic agents, with the extensive use of corticoids, most of which involve significant side effects^{27, 161}. Therefore, selectively blocking the activity and migration of CD4⁺ lymphocytes by targeting PI3K γ has become an attractive therapeutic approach for SLE treatment. This strategy is based on experimental data generated using the multigenic murine model of SLE in the MRL-*lpr* mouse^{27, 162}. The MRL-*lpr* mouse spontaneously develops SLE-like symptoms driven by mutations at several loci, and consistent with human disease, manifests as glomerulonephritis and renal failure. MRL-*lpr* mice exhibit an expanded population of circulating CD4⁺ memory cells that display increased levels of phosphorylated Akt, indicative of PI3K γ activation²⁷. Selective inhibition of PI3K γ in MRL-*lpr* mice with AS605240 has been found to result in reduced glomerulonephritis and improved lifespan of animals relative to the vehicle-treated control group, with no adverse effects detected after 3 months of treatment²⁷. Protection was also observed when AS605240 was administered therapeutically, after the onset of disease. Animals with established disease were treated with AS605240 and were shown to display reduced p-Akt levels in CD4⁺ T cells, where the circulating memory population was reduced in proportion and number in response to inhibitor treatment. Moreover, the incidence of DNA-specific

autoantibodies and immune complexes was also reduced in treated animals, which correlated with improved kidney function^{27, 162}. In light of these data indicating that PI3K γ inhibition using AS605240 is a viable therapeutic for the treatment of SLE in the MRL-*lpr* mouse, it will be important to assess whether long-term blockade of PI3K γ is effective to inhibit CD4⁺ memory T cell survival and/or migration in the treatment of human SLE.

Human rheumatoid arthritis (RA) is a chronic systemic inflammatory condition typified by massive cellular infiltration to inflamed joints comprised of both innate and adaptive immune cell subsets. Inflammation is perpetuated through the release of inflammatory mediators and chemoattractants by infiltrating cells, which results in synovial hyperplasia, pannus formation and the erosion of cartilage and bone in distal joints. In murine models of RA disease is initiated by B and T lymphocytes, which release inflammatory factors responsible for the recruitment of innate cells, such as neutrophils and macrophages that together mediate tissue damage^{8, 163}.

Collagen-induced arthritis (CIA) in rodents is one such model of chronic joint inflammation and is routinely used to test the efficacy of anti-rheumatic drugs due to the semblance between the pathobiology of murine CIA and human RA disease^{164, 165}. Oral administration of AS605240 has been found to significantly reduce leukocyte infiltration to the joints of animals with CIA compared with vehicle-control treatment, suggesting that the migration and infiltration of leukocytes is dependent on PI3K γ signalling in this model⁸. PI3K γ blockade with AS605240 has been shown to be effective in controlling inflammation when administered both at disease onset and during established disease, and mimics the protective effect that is observed in p110 γ -deficient animals⁸. Cellular analyses revealed that whilst PI3K γ inhibition led to impaired migration of lymphocytes to inflamed joints, the main defect leading to amelioration of disease was as a result of reduced neutrophil accumulation in the synovium⁸. During chronic disease, neutrophils predominate the RA inflammatory infiltrate where they accumulate in the synovial fluid and contribute to cartilage erosion through the release of proteolytic enzymes and toxic oxidative products.

Consistent with reduced neutrophil accumulation observed in CIA, PI3K γ inhibition with AS605240 has been shown to effectively block symptoms of a lymphocyte-independent

α CII-induced model of murine arthritis through the suppression of neutrophil migration^{8, 166}. Treatment of arthritic mice with AS605240 in this model resulted in reduced paw swelling and decreased proliferation of leukocytes that had infiltrated the synovium, which ultimately resulted in improved cartilage integrity compared with vehicle-treated control mice⁸. Furthermore, the therapeutic treatment of both CIA and α CII-induced arthritis with AS605240 was shown to suppress disease to a greater extent than a currently marketed therapeutic for RA tested in the same study⁸.

Another debilitating chronic inflammatory condition in humans is multiple sclerosis (MS). Although the aetiology of human multiple sclerosis remains unclear, there is significant experimental evidence derived from the analysis of a murine model of MS, experimental autoimmune encephalomyelitis (EAE) to suggest that MS has, at least in part, an autoimmune pathology towards CNS peptides¹⁶⁷⁻¹⁷¹. EAE mimics both the priming of autoreactive lymphocytes in secondary lymphoid organs and the migration of activated CD4⁺ Th1 and Th17 cells to the CNS. Activated Th1 and Th17 cells that infiltrate the brain and spinal cord of EAE-diseased mice directly contribute to tissue pathology through the release of inflammatory mediators, which induce the recruitment of innate effectors such as neutrophils and macrophages, culminating in the degradation of oligodendrocytes and the onset of paralysis^{170, 171}. The role of PI3K γ in the priming of pathogenic Th1 and Th17 cells during EAE progression has been characterised by our own laboratory and by others^{9, 139}. PI3K γ signalling has been shown to be critical for the induction of EAE and as such, p110 γ ^{-/-} mice are protected from the clinical symptoms of EAE. Specifically, upon immunisation with CNS peptides, p110 γ ^{-/-} animals display impaired CD4⁺ Th1 and Th17 cell priming in secondary lymphoid organs that correlates with the delayed appearance of antigen-specific CD4⁺ cell populations both in the spleen and the CNS, relative to wildtype littermates^{9, 139}. Consistent with the requirement of Th1 and Th17 cells for the induction of EAE disease, the adoptive transfer of primed wildtype CD4⁺ cells to a p110 γ ^{-/-} host has been shown to be sufficient to restore disease⁹.

Data from our own laboratory has extended this phenotype in p110 γ ^{-/-} mice to show that defective CD4⁺ lymphocyte priming is driven by multiple mechanisms, where the impaired migration of antigen-loaded dendritic cells to secondary lymphoid organs in addition to an intrinsic deficiency of the CD4⁺ cell population contributes to ameliorated disease¹³⁹.

PI3K γ signalling has been previously established to mediate the migration of activated dendritic cells¹³⁷, and in the context of EAE, is required for the trafficking of processed antigen to the skin-draining lymph nodes^{139, 172}. The migration of antigen-loaded dendritic cells to secondary lymphoid organs is a crucial process that is required for the initiation of autoimmune responses towards CNS peptides after subcutaneous immunisation. In addition to impaired dendritic cell migration in p110 γ ^{-/-} mice during EAE, the activation and proliferation of Th cells isolated from the spleens of naïve p110 γ ^{-/-} mice were also found to be compromised, where p110 γ ^{-/-} CD4⁺ cells displayed reduced proliferation *in vitro* in response to anti-CD3/anti-CD28 TCR stimulation and reduced Th1 differentiation under polarising conditions relative to wildtype CD4⁺ cells¹³⁹. Furthermore, although not directly assessed in the aforementioned study by Comerford *et al.* (2012), impaired migration of activated CD4⁺ Th1 and Th17 effector cells to the inflamed CNS may also have contributed to reduced disease severity in p110 γ -deficient animals, since the migration of activated lymphocytes is known to be dependent on PI3K γ signalling pathways⁹. Collectively, both intrinsic and extrinsic defects in CD4⁺ Th effector cell priming were shown to culminate in EAE disease protection in p110 γ ^{-/-} mice.

However, another study published by Berod *et al.* (2011), which similarly described ameliorated EAE disease in p110 γ ^{-/-} mice, presented conflicting data regarding the role of PI3K γ in Th1 and Th17 effector cell differentiation. These authors found PI3K γ to be dispensable for the differentiation of IFN- γ -producing Th1 and IL-17-producing Th17 cells when cultured from naïve CD4⁺ splenocytes *in vitro*⁹. This led them to conclude that the impaired Th effector priming and reduced disease severity observed in p110 γ ^{-/-} mice was due solely to the defective migration of p110 γ -deficient dendritic cells and activated CD4⁺ lymphocytes. Consistent with reduced EAE disease severity in p110 γ ^{-/-} mice described by both Comerford *et al.* (2012) and Berod *et al.* (2011), the inhibition of PI3K γ -dependent leukocyte migration with systemic AS605240 treatment in wildtype animals at the onset of EAE disease was found to ameliorate the clinical symptoms and cellular pathology of EAE. Reduced disease severity correlated with decreased numbers of pathogenic CNS-infiltrating Th1 and Th17 cells and enhanced remyelination and axon numbers in the diseased spinal cord^{9, 139}.

Collectively, experimental data generated in murine models of autoimmunity has been useful in defining the functional roles of PI3K γ in the immune system and suggest that the therapeutic targeting of PI3K γ -dependent migration is a viable approach for the treatment of human autoimmune conditions such as systemic lupus erythematosus, rheumatoid arthritis and multiple sclerosis. Furthermore, in addition to the blockade of PI3K γ signalling alone, the dual inhibition of PI3K γ and PI3K δ isoforms that are co-expressed by leukocytes has proven beneficial in the treatment of such inflammatory disorders¹⁷³. As described in the previous section 1.6.2, PI3K δ signalling is the predominant PI3K isoform required for the differentiation and maturation of both B and T lymphocytes. Therefore, the dual inhibition of PI3K γ and PI3K δ mediates the suppression of both the development and migration of lymphocyte effectors during autoimmunity to restrict proinflammatory cytokine signalling and control inflammation¹⁷³. In fact, a dual p110 γ and p110 δ inhibitor named TG100-115 developed by TargeGen was trialled in 2005 and released on the human therapeutics market to treat inflammatory conditions^{174, 175}.

To summarise, PI3K γ is a crucial signalling complex required for the induction of leukocyte migration during both normal immune responses and for the aberrant migration of cells during inflammatory autoimmune diseases. However, although the function of PI3K γ as an enzymatic complex has been characterised during cell migration, the studies described above do not address the molecular regulation of PI3K γ signalling within migrating leukocytes or the contribution of distinct PI3K γ regulatory adaptor subunits, p84 and p101, to these processes.

1.6.4 Roles for Class I PI3K enzymes in cancer initiation and progression

Dysregulated signalling through PI3K family pathways has been associated with the establishment and progression of cancer, where oncogenesis is often coupled with the hyperactivation of PI3K lipid-kinase activity and/or the inactivation of PTEN or SHIP phosphatases that regulate PIP₃ distribution and accumulation^{31, 99, 135, 176}. For example, gain-of-function mutations within *Pik3ca* (p110 α) coupled with increased signalling through Akt/mTOR pathways is a well-documented driver of PI3K-mediated oncogenesis¹⁷⁷⁻¹⁸⁰. Mutations in *Pik3ca* have been reported in many human cancer types, where they have been identified to cluster in mutation ‘hotspots’ predominantly within the helical and kinase domains of p110 α . These mutations have been found to most often arise

late in tumour development and coincide with the adoption of an invasive phenotype¹⁷⁷. Genetic analyses have also identified reduplication or amplification of chromosomal regions containing *Pik3ca*, which has been found to contribute to oncogenesis of a number of human cancers¹⁸¹.

Whilst the oncogenic potential of p110 α requires one or more activating mutations, it has been shown that over-expression alone of p110 β , p110 δ or p110 γ catalytic subunits in their wildtype forms is sufficient to induce cell transformation³¹. This may explain the rarity of p110 β , p110 δ and p110 γ mutations in human cancers relative to p110 α . The intrinsic transforming potential of p110 β , p110 δ and p110 γ isoforms was demonstrated in chicken embryonic fibroblasts, where the over-expression of p110 β , p110 δ or p110 γ was shown to result in cell transformation and loss of cell contact growth inhibition^{31, 182}. This effect was found to be dependent on the lipid-kinase but not protein-kinase activity of PI3K enzymes and was further enhanced by the forced membrane-targeting of p110³¹. Heightened lipid-kinase activity driven by over-expression of p110 β , p110 δ or p110 γ subunits resulted in strong constitutive Akt signalling where the transforming potential of p110 γ and p110 β (but not p110 δ) was found to be dependent on ras-GTP³¹.

One mechanism by which over-expression of wildtype p110 β drives cellular transformation was identified by Dbouk *et al.* (2012) using structural analyses that uncovered the presence of a lysine residue at position 342 (K342), in comparison to other p110 isoforms that carry asparagine residues at analogous positions^{129, 183}. Structurally, a lysine residue in this position was found to destabilise the C2-iSH2 interface between p85 and p110 β subunits¹²⁹. This binding interface has been shown to be involved in the inhibitory regulation of p110 kinase-activity by p85 (described in section 1.4.2) and the weakening of this interaction therefore renders wildtype p110 β more transforming than other wildtype isoforms of p110. In fact, the transforming nature of p110 β was reversed by the mutation of lysine to asparagine at position 342 (K342N) and likewise, the mutation of the analogous asparagine residue within p110 α to lysine (N345K) was shown to be oncogenic^{129, 183}.

A number of studies have implicated PI3K γ in the progression of various cancer types, where PI3K γ -specific inhibitors have been found to suppress tumour growth and metastasis

in vitro and *in vivo*^{33, 34, 76, 122, 176, 184}. Not surprisingly, the metastasis of many invasive carcinomas has been found to be PI3K γ -dependent and is consistent with the established role of PI3K γ in directed cell migration. In keeping with the transforming potential of p110 γ *in vitro* (described above)³¹, up-regulated expression of p110 γ has been identified in human pancreatic intraepithelial neoplasia and ductal carcinoma^{185, 186}. Tumourigenesis of these cancer types was found to correlate with enhanced PI3K γ activation as determined by increased levels of PIP₃ and phosphorylated Akt. In addition to the tumour-promoting role of p110 γ , the gene locus for the p101 adaptor subunit (*Pik3r5*) of PI3K γ has been identified as a common site of retroviral insertion in T-cell lymphomas¹⁸⁷ and the over-expression of p101 in MOLT-4 and Jurkat T lymphocyte cell lines has been found to protect T cells from UV-induced apoptosis¹³⁵.

As described in previous sections, lymphocytes co-express PI3K γ and PI3K δ . In a murine model of T cell acute lymphoblastic leukemia (T-ALL), dysregulation of PI3K γ and PI3K δ signalling pathways has been shown to contribute to the development and progression of disease¹⁷⁶. In keeping with this, the dual inhibition of p110 γ and p110 δ with isoform-selective inhibitors was found to result in reduced T-ALL disease burden and prolonged survival of diseased mice, where the blockade of PI3K γ and PI3K δ signalling pathways was shown to activate pro-apoptotic pathways in leukemic cells¹⁷⁶. Therefore, as described for selected autoimmune conditions in section 1.6.3, the dual inhibition of PI3K γ and PI3K δ may be useful in the treatment of blood cancers.

It is well established that the infiltration of immune cell subsets into tumours influences the progression of solid cancers, where both tumour-promoting and suppressive effects have been reported depending on the infiltrating population. For example, the invasion of inflammatory myeloid cells into tumour masses has been shown to create an environment conducive to tumour growth and the stimulation of angiogenesis¹⁸⁸⁻¹⁹⁰, in addition to the presence of myeloid-derived suppressor cell populations within tumours that suppress T cell responses¹⁹¹⁻¹⁹³. PI3K γ signalling in inflammatory myeloid cells has been shown to induce the expression of surface $\alpha 4\beta 1$ integrin, which facilitates the extravasation of these cells and their invasion into tumours, thereby promoting tumour growth¹⁹⁴. In mice, the inhibition of PI3K γ activity with AS605240 prevented the induction of $\alpha 4\beta 1$ -integrin expression by inflammatory myeloid cells. This was shown to suppress tumour growth as a

result of reduced intratumoural inflammation and the inhibition of angiogenesis¹⁹⁴. Furthermore, myeloid cells from p110 γ -deficient mice (both p110 $\gamma^{-/-}$ and p110^{KD/KD} strains) were similarly found to lack $\alpha 4\beta 1$ expression and displayed reduced adhesion to endothelial cells¹⁹⁴.

Upon examination of the molecular activation of PI3K γ signalling in tumour-infiltrating inflammatory myeloid cells, a novel scenario was revealed where p101/p110 γ PI3K γ heterodimers were found to be activated downstream of GPCRs, whereas p84/p110 γ PI3K γ heterodimers were found to exclusively couple to activated RTKs¹⁹⁴. The activation of p84/p110 γ in response to RTK stimulation was found to mediate myeloid cell migration in this model and represents the first description of PI3K γ acting downstream of a receptor tyrosine kinase. As previously outlined (in further detail) in section 1.5.3, it remains unclear whether the activation of p84/p110 γ in response to VEGFR stimulation with VEGF-A is mediated by the direct association of PI3K γ with the intracellular phosphotyrosine motifs of the activated RTK or whether PI3K γ is cross-activated by an undefined GPCR that is activated in parallel to VEGFR¹⁹⁴.

Previous data generated by our laboratory using siRNA-mediated gene knockdown of PI3K γ subunits revealed the requirements for catalytic and adaptor subunits of PI3K γ for mammary carcinoma cell survival and metastasis in the invasive human breast cancer cell line, MDA.MD.231¹²³. The knockdown (KD) of p101 and p110 γ expression was found to ablate PI3K γ signalling, as determined by the complete inhibition of p110 γ membrane localisation and Akt phosphorylation upon cell stimulation relative to control KD cells. This disruption of PI3K γ signalling in p101 KD and p110 γ KD cells resulted in the inhibition of PI3K γ -dependent chemotaxis *in vitro* and the suppression of MDA.MB.231 cell metastasis to the lungs of SCID mice after intravenous transfer *in vivo*¹²³. Further investigation indicated that PI3K γ signalling mediated by p101/p110 γ heterodimers regulated cell survival and anoikis in MDA.MB.231 cells, which was found to be consistent in the 4T1.2 murine mammary epithelial carcinoma line¹²³.

In contrast to the p101 adaptor protein, siRNA-mediated knockdown of p84 expression was found to enhance the metastatic potential of MDA.MB.231 cells. Heightened tumorigenicity in the absence of p84 was coupled with the persistence of p110 γ at the cell

membrane and constitutive Akt phosphorylation, indicative of uncontrolled PI3K γ activity¹²³. These data suggest that p84 possesses novel tumour suppressor function that is required for the control of PI3K γ activity. Although the molecular mechanisms involved in the regulation of PI3K γ signalling and tumour suppression mediated by p84 in this model were not explored, these data implicate p84 in the regulation of PI3K γ signalling in MDA.MB.231 cells.

In further support of a suppressive role for p84, a recent high-throughput screen of over 2,136 primary human breast cancer samples revealed that p84 is commonly down-regulated in numerous neoplasia and carcinoma types¹⁹⁵. This study by Curtis *et al.* (2012) utilised both genome and transcriptome analyses of samples from an extensive cohort of breast cancer patients with long-term clinical follow up to elucidate breast cancer subgroups and their molecular drivers. For instance, within invasive ductal carcinomas, which represented a large breast cancer subgroup, p84 was found to be significantly down-regulated in >80% of patient samples¹⁹⁵. The down-regulation or loss of p84 expression described by Curtis *et al.* (2012) is consistent with cancer genome mutation and copy number alteration data compiled in the cBio Cancer Genomic Portal database (<http://www.cbioportal.org/>; accessed February 2015)^{196, 197}. Here, among cancer studies where data was available for *Pik3r6* (p84), 78% of studies reported only mutation and/or deletion alterations to *Pik3r6* in comparison to 4% of studies where solely amplification events were documented. Together, these two large-scale genome and transcriptome analyses provide evidence that p84 is commonly deleted or down-regulated in human invasive breast cancer. This is consistent with data generated in our own laboratory, which implies that p84 possesses tumour suppressor function in human breast cancer cell lines.

In summary, it has been demonstrated in numerous cancer types that the over-activity of PI3K γ signalling (caused by either the up-regulation of p110 γ and p101 subunits or the loss of p84 expression) leads to enhanced tumourigenicity. Therefore, unlike the tumour-promoting potentials of p110 γ and p101, p84 possesses novel tumour suppressor function. Although not defined as yet, the tumour suppressor function of p84 appears to be dependent on a regulatory role of p84 during PI3K γ signalling. Therefore, the characterisation of p84 function in the activation and termination of PI3K γ signalling is of high priority, since at this point the molecular regulation of PI3K γ signalling remains

unclear (refer to section 1.5.4). However, based on known regulatory mechanisms that exist for Class IA PI3K enzymes (described in section 1.4.2), it could be proposed that the regulation of PI3K γ activity by p84 and the heterodimerisation of p84 with p110 γ may be dependent on the transient phosphorylation of the p84 adaptor subunit. An examination of the phosphorylation of p84 during PI3K γ signalling should therefore be performed in order to elucidate such mechanisms.

1.7 Advances in genome-editing technologies

As described in section 1.4.3 and Table 1.2, genetically-modified mice with specific gene deletions are powerful tools to study the individual contributions of genes and proteins to cellular functions. Consistent with this, the roles of p110 γ and p101 PI3K γ subunits have been defined using p110 γ - and p101-deficient mouse strains (outlined in Table 1.2). At the time of writing this thesis, efforts by many research groups to create a p84-deficient mouse had been unsuccessful using conventional embryonic stem cell (ES cell) mutagenesis methods. Due to the co-expression of p84 and p101 adaptor proteins in cells such as leukocytes, the inexistence of a p84-deficient genetically-modified mouse made it difficult to elucidate the distinct contributions of p84 and p101 adaptor subunits to PI3K γ signalling or whether redundancy existed within the PI3K γ system. Therefore, the generation and characterisation of a p84 knockout mouse was of high priority.

Recently, two new genome-editing technologies, CRISPR and TALEN nuclease targeting have become available. The primary advantage of CRISPR and TALEN approaches is the rapid time in which genetically-modified knockout animals can be generated relative to conventional embryonic stem cell mutagenesis methods. In addition to time advantages, genome-editing mediated by CRISPR- and TALEN-based strategies has been found to be more efficient than traditional ES cell mutagenesis methods, as measured by the frequency of successful target site mutations¹⁹⁸⁻²⁰⁰.

The CRISPR-Cas system (Clustered Regularly Interspaced Short Palindromic Repeat - Cas 9 nuclease) is based on an adaptable immune mechanism used by bacteria to protect themselves from viruses and transferred foreign plasmids²⁰¹⁻²⁰³. This defence mechanism involves the incorporation of sequences from invading DNA between CRISPR repeat sequences in the bacterial genome, forming CRISPR repeat arrays. RNA transcripts

processed from these arrays (known as crRNA) consist of a variable region transcribed from the incorporated foreign DNA (known as the protospacer region) fused to a CRISPR repeat. Each short crRNA transcript complexes with another RNA known as the transactivating CRISPR RNA (tracrRNA) and the complex is bound by the Cas9 nuclease. The protospacer-encoded portion of the crRNA then guides this CRISPR-Cas9 complex to the foreign invading DNA, where it binds complimentary target sequences. Homology-mediated binding of CRISPR-Cas9 complexes to foreign DNA induces the cleavage of target viral or plasmid DNA by Cas9, which is subsequently degraded.

The ability to customise CRISPR-Cas9 complexes (composed of crRNA, tracrRNA and Cas9 elements) with a desired variable region as the protospacer sequence has been harnessed to guide Cas-9 nuclease activity to desired DNA targets and induce designated double stranded breaks within the genome. Customised CRISPR strategies involve the incorporation of two elements into the target cell, a guide RNA (gRNA), consisting of a designed crRNA (where 20 nucleotides at the 5' end are complementary to the genomic target region) fused to a fixed tracrRNA, and the Cas9 nuclease (as either full-length protein or mRNA transcript). With this customised approach, the RNA-DNA base complementarity between the crRNA and the genomic target guides the Cas9 nuclease to the target site where it facilitates double stranded breaks^{202, 204}. The composition of CRISPR-Cas9 elements is shown in **Figure 1.10**

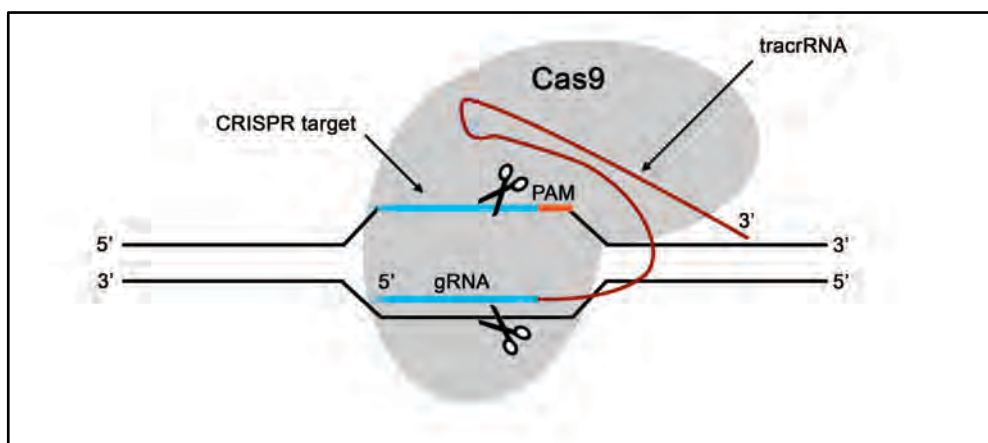


Figure 1.10: CRISPR-Cas targeted gene-editing

Since initial demonstrations in 2012 that Cas9 could be targeted to specific DNA sequences *in vitro*²⁰¹, a multitude of manuscripts published in 2013 reported that Cas9

could be programmed using CRISPR strategies to target the genomes of bacteria, human cell lines, zebrafish, yeast, mice, rats, and rabbits, amongst others²⁰⁴⁻²⁰⁹. In addition to simple deletions by non-homologous end-joining mechanisms, Cas9-induced double stranded breaks have also been used to introduce desired coding sequences through homology-directed repair mechanisms utilising both plasmid DNA and oligonucleotide donor templates^{205, 210}.

Methodologies to generate genetically-modified mice using CRISPR-Cas9 techniques have been established more recently and involve the direct injection of gRNA constructs and Cas9 mRNA into fertilised mouse zygotes. Injected zygotes are implanted into pseudo-pregnant female surrogates by oviduct transfer and after three weeks gestation, CRISPR-modified pups can be screened by sequencing PCR.

Another recently developed customisable gene-editing technology is TALEN (Transcription Activator-Like Effector Nuclease-based genome editing), which like CRISPR, is based on a DNA-targeting mechanism identified in bacteria^{202, 211, 212}. Natural TAL effector proteins are produced by bacterial plant pathogens from the *Xanthomonas* genus where upon infection, TAL effector proteins bind specific sequences within the plant host DNA resulting in the alteration of gene expression within the plant cells and the development of disease. *Xanthomonas* TAL effector proteins consist of an effector domain coupled to a DNA-binding domain composed of linked 33-35 amino acid repeat sequence polypeptides that each recognise and bind a single DNA nucleotide. Nucleotide recognition and TALE specificity is mediated by two hypervariable residues present at positions 12 and 13 of each amino acid repeat sequence, which are called the repeat-variable di-residues (RVDs). Therefore, through the linking of amino acid repeat sequences with defined RVDs (specific to the DNA target), a TALE polypeptide sequence is capable of recognising and binding any specific genomic target of contiguous DNA²¹².

The specificity and DNA-binding of TAL effector proteins has led to the development of customised TALE polypeptides coupled to the FokI nuclease protein, which act in pairs and can be engineered to target and induce double stranded breaks at specific genomic target sequences. As for natural TALE proteins, the specificity of customised TALENs is achieved by linking 33-35 amino acid repeat sequences with varied RVDs (according to the TALE code; presented in **Figure 1.11**) to design an effector polypeptide that allows the precise targeting and manipulation of a chosen genomic target sequence²⁰². Customised

TALEN pairs have been successfully used to target and genetically-modify genomic DNA within human cell lines, plant species such as rice and the genomes of organisms such as *drosophila melanogaster*, zebrafish and mice^{203, 211}.

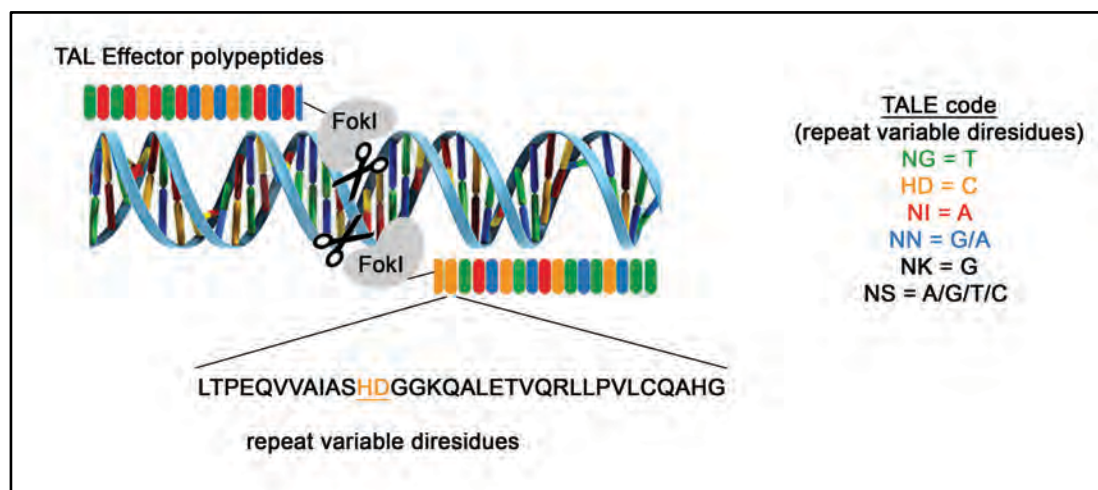


Figure 1.11: TALEN gene-targeting

1.8 The research project

PI3K γ is a dual specificity protein- and lipid-kinase composed of a p110 γ catalytic subunit bound to one of two regulatory adaptor subunits, p84 or p101. PI3K γ components are highly expressed in motile cells of the haematopoietic system, where the signal transduction mediated by PI3K γ heterodimeric enzymes activated downstream of GPCRs is required for the induction of directed cell migration towards chemotactic gradients. Consistent with this, p110 γ ^{-/-} leukocytes display reduced chemotaxis *in vitro*⁷ and p110 γ ^{-/-} mice exhibit protection from inflammatory conditions such as experimental autoimmune encephalomyelitis (EAE), rheumatoid arthritis and asthma, where the migration of immune cells to inflammatory sites is impaired relative to wildtype controls^{8, 9, 28}. However, despite functional data generated in studies utilising p110 γ -deficient mice and the inhibition of PI3K γ catalytic activity with the isoform-selective inhibitor AS605240, there is little known about the molecular regulation of PI3K γ signal transduction by the distinct adaptor subunits. In fact, the molecular events that control the termination of transient PI3K γ signalling are completely unknown. The importance of signal regulation has been highlighted by data demonstrating that aberrant PI3K γ signalling leading to the heightened

and/or prolonged lipid-kinase activity of p110 γ results in cellular transformation and oncogenesis. Therefore, a detailed understanding of the molecular mechanisms regulating PI3K γ signalling is required to comprehend the function of PI3K γ during normal cell function and also during disease when signalling becomes dysregulated.

Least is known about the role of the p84 adaptor subunit in PI3K γ signalling, which compared to the p101 adaptor, is less capable of transducing robust adaptor-mediated PI3K γ signalling characterised by PIP₃ accumulation at the leading cell edge and the induction of phosphorylated Akt. For this reason, it has been proposed that p84 may possess additional functions in the regulation of PI3K γ signalling. Therefore, the goals of this project are 1) to improve our understanding of the function and regulation of the p84 adaptor protein during PI3K γ signalling by examining the phosphorylation of p84, 2) to generate a novel p84-deficient mouse and using it, further our understanding of the specific roles of p84 in PI3K γ -dependent immune processes and 3) to establish a proteomics model that can be used to study p84-dependent mechanisms in autoreactive CD4⁺ cells that infiltrate the CNS during experimental autoimmune encephalomyelitis (EAE). Experiments addressing these three research questions are presented in Results Chapters 3, 4 and 5, respectively.

Chapter 3

A known regulatory mechanism controlling the lipid-kinase activity of Class I PI3K enzymes is through transient phosphorylation events that influence the heterodimerisation of the catalytic subunit to an adaptor protein^{66, 108, 124}. Phosphorylation-dependent regulation such as this has been established for the Class IA p85 adaptor subunit that is transiently phosphorylated to modulate the activity of PI3K α and PI3K β lipid-kinases¹⁰⁸. However, phosphorylation-dependent regulation of the p84 adaptor subunit during PI3K γ signalling is yet to be described.

The hypothesis tested in Chapter 3 is:

The p84 adaptor subunit is transiently phosphorylated during PI3K γ signalling, which is required for the regulation of PI3K γ lipid-kinase activity.

The following aims have been developed to test this hypothesis:

- 1) Assess the phosphorylation status of p84 at rest and in response to PI3K γ signal activation
- 2) Develop p84 expression constructs where regulatory (S/T/Y) phosphorylation sites within p84 are mutated to alanine residues
- 3) Determine the requirement of regulatory phosphorylation sites for the function of p84 in the context of PI3K γ signalling and PI3K γ -dependent cell migration

Chapter 4

The individual contributions of the p84 and p101 adaptor subunits to PI3K γ -dependent processes and the degree of redundancy, if any, that exists between adaptor subunits remain unclear. Whilst the requirement of p110 γ has been determined using experimental models in p110 γ -deficient mice (p110 γ ^{-/-} and p110 γ ^{KD/KD} strains) and the p110 γ isoform-selective inhibitor AS605240, adaptor subunit function in these processes is unclear. This is due in large part to the co-expression of p84 and p101 in the majority of cell types and a lack of specific reagents with which to distinguish their function in the context of PI3K γ signalling. Some information regarding the role of p101 in PI3K γ -dependent cell function has been generated using the p101-deficient mouse (p101^{-/-}), which has been characterised in terms of leukocyte biology^{130, 157}. At the commencement of this project there was no p84-deficient mouse available to assess the specific role of p84 in PI3K γ -dependent cell functions. However at the beginning of the final year of this project, CRISPR genome-editing technology became available, which would allow the rapid generation of genetically-modified mouse strains.

The hypothesis tested in Chapter 4 is:

The p84 adaptor subunit has non-redundant functions in the regulation of PI3K γ -dependent leukocyte migration.

The following aims have been developed to test this hypothesis:

- 1) Generate a p84-deficient mouse strain (Pik3r6^{-/-}) using CRISPR and TALEN genome-editing technologies

- 2) Determine the effect of loss of p84 expression on PI3K γ subunit expression and lipid-kinase activity
- 3) Conduct initial characterisation of the $\text{Pik3r6}^{-/-}$ mouse by assessing the requirement of p84 for mast cell maturation and effector function, thymocyte development and neutrophil migration
- 4) Examine the effect of p84 deficiency on the development of experimental autoimmune encephalomyelitis (EAE) in $\text{Pik3r6}^{-/-}$ mice

Chapter 5

The induction of experimental autoimmune encephalomyelitis (EAE) has been previously shown in our laboratory to be suppressed in $\text{p110}\gamma^{-/-}$ mice as a result of impaired dendritic cell migration to secondary lymphoid organs and defective priming of autoreactive CD4^+ Th1 and Th17 cells¹³⁹. This correlated with reduced numbers of CNS-infiltrating Th1 and Th17 cells and ameliorated disease symptoms in $\text{p110}\gamma^{-/-}$ animals relative to wildtype controls. Whilst it has been established that Th1 and Th17 cells initiate pathology within the inflamed CNS, the mechanisms that allow these effector cells to migrate to and infiltrate the immuno-privileged CNS are not well understood. A large-scale quantitative ICPL proteomic analysis method will therefore be developed as an initial study to map the critical processes utilised by CNS-infiltrating CD4^+ effector cells during EAE progression. Then if time permits, the proteomes of activated CD4^+ effector cells from wildtype and p84-deficient mice will be compared during effector cell priming and disease development to determine those cell processes that are dependent on p84 and PI3K γ signalling.

The hypothesis tested in Chapter 5 is:

Comparison of the proteomes of antigen-activated wildtype and p84-deficient CD4^+ T cells will provide insight into p84-dependent signal transduction processes.

The following aims have been developed to test this hypothesis:

- 1) Optimise the isolation of target CD4^+ cells from the inflamed CNS of wildtype mice at various stages of EAE disease progression (disease onset, peak-disease and remission phases)

- 2) Assess the efficiency of Isotope-coded protein-labelling (ICPL) isotopic labels for the detection and quantification of proteins isolated from CD4⁺ cells
- 3) Compare the proteomes of CD4⁺ cells isolated from the CNS of wildtype mice during EAE at disease onset, peak-disease +/- remission phases of disease in two independent models of EAE (MOG₃₅₋₅₅-induced chronic EAE in C57Bl/6 mice and PLP₁₃₉₋₁₅₁-induced relapsing-remitting EAE in SJL/J mice) to elucidate key processes adopted by autoreactive cells during pathogenesis using ICPL
- 4) Compare the proteomes of CD4⁺ Th effector cells isolated from wildtype and p84-deficient (*Pik3r6*^{-/-}) mice during the priming phase in secondary lymphoid organs, upon migration through the blood and upon infiltration into the inflamed CNS during EAE disease progression

**Note: This aim (4) is time permitting and dependent on the availability of the p84-deficient (*Pik3r6*^{-/-}) mouse developed in Results Chapter 4.*

Chapter 2: Methods and Materials

Chapter 2: Methods and materials

2.1 Mice

2.1.1 Housing and maintenance

Wildtype mice were sourced from the Waite Laboratory Animal Services Breeding Facility, South Australia (C57Bl/6), and the Australian Resources Centre Western Australia (SJL/J and SCID). Genetically modified p84-deficient mice (C57Bl/6 *Pik3r6*^{-/-}) were generated using CRISPR technology (refer to section 2.1.2) in conjunction with the South Australian Gene Editing Facility (SAGE) at the University of Adelaide Laboratory Animal Services facility. All animals were housed at the University of Adelaide Laboratory Animal Services facility for the duration of experimental protocols. All experimental procedures employed in this study were approved by the University of Adelaide Animal Ethics Committee. At all times, the principles of reduce, refine and replace were adhered to and animal suffering was kept to a minimum.

2.1.2 CRISPR gRNA construct design and injection

The guide RNA (gRNA) construct for CRISPR gene-targeted mutation of *Pik3r6* and Cas9 RNA components were designed and synthesised by ToolGen Genome Engineering (Seoul, Korea). The *Pik3r6*-targeted gRNA sequence was designed with homology to a target sequence within exon 1; the gRNA sequence is as follows: 5'-CTTACCCTGATTGCTCTGGA-3'. *Pik3r6*^{-/-} mice were generated by the direct injection of pre-prepared gRNA and Cas9 RNA components into fertilised zygotes. Briefly, female C57Bl/6 donors were super-ovulated with the administration of PMSG hormone to stimulate egg production and HCG to induce ovulation, prior to mating with male C57Bl/6 mice. Fertilised zygotes were harvested from mated donor females, microinjected with gRNA and Cas9 RNA components *in vitro* then implanted by oviduct transfer into pseudo-pregnant female surrogate mice. A total of 150 zygotes (derived from 12 mated donor females) were injected with *Pik3r6*-targeted CRISPR components, which were implanted into 6 female surrogates. Five litters of CRISPR-modified pups were born giving a total of 25 animals for screening (16 male, 9 female).

2.1.3 TALEN design and injection

Paired TALEN constructs (FokI-nuclease-coupled TAL effector polypeptides) for gene-targeted mutation of *Pik3r6* were designed and synthesised by ToolGen Genome

Engineering. The *Pik3r6* TALEN target sequence within exon 1 is as follows: 5'-TGTGGAGCTGGACTTCCAGAGGAGTGTACAGGCTGTGCTGCGAGAGCTCAACA-3'; where the left and right TALENs bind to the underlined *Pik3r6* sequences that are separated by a spacer sequence defined by italics. *Pik3r6*^{-/-} mice were generated by the direct injection of pre-prepared TALEN constructs into fertilised zygotes as described above for CRISPR-induced mutagenesis. A total of 25 zygotes (derived from 2 mated donor females) were injected with TALEN constructs, which were implanted into a single female surrogate. A single litter of 7 TALEN-modified pups were born (6 male, 1 female).

2.2 Expression construct design and DNA cloning

2.2.1 Cloning p84 expression constructs

Human full-length p84 cDNA (codon-optimised for mammalian expression) was synthesised with a C-terminal HA tag and 5' XhoI / 3' EcoRI restriction sites (termed p84(h)OPT) by GenScript (Piscataway, NJ, USA), which was delivered as a cloned construct in the pUC57 shuttle vector. p84(h)OPT cDNA was subsequently subcloned using XhoI/EcoRI restriction sites from the purchased pUC57 construct into the retroviral pMSCV expression system (pMSCV-p84-HA) (Clontech Laboratories Inc., Mountain View, CA, USA) and sequenced using pMSCV forward/reverse and p84(h)OPT F1, F2, F3, R1, R2 and R3 sequencing primers (refer to **Table 2.1**).

2.2.2 Site-directed mutagenesis of p84 expression constructs

The retroviral pMSCV-p84-HA expression construct was modified by site-directed mutagenesis PCR to generate pMSCV-p84-S358A-HA and pMSCV-p84-T607A-HA expression mutants. Mutagenic primers were purchased from Sigma Aldrich (St. Louis, MO, USA) and are listed in **Table 2.1**. Mutagenesis was performed using the QuikChange II site-directed mutagenesis kit (Agilent Technologies, Santa Clara, CA, USA) according to supplier protocols. The sequences of resultant pMSCV-p84-S358A-HA and pMSCV-p84-T607A-HA expression constructs were confirmed by PCR sequencing using p84(h)OPT F2 and R2 sequencing primers (**Table 2.1**). Orbitrap LTQ XL ETD LC-mass spectrometry was used to confirm the amino acid sequences of p84-S358A-HA and p84-T607A-HA proteins isolated from MDA.MB.231 cells transfected with pMSCV-p84-S358A-HA and pMSCV-p84-T607A-HA vectors.

2.2.3 Transfection and retroviral transduction of p84 expression vectors

MDA.MB.231 and HEK293FT cells were transiently transfected with pMSCV control (empty vector control) or pMSCV-p84-HA expression constructs using Lipofectamine2000 (Life Technologies, Carlsbad, CA, USA), according to supplier protocols. Briefly, cultured adherent cells at 90% confluency were incubated with pre-mixed Lipofectamine2000:DNA complexes in Opti-MEM I reduced serum medium (Gibco, Life Technologies) with 5% foetal calf serum for 6 hours before transfection medium was replaced with complete growth medium (refer to section 2.3.1). Cells were tested for construct expression and utilised in experimental procedures at 24-36 hours post-transfection.

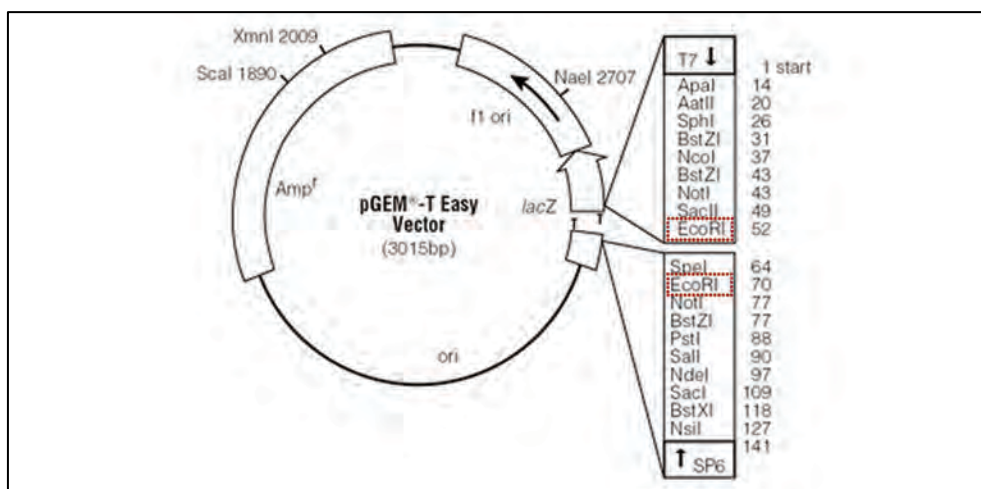
Stable MDA.MB.231 expression cell lines were generated by retroviral transduction of pMSCV control, pMSCV-p84-HA, pMSCV-p84-S358A-HA and pMSCV-p84-T607A-HA constructs, as described in Akekawatchai *et al.*¹³¹. Briefly, HEK293T cells were transiently transfected with pMSCV expression constructs (12µg) in conjunction with retroviral packaging plasmids, pVSV and pGP (9µg each; Stratagene, Agilent Technologies) to elicit retroviral virion production over 48 hours. MDA.MB.231 cells were incubated with purified viral supernatants for 8-12 hours before replacement with complete growth medium for MDA.MB.231 cells (refer to section 2.3.1). Antibiotic selection (puromycin 6µg/mL; Sigma Aldrich) was incorporated into cell culture medium 48 hours post-transduction to select clones with successfully integrated p84 expression constructs.

2.2.4 DNA sequencing

All primers utilised for DNA sequencing are listed in **Table 2.1**. Sequencing PCR reactions consisted of Big Dye Sequencing Mix (1µl), Big Dye Buffer (3µl), primer (4µl at 10pmol/reaction), DNA (25-50ng) and PCR-grade water (up to 20µl total reaction volume). The reaction cycle used for sequencing reactions is defined as follows: denaturation at 96°C for 10 seconds, annealing at 50°C for 30 seconds, extension at 60°C for 4 minutes; 25 cycles; hold at 4°C end. Sequencing PCR products were purified using isopropanol precipitation, where 1µl aqueous molecular biology grade glycogen stock (Thermo Fisher Scientific, Bremen, Germany) was added to the sequencing reaction (20µl volume) prior to addition of 20µl dH₂O and 60µl isopropanol (60% isopropanol final). The mixture was vortexed thoroughly, incubated at room temperature for 15 minutes, then centrifuged at 4°C for 25 minutes at maximum speed to precipitate the DNA. The DNA pellet was washed once in 200µl ice-cold 70% ethanol, centrifuged at 4°C for 15 minutes

at maximum speed and the supernatant was carefully aspirated. DNA was briefly air-dried, then stored at -20°C until analysis on DNA sequencing instruments at the IMVS Sequencing Centre, SA Pathology.

TA-cloning for DNA sequencing of genomic DNA isolated from CRISPR- and TALEN-modified pups was performed using the pGEM-Teasy Vector System (Promega, Madison, WI, USA), according to supplier protocols. The vector map for pGEMT-Teasy is shown below.



2.3 Cell lines and *ex vivo* cell culture

2.3.1 MDA.MB.231 and HEK293FT cell culture

MDA.MB.231 human mammary carcinoma cells were cultured in RPMI 1640 (Gibco, Life Technologies) supplemented with 10% foetal calf serum, 2mM L-glutamine (IMVS, SA, Australia), 10mM HEPES (IMVS), 1mM sodium pyruvate (Gibco, Life Technologies) and 0.2 U/mL penicillin/gentamycin (IMVS). HEK293FT human embryonic kidney cells were cultured in DMEM (Gibco, Life Technologies) supplemented with 10% foetal calf serum and 0.2 U/mL penicillin/gentamycin (IMVS). Cell density of adherent cell lines was maintained as required, where cells were released from adherent conditions by brief incubation with warmed PBS / 0.25% trypsin / 0.2 g/l EDTA. Cells were incubated at 37°C and 5% CO_2 .

2.3.2 BMMC culture from total bone marrow isolates

Mature bone marrow-derived mast cells (BMMC) were cultured from the total bone marrow of 5 week-old female wildtype and *Pik3r6^{-/-}* mice. Bone marrow cells were flushed

from the tibias and femurs of mice and the differentiation and maturation of mast cells was induced from BM-derived stem cells by culturing cells in IL-3 supplemented media (DMEM (Gibco, Life Technologies) supplemented with 20% WEHI-3 conditioned medium) over 6 weeks (weeks 1-3: 3ng/mL IL-3; weeks 4-6: 4ng/mL IL-3), as described in Yip *et al.*²¹³. The maturity of BMMC cultures were assessed by phenotypic analysis of May-Grunwald Giemsa stained cells and flow cytometric analysis (refer to section 2.5.11) of mature c-kit⁺/FcεRI⁺ cells using antibodies listed in **Table 2.2**.

2.4 *In silico* analyses

2.4.1 *In silico* phospho-prediction database analyses

Six phosphorylation prediction tools were used to evaluate potential phosphorylation sites within p84 (Pik3r6 amino acid sequence; NCBI: NP_001010855.1 / Swiss-Prot: Q5UE93.1); DiPhos1.3, NetPhorest2.0, GPS2.1, NetPhos2.0, NetPhosK1.0 and ScanSite3 programs were accessed May 2014. The (S/T/Y) phosphorylation sites predicted with highest confidence (high stringency settings) from each analysis tool were compiled.

DiPhos1.3, (<http://www.dabi.temple.edu/diphos/>).

NetPhorest2.0, (<http://netphorest.info/>).

GPS2.1, (<http://gps.biocuckoo.org/>).

NetPhos2.0, (<http://www.cbs.dtu.dk/services/NetPhos/>).

NetPhosK1.0, (<http://www.cbs.dtu.dk/services/NetPhosK/>).

ScanSite3, (<http://scansite3.mit.edu/>).

2.4.2 Database mining

The cBio Cancer Genomic Portal database for large-scale cancer genomics datasets (<http://www.cbioportal.org/>) was interrogated for data regarding mutation and copy number alterations (CNA) for the *Pik3r6* gene under the search conditions ‘all cancer studies’.

The regulation of *Pik3r6* expression in human cancer samples was investigated using the OncoPrint database, which generates gene expression signatures from large-scale human cancer genomic datasets (<https://www.oncoPrint.org/>). The *Pik3r6* gene was searched

against ‘cancer vs. cancer’ datasets, the largest dataset was determined to be Curtis *et al.* Nature (2014) [PMCID: PMC3440846]¹⁹⁵.

2.5 *In vitro* techniques

2.5.1 Immunoprecipitation and LDS-PAGE

MDA.MB.231 cells were serum starved for 4 hours at 37°C, 5% CO₂ in serum starvation media (RPMI 1640 supplemented with 0.1% foetal calf serum, 2mM L-glutamine (IMVS), 10mM HEPES (IMVS), 1mM sodium pyruvate (Gibco, Life Technologies) and 0.2 U/mL penicillin/gentamycin (IMVS)) before stimulation with 100ng/mL recombinant CXCL12 (kindly provided by Professor Ian Clark-Lewis, UBC, Vancouver, Canada) for designated time periods (0-20 minutes). Stimulation was ceased by transferring cells to ice, washing cells twice with ice-cold PBS and cell lysis in an NP-40 lysis buffer (refer to section 2.8.8) for 1 hour on ice. Lysates were cleared by centrifugation at 20 000 x g for 10 minutes at 4°C and the protein concentration of lysates was quantitated using a Coomassie Plus (Bradford) Assay (Pierce, Thermo Fisher Scientific), according to supplier protocols. Lysates were stored at -20°C if required or used for immunoprecipitation or LDS-PAGE procedures immediately.

For immunoprecipitation of p84-HA, lysates were incubated overnight with 4µl anti-HA antibody (refer to **Table 2.2**) per 1mg total protein lysate (in 1mL) at 4°C with gentle rotation. Antibody/protein complexes were precipitated using FastFlow Protein G linked sepharose beads (GE Healthcare Life Sciences, Pittsburgh, PA, USA), according to supplier protocols. Bead-bound immunoprecipitates were washed three times with ice-cold NP-40 lysis buffer (refer to section 2.8.8) with centrifugation steps performed at 9000 rpm for 25 seconds each in a pre-cooled Eppendorf benchtop centrifuge.

Total cell lysates or immunoprecipitates were denatured by incubation with NuPAGE LDS sample buffer (4x) (Life Technologies, Invitrogen) and 50mM Dithiothreitol (DTT) for 10 minutes at 70°C, then proteins were separated by LDS-PAGE using BOLT NuPAGE 4-12% polyacrylamide gels and BOLT LDS-PAGE gel tanks (Life Technologies, Invitrogen).

2.5.2 Coomassie Brilliant Blue staining

LDS-PAGE gels were completely covered with Coomassie Brilliant Blue G-250 stain (refer to section 2.8.10) and incubated overnight at 4°C with gentle shaking. Gels were destained with dH₂O at 4°C for 4 hours and imaged using the ChemiDoc MP Imaging System (Bio-rad Laboratories Inc., Hercules, CA, USA). Protein bands for mass spectrometry analysis were manually excised using a scalpel.

2.5.3 Western blot analysis

Proteins separated by LDS-PAGE were transferred to PVDF Transfer Membrane (Thermo Fisher Scientific) using a Trans-Blot SD Semi-Dry Transfer Cell (Bio-rad Laboratories Inc.), according to manufacturer's instructions. Membranes were blocked with Western Blocking Reagent (Roche Diagnostics Australia, NSW, Australia) and protein was detected by incubating membranes with specific primary and secondary antibodies as directed by the supplier (refer to **Table 2.2** for antibody details and dilutions). Signal derived from HRP-coupled secondary antibodies was visualised using Immobilon Western Chemiluminescent-HRP substrate (Merck Millipore, Billerica, MA, USA) and imaged using the ChemiDoc MP Imaging System (Bio-rad Laboratories Inc.).

For immuno dot blots, protein samples were spotted onto PVDF membranes in defined positions rather than gel separation by LDS-PAGE. The detection of proteins using primary and secondary antibodies was performed as described above for Western blot methods. Adriana Caon kindly performed the immuno dot blot for detection of p84-p-Thr607 using purified phospho-specific antibodies raised against a p84 peptide phosphorylated on Thr607. Manuela Klingler-Hoffmann kindly performed the immuno dot blot for the detection of phosphorylation of a p84 peptide that had been incubated with Akt during an *in vitro* kinase assay.

2.5.4 Enzyme-linked immunosorbent assay (ELISA)

High protein-binding EIA/RIA ELISA trays (Corning Costar, Bloomington, MN, USA) were coated with antigen-specific capture antibodies diluted in ELISA coating buffer (0.1M NaHCO₃) overnight at 4°C, according to supplier protocols. Trays were washed 3 times with PBS / 0.05% Tween20 and incubated with diluted samples for 2 hours at room temperature, prior to 3 wash steps and incubation with antigen-specific HRP-coupled detection antibodies for 1 hour at room temperature. Signal detection was developed using TMB-ELISA Substrate Solution (Thermo Fisher Scientific) according to supplier protocols

and absorbance was analysed using a Biotrak II microplate reader (Amersham Biosciences, USA). The detection of BMMC-derived IL-6 and TNF α was performed using mIL-6 and mTNF OptEIATM kits (BD Biosciences, San Jose, CA, USA), according to kit protocols (refer to section 2.5.13). Adriana Caon kindly performed the ELISA for detection of IgG from immunised rabbit serums during antibody production experiments.

2.5.5 XTT/PMS proliferation assay

Redox activity was used to assess the extent of cell proliferation by PMS-mediated XTT reduction of MDA.MB.231 cells in culture. MDA.MB.231 cells were seeded to 96-well culture plates (Corning Plasticware, Sigma Aldrich) at a density of 500 cells/well and redox activity was measured on days 0, 3, 4 and 5 by incubation with PMS/XTT (Sigma Aldrich), according to supplier protocols. Briefly, 1mg/mL 2,3-Bis(2-methoxy-4-nitro-5-sulphophenyl)-2H-tetrazolium-5-carboxanilide (XTT) and 0.383mg/mL N-methyl dibenzopyrazine methyl sulphate (PMS) were combined in a 50:1 ratio and 50 μ l was incubated with cells for 2 hours at 37°C, 5% CO₂. Absorbance was measured at 490nm (Ref 650nm) using a Biotrak II microplate reader (Amersham Biosciences, USA).

2.5.6 Soft agar 3D attachment-independent growth assay

The ability of single cancer cells to form attachment-independent cell spheres was assessed by growth in bacto-agar as a measure of oncogenic colony formation. MDA.MB.231 cells were seeded to 0.3% bacto-agar in complete Iscove's Modified Dulbecco's Medium (IMDM supplemented with 10% FCS, 0.2 U/mL penicillin/gentamycin (IMVS) and fungizone (IMVS)) at a density of 2000 cells/well in 1mL, which was overlaid onto a pre-set layer (1mL) of 0.7% bacto-agar / IMDM in 6-well culture trays (Corning Plasticware, Sigma Aldrich). Cells were incubated for 2 weeks at 37°C, 5% CO₂ to allow sphere formation from single cells, then sphere colonies were stained with Crystal Violet solution diluted in PBS (0.01%) overnight at room temperature. The number of colonies was quantified using QuantityOne Analysis Software (Bio-Rad Laboratories Inc.).

2.5.7 Membrane fractionation

The subcellular fractions of MDA.MB.231 cells were isolated using the Subcellular Protein Fractionation Kit (Pierce, Thermo Fisher Scientific), according to kit instructions. Membrane fraction lysates were equalised using the Coomassie Plus (Bradford) Assay (Pierce, Thermo Fisher Scientific) and samples were analysed by LDS-PAGE and Western blot as described in sections 2.5.1 and 2.5.3.

2.5.8 Incucyte migration assay

The migration of MDA.MB.231 cells was assessed using the live-cell imaging Incucyte tracking system following the introduction of a scratch wound. Cells were seeded to 24-well Essen ImageLock grid culture trays and cultured to 85% cell confluency in complete media (refer to section 2.3.1). Prior to imaging, cells were incubated with Mitomycin C (Sigma Aldrich) for 2 hours to block proliferation, before the application of a scratch wound of defined width using the Essen Scratch Tool. The ability of cells to directionally migrate to colonise the scratch wound was then imaged hourly for 40 hours using the Incucyte Live-Cell Imaging System and software (Essen Instruments, Ann Arbor, MI, USA) and the mean relative wound density was calculated for four biological replicates in each experiment.

2.5.9 PCR

Conventional PCR reactions (25µl total volume) were assembled using 100-200ng of template DNA and specific primers listed in **Table 2.1** (25pmol/primer), in addition to either 1x MyTaq Buffer/Polymerase mix (Bioline, Alexandria, NSW, Australia) or 1x Dynazyme buffer and 0.25µl/reaction Dynazyme Polymerase (Thermo Fisher Scientific), according to supplier's instructions. Reactions were performed using a Thermal Cycler (Bio-Rad Laboratories Inc.) using the following cycle conditions: pre-cycle incubation: 96°C, 2 minutes; denaturation: 96°C, 30 seconds; annealing: T_m of primers -2°C, 45 seconds; extension: 72°C, 1 minute/kb of expected amplification product; repeat denaturation/annealing/extension steps 35 times; hold at 4°C until end. Amplification products were separated by agarose gel electrophoresis using 1.5% agarose gels and visualised by GelRed (Biotium Inc., Hayward, CA, USA) incubation for 15 minutes and ChemiDoc MP Imaging (Bio-Rad Laboratories Inc.).

Quantitative PCR (qPCR) was performed with cDNA templates produced from total RNA isolated using an RNeasy Micro kit (Qiagen Sciences, Maryland, USA), according to kit instructions. cDNA synthesis was performed using 1µg RNA (or total extracted RNA if <1µg) according to the Roche cDNA synthesis kit (Roche Diagnostics, Australia). qPCR reaction mixes were prepared with the LightCycler 480 SYBR Green I Master Mix (Roche Applied Science, Mannheim, Germany) according to supplied protocols and reactions were run on a LightCycler 480 Real-Time PCR System (Roche Applied Science). Data were

analysed using LightCycler 480 software version 1.5 (Roche Applied Science). Gene expression was calculated relative to the reference gene RPLP0.

All primers utilised for conventional and quantitative PCR methods are listed in **Table 2.1**.

2.5.10 Flow cytometry

Tissue samples (spleen, lymph node, thymus, bone marrow) were collected and single cell suspensions were prepared by tissue homogenisation through a 70µm cell strainer, incubation with mouse red cell removal buffer (MRCRB; refer to section 2.8.4) for 10 minutes at 37°C followed by a single wash step in PBS. Blood samples were collected and incubated with MRCRB for 15 minutes at 37°C, then washed three times with PBS to remove lysed red cells. CNS-infiltrating cell suspensions were prepared by homogenisation of brain and spinal cord tissues through a 70µm cell strainer into PBS, then pelleted CNS samples were applied to a 70%/40% Percoll (Sigma Aldrich) gradient in HBSS (Gibco, Invitrogen) and centrifuged at 1000 x g for 25 minutes at room temperature (brake removed). Isolated leukocytes were subjected to red cell lysis with MRCRB for 5 mins at 37°C and then washed once with PBS.

1 x 10⁶ cells/well were plated to 96-well U-bottom trays (Corning Plasticware, Sigma Aldrich) and cells were washed twice with cold PBS. All centrifugation steps were performed at 400 x g for 2 minutes at 4°C.

Cells were incubated with 50µl/well LIVE/DEAD fixable near-IR dead cell stain kit (Life Technologies), diluted 1:1000 in PBS for 20 minutes at room temperature in the dark, then washed twice with PBS/BSA/Azide (refer to section 2.8.5). Fc receptors were subsequently blocked with 50µl/well murine gamma globulin for 20 minutes at room temperature in the dark, then 10µl/well diluted directly-conjugated primary antibodies were applied to the blocked cells (refer to **Table 2.2** for antibody details and final dilutions) and incubated for 30 minutes at 4°C in the dark. Stained cells were washed twice in cold PBS/Azide (refer to section 2.5.6) and either acquired immediately or fixed in 1% paraformaldehyde solution (refer to section 2.8.7) and stored at 4°C in the dark. If biotin-conjugated antibodies were used, an additional step was included after incubation with the primary antibody where stained and washed cells were incubated with streptavidin-647 (refer to **Table 2.2**) for 15 minutes at 4°C in the dark, then washed twice in cold PBS/Azide and acquired.

For intracellular cytokine staining, following the incubation of cells with surface stain directly-conjugated primary antibodies, cells were permeabilised overnight using a Foxp3 Staining Buffer Set (eBioscience, San Diego, CA, USA), according to supplier protocols. Permeabilised cells were stained with directly-conjugated antibodies against intracellular antigens (refer to **Table 2.2** for antibody details and final dilutions) for 30 minutes at 4°C in the dark and washed as directed. Cells were finally fixed in 1% paraformaldehyde solution and stored at 4°C in the dark until acquisition.

Samples were acquired using the BD FACSAria III instrument (BD Biosciences) in conjunction with FACSDiva Software (BD Biosciences) and then analysed using FlowJo version 10.0.7 (Tree Star, Ashland, OR, USA).

2.5.11 BMMC β -hexaminidase release assay

Mature BMMC cells (from 6 week-old cultures) were resuspended to 1×10^6 cells/mL in 3ng/mL IL-3 supplemented growth media (DMEM/WEHI-3; refer to section 2.3.2) and sensitised overnight at 37°C, 5% CO₂ with 2 μ g/mL IgE anti-DNP mAb (clone SPE-7; Sigma Aldrich). Sensitised cells were washed twice in Tyrodes buffer (refer to section 2.8.9), resuspended to 8×10^6 cells/mL and 8×10^4 cells/well were plated to V-bottom trays (Corning Costar). Cells were then pre-incubated with +/- AS605240 (1 μ M)(Echelon Biosciences Inc., Salt Lake City, UT, USA) and +/- adenosine (20 μ M)(Sigma Aldrich) for 30 minutes at 37°C. Degranulation was induced with the addition of DNP-HSA antigen (Sigma Aldrich) at 10ng/mL in Tyrodes buffer for 1 hour at 37°C, 5% CO₂ and the extent of β -hexaminidase release was assessed by calculating the ratio of β -hexaminidase released into the supernatant relative to β -hexaminidase associated with the cell pellet. The V-bottom tray was centrifuged and 10 μ l of the supernatant was transferred to a 96-well flat bottom tray (Corning Costar) and the remaining supernatant was discarded. Cell pellets were lysed with the addition of 20 μ l/well 0.5% Triton-X100 solution and 10 μ l of the lysate was transferred to a 96-well flat bottom tray. 50 μ l PNAG substrate (p-Nitrophenyl-N-acetyl-Beta-D-glucosaminide, 4mM; Sigma Aldrich) was added to supernatant and cell lysate samples and developed for 45 minutes at 37°C, 5% CO₂. Finally, 150 μ l 0.2M glycine was added to each well and the absorbance was acquired at 405nm on a Biotrak II microplate reader (Amersham Biosciences, USA).

2.5.12 BMMC cytokine release assay

Mature BMMC cells (from 6 week-old cultures) were resuspended to 1×10^6 cells/mL in 3ng/mL IL-3 supplemented growth media (DMEM/WEHI-3; refer to section 2.3.2) and sensitised overnight at 37°C, 5% CO₂ with 2µg/mL IgE anti-DNP mAb (clone SPE-7). Sensitised cells were washed twice with warmed PBS, resuspended to 1.5×10^6 cells/mL in BMMC culture medium (DMEM/WEHI-3) and 3×10^5 cells/well were seeded to U-bottom 96-well trays (Corning Costar). Cells were then pre-incubated with +/- AS605240 (1µM)(Echelon Biosciences Inc.) and +/- adenosine (20µM)(Sigma Aldrich) for 30 minutes at 37°C. The activation of sensitised BMMC was induced with the addition of 10ng/mL DNP-HSA antigen (Sigma Aldrich) and cytokine production and release was allowed for 6 hours at 37°C, 5% CO₂. Supernatants were collected and the levels of soluble IL-6 and TNFα were measured by ELISA using BD OptEIA™ kits for mIL-6 and mTNFα (BD Biosciences).

2.5.13 *In vitro* transwell chemotaxis assay

Total bone marrow cells were isolated from the tibias and femurs of 6 week-old male C57Bl/6 wildtype and Pik3r6^{-/-} mice, washed once in PBS and subjected to red cell lysis in MRCRB (refer to section 2.8.4) for 5 mins at 37°C. Cells were washed three times in pre-warmed chemotaxis buffer (RPMI no phenol, 5mg/mL BSA, 25mM HEPES) and resuspended to 5×10^6 cells/mL. IL-8 dilutions (0, 1, 10 and 50nM) were prepared in chemotaxis buffer and 600µl/well was plated to the lower chamber of HTS Transwell 24-well plates with 3.0µm polycarbonate membranes (Corning Inc., NY, USA), prior to the addition of 400µl cell suspension to the upper chamber of the transwells. Trays were incubated for 30 minutes at 37°C, 5% CO₂ then transwell inserts were removed. The cells that had migrated through to the lower transwell chamber were stained by flow cytometry as described in section 2.5.10. Neutrophils were defined as CD11b⁺Gr-1⁺ and detected using anti-CD11b-PECy7 and anti-Gr-1-PE antibodies (refer to **Table 2.2**), where the migration index of neutrophils across samples was normalised and calculated relative to BD Calibrite unlabelled beads (BD Biosciences).

2.5.14 *In vitro* Akt phosphorylation in bone marrow cells

Total bone marrow cells were isolated from the tibias and femurs of 6 week-old male C57Bl/6 wildtype and Pik3r6^{-/-} mice, washed once in PBS and subjected to red cell lysis in MRCRB (refer to section 2.8.4) for 5 mins at 37°C. Bone marrow cells were then washed 3

times in warmed PBS and serum starved for 3 hours at 37°C 5% CO₂ in serum starvation media (RPMI 1640 supplemented with 0.1% foetal calf serum, 2mM L-glutamine (IMVS), 10mM HEPES (IMVS), 1mM sodium pyruvate (Gibco, Life Technologies) and 0.2 U/mL penicillin/gentamycin (IMVS)). Cells were stimulated with 10nM IL-8 for 0, 1 or 5 minutes. Stimulation was ceased by transferring cells to ice, washing cells twice with ice-cold PBS and cell lysis in an NP-40 lysis buffer (refer to section 2.8.8) for 1 hour on ice. Lysates were cleared by centrifugation at 20 000 x g for 10 minutes at 4°C and the protein concentration of lysates was quantitated using a Coomassie Plus (Bradford) Assay (Pierce, Thermo Fisher Scientific), according to supplier protocols. Lysates were separated by LDS-PAGE and analysed by Western blot for the detection of phosphorylated Akt (refer to sections 2.5.1 and 2.5.3).

2.6 *In vivo* techniques

2.6.1 Phospho-specific antibody production

A phospho-specific p84 antibody (anti-p84-pThr607) was raised against a synthetic phosphorylated p84 peptide (CRPREVpTVSLRA) in a rabbit using a four-dose immunisation regime. The phospho-peptide was conjugated to the mcKLH hapten using the Imject EDC Carrier Protein spin kit (Thermo Fisher Scientific) and dialysed overnight through four changes of PBS. The hapten-coupled phospho-peptide was then used to immunise a rabbit according to the following regime: 1st dose (week 0), 500µg/animal; 2nd dose (week 3), 250µg/animal; 3rd dose (week 6), 250µg/animal; 4th dose (week 9), 250µg/animal. A pre-bleed was collected prior to the first immunisation to establish baseline serum IgG levels, a test bleed was performed prior to the final immunisation at week 7.5 and the final serum collection was performed at week 10.5. Serum titres were assessed by ELISA as described in section 2.5.4.

2.6.2 Experimental haematogenous metastasis

MDA.MB.231 cells transduced with pMSCV control, pMSCV-p84-HA, pMSCV-p84-S358A-HA and pMSCV-p84-T607A-HA expression vectors were transferred intravenously at 2×10^5 cells/mouse into 8-10 week old female Severe Combined Immuno-Deficient (SCID) mice and metastatic lung nodules were allowed to form for 7 weeks. Mice were monitored daily for clinical symptoms and distress according to University of Adelaide animal ethics approvals and NH&MRC guidelines. At the completion of the

experiment, lungs were harvested and separated into individual lobes prior to the enumeration of metastatic surface nodules. Lungs were subsequently imaged using a Leica MZ16FA Stereomicroscope (Leica Microsystems, Wetzlar, Germany).

2.6.3 Induction of chronic MOG₃₅₋₅₅-induced EAE

Chronic experimental autoimmune encephalomyelitis (EAE) disease was induced in 8-10 week old female C57Bl/6 mice with the subcutaneous injection of 50µg MOG₃₅₋₅₅ peptide (MEVGWYRSPFSRVVHLYRNGK) (GL Biochem, China) emulsified in a Complete Freund's Adjuvant (CFA) preparation for MOG (85% mineral oil / 15% mannide monooleate (Sigma Aldrich) with 8.33mg/mL *Mycobacterium tuberculosis* (Difco Laboratories, Becton Dickinson, NT, USA)). Briefly, MOG peptide was dissolved in endotoxin-free PBS and mixed at a 1:1 ratio with CFA by passing the mixture through a stopcock with two syringes until a thick emulsion was achieved. MOG/CFA was injected subcutaneously into the hind flanks (50µl/flank) and the scruff of the neck (20µl), in conjunction with 300ng/dose pertussis toxin (List Biological Laboratories Inc., CA, USA) in endotoxin-free PBS administered intravenously in two doses; 2 hours prior to MOG/CFA immunisation and a second dose on day 2 post-disease induction. EAE clinical disease scores and signs of distress were monitored daily according to University of Adelaide animal ethics approvals and clinical disease symptoms were scored according to **Table 2.3**.

2.6.4 Induction of relapsing-remitting PLP₁₃₉₋₁₅₁-induced EAE

Relapsing-remitting experimental autoimmune encephalomyelitis (EAE) disease was induced in 8-10 week old female SJL/J mice with the subcutaneous injection of 50µg PLP₁₃₉₋₁₅₁ peptide (HSLGKWLGHDPDKF) (Biomedical Research Centre, University of British Columbia, Vancouver BC, Canada) emulsified in a Complete Freund's Adjuvant (CFA) preparation for PLP (85% mineral oil / 15% mannide monooleate (Sigma Aldrich) with 8.33mg/mL *Mycobacterium tuberculosis* and 0.5mg/mL *Mycobacterium butyricum* (Difco Laboratories, Becton Dickinson)). Briefly, PLP peptide was dissolved in endotoxin-free PBS and mixed at a 1:1 ratio with CFA by passing the mixture through a stopcock with two syringes until a thick emulsion was achieved. PLP/CFA was injected subcutaneously into the hind flanks (50µl/flank), in conjunction with 300ng/dose pertussis toxin (List Biological Laboratories Inc.) in endotoxin-free PBS administered intravenously in two doses; 2 hours prior to PLP/CFA immunisation and a second dose on day 2 post-disease induction. EAE clinical disease scores and signs of distress were monitored daily

according to University of Adelaide animal ethics approvals and clinical disease symptoms were scored according to **Table 2.3**.

2.7 Proteomics

All proteomics methods and experimentation were performed in conjunction with the Adelaide Proteomics Centre under the guidance of Professor Peter Hoffmann. I would like to acknowledge the contribution of past and present staff of the Adelaide Proteomics Centre who have worked on this project; Georgia Arentz, Michelle Hooi, Chris Cursaro, James Eddes, Johan Gustafsson and Tomas Koudelka.

2.7.1 Orbitrap LTQ XL ETD LC-MS for p84 phosphorylation studies

Sample preparation

Gel bands were excised, washed in 500 μ L of 50mM ammonium bicarbonate and de-stained with 100mM ammonium bicarbonate in 30% acetonitrile (ACN). Protein was reduced using 0.5 μ mol dithiothreitol (DTT) in 100mM ammonium bicarbonate, alkylated using 2.75 μ mol iodoacetamide (IAA) in 100mM ammonium bicarbonate and digested overnight using 100ng modified porcine trypsin (Promega) in 5mM ammonium bicarbonate 10% acetonitrile. 30 μ L of 0.1% formic acid (FA) was added and sonicated for 15 min. Peptides were extracted and two subsequent extractions steps were performed with sonication for 15 minutes using 50 μ L of 0.1%FA in 50% ACN and 50 μ L of 100% ACN, respectively. Peptides were purified and concentrated using Pierce C18 spin columns (Thermo Fisher Scientific). The volumes of peptide extracts were reduced by vacuum centrifugation (to approximately 1 μ L), then resuspended with 0.1% TFA in 2% ACN to a total volume of 10 μ L. 5 μ L of the sample was injected into the liquid chromatography system.

Liquid chromatography mass spectrometry

Peptides were separated on an HPLC system (UltiMate 3000; Dionex) using a separation column (Thermo Fisher Scientific) (Acclaim PepMap RSLC, C18, pore size 100 Å, particle size 2 μ m, 75 μ m inner diameter (ID) \times 15 cm length) and a trapping column (Thermo Fisher Scientific) (Acclaim PepMap100, C18, pore size 100 Å, particle size 3 μ m, 75 μ m ID \times 2 cm length). The HPLC system was coupled to an LTQ Orbitrap XL mass spectrometer (Thermo Fisher Scientific), using the following buffer system: (A) 2% ACN,

0.1% FA in H₂O; (B) 80% ACN, 0.1% FA in H₂O. For in-line desalting and concentration, 5 μL of digests were loaded onto the trap column and washed for 5 min with 100% (A) at a flow rate of 5 μL/min. Peptides were eluted at 300 nL/min with the following 100 min gradient: 4% (B) for 10 min, gradient to 40% (B) over 50 min, gradient to 90% (B) in 20 min, 90% (B) for 10 min, gradient from 90% to 4% (B) in 30 sec, 4% (B) for 19.5 min. The effluent from the HPLC column was directly electrosprayed into the mass spectrometer. The LTQ Orbitrap XL instrument was operated in data-dependent mode to automatically switch between full scan MS and MS/MS acquisition. Instrument control utilised Thermo Tune Plus and Xcalibur software (Thermo Fisher Scientific). Full scan MS spectra (from m/z 300-1700) were acquired in the Orbitrap analyser and resolution in the Orbitrap system was set to $r = 60\ 000$. The standard mass spectrometric conditions for all experiments were: spray voltage, 1.25kV; no sheath and auxiliary gas flow; heated capillary temperature, 200°C; predictive automatic gain control (AGC) enabled, and an S-lens RF level of 50-60%. All unassigned charge states and charge states of 1 were rejected. An inclusion list for the parents' masses and their neutral losses of 98 was generated. The parent peptide ions were sequentially isolated and fragmented in the high-pressure linear ion trap by low-energy CID. However, MS₂ scans were carried out on the most intense peptide ions with charge states ≥ 2 and minimum signal intensity of 500 if no parent masses were detected. A repeat count of 1 and exclusion duration of 180s was taken into account before the same mass was acquired again. An activation $q = 0.25$, activation time of 15ms and normalised collision energy of 35% were used. The resulting fragment ions were scanned out in the low-pressure ion trap at the "normal scan rate" (33 333 amu/s) and recorded with the secondary electron multipliers. Nine data dependent for CID-MS measurements were carried out in the LTQ using the same settings as the CID/MS₂.

Data analysis

Samples were subjected to the Proteome Discoverer software (Thermo Fisher Scientific) to set up the workflow prior to submission to MASCOT (Version 2.2; Matrix Science Inc., Boston, USA) by the Proteome Discoverer Daemon (Thermo Fisher Scientific). Peak lists in the range from 350 m/z to 5000 m/z were searched against the SwissProt 2014_08 database. Search parameters for fixed modifications were carbamidomethyl (C) and for variable modifications were oxidation (M), phosphorylation (ST) and phosphorylation (Y). The MSMS scans of the samples were also analysed manually to confirm the phosphorylation sites using the Thermo Scientific Xcalibur software (Version 2.0.7).

2.7.2 *In vitro* Akt kinase assay

The AKT1 Kinase Enzyme System (Promega, Madison, WI, USA) was used to assess the phosphorylation of full-length p84 protein, digested p84 peptides and a p84 synthetic peptide (CRPREVTVSLRA), according to kit protocols. Briefly, the protein or peptide samples were buffered and incubated with Akt kinase, DTT and ATP for 30 minutes, prior to isolation and mass spectrometry analyses. The extent of phosphorylation at Thr607 was compared with a synthetic p84 phospho-peptide (CRPREV**p**TVSLRA) by immunoblot methods using an anti-phospho-(Ser/Thr) Akt substrate antibody that detects phosphorylation at an Akt kinase phosphorylation consensus site. The precise position of the phosphorylation was confirmed by mass spectrometry using the UltrafleXtreme MALDI-TOF/TOF system (Bruker Daltonics), as described below.

Peptides were purified from the kinase assay using a C18 ZipTip (Merck Millipore, Darmstadt, Germany) and were diluted to a concentration of 1pmol/μL with 0.1% trifluoroacetic acid (TFA). 1μL of sample was spotted onto an 800μm AnchorChip target plate (Bruker Daltonics) and allowed to dry. 1μL of matrix (alpha-cyano-cinnamic acid, 0.5 mg/mL in water/acetonitrile/TFA 10/90/0.1) was spotted onto the same positions on the target plate and dried. Mass spectra were acquired on an UltrafleXtreme MALDI-TOF/TOF mass spectrometer (Bruker Daltonics) operating in reflective positive mode. Instrument settings were set in flexControl software (Version 3.3; Bruker Daltonics). Sample m/z range was set to 800-5000 Da. Two thousand shots were collected for the external calibration and ten thousand shots were collected for the sample spots. External calibration was performed using a 1:50 dilution of peptide calibration standard 2 (Bruker Daltonics) in the range 1000-4000 Da, which was analysed under the same conditions as the sample. Spectra from each analysed spot were obtained at various locations over the surface of the matrix spot at an intensity determined by the operator. The MS spectra obtained were analysed using flexAnalysis software (Version 3.3; Bruker Daltonics) employing smoothing, background subtraction and peak detection algorithms.

2.7.3 Parallel reaction monitoring (PRM)

LC-ESI-MS/MS was performed using an Ultimate 3000 nano-flow system (Dionex) coupled to an Impact II QTOF mass spectrometer (Bruker Daltonics) via an Advance CaptiveSpray source (Bruker Daltonics). 20mL of each trypsin digested sample was loaded

onto a trapping column (Acclaim PepMap100, C18, pore size 100 Å, particle size 3µm, 75µm ID × 2 cm length, Thermo Scientific) at 3ml/min using 0.1% FA, 5% ACN in water. Peptide separation was then performed on a Acclaim PepMap RSLC column (C18, pore size 100 Å, particle size 2µm, 75µm internal diameter × 15cm length, Dionex) at 0.3ml/min using a linear gradient of 5-45% ACN in 0.1% FA over 40 min. PRM was performed on the QTOF using the following parameters for the peptide ELVLFRLPR; m/z 571.8559, collision energy of 20.1, and an isolation width of 10. The following parameters for the peptide SVQAVLR; m/z 386.7374, collision energy of 14.5, and an isolation width of 10. Data was analysed using the open source software Skyline where it was compared to a Pik3r6 spectral library acquired from previous experiments (refer to section 2.7.1). The following Skyline settings were used; trypsin digestion, up to 2 missed cleavages, variable modifications of carbamidomethyl and oxidation, and mass error tolerance of 40 ppm.

2.7.4 Isotope-Coded Protein Labelling (ICPL) analyses: Sample preparation

Single cell suspensions were generated from brain and spinal cord (CNS) tissues by enzymatic dissociation in 2mg/mL collagenase D (Roche Diagnostics, Australia) and 10U DNaseI (Sigma Aldrich) for 1 hour at room temperature prior to homogenisation through a 70µm cell strainer into PBS. Pelleted CNS samples were applied to a 70%/40% Percoll (Sigma Aldrich) gradient in HBSS (Gibco, Invitrogen) and centrifuged at 1000 x g for 25 minutes at room temperature (brake removed). Isolated leukocytes were subjected to red cell lysis with MRCRB (section 2.8.4) for 5 mins at 37°C. Cells were resuspended in 0.1% BSA/PBS and CD4⁺ cells were isolated using Invitrogen DynaBead positive Isolation for CD4⁺ cells and Detach-a-Bead for mouse CD4 kits, according to provided protocols (Invitrogen). Unactivated control samples were isolated from the spleens of naïve mice, where cells isolated by homogenisation through a 70µm cell strainer into PBS, red cell lysis in MRCRB for 10 minutes at 37°C and CD4⁺ cell purification as described for CNS samples above. Cells were washed three times in ice-cold PBS, then lysed to extract either protein for ICPL labelling or RNA for quantitative PCR. For protein extraction, cells were lysed for 10 minutes on ice with NP-40 lysis buffer (section 2.8.8), then lysates were cleared by centrifugation at maximum speed and stored at -80°C until processing. mRNA transcript levels of selected protein candidates identified during ICPL analyses were assessed by quantitative PCR according to section 2.5.9.

2.7.5 ICPL analyses: Labelling, LDS-PAGE and peptide isolation

15µg protein from each control or disease stage (naive control, disease onset, peak-disease +/- remission) were reduced, alkylated and then labeled with ICPL 0, ICPL 6 and ICPL 10 for MOG₃₅₋₅₅-EAE samples or with ICPL 0, ICPL 4, ICPL 6 and ICPL 10 for PLP₁₃₉₋₁₅₁-EAE samples, respectively, according to protocols provided with the SERVA ICPL Quadruplex PLUS Kit (SERVA, Heidelberg, Germany). Following labelling, samples were combined (triplex for MOG₃₅₋₅₅-EAE; 45µg total protein or quadruplex for PLP₁₃₉₋₁₅₁-EAE; 60µg total protein). Protein was then precipitated using acetone precipitation as described in SERVA provided protocols followed by solubilisation in 20µL 1x LDS loading buffer with 20mM DTT using sonication. Samples were heated at 95°C for 10 min, allowed to cool and separated by LDS-PAGE on 1mm 4-12% NuPAGE Bis-Tris gels (Invitrogen) using MOPS running buffer at 200V for 50 min.

Following separation, gel bands were visualised using Colloidal Coomassie Blue staining (Amersham Biosciences, USA) prior to manual excision and in-gel reduction (DTT), alkylation (iodoacetamide) and tryptic digestion (100ng modified porcine trypsin, Promega, Madison, WI, USA). Peptides were extracted from the gel plugs using sonication in 50% ACN with 0.1% TFA followed by 100% ACN. Combined peptide eluates for each gel band were dried down in a vacuum centrifuge and each was reconstituted using 2% ACN with 0.1% TFA.

2.7.6 ICPL triplex: HPLC, fraction collection and mass spectrometry

An Agilent 1100 system was operated using binary gradients of mobile phase A (0.1% TFA in 95% H₂O, 5% ACN) and B (0.1% TFA in 95% ACN, 5% H₂O). The Agilent 1100 was controlled using the Hystar software platform (V3.2-SR2, Bruker Daltonics, Bremen, Germany). Peptide samples were eluted and separated directly over an Acclaim PepMap100 C18 analytical column (180µm i.d. × 15cm, 5µm particle size, 100 Å, Dionex) at a flow rate of 1µL/min. The peptides were eluted with an ACN gradient of 0% B for 10 min, 0 to 48% solvent B in 54 min, 48 to 60% solvent B in 5 min, 60 to 80% solvent B in 0.5 min, followed by 80% B for 5 min.

Fifteen-second fractions were collected onto a MTP 384 MALDI 800µm AnchorChip target (Bruker Daltonics) using a Proteineer Fraction Collector (Bruker Daltonics). A supporting liquid (50% ACN in 0.1% TFA) was added discontinuously over the last 2 sec

during deposition onto the MALDI target via sheath flow to reduce peak tailing. After the spots were air-dried, 1 μ L of α -cyano-4-hydroxycinnamic acid (CHCA) matrix solution was added manually to each fraction according to Zhang *et al.*^{214, 215} and allowed to dry. For calibration spots 1 μ L of Bruker Daltonics Peptide Calibration Standard II (dissolved in 125 μ L of 0.1% TFA) was mixed with 99 μ L of 30% ACN in 0.1% TFA and 600nL deposited onto the target. After drying, 0.8 μ L of matrix solution was subsequently added and left to dry.

MS analysis was performed on an Ultraflex III MALDI-TOF/TOF system (Bruker Daltonics) in reflectron positive ion mode, using WARP-LC (V1.2; Bruker Daltonics) interfaced with flexControl. Laser power and detector gain was operator determined to provide optimal MS intensity and resolution. 500 and 400 laser shots were collected for both sample and calibration spots respectively using an acquisition m/z range of 700-4500. Following MS collection, MS spectra were smoothed (Gaussian, 1 cycles, width - m/z 0.05), and baseline subtracted (TopHat). Peak masses and intensities were detected with flexAnalysis using the SNAP algorithm.

WARP-LC was used to calculate a compound list for automated MS/MS based on a preset LC-MALDI method. MS/MS instrument settings were defined by the LIFT method. Following automated MS/MS acquisition, MS/MS spectra were imported into Proteinscape version 3.0.0346 (Bruker Daltonics) and submitted to Mascot (V2.3.02) for identification using the following search parameters: Taxonomy, *Mus musculus*; Database, Swiss-Prot release 2013_04; Maximum missed cleavages, 1; MS tolerance, 50ppm, MS/MS tolerance, 0.8Da; Enzyme, Arg C; Variable modifications, oxidation (M), ICPL_0 (Lysine), ICPL_0 (Protein N-terminal), ICPL_6 (Lysine), ICPL_6 (Protein N-terminal), ICPL_10 (Lysine), ICPL_10 (Protein N-terminal); fixed modifications; carbamidomethyl (cysteine).

2.7.7 ICPL quadruplex: HPLC, fraction collection and mass spectrometry

An UltiMate 3000 RS Nano/Cap System (Dionex, California, USA) was operated using binary gradients of mobile phase A (0.05% TFA in 98% H₂O, 2% ACN) and B (0.04% TFA in 80% ACN, 20% H₂O) and controlled using Hystar (V3.2-SR2; Bruker Daltonics). A micro-WPS-3000 autosampler (Dionex) injected 5 μ L samples onto an Acclaim Pepmap 100 trap column (75 μ m \times 2cm, 3 μ m, 100 Å). Sample loading was performed at 3 μ L/min at 0% B for 10 min. For analytical separation the trap was switched inline to an Acclaim

Pepmap100 C-18 analytical column (75 μ m \times 15cm, 3 μ m; Dionex) running at 300nL/min. Peptides were eluted with 4-8% B in 1 min, 8-42% B in 44 mins, 42-90% B in 5 min followed by 90% B for 10 min.

Fifteen-second fractions were collected onto an MTP 384 MALDI 800 μ m AnchorChip target (Bruker Daltonics) using a Proteineer Fraction Collector (Bruker Daltonics), as described in Gustafsson *et al.*²¹⁶. Briefly, eluate was mixed with CHCA matrix, supplied by a syringe pump (Cole-Parmer, Illinois, USA), in a MicroTee junction (PEEK, 1/32 in, Upchurch Scientific). Matrix consisted of 748 μ L 95% ACN in 0.1% TFA, 36 μ L saturated CHCA in 90% ACN and 0.1% TFA, 8 μ L of 10% TFA and 8 μ L of 100mM ammonium phosphate. 1 μ L of Peptide Calibration Standard II (Bruker Daltonics) dissolved in 125 μ L 0.1% TFA was mixed with 99 μ L 30% ACN in 0.1% TFA and 150 μ L of matrix. 600nL of this mixture was deposited onto calibration spots.

MS and MS/MS analyses were performed using an UltrafleXtreme MALDI-TOF/TOF system (Bruker Daltonics) in reflectron positive ion mode, using WARP-LC (V1.2; Bruker Daltonics) interfaced with flexControl. Laser power was operator determined to provide optimal MS intensity and resolution. 3000 laser shots were collected for both sample and calibration spots. Acquisition settings: m/z range of 700-4000, 5.0 \times reflector gain and 2.00 GS/s acquisition rate. MS spectra were smoothed (Gaussian, 1 cycles, width - m/z 0.02), and baseline subtracted (TopHat). Peak masses and intensities were detected in flexAnalysis using the SNAP algorithm.

WARP-LC was used to calculate a compound list for automated MS/MS based on a preset LC-MALDI method. MS/MS instrument settings were defined by the LIFT method. Following automated MS/MS acquisition, MS/MS spectra were imported into Proteinscape version 3.0.0346 (Bruker Daltonics) and submitted to Mascot (V2.3.02) for identification using the following search parameters: Taxonomy, *Mus musculus*; Database, Swiss-Prot release 2013_04; Maximum missed cleavages, 1; MS tolerance, 50ppm; MS/MS tolerance, 0.8Da; Enzyme, Arg-C; Fixed modifications, carbamidomethyl (C); Variable modifications, Oxidation (M), ICPL_0 (Lysine), ICPL_0 (Protein N-terminal), ICPL_4 (Lysine), ICPL_4 (Protein N-terminal), ICPL_6 (Lysine), ICPL_6 (Protein N-terminal), ICPL_10 (Lysine), ICPL_10 (Protein N-terminal) . To prepare a list of candidate peptides

for quantitation, all protein identifications with at least one identification with an ion score greater than the identity threshold were accepted.

2.7.8 ICPL analyses: Determination of peptide and protein ratios

Peptide identifications were exported from Proteinscape to tab delimited text and LC-MALDI data was converted to the open mzMXL format using CompassXport (version 1.3; Bruker Daltonics). For each ICPL labeled peptide, the expected monoisotopic m/z of the corresponding ICPL 0, ICPL 4, ICPL 6 and ICPL 10 labeled peptides were calculated and their intensities extracted from the data as follows: the spectra from the LC-MALDI fraction from which the identification was made, and both the preceding and following two fractions (a 75 second window) were loaded into R using the mzR package²¹⁷ and m/z peaks were detected using the MALDIquant package²¹⁸; the intensity of peaks with 0.1Da of each calculated ICPL m/z were then extracted from each spectrum and summed to give an intensity for each ICPL labeled species (where peak detection failed, the maximum signal within 0.05 Da of the expected m/z was taken). For peptides with a single ICPL label, the intensity of ICPL 6 monoisotopic peak was corrected by subtracting the predicted intensity of the overlapping third isotope of the ICPL 4 labeled species. The correction factor was determined empirically from the dataset by examining the relative heights of the isotopes of all peptides identified as being modified with two or more ICPL 4 labels. The ICPL 4, ICPL 6 and ICPL 10 intensities were each divided by the ICPL 0 signal to give ratios for each peptide. Log₂ ratios were then normalised by subtracting the mean log₂ ratios for ICPL 4 / ICPL 0, ICPL 6 / ICPL 0 and ICPL 10 / ICPL 0 for the dataset. Finally, protein regulations were expressed as the mean of the log₂ of their peptide ratios.

The spectra for the regulated 23 proteins (presented in Tables 5.1 and 5.2) were manually inspected and reviewed for accuracy. The annotated spectra and extracted ion chromatograms are provided and can be accessed online (www.pubs.acs.org/doi/suppl/10.1021/pr500158r) as Supporting Information associated with the published manuscript.

Differential regulation of protein expression was defined as at least 2-fold change in peptide intensity of a disease stage sample (ICPL_4, ICPL_6, ICPL_10; either increase >2.0 or decrease <0.50 fold-change) relative to the naive control sample (ICPL_0; defined as 1). This conservative threshold was based on preliminary control analysis of the

technical variance associated with ICPL labelling, where protein extract from CD4⁺ cell lysate from naïve spleen samples were split into 4 aliquots, labelled with ICPL Quadruplex labels, then combined and quantitatively analysed following the described experimental workflow (sections 2.7.2 and 2.7.4). From 4 prominent protein bands the experimental deviation from 1:1 was determined. The mean and standard deviations relative to ICPL_0 were determined [ICPL_0 : ICPL_4 : ICPL_6 :ICPL_10][1 : 0.85 : 0.95 : 0.90]. The standard derivation for the ratios were low; 0.2011 for ICPL _4, 0.1332 for ICPL_6 and 0.1442 for ICPL_10. The mean of the standard deviation was 0.1595 and to be conservative we defined the regulation window, which is considered to be above the technical variation, by being 2 times the mean standard deviation below the lowest and above the highest value (0.531- 1.269). Considering these values, protein regulation was considered as significant if there was at least a 2-fold change in regulation.

2.8 Antibodies and General Reagents

2.8.1 Primers and antibodies

Primers used in this study were purchased from Sigma Aldrich and are listed in **Table 2.1**. All primers were resuspended to 100µM in PCR grade H₂O and stored at -20°C. Antibodies used in immunoprecipitation, Western blot, flow cytometry and immunofluorescence are listed in **Table 2.2**.

2.8.2 Phosphate buffered saline (PBS) / Tris buffered saline (TBS)

PBS and TBS solutions were obtained from the Technical Services Unit at the School of Molecular and Biomedical Sciences, The University of Adelaide.

2.8.3 Diethyl Pyrocarbonate (DEPC) reagents for RNA isolation

RNase-free water and ethanol solutions were prepared using DEPC (Sigma Aldrich). DEPC-H₂O was prepared by diluting DEPC 1/1000 in Milli-Q water and the solution was autoclaved before use. DEPC-H₂O was used to prepare a 70% ethanol solution, then DEPC was added at 1/1000 and the solution was autoclaved before use to generate DEPC-70% ethanol.

2.8.4 Murine Red Cell Removal Buffer (MRCRB)

MRCRB is 140mM NH₄Cl, 17mM Tris, pH7.2 and is prepared as required by mixing two pre-prepared solutions; parts A and B. part A is prepared by solubilising 8.3g NH₄Cl in 1L

Milli-Q water; part B is prepared by solubilising 20.594g Tris in 1L Milli-Q water and adjusting the pH to 7.65. The final buffer is prepared as required by mixing parts A and B in a 9:1 ratio (A:B), adjusting the pH to 7.2 and filter sterilisation using a 0.2 μm filter. MRCRB stored at 4°C.

2.8.5 PBS/BSA/Azide

PBS/BSA/Azide solutions for flow cytometry were prepared with the addition of 1% BSA (Sigma Aldrich) and 0.04% sodium azide (Ajax Finechem) to PBS. Stored at 4°C.

2.8.6 PBS/Azide

PBS/Azide solutions for flow cytometry were prepared with the addition of 0.04% sodium azide (Ajax Finechem) to PBS. Stored at 4°C.

2.8.7 Paraformaldehyde solutions (PFA)

4% PFA was prepared by dissolving 4g of paraformaldehyde (Sigma Aldrich) in 100mL 1x PBS overnight with constant stirring at 50°C. 4% PFA was stored at -20°C. 1% PFA solution was prepared by diluting 4% PFA 1:4 in 1x PBS and was stored at 4°C.

2.8.8 NP-40 lysis buffer

The NP-40 lysis buffer used for all protein lysis in this study was composed of 1% NP-40, 50mM Tris pH 7.5, 200mM NaCl and 1mM EDTA. The lysis buffer was stored at 4°C and supplemented with 2mM Na_3VO_4 , 50mM NaF, 10mM phenylmethylsulfonyl fluoride and protease inhibitor cocktail diluted 1:100 (Sigma Aldrich) immediately prior to use.

2.8.9 Tyrodes buffer

Tyrodes buffer for BMMC β -hexaminidase assays was prepared by mixing 10mL 1M HEPES, 7.54g NaCl, 0.37g KCl, 0.206g CaCl_2 , 0.203g MgCl_2 , 1.008g D-glucose, 1g BSA to a final volume of 1L in Milli-Q water. The solubilised buffer was sterilised through a 0.2 μm filter and stored sterile at 4°C.

2.8.10 Coomassie Brilliant Blue G-250 (CBB)

CBB stock was prepared fresh as required. For 75mL, 6.5g ammonium sulphate was dissolved in Milli-Q water to a volume of 61 mL, then 1.5mL 85% phosphoric acid, 1.25mL G-250 dye stock and 15.5mL methanol was added.

2.9 Statistical analyses

Statistical analysis was performed using GraphPad Prism v6 (GraphPad Software, San Diego, CA, USA). Data are summarised and presented as mean \pm standard error. Unless otherwise stated, statistical tests used for analyses are unpaired two-tailed *t*-tests with statistical significance defined as follows: * $p < 0.05$; ** $p < 0.01$, *** $p < 0.001$, **** $p < 0.0001$. Densitometry analysis for Western blots was performed using ImageJ 1.47v (National Institute of Health, Bethesda, MD, USA).

Table 2.1: Primers used in this study

Primer name	Sequence (5' – 3')	Type
pMSCV forward	CCCTTGAACCTCCTCGTTTCGACC	sequencing
pMSCV reverse	CAGCGGGGCTGCTAAAGCGCATGC	
p84(h)OPT F1	CACTGTGGCTCTCGATTGTG	sequencing
p84(h)OPT F2	GACTTCCTGATGCCTGGAT	
p84(h)OPT F3	GTCACCGAGGTGGTCAAATC	
p84(h)OPT R1	GTGAGGTTCTGCTCAGCGAT	sequencing
p84(h)OPT R2	TCACTCCTGGCAGCATCTC	
p84(h)OPT R3	TGAATCTGGATGTTGTTTGTCC	
p84(h)OPT S358A mut	GCTGCCTGCACCTGGAGCCCCTGAGATGGA	
p84(h)OPT S358A as	TCCATCTCAGGGGCTCCAGGTGCAGGCAGC	
p84(h)OPT T607A mut	ACCACGCGAAGTGGCCGTCTCCCTGAG	mutagenesis
p84(h)OPT T607A as	CTCAGGGAGACGGCCACTTCGCGTGGT	
p84 screen F	ATTGCTACTGGGCACCCTTC	PCR / seq
p84 screen R	GACAGAAATGGAAGGACGGGATAG	
p84 CRISPRlong F	AGTGGGAATGATACAGCAGGAC	PCR / seq
p84 CRISPRlong R	TCCGAACTCGTGAGTGGAAG	
mu p84 variant 1 F	GAGCTGGAGAAGGCAGAAAGC	qPCR
mu p84 variant 1 R	GGATGCCTGTGGCCTTAGTG	
mu p84 predicted X1 F	TGCTCAGAGAGCTGGAGAAGAAA	qPCR
mu p84 predicted X1 R	GGATGCCTGTGGCCTTAGTG	
mu p101 F	CTGCCCTGGAAAGACAGCAT	qPCR
mu p101 R	CCAAGCAAGGACTATCCTGAGAGT	
mu p110 γ F	GGCCGCTGGTGGATGAC	qPCR
mu p110 γ R	GTGAACACACTCTCGTGGTCCTT	
mu Annexin A1 F	GCAACCATCATTGACATTCTTACC	qPCR
mu Annexin A1 R	TGTAAGTACGCGGCCTTGATC	
mu Annexin A2 F	AAGGACATCATCTCTGACACATCTG	qPCR
mu Annexin A2 R	GCTCGTCTGCCCTTTGCA	
mu S100A4 F	TTGAGGGCTGCCAGATAAG	qPCR
mu S100A4 R	GCAAACACTACCCCAACACTTCA	
mu S100A9 F	GAAGCCCTCATAAATGACATCATG	qPCR
mu S100A9 R	CATCAGCATCATACTCCTCAAAG	
mu RPLP0 F	TGCAGATCGGGTACCCAAC	qPCR
mu RPLP0 R	ACGCGCTTGTACCCATTGA	

Table 2.2: Antibodies used in this study

WESTERN BLOT and IMMUNOPRECIPITATION					
Name	Clone	Catalog #	Provider	Species / Isotype¹	Dilution²
HA tag	C29F4	3724	Cell Signalling Technology	rabbit IgG mAb	1/10 000
p84.2	-	N/A	Home-made	rabbit polyclonal	1/200
p87 ^{PIKAP}	K-17	sc-241593	Santa Cruz Biotechnology	goat polyclonal IgG	1/500
p84-pThr607	-	N/A	Home-made <i>phospho-specific</i>	rabbit polyclonal	1/200
p110 γ	D55D5	5405	Cell Signalling Technology	rabbit IgG mAb	1/1000
p101 (R87)	-	N/A	Home-made	rabbit polyclonal	1/1000
Akt (pan)	11E7	4685	Cell Signalling Technology	rabbit IgG mAb	1/2000
phospho Akt (Ser473)	193H12	4058	Cell Signalling Technology	rabbit IgG mAb	1/1000
phospho- (Ser/Thr) Akt substrate	110B7E	9614	Cell Signalling Technology	rabbit IgG mAb	1/1000
β -actin	AC-15	A1978	Sigma-Aldrich	mouse IgG1 mAb	1/10 000
pan-cadherin	28E12	4073	Cell Signalling Technology	rabbit IgG mAb	1/1000
rabbit IgG-HRP	-	31460	Thermo Scientific	goat polyclonal	1/100000
mouse IgG-HRP	-	31480	Thermo Scientific	goat polyclonal	1/20 000

FLOW CYTOMETRY

Antibody name	Clone	Catalog #	Provider	Species / Isotype¹	Dilution³
----------------------	--------------	------------------	-----------------	--------------------------------------	-----------------------------

Leukocyte staining

CD3 - PECy7	145-2C11	25-0031-82	eBioscience	Hamster (Ar) IgG	1/240
CD4 - BV450	RM4-5	560468	BD Biosciences	Rat IgG2a	1/240
CD8 - BV510	53-6.7	563068	BD Biosciences	Rat IgG2a	1/240
CD44 - biotin	IM7	553132	BD Biosciences	Rat IgG2b	1/210

IL-17A - PE	TC11-18H10	559502	BD Biosciences	Rat IgG1	1/180
IFN γ - FITC	XMG1.2	554411	BD Biosciences	Rat IgG1	1/180
FoxP3 - PerCPCy5.5	FJK-16s	45-5773-82	eBioscience	Rat IgG2a	1/120
CD45.2 - PerCPCy5.5	104	45-0454-82	eBioscience	Mouse IgG2a	1/300
B220 - PerCPCy5.5	RA3-6B2	552771	BD Biosciences	Rat IgG2a	1/240
CD11b - PECy7	M1/70	552850	BD Biosciences	Rat IgG2b	1/240
Gr-1 - PE	RB6-8C5	553128	BD Biosciences	Rat IgG2b	1/300
F4/80 - FITC	BM8	11-4801-85	eBioscience	Rat IgG2a	1/180

Thymocyte staining

CD3 - biotin	17A2	13-0032-82	eBioscience	Hamster (Ar) IgG	1/240
CD4 - biotin	H129.19	553649	BD Biosciences	Rat IgG2a	1/240
CD8 - biotin	53-6.7	553029	BD Biosciences	Rat IgG2a	1/180
CD11c - biotin	HL3	553800	BD Biosciences	Hamster (Ar) IgG1	1/180
Gr-1 - biotin	RB6-8C5	553125	BD Biosciences	Rat IgG2b	1/180
CD45R - biotin	RA3-6B2	553086	BD Biosciences	Rat IgG2a	1/180
CD25 - PE	7D4	558642	BD Biosciences	Rat IgM	1/180
CD44 - BV450	IM7	560451	BD Biosciences	Rat IgG2b	1/180
Streptavidin - 647	-	S-32357	Molecular Probes	-	1/250

Mast cell staining

c-kit - PE	2B8	561075	BD Biosciences	Rat IgG2b	1/200
Fc ϵ RI - APC	MAR-1	17-5898-82	eBioscience	Hamster (Ar) IgG	1/100

CELL ISOLATION

Antibody name	Clone	Catalog #	Provider	Species / Isotype	Dilution ⁴
Dynabeads Mouse CD4	-	11445D	Invitrogen	-	25 μ l per 1x10 ⁷ cells

¹ Hamster (Ar), Armenian Hamster² Dilution of antibodies for Western blot in TBS/Tween (0.05%)³ Dilution of antibodies for flow cytometry in PBS/BSA/Azide with murine gamma globulin; dilution is final⁴ Dilution of antibodies for cell isolation in Invitrogen Isolation Buffer (PBS/0.1% BSA/2mM EDTA; pH7.4)

Table 2.3: Clinical disease scoring of murine experimental autoimmune encephalomyelitis

Experimental Autoimmune Encephalomyelitis (EAE) DISEASE SCORING		Disease stage designation (ICPL)	
SCORE	SYMPTOMS		
0.5	Good but reaching for front/back paws when held by the tail	Disease onset	Remission
1	Partially flaccid tail <i>and</i> some difficulty up-righting when placed on back		
2	Fully flaccid tail <i>or</i> difficulty up-righting when placed on back		
2.25	Fully flaccid tail <i>and</i> difficulty up-righting when placed on back		
2.5	Fully flaccid tail <i>and</i> some hind limb paralysis (ataxia)	Peak-disease	
3	Hind limb paralysis		
3.25	Hind limb paralysis <i>and</i> favouring one paw		
3.5	Hind limb paralysis <i>and</i> some fore limb paralysis		
4	Hind limb paralysis <i>and</i> (mostly) fore limb paralysis		
4.5	Paralysis and looking very sick		
5	Moribund		

ICPL - Isotope-coded protein labelling

Chapter 3: Regulatory phosphorylation sites within p84

Chapter 3: Identification and characterisation of regulatory phosphorylation sites within p84 in the context of PI3K γ signalling and implications for cell migration

3.1 Introduction

Of the three PI3K γ subunits, least is known about the p84 adaptor protein and the distinct role of this subunit in the regulation of PI3K γ signalling at the molecular level. This is largely due to the absence of structural or domain data for p84 and a lack of high-quality p84-specific reagents, which has limited the examination of p84 interactions with the p110 γ catalytic subunit and the regulation of its activity. One established mechanism by which PI3K enzyme complexes are regulated involves the transient phosphorylation of PI3K subunits that can facilitate or prevent protein interactions within the enzyme complex. However to date, post-translational modifications to p84, including the phosphorylation of p84 during PI3K γ signalling downstream of GPCRs, has not been examined. Therefore, the goal of the experiments outlined in this chapter was to assess the phosphorylation of p84 during PI3K γ signal activation and determine the role of regulatory phosphorylation for the function of p84. A number of *in silico*, proteomic and biochemical approaches were utilised in order to assess the phosphorylation of p84. Following this, the functions of regulatory phosphorylation sites within p84 were investigated in the context of PI3K γ signal activation, p84 heterodimerisation with p110 γ , subcellular localisation of PI3K γ subunits and cell migration.

3.2 Results

3.2.1 *In silico* prediction of phosphorylation sites within p84

Using a number of bioinformatic database tools, phosphorylation sites within p84 were predicted based on the amino acid sequence of p84 and known kinase consensus sequences. **Table 3.1** summarises the highest ranking predicted phosphorylation sites within p84 compiled from DiPhos 1.3, NetPhorest 2.0, GPS 2.1, NetPhos 2.0, NetPhosK 1.0 and Scansite3 prediction tools. The top ranked phosphorylation site within p84 predicted by GPS 2.1, NetPhorest 2.0 and Scansite 3 tools was found to be threonine 607 (Thr607). In addition, another predicted phosphorylation site, Serine 358 (Ser358), was identified by five of the six bioinformatic tools. Together, these two sites Ser358 and

Thr607 represented the top 2 predicted phosphorylation sites within p84. Moreover, Thr607 and Ser358 residues were predicted to be phosphorylated by Akt/PKB and GSK-3 kinases, respectively, which are known downstream effectors of the PI3K γ signalling pathway^{91, 219, 220}.

3.2.2 Identifying phosphorylation sites within p84

There are limited high-quality reagents available to specifically detect endogenous expression of p84. A commercial antibody (anti-p87^{PIKAP}) from Santa Cruz Technologies and an in-house antibody (anti-p84.2) were tested by Western blot analysis and immunoprecipitation (IP/WB) for specificity and sensitivity to endogenous p84. It was found that neither antibody could adequately detect p84 from either lysates (**Figure 3.1 (left)**) or immunoprecipitates (**Figure 3.1 (right)**). A weak protein band at approximately 84 kDa could be detected by IP/WB using the anti-p84.2 antibody (as shown in **Figure 3.1 (right)**), however the result was messy and produced many non-specific bands. For this reason, detection of p84 using anti-p84.2 was deemed neither specific nor sensitive enough for planned experiments investigating the functional role of p84 in PI3K γ signalling.

Therefore, due to the described challenges regarding the detection and isolation of endogenous p84, in conjunction with the requirement for large amounts of protein in order to conduct phospho-proteomic analyses, the following protein over-expression approach was devised to specifically analyse p84. In order to determine the phosphorylation status of p84 isolated from stimulated cells, a p84 expression construct was designed where p84 was expressed with an HA fusion tag that could be used to specifically immunoprecipitate the protein. A synthetic expression-optimised p84-HA fusion construct (p84(h)OPT-HA) was produced in the pUC57 shuttle vector by Genscript using XbaI and SalI restriction sites, as shown in **Figure 3.2 (A-C)**. The p84-HA construct was then subcloned from the shuttle vector into the retroviral expression vector pMSCVpuro using XhoI and EcoRI restriction sites (**D, E**), which was confirmed by gel electrophoresis of digested plasmid products (**F**).

The expression of p84-HA in MDA.MB.231 cells transiently-transfected with pMSCV-p84(h)OPT-HA was readily detected by Western blot analysis of cell lysates using an HA-specific antibody, compared with cell lysates from control cells transfected with the empty pMSCV vector, as shown in **Figure 3.3 (A)**. The HA-specific antibody was also used to

immunoprecipitate p84-HA from total cell lysates produced from MDA.MB.231 cells transfected with the pMSCV-p84(h)OPT-HA expression vector, which could be detected by Coomassie Brilliant Blue staining (CBB) compared with the vector control IP (cells transfected with pMSCV empty vector) that lacked p84-HA expression (**Figure 3.3 (B)**). Collectively, these data suggest that expression of p84 using the pMSCV-p84(h)OPT-HA expression system was a suitable method to express and isolate sufficient amounts of p84 for proteomic analysis and detection of phospho-amino acids.

Using p84-HA expression and immunoprecipitation from transfected MDA.MB.231 cells as described above, p84 was isolated for phospho-proteomic analyses to detect phosphorylation events induced by GPCR stimulation. Specifically, p84-HA was expressed in human mammary carcinoma MDA.MB.231 cells by transient transfection with pMSCV-p84-HA and cells were stimulated for 0, 1, 5, 10 and 20 minutes with CXCL12 to activate PI3K γ signalling downstream of CXCR4. Vector control cells (transfected with pMSCV only) were used as a negative control for p84-HA detection. Total cell lysates from stimulated cells were subjected to immunoprecipitation with the HA-specific antibody to isolate p84-HA, then precipitates were separated by LDS-PAGE and gels were stained with Coomassie Brilliant Blue. A prominent protein band at approximately 84 kDa was observed in p84-HA stimulated samples compared with the vector control IP, which was confirmed to be p84-HA by Western blot analysis as shown in **Figure 3.4 (A)**. Bands representing p84-HA were manually excised and prepared for mass spectrometry through reduction, alkylation, tryptic digestion and peptide purification techniques (refer to Materials and Methods section 2.7.1). Peptide samples were analysed and the identity of p84 was verified with 69-73% peptide coverage, as depicted in **Figure 3.4 (B-F)**. A summary of post-translational modifications identified within p84 isolated from cell lysates upon CXCL12 stimulation is presented in **Table 3.2**, where phosphorylation, oxidation and methylation modifications were considered according to the data analyses methods defined in section 2.7.1. Phosphorylation of p84 on Ser358 was identified from each sample (unstimulated and stimulated), suggesting that Ser358 phosphorylation is constitutive. The extent of Ser358 peptide phosphorylation was estimated by calculating the ratio of phospho-peptide relative to non-phospho-peptide detected, which was determined to range from 5-17% (*data not shown*). A representative MS/MS spectrum demonstrating phosphorylation on Ser358 is presented in **Figure 3.5 (A)** and the position of Ser358 within the p84 sequence is shown in **(B)**.

Unlike p-Ser358 that was readily identified within p84 isolated from stimulated cell lysates, no further phosphorylation was identified, including the expected phosphorylation on Thr607 that was predicted with highest confidence by *in silico* prediction tools. Although speculative, two reasons for the lack of phosphorylated Thr607 (p-Thr607) detection in these analyses were proposed. Firstly, that the phosphorylation of Thr607 is a brief transient event and the described isolation method failed to detect the induction of p-Thr607. Secondly, that transient phosphorylation of Thr607 occurs to a lesser extent than the constitutive Ser358 phosphorylation observed and may therefore be lost due to the extensive sample manipulation involved in extracting p84 from total cell lysates, despite the presence of phosphatase inhibitors. An alternative scenario, which cannot be ruled out, is that p84 is not phosphorylated on Thr607, contrary to *in silico* predictions.

Since Akt kinase was predicted with high confidence to phosphorylate p84 on Thr607, an *in vitro* kinase assay was performed using active Akt kinase to induce phosphorylation of p84 isolated from cells, both at the peptide and protein levels. **Figure 3.6** shows the experimental design. For phosphorylation at the peptide level (**A**), p84-HA was immunoprecipitated from MDA.MB.231 cells transfected with pMSCV-p84-HA, then precipitates were separated by LDS-PAGE and stained with CBB. Bands representing p84-HA (*dotted box*) were excised and protein was digested with trypsin. The resultant peptide solution was buffered and then incubated with active Akt to stimulate phosphorylation of Thr607 before analysis by mass spectrometry. For phosphorylation at the protein level (**B**), p84-HA was immunoprecipitated from MDA.MB.231 cells transfected with pMSCV-p84-HA then incubated with Akt kinase whilst bound to the immunoprecipitation sepharose beads to stimulate the phosphorylation of Thr607. Precipitates were then denatured, separated by LDS-PAGE and stained with Coomassie Brilliant Blue. The dotted box represents p84-HA protein bands and the large band at approximately 55 kDa represents the Akt enzyme. p84 bands were excised and analysed by mass spectrometry for detection of p84 phosphorylated on Thr607. A vector control immunoprecipitation (v) was included to ensure the specific immunoprecipitation of p84-HA. Using the described approaches, proteomic analyses of p84 isolated and stimulated *in vitro* with Akt did not detect p-Thr607.

To determine whether Akt kinase was capable of phosphorylating a p84 peptide (12 amino acids in length that included Thr607 (CRPREVTVSLRA)), an *in vitro* kinase assay was performed comparing synthetic non-phosphorylated and phosphorylated p84 peptides to the non-phosphorylated peptide incubated with Akt. In keeping with *in silico* predictions, the amino acid sequence surrounding Thr607 (RPREVT) shown in **Figure 3.7 (A)** represents an Akt kinase consensus motif for phosphorylation (RXRXXS/T), as depicted in **(B)**. Upon incubation of the non-phosphorylated p84 peptide with Akt, it was found that Akt mediated the phosphorylation of p84 at an Akt phosphorylation consensus site, as detected by Western dot blot presented in **Figure 3.7 (C)**. This Western blot assay utilised a commercial antibody (anti-phospho-(Ser/Thr) Akt substrate) that detects phosphorylation at an Akt phosphorylation consensus site (R.X.R.X.X.S/T), such as Thr607 within the p84 peptide. In addition to detection by Western dot blot, the p84 peptide product isolated from this incubation with Akt was confirmed to encompass phosphorylation specifically on residue Thr607 by mass spectrometry, as shown in **Figure 3.7 (D)**. Further evidence to suggest that Akt mediates phosphorylation of p84 on Thr607 was provided by the co-precipitation of Akt with p84, suggesting an interaction between the two proteins. As shown in **Figure 3.8**, similar amounts of Akt were detected to co-precipitate with p84-HA from unstimulated and stimulated cell lysates.

Based on the evidence provided above suggesting that Akt can phosphorylate p84 on Thr607, a method was devised to generate an antibody to specifically detect p84 phosphorylated on Thr607. Since Akt is a major effector of PI3K γ signalling, transient phosphorylation of p84 on Thr607 by Akt may represent a regulatory feedback mechanism influencing the activity of p84. Whilst p84 was also determined to be phosphorylated on Ser358, an antibody to detect this phosphorylation was not pursued since Ser358 phosphorylation was shown to be constitutive.

A phospho-specific antibody against p84 phosphorylated at Thr607 (anti-p84-pThr607) was raised in rabbits using a phosphorylated p84-pThr607 immunising peptide (CRPREV**p**TVSLRA; refer to Materials and Methods section 2.6.1). However, whilst IgG serum titres after three peptide immunisations appeared to show considerable antibody production (**Figure 3.9 (A)**) and the antibodies within the harvested serum were sufficient to detect the immunising peptide by immuno dot blot (*data not shown*), after purification, the anti-p84-pThr607 antibody was not capable of immunoprecipitating and detecting

phosphorylated p84 from cells to a sufficient level (**Figure 3.9 (B) left blot**). Although a weak band could be seen at the correct molecular weight of approximately 84 kDa, which was shown to increase very slightly after 5 minutes stimulation with CXCL12, detection at this level was not convincing when compared with the Western blot of duplicate lysates using the anti-HA antibody to detect p84-HA as a control (**Figure 3.9 (B) right blot**). The stimulation time-frame assessed was extended to 20 minutes (0, 1, 5, 10 and 20 minutes CXCL12 stimulation)(*data not shown*), however phosphorylated p84 was not detected using the anti-p84-pThr607 antibody at any of these time-points. The inability to detect phosphorylated p84 using this phospho-specific antibody indicates that either p84 was not phosphorylated at Thr607 at 0 or 5 minutes stimulation with CXCL12 or that the raised anti-p84-pThr607 antibody was not sufficient to detect phosphorylated p84-pThr607. Collectively, the experiments presented here and in Figure 3.1 investigating the sensitivity and specificity of commercial, in-house and phospho-specific p84 antibodies demonstrate that currently available antibodies were not sufficient to detect p84 or p84 phosphorylated on Thr607. It was therefore concluded that detection of p84 would require the expression of the pMSCV-p84-HA construct in MDA.MB.231 cells and the detection of p84 using the HA fusion tag (anti-HA).

3.2.3 Development of an expression system to detect and immunoprecipitate wildtype and mutant p84 proteins

The role of p84 expression and the function of Ser358 and Thr607 putative phosphorylation sites were examined in MDA.MB.231 mammary carcinoma cells in the context of PI3K γ signal regulation and cancer cell biology. In order to generate stable MDA.MB.231 cell lines expressing p84-HA and determine the role of Ser358 and Thr607 residues in p84 function, the pMSCV-p84-HA retroviral expression vector was mutated to encode p84-HA where Ser358 and Thr607 residues were mutated to alanine residues. Site-directed mutagenesis of the p84(h)OPT-HA sequence to mutate S358 \rightarrow A358 and T607 \rightarrow A607 required the substitution of two nucleotides (AGC (serine) \rightarrow GCC (alanine)) or one nucleotide (ACC (threonine) \rightarrow GCC (alanine)), respectively, as shown in **Figure 3.10 (A-C)**. This produced pMSCV-p84-S358A-HA and pMSCV-p84-T607A-HA vectors that would result in the expression of mutant p84-S358A and p84-T607A proteins. The successful mutation of the pMSCV-p84-HA parental vector was confirmed by DNA sequencing of plasmid preparations and proteomic analysis of mutant p84 proteins

expressed by transient transfection of MDA.MB.231 cells. The mutation of p84-S358A is demonstrated in **Figure 3.11 (upper section)** as shown by amino acid sequence (**A**), DNA sequencing and alignment (**B**) and mass spectrometry of p84-S358A isolated from transfected cells (**C, D**). The mutation of p84-T607A is demonstrated in **Figure 3.11 (lower section)** as shown by amino acid sequence (**E**), DNA sequencing and alignment (**F**) and mass spectrometry of p84-T607A isolated from transfected cells (**G, H**).

Retroviral expression constructs encoding wildtype p84 (pMSCV-p84-HA) and mutant p84 proteins (pMSCV-p84-S358A-HA and pMSCV-p84-T607A-HA) were then transduced into MDA.MB.231 cells and the stable expression of p84 proteins were confirmed by Western blot analysis, compared with the vector control cell line (pMSCV empty; depicted as 'v'), as shown in **Figure 3.12 (A)**. The expression levels of wildtype and mutant p84 proteins shown in **Figure 3.12 (A) (upper panel)** were found to be equivalent when normalised to the expression of β -actin as a cell lysate loading control shown in **Figure 3.12 (A) (lower panel)**. Immunoprecipitation of wildtype and mutant p84 proteins using the HA fusion tag was also found to be equivalent, as determined by Coomassie Brilliant Blue staining of anti-HA precipitates separated by LDS-PAGE, shown in **Figure 3.12 (B)**. The stained protein bands representing p84-HA, p84-S358A-HA and p84-T607A-HA were observed at approximately 84 kDa, as expected, and determined to be immunoprecipitated specifically by anti-HA as shown by the absence of a protein band in the vector control cell line (that lacked the HA tag) (**Figure 3.12 (B)**). These data suggest that wildtype p84 and mutant p84 proteins are expressed at equal levels in transduced MDA.MB.231 cell lines and that the stability of p84 expression is not dependent on Ser358 or Thr607 residues.

3.2.4 Investigating the tumour suppressor function of p84 and the role of Ser358 and Thr607 phosphorylation sites

The role of p84 was then assessed in a model of experimental haematogenous metastasis of MDA.MB.231 cells to the lung. This assay mimics the later stages of breast cancer metastasis and it examines the ability of carcinoma cells to survive as single cells in the blood, adhere to the endothelial vessels of lung capillaries, extravasate and invade the lung parenchyma and form secondary tumours²²¹. MDA.MB.231 cells transduced to express wildtype p84, p84-S358A or p84-T607A mutant proteins were injected intravenously into

SCID mice. Seven weeks later, lungs were harvested, lobes of the lungs separated and surface lung nodules were enumerated. The expression of both wildtype p84 and p84-S358A were found to reduce the metastatic capability of MDA.MB.231 cells as shown by a reduction in the number of surface lung nodules relative to the vector control cell line, shown in **Figure 3.13 (A, B)**. The suppressive effect of p84 expression on MDA.MB.231 cell metastasis was found to be dependent on Thr607, since in contrast to cells expressing wildtype p84, the expression of p84-T607A resulted in a comparable number of metastases to the vector control cell line (**Figure 3.13 (A, B)**). Unlike Thr607, the mutation of Ser358 to alanine (p84-S358A) did not alter the tumour suppressor function of p84, suggesting that Ser358 is dispensable for the tumour suppressor function of p84. The ratio of surface lung nodules relative to the vector control for each p84-expressing cell line is presented in **Figure 3.13 (A)** and representative lung images are presented in **Figure 3.13 (B)**, where the black arrows indicate examples of metastatic MDA.MB.231 surface lung nodules. These data suggest that p84 possesses tumour suppressor function and that the suppression mediated by p84 is dependent on Thr607.

3.2.5 The effect of wildtype and mutant p84 protein expression on PI3K γ signal activation

Since wildtype p84 was shown to possess tumour suppression function, it was hypothesised that increased expression of wildtype p84 may have an effect on PI3K γ signal activation and that this effect would be dependent on Thr607. To test this hypothesis, the induction of PI3K γ -mediated phosphorylated Akt (p-Akt) was examined in MDA.MB.231 cells transduced to express wildtype p84, p84-S358A or p84-T607A proteins. The induction of p-Akt is a well-established read-out of PI3K γ -dependent PIP₃ accumulation downstream of GPCR activation and was induced in the present study with CXCL12 stimulation. However, it is important to note that endogenous p101 is present in these cells and that this assay is not capable of distinguishing between PI3K γ signalling (as measured by p-Akt induction) mediated by p84/p110 γ as opposed to p101/p110 γ enzymes. Phosphorylation of Akt on Ser473 was observed after 5 minutes CXCL12 stimulation, as shown by the vector control cell line (**Figure 3.14 (A) upper panel left**), and the expression of wildtype p84 or mutant p84-S358A, p84-T607A proteins did not significantly alter the level or kinetics of Akt phosphorylation (**Figure 3.14 (A) lower panels left**). The induction of p-Akt was confirmed to be PI3K γ -dependent using the

isoform-selective inhibitor AS605240 (**Figure 3.13 (A, B, C) right panels**). The expression of wildtype and mutant p84-HA proteins and total Akt were detected from cell lysates, which represented expression and loading controls, respectively, as shown in **Figure 3.14 (B, C)**. Collectively, these data suggest that the activation of PI3K γ signalling, as measured by p-Akt induction, is not affected by the over-expression of p84 or the loss of Ser358 or Thr607 residues, at least during the stimulation time frame investigated (0-20 minutes). Instead, these data suggest that p-Akt induction is independent of p84 and is generated through the actions of p101/p110 γ heterodimers.

3.2.6 The effect of wildtype and mutant p84 protein expression on MDA.MB.231 cell proliferation and 3D growth

The data presented in the previous section suggested that the tumour suppressor function of p84 was not as a result of altered PI3K γ signal activation. It was therefore examined whether the expression of wildtype p84 mediated tumour suppression through indirect effects on cell proliferation and/or 3D carcinoma cell growth. However, consistent with comparable p-Akt induction between vector control and p84-expressing cell lines, no difference in the proliferation of transduced MDA.MB.231 cell lines was observed, as demonstrated in **Figure 3.15 (A)**. Though primarily controlled through the actions of PI3K α and PI3K β isoforms, the proliferation of some cell types has been shown to require contributions from PI3K γ signalling^{2, 34, 160}. Albeit, the data presented in **Figure 3.15 (A)** indicates that reduced lung metastases observed in MDA.MB.231 cells expressing wildtype p84 (shown in Figure 3.13) was not as a result of a decreased intrinsic ability of the cells to proliferate.

The ability of carcinoma cells to form attachment-independent 3D colonies in bactoagar is an established method to assess their oncogenic potential. In accordance with reduced metastases of MDA.MB.231 cells transduced to express wildtype p84 *in vivo* (Figure 3.13), the expression of wildtype p84 was found to modestly decrease the oncogenic potential of MDA.MB.231 cells *in vitro* relative to the vector control cell line, as shown in **Figure 3.15 (B)**. Expression of a similar amount of p84-S358A further reduced the number of 3D colonies formed. In contrast, the expression of p84-T607A by MDA.MB.231 cells led to a significant increase in the number of 3D colonies formed, relative to the expression wildtype p84 (**Figure 3.15 (B)**). These data indicated that the suppression of oncogenic

potential *in vitro* mediated by wildtype p84 was dependent on Thr607, but not Ser358, as was the case for *in vivo* metastases. These data further support previous findings¹²³ that indicate p84 to possess tumour suppressor function in MDA.MB.231 cells, and that the function of p84 in this context is dependent on Thr607.

3.2.7 Assessing the formation of p84/p110 γ heterodimers and their translocation to the membrane

Initial data indicated that p84 suppresses the oncogenic potential and metastasis of MDA.MB.231 cells *in vitro* and *in vivo*, however, the PI3K γ -dependent induction of p-Akt signalling was unaffected by p84 expression. Therefore, it was proposed that p84 may be involved in the regulation of PI3K γ signalling, specifically, the termination of the transient signal rather than the activation of PI3K γ signalling cascades. To assess this, the ability of p84 to dimerise with p110 γ was examined, in addition to the subcellular localisation of the subunits in order to ascertain whether p84/p110 γ enzymes were present at the membrane. The recruitment of PI3K γ complexes to the plasma membrane is required for the activation of their lipid-kinase activity and therefore, according to the accepted model of PI3K enzyme activation, the detection of p84/p110 γ heterodimers at the membrane would imply the formation of a PI3K γ enzyme capable of lipid-kinase activity. The extent of p84/p110 γ dimerisation was measured by the precipitation of p84-HA from CXCL12 stimulated cell lysates and the detection of co-precipitated endogenous p110 γ by Western blot analysis (**Figure 3.16**). Wildtype p84 was found to maintain a degree of basal dimerisation with p110 γ , as shown by a modest p110 γ co-precipitated protein band detected in the unstimulated (0) sample, which was further induced upon CXCL12 stimulation and peaked at 10 minutes stimulation (**Figure 3.16 (A) top panel**). This result represents the first description of inducible heterodimerisation between p84 and p110 γ . Of note, the formation of this induced p84/p110 γ dimer observed at 10 minutes stimulation occurred after the induction of p-Akt in these cells. This provides further evidence to suggest that p-Akt generated at 5 minutes stimulation (see Figure 3.14) was not produced by the enzymatic activity of p84/p110 γ heterodimers, thereby indicating that p84 does not participate in the induction phase of PI3K γ signalling. In contrast to wildtype p84, whilst p84-T607A maintained a comparable basal interaction with p110 γ in the absence of stimulation, heterodimerisation between p84-T607A and p110 γ could not be induced above

unstimulated levels (**Figure 3.16 (A) middle panel**). This suggests that Thr607 is required for p84 to form the inducible heterodimer with p110 γ in response to CXCL12 stimulation. Albeit at a lower level, the dimerisation of p84-S358A with p110 γ was found to follow the same induction pattern as wildtype p84 (**Figure 3.16 (A) bottom panel**), suggesting that Ser358 is not required for p84 interactions with p110 γ . A number of controls were employed in this assay and demonstrated that p84, p84-S358A and p84-T607A were immunoprecipitated with equal efficiency from each sample (**Figure 3.16 (B)**), that endogenous p110 γ was expressed at equal levels in each cell line (**Figure 3.16 (C) upper**) and that equal amounts of total lysate were used for each condition, as determined by the detection of β -actin (**Figure 3.16 (C) lower**). Control immunoprecipitations are shown in **Figure 3.16 (D)** and confirm that p110 γ is not precipitated non-specifically with the anti-HA antibody or immunoprecipitation beads. The induction of p84/p110 γ heterodimerisation, as determined by Western blot detection of co-precipitated p110 γ , was quantified using ImageJ densitometry from 3 independent experiments as shown in **Figure 3.16 (E)**.

As described above, the lipid-kinase activity of PI3K γ enzymes requires the adaptor-mediated translocation of the p110 γ catalytic subunit to the plasma membrane, where it is proximal to lipid substrates. To establish whether p84/p110 γ heterodimers induced at 10 minutes CXCL12 stimulation were present at the membrane, the membrane localisation of p84 and p110 γ subunits were assessed in transduced MDA.MB.231 cells. Cells transduced to express wildtype and mutant p84 proteins were stimulated with CXCL12 and lysed, then the membrane fraction of the lysate was isolated by subcellular fractionation. **Figure 3.17** depicts the detection of endogenous p110 γ (**A**) and p84 proteins (**B**) within the membrane fraction of stimulated cells as detected by Western blot, in addition to the detection of cadherin as a membrane fraction control (**C**). In the vector control cell line, p110 γ was shown to be recruited to the membrane at 1 minute stimulation. The detection of p110 γ within the membrane fraction was then shown to decrease after 1 minute stimulation, suggesting that PI3K γ participates in transient signalling at the membrane (**Figure 3.17 (A) top panel**). The recruitment of p110 γ in cells transduced to express wildtype p84 and p84-S358A was found to reflect the kinetics observed for the vector control cell line (**Figure 3.16 (A) second and fourth panels**), indicating that the expression of p84 does not influence the membrane recruitment of p110 γ . Consistent with this, p84 and p84-S358A

were detected at very low levels within the membrane fraction and did not increase above unstimulated levels (**Figure 3.17 (B)**). As suggested previously, these data provide further evidence to indicate firstly, that the recruitment of p110 γ to the membrane at 1 minute in these cells is mediated by p101, and secondly, that the p84/p110 γ dimer observed at 10 minutes CXCL12 stimulation is not present at the plasma membrane and is therefore unlikely to represent an active PI3K γ enzyme, since it is not in proximity to its lipid substrates. Although not specifically assessed, due to the absence of p84/p110 γ heterodimers (detected at 10 minutes stimulation) within the membrane fraction, it could be speculated that p84/p110 γ complexes are instead present within the cytosol.

In contrast to the transient membrane recruitment of endogenous p110 γ in the vector control cell line and cells expressing wildtype p84 and p84-S358A, the membrane recruitment of p110 γ in cells transduced to express p84-T607A was found to be delayed and persistent (**Figure 3.17 (A) third panel**). Furthermore, p84-T607A was shown to have increased localisation at the membrane relative to wildtype 84 and p84-S358A (**Figure 3.17 (B) middle panel**). The detection of total cadherin was used to confirm equivalent loading of membrane fractions across samples (**Figure 3.17 (C)**). The purity of cytosolic, membrane and nuclear fractions attained using subcellular fractionation methods were demonstrated by Western blot detection of cytosolic (calpain 1), membrane (cadherin) and nuclear (HDAC2) proteins (**Figure 3.17 (D)**). The recruitment of p110 γ to the membrane in response to CXCL12 stimulation was quantified using ImageJ densitometry from 3 independent experiments, as shown in **Figure 3.17 (E)**.

3.2.8 Implications of p84 expression on MDA.MB.231 cell migration

Data presented in the current study demonstrate that the loss of Thr607 (p84-T607A) within p84 prevents p84-mediated tumour suppression and that cells transduced to express mutant p84-T607A exhibited a similar phenotype to MDA.MB.231 cells in which p84 expression had been knocked down (p84 KD). In a previous publication produced by the laboratory, p84 KD cells were shown to display enhanced metastatic potential relative to wildtype MDA.MB.231 cells¹²³ using the same assay of haematogenous metastasis presented in Figure 3.13. Increased metastasis of p84 KD cells was coupled with constitutive membrane localisation of p110 γ ¹²³, indicating that loss of p84 resulted in increased PI3K γ signalling driven by p101/p110 γ enzymes. Therefore in the present study,

the migratory capacities of MDA.MB.231 p84 KD cells and cells transduced to express p84-T607A were assessed using an Incucyte migration assay, which allowed the tracking of directed cell migration in real-time (**Figure 3.18**). In this assay, cell proliferation was blocked with Mitomycin C, then a scratch of defined width was introduced to a confluent cell layer and the migration of cells to colonise the scratch wound was measured. **Figure 3.18** shows the rate of directed cell migration during a 40-hour incubation (**A**) and representative images taken at 20 hours are shown (**B**). Relative to cells expressing wildtype p84, it was found that p84 KD cells (that lacked p84-mediated tumour suppressor function) migrated at a significantly faster rate, as shown in **Figure 3.18 (A, B)**. Although not to the same extent as p84 KD cells, MDA.MB.231 cells expressing p84-T607A were also shown to migrate significantly faster than those expressing wildtype p84. These data suggest that in the absence of p84 (p84 KD) or where p84 lacks Thr607 (p84-T607A), cells do not exhibit the tumour suppression conferred by p84. The migration of MDA.MB.231 cells in this assay was confirmed to be PI3K γ -dependent as shown by significantly inhibited migration of AS6065240-treated cells (**Figure 3.18 (A) and (B) lower panel**).

3.3 Summary

Collectively, these data presented in Chapter 3 describe the identification of two putative phosphorylation sites within p84, Ser358 and Thr607, in a study that represents the first detailed analyses of post-translational modifications to p84 with a specific focus on phosphorylation. The characterisation of these potential regulatory phosphorylation sites revealed that the tumour suppressor function of p84 in MDA.MB.231 cells is dependent on Thr607. Specifically, whilst the expression of wildtype p84 suppressed the oncogenic potential *in vitro* and metastasis *in vivo* of human mammary carcinoma MDA.MB.231 cells, it was found that the mutation of Thr607 to alanine reversed this effect. It was shown that Akt, a prominent downstream effector of PI3K γ signalling, was capable of interacting with p84 and phosphorylating Thr607 *in vitro*, suggesting that phosphorylation of p84 on Thr607 may represent a feedback loop within PI3K γ signalling. Moreover, Thr607 was shown to be required for p84 to form an inducible heterodimer with p110 γ in a complex sequestered from active signalling at the membrane. Temporal analysis revealed that the interaction between p84 and p110 γ occurred after the induction of initial PI3K γ signalling mediated by p101/p110 γ complexes (as measured by p-Akt induction), suggesting that the Thr607-dependent interaction between p84 and p110 γ represents negative feedback

potentially involved in the termination of signalling. This represents a novel mechanism of PI3K γ signal regulation in the control of carcinoma cell migration and metastasis.

Table 3.1: Predicted phosphorylation sites within p84.

Six bioinformatic prediction tools were used to identify potential phosphorylation sites within the human p84 sequence (NCBI Reference Sequence: NP_001010855.1). The top 20 (S/T/Y) phosphorylation sites from each prediction program and predicted kinases were compiled. Prediction tools accessed May 2014.

DiPhos 1.3 (<http://www.dabi.temple.edu/diphos/>); *NetPhorest 2.0* (<http://netphorest.info/>); *GPS 2.1* (<http://gps.biocuckoo.org/>);

NetPhos 2.0 (<http://www.cbs.dtu.dk/services/NetPhos/>); *NetPhosK 1.0*

(<http://www.cbs.dtu.dk/services/NetPhosK/>); *ScanSite3* (<http://www.scansite3.mit.edu/>).

position		Peptide	site		Kinase	Prediction tool*
start	end		sequence	residue		
1	7	**MESSDVE	S	3	-	DiPhos1.3
1	8	*MESSDVEL	S	4	-	DiPhos1.3
15	29	QAVLRELSTQAPALQ	S	22	CAMK	GPS 2.1
18	28	LRELSTQAPAL	T	23	ATM/ ATR	NetPhorest 2.0
33	43	GMWRWLSLHKKV	S	38	PKC	NetPhorest 2.0
43	57	VERDPGKSPVLVRIL	S	50	CMGC/GSK/GSK3A	GPS 2.1
91	99	TEELYQRIY	Y	95	SRC	NetPhos2.0 / NetPhosK
103	117	TRLLTLPTPYCTVAL	T	110	STE/STE7/MAP2K6	GPS 2.1
177	191	EAAQAQQTPEFCMRH	T	184	STE/STE7	GPS 2.1
212	222	RKIQASPRRTL	S	217	p38MAPK	NetPhos2.0 / NetPhosK
					CDK1/ 2/ 3/ 5	NetPhorest 2.0
236	246	MASEASPSREG	S	241	cdk5	NetPhos2.0 / NetPhosK
					-	DiPhos1.3
					CLK	NetPhorest 2.0
239	247	EASPSREGH	S	243	-	NetPhos2.0 / NetPhosK
					-	DiPhos1.3
251	259	LEEIYCSLL	Y	255	-	NetPhos2.0 / NetPhosK
304	312	LRPRSQRRL	S	308	PKA/ DNAPK	NetPhos2.0 / NetPhosK
					-	DiPhos1.3
309	317	QLRLSADLE	S	313	cdc2/ PKA	NetPhos2.0 / NetPhosK
330	338	LARVSVLST	S	334	PKA	NetPhos2.0 / NetPhosK
					-	DiPhos1.3
333	341	VSVLSTDSG	S	337	CKI	NetPhos2.0 / NetPhosK
335	345	VLSTDSGIERD	S	340	CKII	NetPhos2.0 / NetPhosK
					CK2	NetPhorest 2.0
342	353	ERDLPTGADEL	T	348	-	DiPhos1.3
					CK2	NetPhorest 2.0
					CMGC/CDK/CDC2/CDK2	GPS 2.1
351	365	DELPAPGSPEMERAG	S	358	GSK3	NetPhos2.0 / NetPhosK
					-	DiPhos1.3
					CDK1/ 2/ 3/ 5	NetPhorest 2.0
393	401	LHRRTGRPS	T	397	PKC	NetPhos2.0 / NetPhosK
397	405	TGRPSGDGE	S	401	-	NetPhos2.0 / NetPhosK
					-	DiPhos1.3

Table 3.1 continued on next page

404	418	GEMPLGVSRSLHTARV	S	411	Other/IKK/IKKb	GPS 2.1
410	420	VSRLHTARVLV	T	415	PKC	NetPhorest 2.0
437	447	LRKRETQKFCL	T	442	PKC	NetPhorest 2.0
441	455	ETQKFCLTPRLSLQL	T	448	STE/STE7/MAP2K3	GPS 2.1
					STE/STE7/MAP2K7	GPS 2.1
					p38MAPK	NetPhos2.0 / NetPhosK
445	459	FCLTPRLSLQLYYIP	S	452	Aurora A (Baso_ST_kin)	ScanSite3
507	515	PSLDTSRV	T	511	-	NetPhos2.0 / NetPhosK
528	542	RMGTQPIYFQIYTVK	Y	535	TK/Trk/TRKB	GPS 2.1
					TK/Trk	GPS 2.1
535	545	YFQIYTVKIFF	T	540	PKC	NetPhorest 2.0
542	556	KIFFSDLSQDPTEDI	S	549	CKII/ DNAPK/ ATM	NetPhos2.0 / NetPhosK
					ATM/ ATR	NetPhorest 2.0
					ATM (DNA_dam_kin)	ScanSite3
569	583	KFPKDGFSRRRGVA	S	576	p38MAPK/ cdk5	NetPhos2.0 / NetPhosK
					-	DiPhos1.3
					CDK1/ 2/ 3/ 5	NetPhorest 2.0
					Cdc2/ Cdk5 (Pro_ST_kin)	ScanSite3
595	605	QKALLSHRPRE	S	600	PKC	NetPhorest 2.0
600	614	SHRPREVTVSLRATG ▲	T	607	AGC/AKT	GPS 2.1
					CAMK/DAPK	GPS 2.1
					CAMK/DAPK/DAPK3	GPS 2.1
					PKB (AKT)	NetPhorest 2.0
					AKT (Baso_ST_kin)	ScanSite3
604	614	REVTVSLRATG	S	609	PKC	NetPhos2.0 / NetPhosK
					PKC	NetPhorest 2.0
618	628	KAIPASDTEVS	S	623	CK2	NetPhorest 2.0
624	632	DTEVSGSSH	S	628	-	NetPhos2.0 / NetPhosK
626	634	EVSGSSHCP	S	630	cdc2	NetPhos2.0 / NetPhosK
644	658	TCLNVNVTEVVKSSN	T	651	STE/STE7/MAP2K2	GPS 2.1
659	673	LAGKFSSTVTNTFRT	T	666	CAMK/CAMKL/LKB	GPS 2.1
663	677	SFSTVTNTFRTNNIQ	T	670	AGC/PKB	GPS 2.1
					TKL/RAF	GPS 2.1
					PKC	NetPhorest 2.0
675	685	NIQIQRDQRL	S	680	ATM/ ATR	NetPhorest 2.0
690	704	LDKDDQRTFRDVVRF	T	697	STE/STE7/MAP2K3	GPS 2.1
					PKC	NetPhorest 2.0
745	756	LMPINTFSGIVQ***	S	750	TKL/MLK	GPS 2.1
					TKL	GPS 2.1

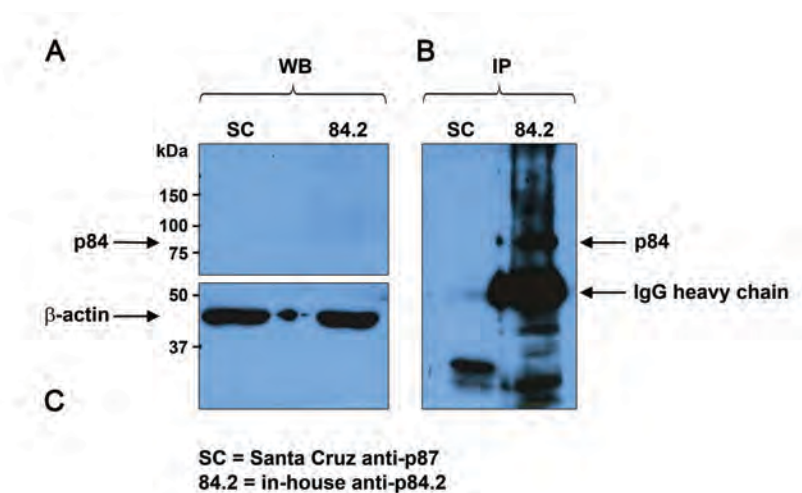
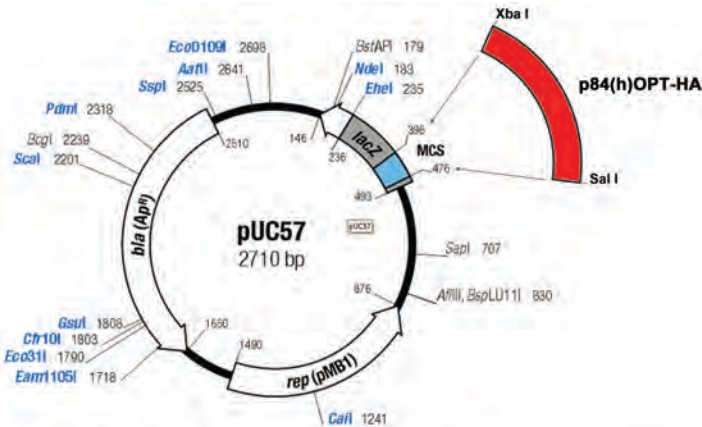


Figure 3.1: Assessing p84-specific antibodies.

Commercially available and in-house antibodies against p84 were tested by Western blot and immunoprecipitation methods to determine specificity and sensitivity against lysates prepared from MDA.MB.231 cells. (A) Western blot assessing the commercial p84 antibody from Santa Cruz (anti-p87^{PIKAP}) and an in-house anti-p84.2 antibody to detect p84 in total cell lysates. The position within the blot where p84 would be detected according to the molecular weight of p84 is designated (*arrow*). (B) Immunoprecipitation / Western blot analysis using Santa Cruz anti-p87^{PIKAP} and in-house anti-p84.2 antibodies to immunoprecipitate and detect p84 from cell lysates. Detection of p84 and immunoglobulin from immunoprecipitates are designated (*arrows*). (C) Control Western blot for β -actin of total cell lysates; detection of β -actin is designated (*arrow*).

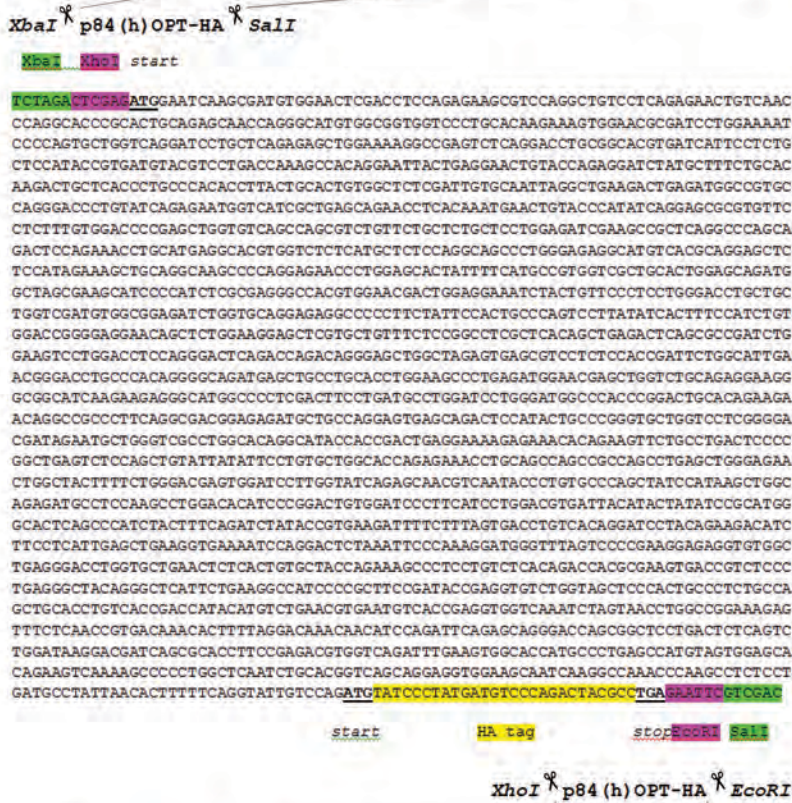
A



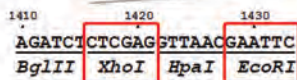
B



C



D



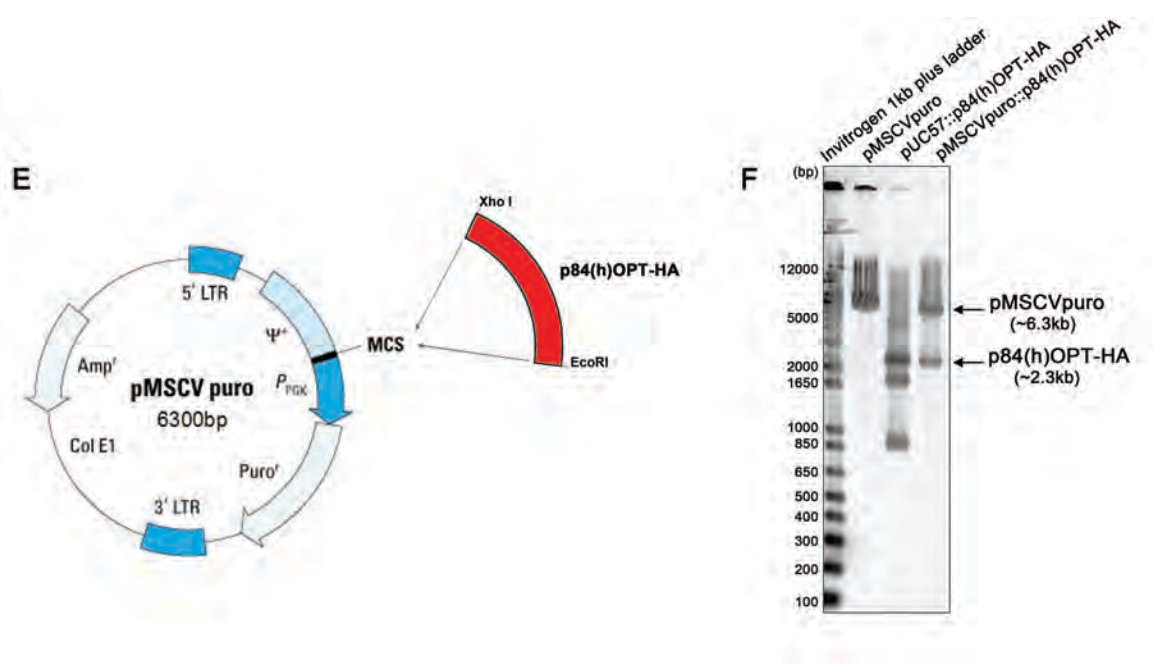


Figure 3.2: Generating a p84 expression construct with an HA fusion tag.

A codon-optimised sequence for human p84 with a C-terminal HA tag was synthesised in the pUC57 shuttle vector and subcloned into the retroviral expression vector pMSCV. (A) Plasmid map of shuttle vector pUC57 with p84(h)OPT-HA cloned into the multiple cloning site (XbaI/Sall). (B) MCS of PUC57. (C) Nucleotide sequence of p84(h)OPT-HA. (D) MCS of pMSCV. (E) Plasmid map of pMSCV with p84(h)OPT-HA cloned into the multiple cloning site (XhoI/EcoRI). (F) Restriction digest of parent pMSCV and subcloned pUC57-p84(h)OPT-HA and pMSCV-p84(h)OPT-HA vectors. pMSCV vector and p84(h)OPT-HA insert fragments are designated (*arrows*).

Intentionally blank

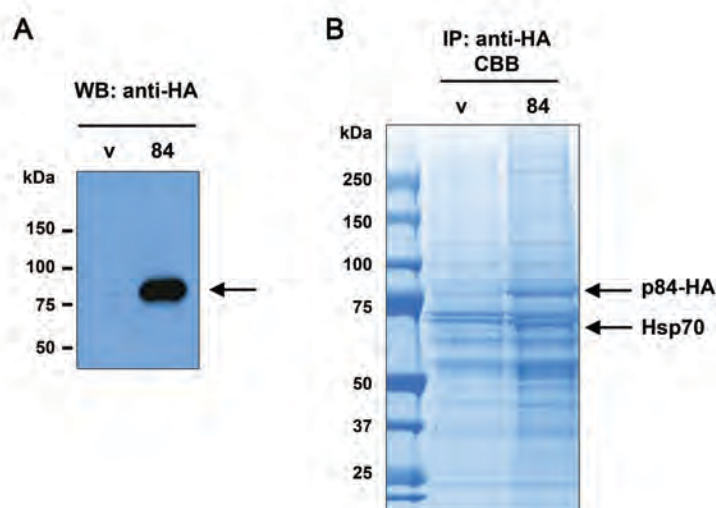


Figure 3.3: Transient expression of p84-HA in transfected MDA.MB.231 cells.

(A) The expression of p84-HA in MDA.MB.231 cells transfected with pMSCV-p84(h)OPT-HA was detected using HA-specific antibodies by Western blot analysis compared with the retroviral vector control. 50 μ g total protein lysates from vector control cells (v) and cells transfected to express p84-HA (84) were separated by LDS-PAGE, transferred to PVDF membrane using semi-dry transblot methods and p84-HA was detected using an anti-HA antibody at 1 : 10 000 dilution; detection of p84-HA is designated (*arrow*). (B) 2mg total protein lysates from vector control cells (v) and cells transfected to express p84-HA (84) were incubated with anti-HA antibody overnight and precipitated using Protein A coupled sepharose beads. Precipitated proteins were separated by LDS-PAGE and stained with Coomassie Brilliant Blue (CBB). Detection of p84-HA and co-precipitated Hsp70 are designated (*arrows*) and their identity confirmed by mass spectrometry.

Figure 3.4: Proteomic analysis of p84-HA precipitated from stimulated MDA.MB.231 cell lysates.

MDA.MB.231 cells transiently transfected with the vector control (v) or pMSCV-p84(h)OPT-HA were stimulated with 100ng/mL CXCL12 for 0-20 minutes. p84-HA was immunoprecipitated from total protein lysates using HA-specific antibodies, precipitates were separated by LDS-PAGE and stained with Coomassie Brilliant Blue. (A) p84-HA was identified by CBB staining (*upper panel*) and confirmed by Western blot analysis (*lower panel*). Protein bands representing p84-HA, Hsp70 and immunoglobulin are designated (*arrows*). p84-HA bands were excised and prepared for mass spectrometry to identify post-translational modifications within p84 induced with stimulation. Retrieved sequence coverage (%) of p84 protein is shown for (B) unstimulated, (C) 1 minute stimulation, (D) 5 minute stimulation, (E) 10 minute stimulation and (F) 20 minute stimulation samples; identified peptides are designated in *red*.

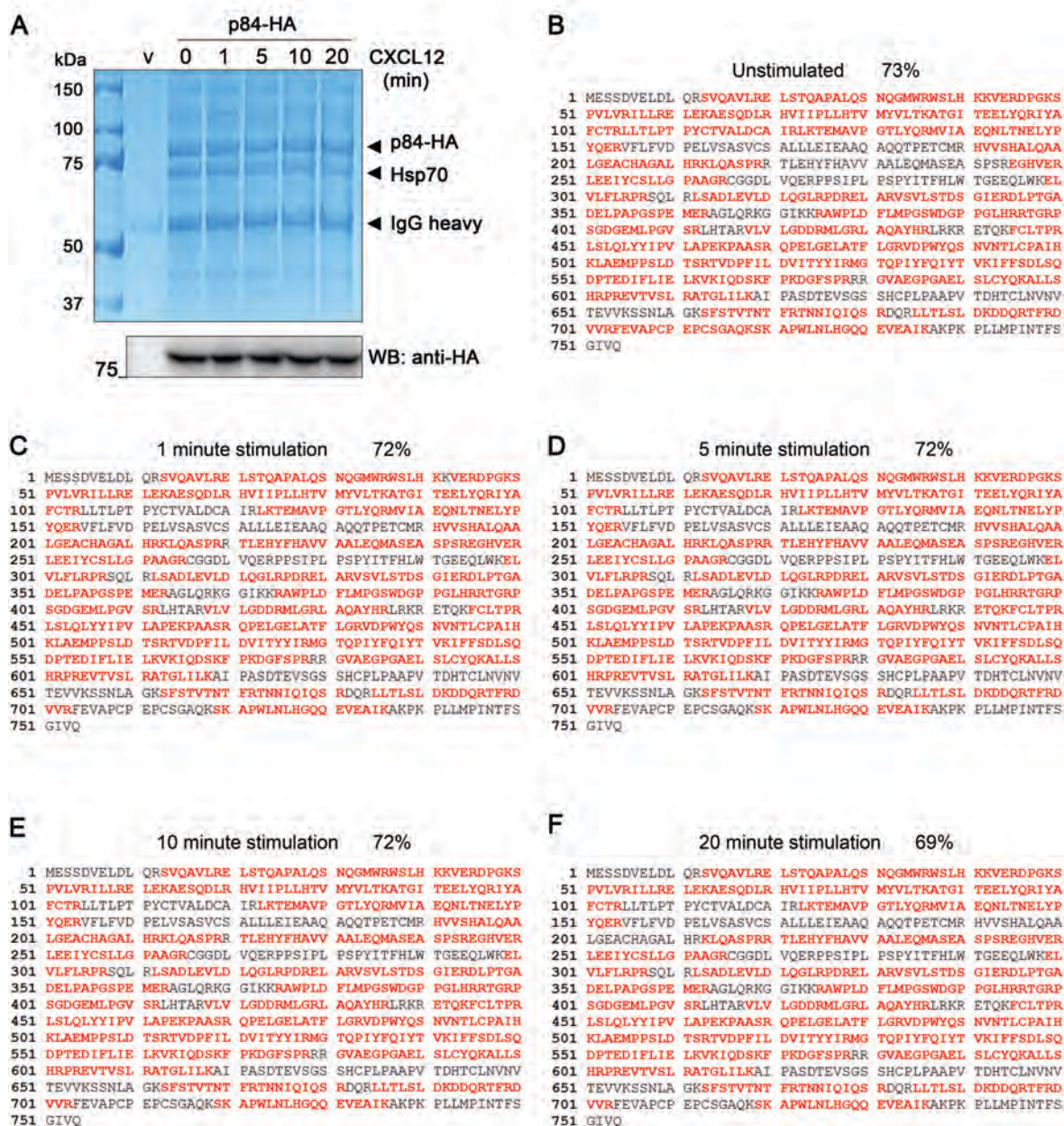


Table 3.2: Summary of post-translational modifications identified within p84.

p84-HA was immunoprecipitated from MDA.MB.231 cell lysates post stimulation with CXCL12 for 0-20 minutes. Peptide modifications included were phosphorylation, oxidation and methylation.

start	Peptide		Modification	Conditions
	end	sequence		
20	36	R.ELSTQAPALQSNQGMWR.W	Oxidation (M)	0 (Ions score 97); 1 (Ions score 85); 5 (Ions score 97); 10 (Ions score 106); 20 (Ions score 90)
71	86	R.HVIIPLLHTVMYVLT.K.A	Oxidation (M)	0 (Ions score 40); 1 (Ions score 44); 5 (Ions score 63); 10 (Ions score 36); 20 (Ions score 40)
123	136	R.LKTEMAVPGTLYQR.M	Oxidation (M)	0 (Ions score 72); 1 (Ions score 87); 5 (Ions score 73); 10 (Ions score 77); 20 (Ions score 77)
137	154	R.MVIAEQNLTNELPYQER.V	Oxidation (M)	0 (Ions score 102); 1 (Ions score 99); 5 (Ions score 79); 10 (Ions score 104); 20 (Ions score 68)
220	244	R.RTLEHYFHAVVAALQEMASEASPSR.E	Oxidation (M)	5 (Ions score 104); 10 (Ions score 23); 20 (Ions score 54)
345	363	R.DLPTGADELPA PGSPEMER.A	Oxidation (M)	0 (Ions score 113); 1 (Ions score 82); 5 (Ions score 99); 10 (Ions score 105); 20 (Ions score 97)
376	395	R.AWPLDFLMPGSWDGPPGLHR.R	Phospho (ST)	0 (Ions score 92); 1 (Ions score 24); 5 (Ions score 105); 10 (Ions score 43); 20 (Ions score 87)
397	412	R.TGRPSGDGEMLPVSR.L	Oxidation (M)	0 (Ions score 42); 1 (Ions score 61); 5 (Ions score 79); 10 (Ions score 67); 20 (Ions score 56)
418	429	R.VLVLGDDRMILGR.L	Oxidation (M)	0 (Ions score 57); 1 (Ions score 61); 5 (Ions score 59); 10 (Ions score 52); 20 (Ions score 59)
502	513	K.LAEMPPSLDTSR.T	Oxidation (M)	0 (Ions score 43); 1 (Ions score 44); 5 (Ions score 62); 10 (Ions score 47); 20 (Ions score 56)
529	542	R.MGTQPIYFQIYTVK.I	Oxidation (M)	0 (Ions score 61); 1 (Ions score 67); 5 (Ions score 61); 10 (Ions score 71); 20 (Ions score 69)
			Oxidation (M)	0 (Ions score 79); 1 (Ions score 84); 5 (Ions score 79); 10 (Ions score 79); 20 (Ions score 71)

Intentionally blank

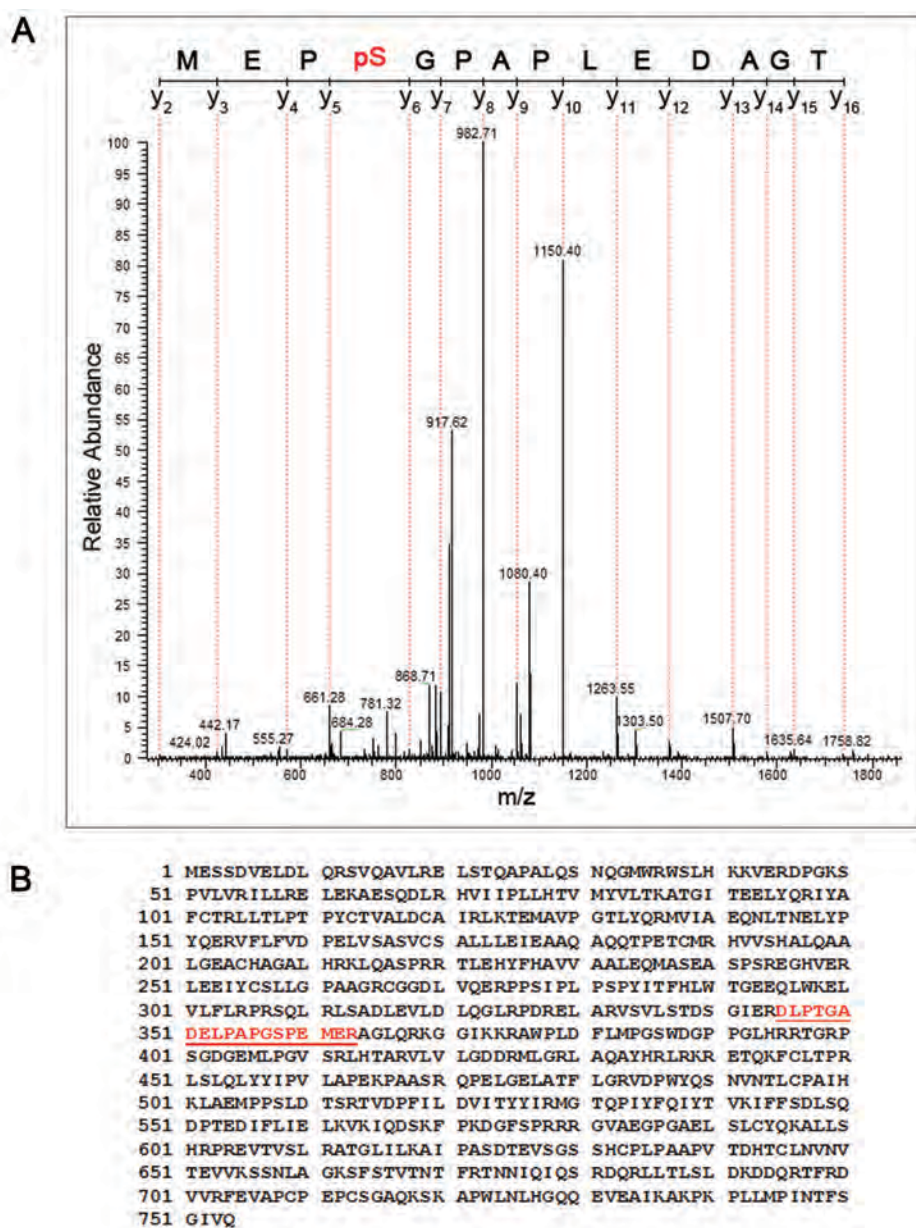
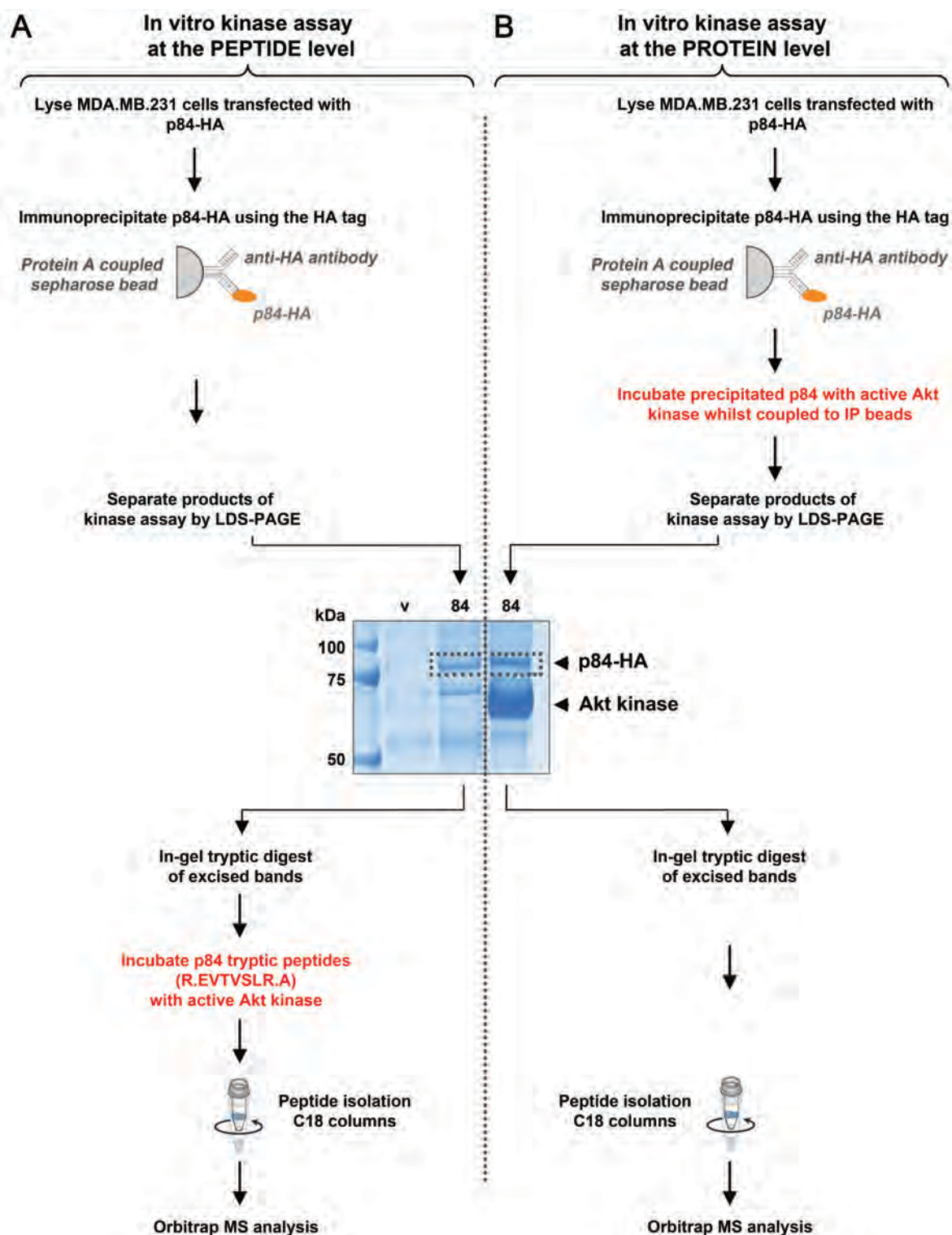


Figure 3.5: p84 is constitutively phosphorylated at Serine 358 (Ser358).

(A) MS/MS spectrum of identified p84 peptide (DLPTGADELPAAGSPEMER) demonstrates phosphorylation at Ser358; mass spectrometry of p84 immunoprecipitated from unstimulated and stimulated MDA.MB.231 cell lysates. (B) Amino acid sequence of p84; tryptic peptide encompassing Ser358 is designated (*red and underlined*).

Figure 3.6: Identifying Thr607 phosphorylation within p84 *in vitro*.

p84-HA was immunoprecipitated from transfected MDA.MB.231 cells and was incubated with active Akt kinase *in vitro* as either peptide substrates or full length protein. **(A)** Workflow for phosphorylation analysis for *in vitro* kinase assay at the peptide level; anti-HA precipitates were separated by LDS-PAGE, stained with Coomassie Brilliant Blue, and bands representing p84-HA (*highlighted by dotted lines*) were excised and digested with trypsin. Tryptic peptides were buffered and incubated with active Akt prior to isolation for mass spectrometry. **(B)** Workflow for phosphorylation analysis for *in vitro* kinase assay at the protein level; p84-HA precipitated using anti-HA was buffered and incubated with active Akt whilst bound to sepharose immunoprecipitation beads. Products from the kinase assay were denatured, separated by LDS-PAGE and stained with Coomassie Brilliant Blue. Bands representing p84-HA (*highlighted by dotted lines*) were excised, tryptic digest was performed and peptides were isolated for mass spectrometry.



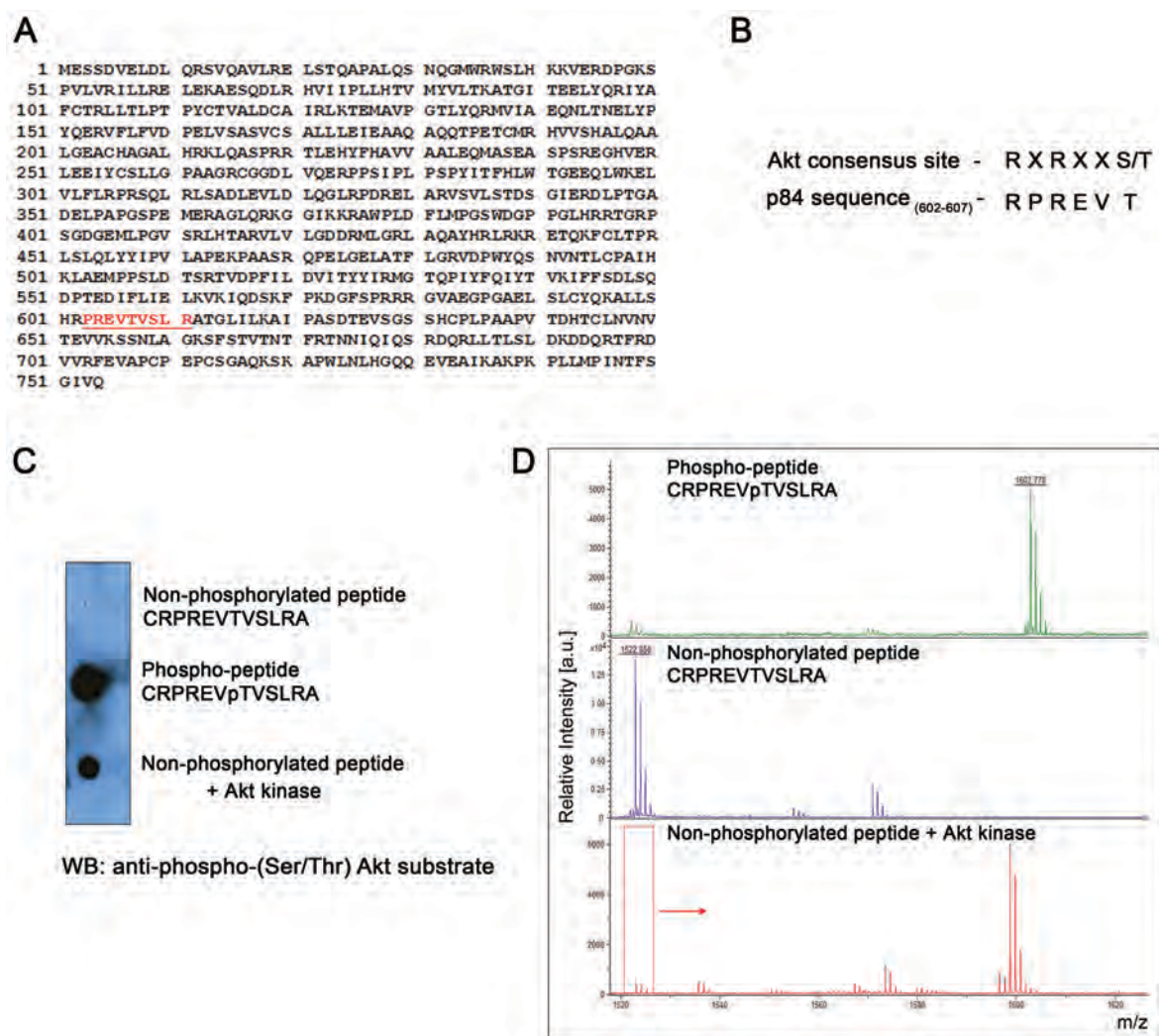


Figure 3.7: Thr607 is part of an Akt phosphorylation consensus site and can be phosphorylated by Akt kinase *in vitro*.

Phosphorylation of Thr607 was confirmed using an *in vitro* Akt kinase assay utilising synthetic p84 peptides. (A) p84 amino acid sequence; the tryptic peptide encompassing Thr607 is designated (*red and underlined*). (B) The residues surrounding Thr607 form an Akt phosphorylation consensus sequence (R.X.R.X.X.S/T). (C) Dot blot of control non-phosphorylated peptide, control phospho-peptide and non-phosphorylated peptide after incubation with active Akt kinase; phosphorylation at an Akt kinase phosphorylation consensus site (R.X.R.X.X.pS/T) was detected using a phospho-(Ser/Thr) Akt substrate antibody. (D) Mass spectrometry analysis of kinase assay products demonstrates phosphorylation on Thr607 after incubation of the non-phosphorylated peptide with Akt.

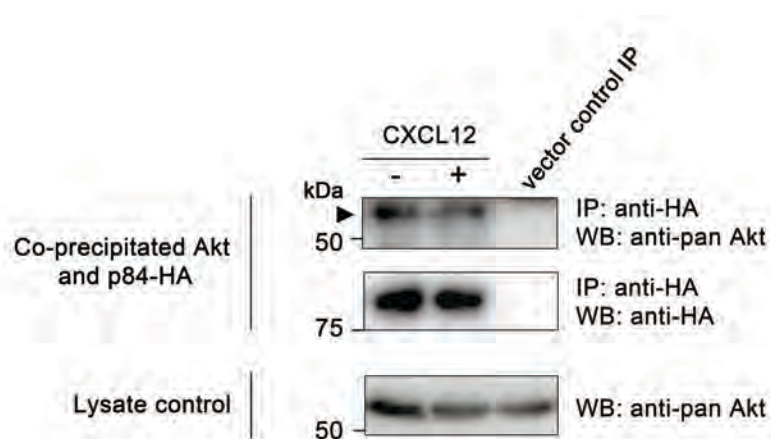


Figure 3.8: Akt interacts with p84.

Co-immunoprecipitation of Akt with p84 from stimulated (100ng/mL CXCL12 for 5 minutes) and unstimulated MDA.MB.231 cells transfected to express p84-HA. p84-HA was precipitated and detected using anti-HA, co-precipitated Akt was detected using anti-pan Akt (designated by *arrow*), in addition to the detection of total Akt using anti-pan Akt from total lysates as a loading control.

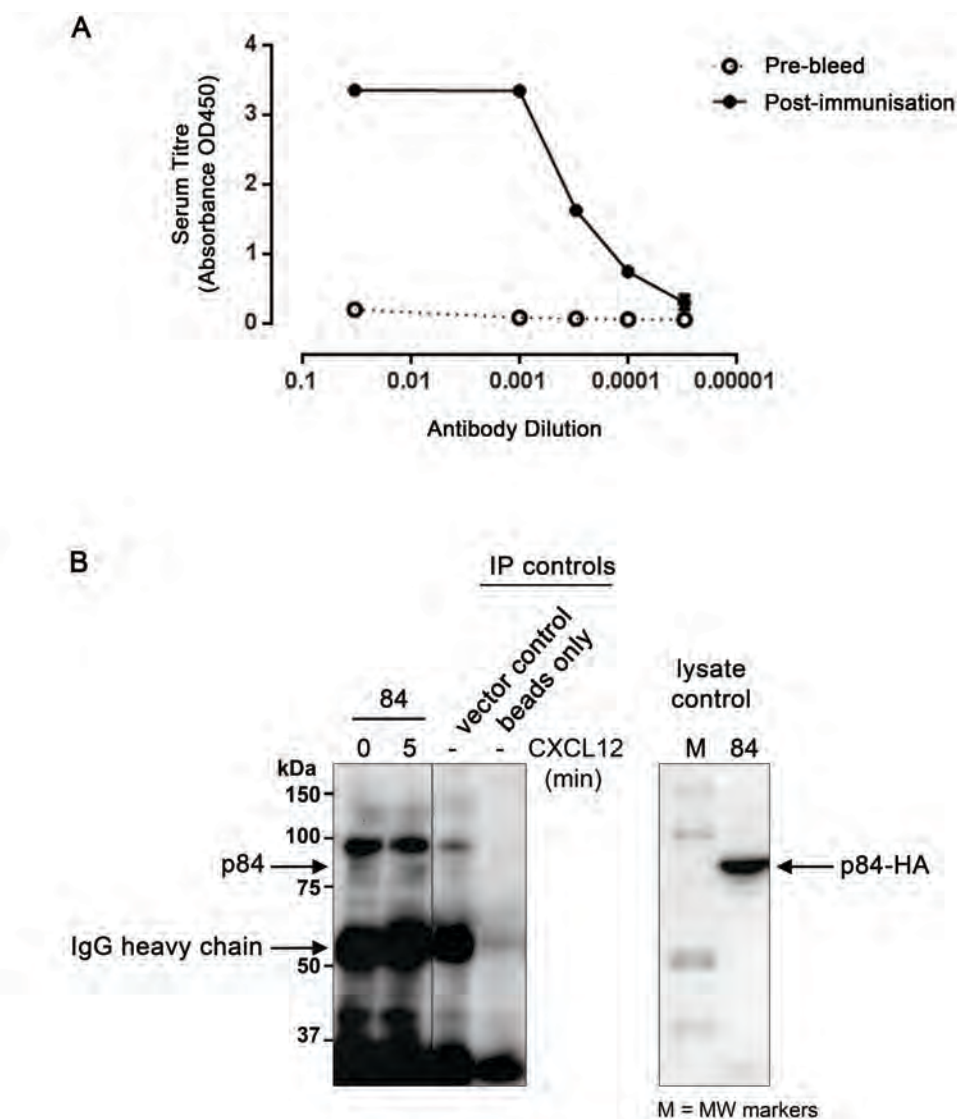


Figure 3.9: Generation of a phospho-specific p84 antibody (anti-p84-pThr607).

A phospho-specific antibody against p84 phosphorylated on Thr607 was generated by rabbit immunisation with a phospho-Thr607 p84 synthetic peptide (CRPREVpTVSLRA). (A) IgG immunoglobulin serum titres from rabbit bleeds harvested pre-immunisation and post-immunisation as determined by ELISA. (B) Immunoprecipitation and Western blot detection of p84 phosphorylated on Thr607 using the anti-p84-pThr607 antibody (*left panel*); MDA.MB.231 cells were transfected to overexpress p84-HA and stimulated for 0 or 5 minutes with 100ng/mL CXCL12; protein bands representing p84 and immunoglobulin are designated (*arrows*). The sensitivity and specificity of the anti-p84-pThr607 antibody (*left panel*) was compared with Western blot detection of p84-HA from total cell lysates where p84 was detected using the HA fusion tag (anti-HA) as a positive control (*right panel*).

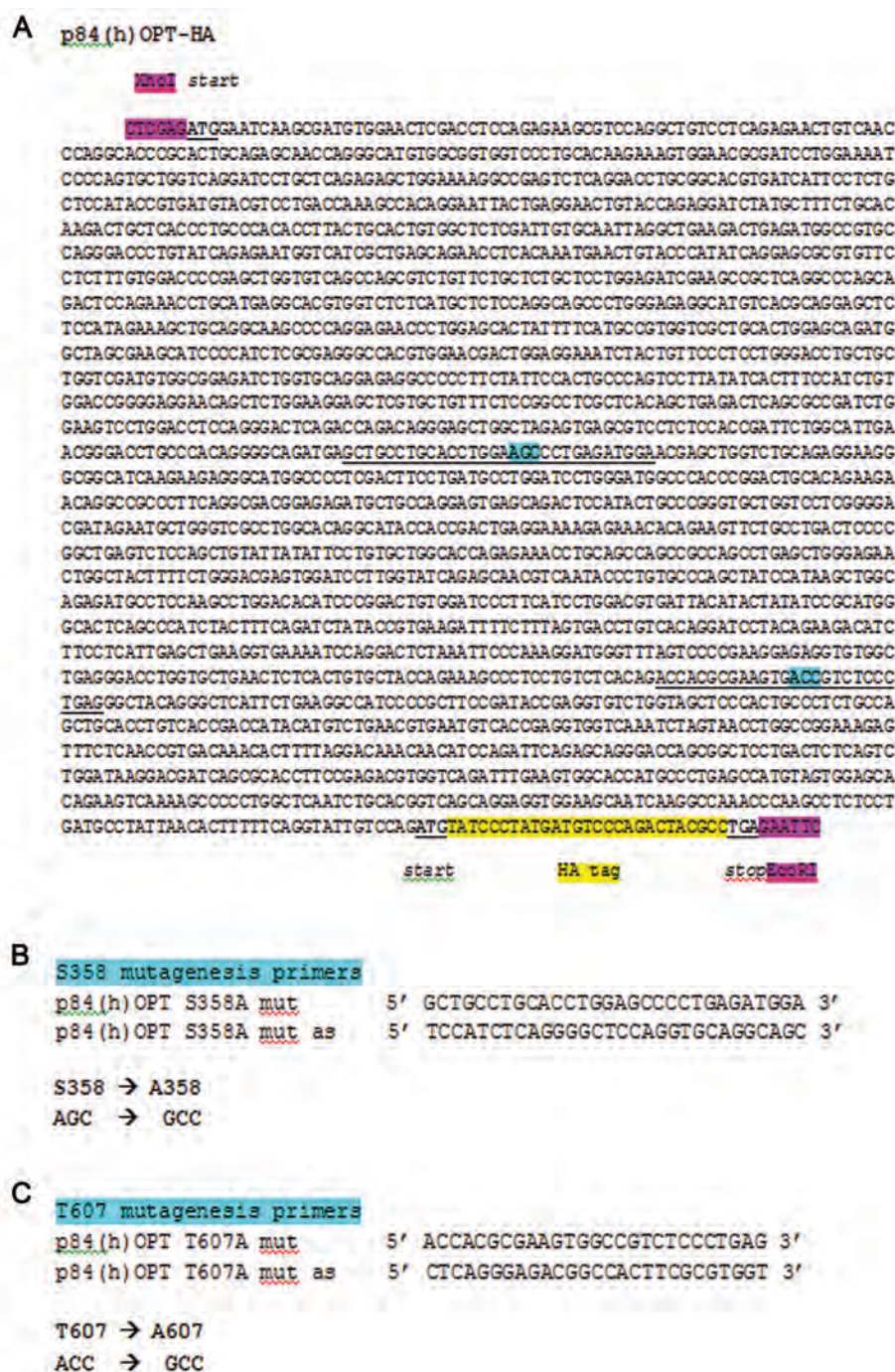


Figure 3.10: Site-directed mutagenesis of Ser358 and Thr607 residues.

pMSCV-p84-HA was modified by site-directed mutagenic PCR to mutate codons representing the putative phosphorylation sites Ser358 and Thr607 from serine/threonine to alanine (GCC codon). (A) Nucleotide sequence for p84-HA is shown with Ser358 and Thr607 target codons highlighted in *blue* and the mutagenic PCR primer targets surrounding these codons *underlined*. (B) Mutagenic primer sequences to mutate Ser358 AGC (serine) to GCC (alanine). (C) Mutagenic primer sequences to mutate Thr607 ACC (threonine) to GCC (alanine).

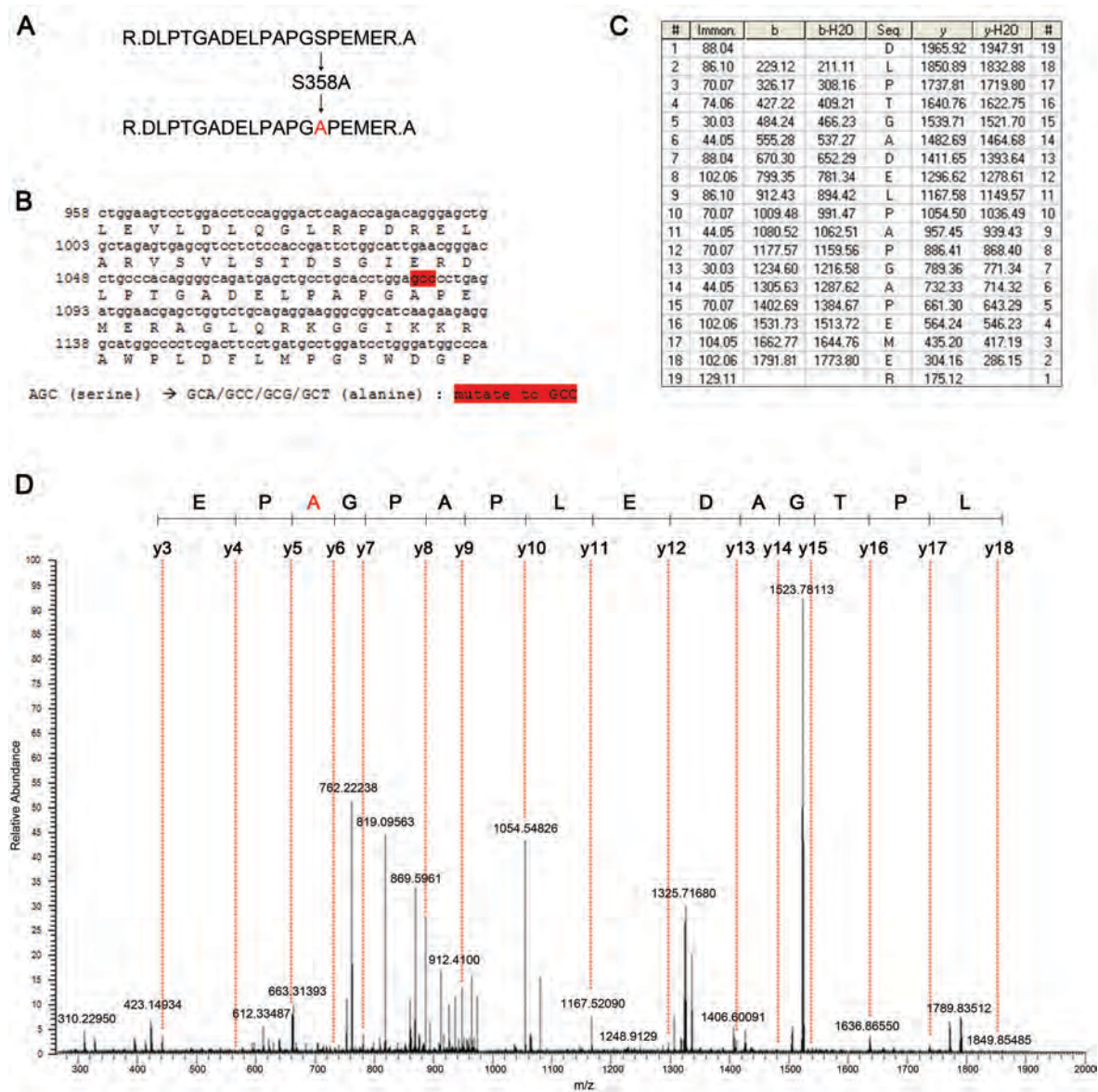


Figure 3.11: Validation of S358A and T607A mutations.

The mutated pMSCV-p84-S358A-HA and pMSCV-p84-T607A-HA expression vectors were validated at the sequence and protein expression levels. (A) The alanine mutation at position 358 (A358). (B) DNA sequencing of pMSCV-p84-S358A-HA confirms mutation to GCC alanine codon. (C, D) Proteomic analysis of p84-S358A-HA immunoprecipitated from MDA.MB.231 cells transfected with pMSCV-p8-S358A-HA confirms alanine mutation at position 358, as determined by mass spectrometry. (E) The alanine mutation at position 607 (A607). (F) DNA sequencing of pMSCV-p84-T607A-HA confirms mutation to GCC alanine codon. (G, H) Proteomic analysis of p84-T607A-HA immunoprecipitated from MDA.MB.231 cells transfected with pMSCV-p8-T607A-HA confirms alanine mutation at position 607, as determined by mass spectrometry.

E

R.PREVTVSLR.A
 ↓
 T607A
 ↓
 R.PREVAVSLR.A

G

#	Immon.	b	b-H2O	Seq	y	y-H2O	#
1	102.06			E	773.45	755.44	7
2	72.08	229.12	211.11	V	644.41	626.40	6
3	44.05	300.16	282.15	A	545.34	527.33	5
4	72.08	399.22	381.21	V	474.30	456.29	4
5	60.04	486.26	468.25	S	375.23	357.22	3
6	86.10	599.34	581.33	L	288.20		2
7	129.11			R	175.12		1

F

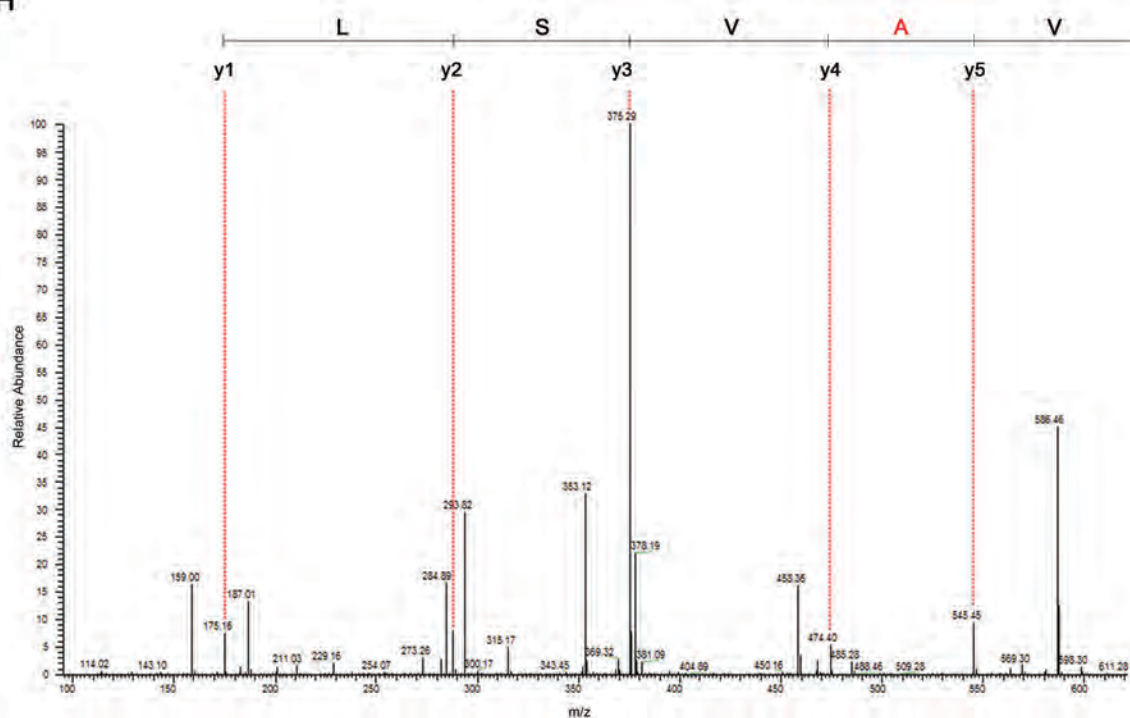
```

1723 ccaaaggatgggttagtccccgaaggagaggtgtggctgagga
      F K D G F S P R R R G V A E G
1768 cctgggtgctgaactctcactgtgctaccagaagccctcctgtct
      P G A E L S L C Y Q K A L L S
1813 cacagaccacgogaagtgcacgtctccctgagggctacagggctc
      H R P R E V A V S L R A T G L
1858 attctgaaggccatccccgcttccgataccgaggtgtctgtgtagc
      I L K A I P A S D T E V S G S
1903 tcccactgocctctgcccagctgcacctgtcaccgaccatacatgt
      S H C P L P A A P V T D H T C

```

ACC (threonine) → GCA/GCC/GCG/GCT (alanine) : mutate to GCC

H



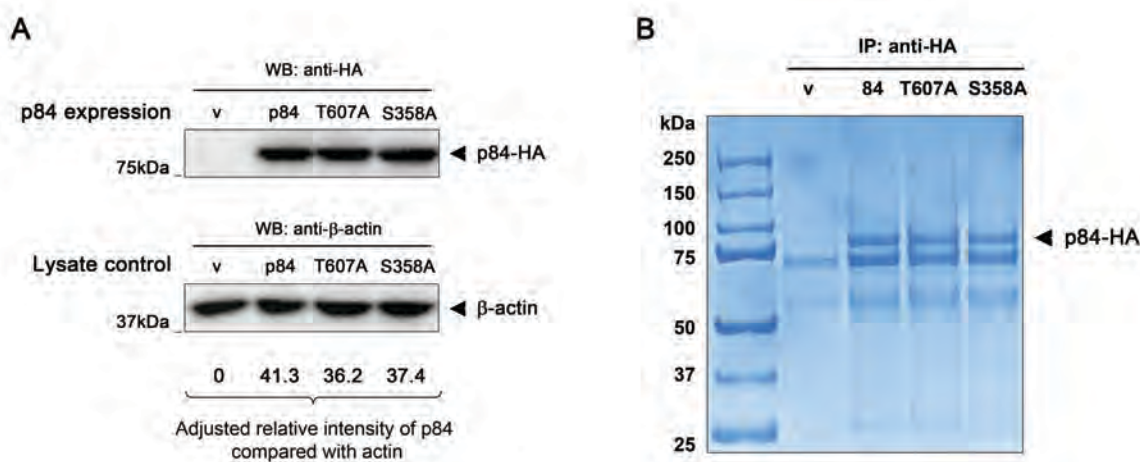


Figure 3.12: Stable transduction of MDA.MB.231 cells with p84 retroviral vectors.

MDA.MB.231 cells were transduced with pMSCV empty vector control (v), pMSCV-p84-HA (84), pMSCV-p84-S358A-HA (S358A) or pMSCV-p84-T607A-HA (T607A) retroviral expression vectors. (A) Equivalent expression of p84-HA, p84-S358A-HA and p84-T607A-HA proteins was confirmed by Western blot analysis of total protein lysates (20 μ g loaded per lane). p84 proteins were detected using anti-HA and compared relative to the expression of β -actin as a loading control, as designated (*arrows*). Densitometry was performed using ImageJ software to calculate the relative intensity of p84 compared with the loading control. (B) p84-HA, p84-S358A-HA and p84-T607A-HA proteins were immunoprecipitated from stable transduced cell lines using anti-HA (2mg total cell lysate), separated by LDS-PAGE and stained with Coomassie Brilliant Blue; isolations of p84 proteins are designated (*arrows*).

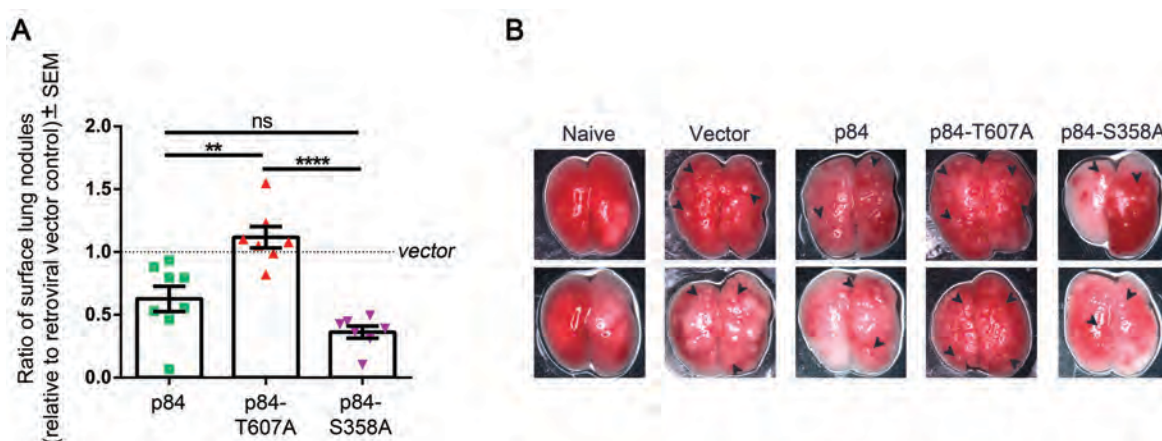


Figure 3.13: p84 expression limits the metastatic capability of MDA.MB.231 cells in a model of experimental haematogenous metastasis.

2×10^5 MDA.MB.231 cells transduced with pMSCV vector control, pMSCV-p84-HA, pMSCV-p84-S358A-HA or pMSCV-p84-T607A-HA vectors were injected intravenously into SCID mice. After 7 weeks lung lobes were separated and surface metastatic lung nodules were counted. **(A)** Ratio of surface lung nodules relative to retroviral vector control (*dotted line*); (n=7), t-test **p<0.01, ****p<0.0001. **(B)** Representative lung images; black arrows indicate examples of surface metastatic lung nodules.

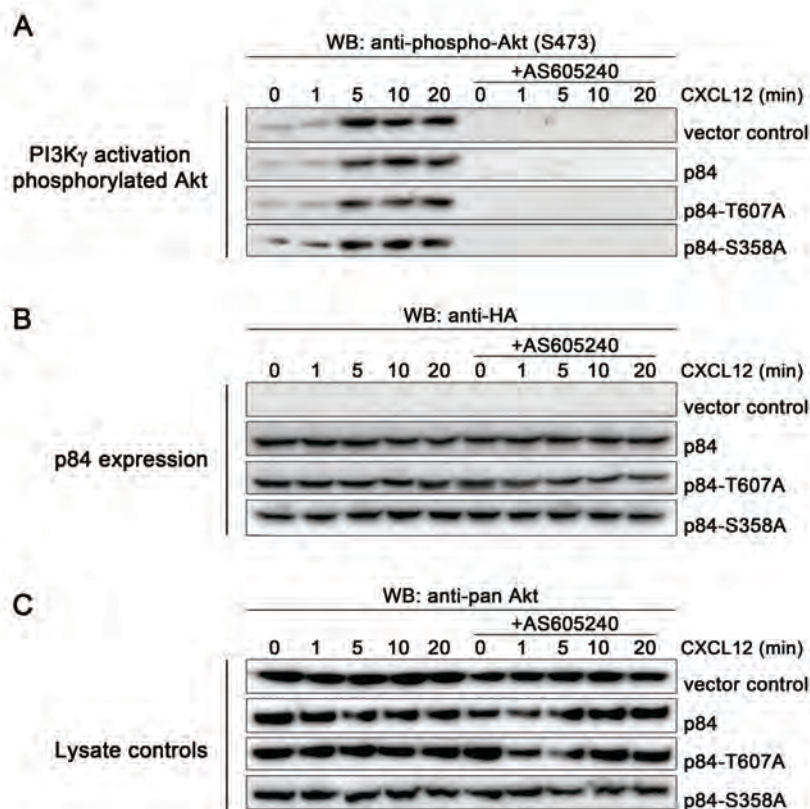


Figure 3.14: Expression of wildtype or mutant p84 proteins does not alter PI3K γ signal activation.

MDA.MB.231 cells transduced with control, pMSCV-p84-HA, pMSCV-p84-S358A-HA, or pMSCV-p84-T607A-HA expression vectors were stimulated with 100ng/mL CXCL12 for 0-20 minutes in the absence or presence of AS605240 to induce PI3K γ signalling, as measured by the induction of phosphorylated Akt. Western blot analysis of 20 μ g cell lysates was used to detect (A) p-Akt (S473), (B) p84 proteins using anti-HA and (C) total Akt as a protein loading control. Representative blot shown.

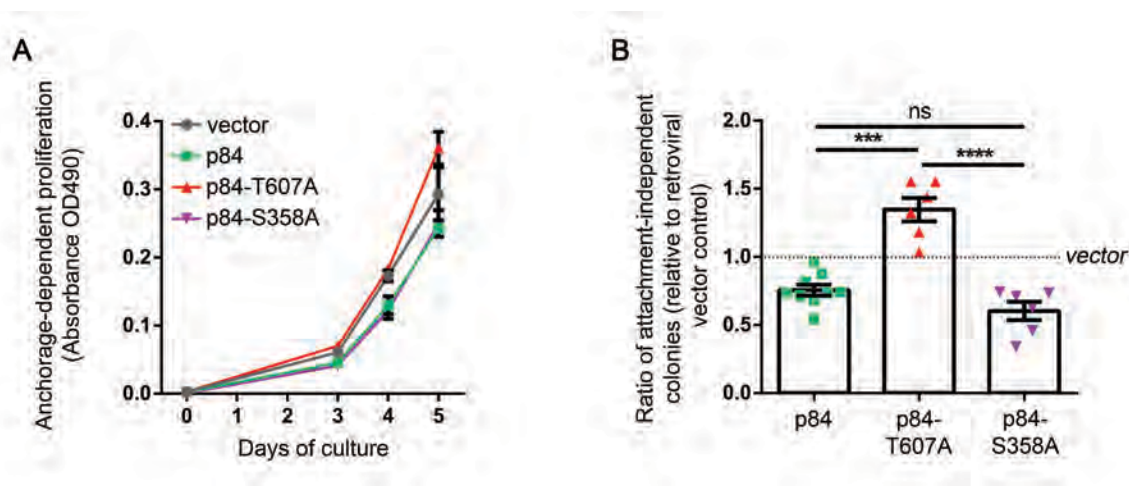


Figure 3.15: Expression of p84 does not alter cell proliferation but affects attachment-independent colony formation of MDA.MB.231 cells *in vitro*.

MDA.MB.231 cells transduced with pMSCV vector control, pMSCV-p84-HA, pMSCV-p84-S358A-HA or pMSCV-p84-T607A-HA vectors were assessed for growth properties. **(A)** An XTT/PMS assay was used to determine the rates of cell proliferation where transduced MDA.MB.231 cells were grown in continuous culture and redox activity was measured on days 0, 3, 4 and 5 of growth; (n=4). **(B)** Transduced MDA.MB.231 cells were assessed for the ability to form spherical cell colonies in bactoagar when cultured for 2 weeks from single cells; plotted as ratio relative to the retroviral vector control cell line (*dotted line*); (n=6), t-test ***p<0.005, ****p<0.001.

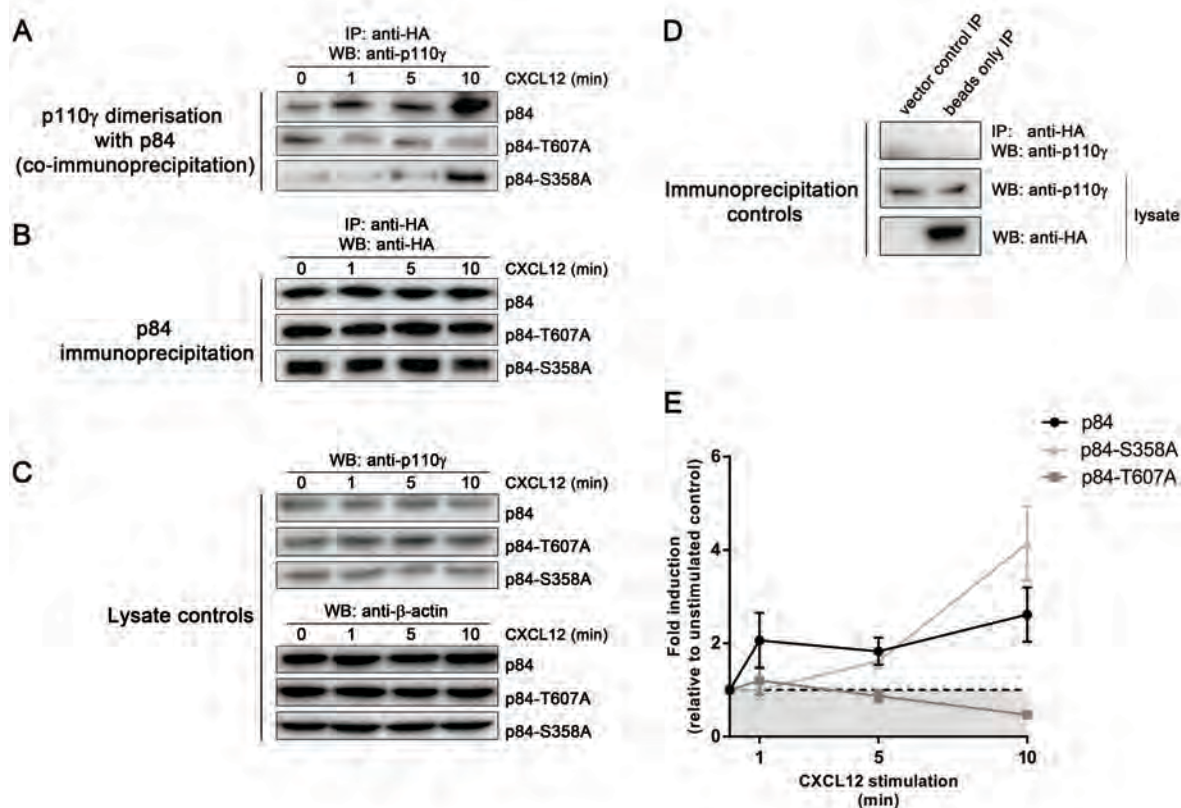


Figure 3.16: p84 forms an inducible heterodimer with p110 γ upon CXCL12 stimulation that is dependent on Thr607.

MDA.MB.231 cells transduced with pMSCV vector control, pMSCV-p84-HA, pMSCV-p84-S358A-HA or pMSCV-p84-T607A-HA vectors were stimulated with 100ng/mL CXCL12 for 0-20 minutes to activate PI3K γ signalling. Wildtype and mutant p84 proteins were immunoprecipitated from total cell lysates using an HA-specific antibody and precipitates were analysed by Western blot. **(A)** Detection of p110 γ (co-precipitated with p84-HA), as a measure of p84/p110 γ heterodimerisation. **(B)** Detection of immunoprecipitated p84. **(C)** Detection of total p110 γ and β -actin from cell lysates were included as loading controls. Representative blot shown. **(D)** Quantitation of p110 γ co-precipitation as a measure of p84/p110 γ heterodimerisation from 3 independent experiments calculated as fold-induction; densitometry performed using ImageJ.

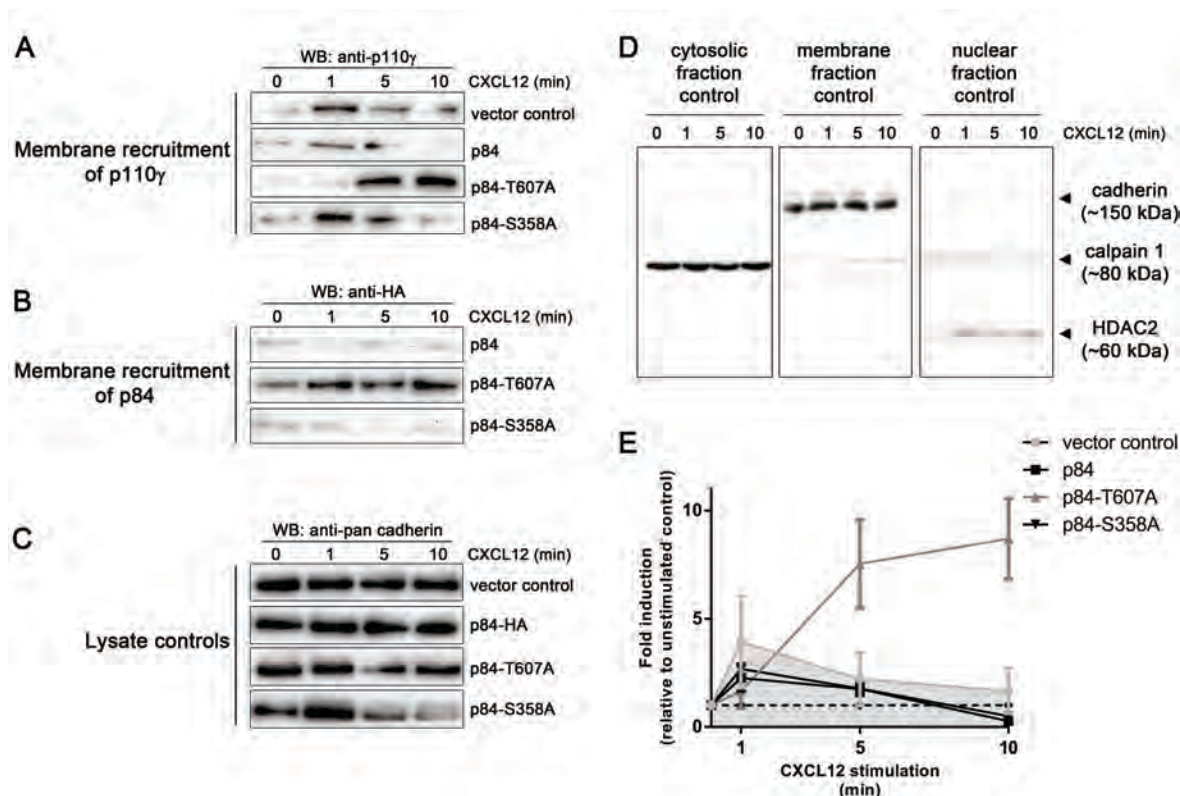
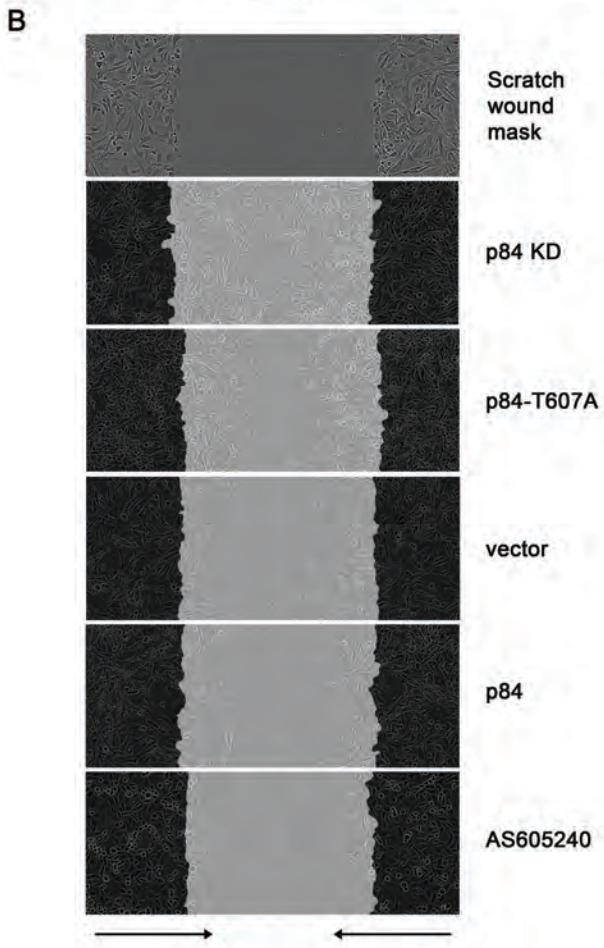
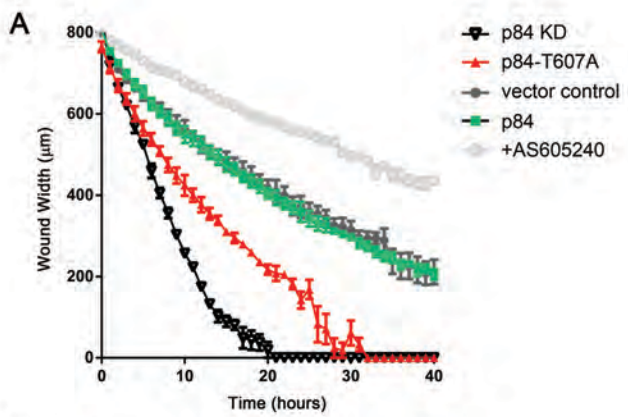


Figure 3.17: Recruitment of p110 γ to the membrane is transient and is not affected by the expression of wildtype p84.

MDA.MB.231 cells transduced with pMSCV vector control, pMSCV-p84-HA, pMSCV-p84-S358A-HA or pMSCV-p84-T607A-HA vectors were stimulated with 100ng/mL CXCL12 for 0-10 minutes to activate PI3K γ signalling. Cells were lysed and the membrane (plasma and endosomal) fraction of the protein lysate was isolated by subcellular fractionation for Western blot analysis. **(A)** Detection of endogenous p110 γ within the membrane fraction. **(B)** Detection of p84 proteins within the membrane fraction using anti-HA. **(C)** Detection of total cadherin was included as a membrane fraction loading control. Representative blot shown. **(D)** Membrane fraction controls; detection of calpain 1 (cytosolic), cadherin (membrane) and HDAC2 (nuclear) proteins; representative blots shown. **(E)** Quantitation of membrane-localised endogenous p110 γ from 3 independent experiments calculated as fold-induction; densitometry performed using ImageJ.

Figure 3.18: MDA.MB.231 cells transduced to express mutant p84-T607A are functionally similar to p84 knockdown cells in a model of PI3K γ -dependent migration.

MDA.MB.231 cells transduced with pMSCV vector control, pMSCV-p84-HA, pMSCV-p84-T607A-HA vectors or the p84 expression knockdown construct pLKO.1shp84 were assessed for directional migration in an Incucyte migration assay. Transduced cells were grown to 90% confluence, incubated with Mitomycin C for 2 hours and then were scratched to create a wound of defined width. PI3K γ dependence was demonstrated by the incubation of wildtype MDA.MB.231 cells with AS605240. **(A)** Rate of cell migration to colonise the scratch wound imaged in real time; (n=3). **(B)** Representative images of wound closure at 20 hours.



Chapter 4: Generating and
characterising a novel p84-deficient
mouse (C57Bl/6 $Pik3r6^{-/-}$)

Chapter 4: Generation, screening and characterisation of a novel p84-deficient mouse (C57Bl/6 *Pik3r6*^{-/-})

4.1 Introduction

The functional roles of PI3K γ , both kinase-dependent and -independent, have for the most part been elucidated using the genetically-modified p110 γ and p101 subunit-deficient mouse strains (p110 γ ^{-/-}, p110 γ ^{KD/KD} and p101^{-/-}). These tools have been invaluable in characterising the functions of PI3K γ signalling in the development, activation and directed cell migration of haematopoietic cells during homeostasis and immune responses (refer to sections 1.6.2 and 1.6.3). However to this point, detailed information regarding the specific role of p84 in PI3K γ signalling and the contribution of p84 to PI3K γ -dependent functions, such as immune cell development and migration have been lacking in the absence of a p84-deficient mouse model. The lack of a p84 knockout mouse has been the most significant limitation holding back research into the role of p84. Therefore, in the present study, CRISPR gene-editing technology was employed to generate a novel p84-deficient mouse (C57Bl/6 *Pik3r6*^{-/-}). Access to CRISPR technology (detailed in Introduction section 1.7) only became available at the commencement of the last year of PhD candidature, therefore the generation and screening of the *Pik3r6*^{-/-} mouse was conducted at a late stage of the project. For this reason, an initial characterisation of the *Pik3r6*^{-/-} mouse was completed to as much detail as possible within the time constraints of the project. The data presented in Chapter 4 represent the generation, screening and initial characterisation of the *Pik3r6*^{-/-} mouse, which has allowed the identification of novel p84-dependent roles within immune cell function.

4.2 Results

4.2.1 Targeting *Pik3r6* using CRISPR gene-editing technology

Genome-editing using CRISPR technology involves the direct injection of CRISPR guide RNA (gRNA) constructs and Cas9 nuclease mRNA transcript components into murine zygotes harvested from impregnated females (reviewed in ^{198, 210}). Within the single fertilised cell, the CRISPR gRNA complexes with Cas9 nuclease through the tracrRNA region and guides the nuclease to the CRISPR gene target via complementary binding interactions. Binding of the CRISPR:Cas9 complex to the genomic target induces the double-stranded cleavage of the target by Cas9 nuclease and leads to the introduction of insertion/deletion mutations through error-prone non-homologous end joining DNA repair pathways (refer to section 1.7 for further detail). A strategy to target *Pik3r6* using CRISPR technology was designed to mediate Cas9 cleavage of a target region within the first exon of *Pik3r6*. **Figure 4.1** depicts the locus (**A**) and exon structure (**B**) of *Pik3r6* on murine chromosome 11, where the CRISPR target region within exon 1 of *Pik3r6* is shown with the complementary guide RNA sequence (**C**). A schematic of the CRISPR:Cas9 interaction with the target sequence is presented in **Figure 4.1 (D)**. The *Pik3r6*-targeted gRNA construct in conjunction with Cas9 components (synthesised by Toolgen) were injected into C57Bl/6n zygotes and implanted into pseudo-pregnant surrogate females. Each successfully implanted zygote that survived through development would potentially carry individual CRISPR-induced mutations within each allele of *Pik3r6* exon 1. Two CRISPR injection/implantation rounds were completed, which resulted in the birth of 25 *Pik3r6*-targeted CRISPR pups in communal litters of 10 and 15 (*Pik3r6* CRISPR #1-10 and #11-25), as depicted in **Figure 4.2**.

4.2.2 Screening CRISPR-induced mutations within *Pik3r6* exon 1

A PCR screening approach was designed and optimised to amplify the region surrounding *Pik3r6* exon 1 and the CRISPR target region (**Figure 4.3 (A)**) in order to verify CRISPR-induced mutations. PCR primers (p84 screen F and p84 screen R) were designed to amplify a 300bp product (**Figure 4.3 (A)**) and were tested for their efficiency by PCR of control C57Bl/6 wildtype DNA using Dynazyme (ThermoScientific) and MyTaq (Bioline) polymerase systems with two different annealing temperature gradients, as shown in **Figure 4.3 (B, C)**. Amplification using Dynazyme polymerase with an annealing temperature of 65°C was found to be optimal, as determined by the sharpest amplification product observed at approximately 300bp in **Figure 4.3 (C) dotted box**. Therefore, these conditions were employed for all further PCR amplifications for screening of *Pik3r6* exon 1. Following amplification, the 300bp PCR screen product was manually excised from the gel and purified for sequencing.

Pik3r6 CRISPR pups #1-25 born from the two zygote injection/implantation rounds (refer to Figure 4.2) were tail-tipped upon weaning as a source of genomic DNA for CRISPR-induced mutation screening. Tail-tips were digested and DNA was isolated for CRISPR screening PCR, described above, to amplify the 300bp region flanking *Pik3r6* exon 1 and the CRISPR target site. The screening PCR products for each of the 25 pups were purified and segregated into two aliquots; an aliquot for direct DNA sequencing and an aliquot that was used to subclone the product into the pGEM-Teasy vector for further sequencing; collectively to reveal the mutational changes to the CRISPR target. DNA sequencing was performed using Big Dye sequencing PCR and the p84 screen F primer, followed by processing at the SA Pathology Sequencing Centre. Cloning of a single PCR amplification unit into pGEM-Teasy and the sequencing of single clones allowed the discrimination between alleles. The mutational changes identified for *Pik3r6* CRISPR pups #1-25 are

depicted by sequence alignments between WT DNA [Query] and *Pik3r6* CRISPR pup DNA [Sbjct] (*upper*) with mutations highlighted in red, and associated sequence chromatograms (*lower*) in **Figure 4.4 (A-Y)**. In cases where more than 2 sequences are presented, such as *Pik3r6* CRISPR #3 and #19, it was concluded that these animals were mosaic. Mosaic animals are generated when the direct injection of CRISPR components is performed at a stage when the fertilised zygote has already undergone one cycle of division, rather than injection at the single cell stage, hence multiple alleles are available for CRISPR-editing. As expected based on the targeting strategy presented in Figure 4.1, the majority of mutations induced by *Pik3r6*-targeted CRISPR editing were within, or immediately 5' to the CRISPR target site within exon 1 of *Pik3r6* (**Figure 4.4**). Furthermore, the efficiency of mutation in the present study was found to be very high with mutation achieved in 24 of the 25 pups (**Figure 4.4**). This is a far superior mutation rate than previously reported for conventional genetic-modification techniques in embryonic stem cells^{200, 205}.

By analysing the CRISPR-induced mutations to *Pik3r6*, it was observed that Δ -10bp deletions were prominent amongst the multi-nucleotides mutations. One common mutation observed immediately 5' of the CRISPR target site, AAACCC Δ -10bp deletion, was identified to result in a frame-shift event that would bring a stop codon into frame, thereby ceasing translation and leading to the production of a truncated non-sense p84 protein. This mutation, if bred to homozygosity, would therefore result in a p84-deficient animal. For this reason, *Pik3r6* CRISPR pups #7 (F), #12 (M) and #22 (F) that each carried AAACCC Δ -10bp deletions on a single allele were retained for breeding as a trio, in order to select and maintain the desired AAACCC Δ -10bp mutation to homozygosity. Unfortunately pup #25 (F) that carried AAACCC Δ -10 deletions on both alleles could not

be utilised for breeding purposes as it died due to unknown causes shortly after weaning. The pups born from the aforementioned AAACCC Δ -10bp #12 (M), #7 (F) and #22 (F) breeding trio were screened for *Pik3r6* alleles using the same PCR screening approach described previously and were used to replace initial breeders until the *Pik3r6* AAACCC Δ -10bp mutation was selected to homozygosity. The resultant line was named C57Bl/6 *Pik3r6*^{-/-}.

4.2.3 Targeting *Pik3r6* with TALEN gene-editing technology and screening of TALEN-induced mutations

A second gene-editing technique, Transcription Activator-Like Effector Nuclease-based genome editing (TALEN), was also employed to generate mutations within *Pik3r6* exon 1. Customised TALEN constructs act in pairs and are composed of multiple linked TAL effector polypeptides that form a DNA-binding domain coupled to a FokI nuclease protein. Each polypeptide has a set of common repeat residues with two variable di-residues specific to a nucleotide within the TALEN target. By linking polypeptides (defined by the specific TALE code to target a corresponding nucleotide sequence), customised TALENs allow the targeted editing of any genomic sequence (reviewed in ^{211, 212})(refer to section 1.7 for further detail). The TALEN strategy to target exon 1 of *Pik3r6* is presented in **Figure 4.5**, where the TALEN target site is shown within exon 1 in (A) and annotated in (B). A schematic representation of the TAL effector polypeptide binding and TALE di-residue code is depicted in **Figure 4.5 (C)**. Like CRISPR-targeting described in the previous section, genome targeting using TALEN technology requires the direct injection of TALEN pairs into zygotes, which are subsequently implanted into pseudo-pregnant surrogate females. A single round of TALEN injection/implantation was completed, which resulted in the birth of 7 *Pik3r6*-targeted TALEN pups (#26-32). An identical PCR screening approach (previously described for CRISPR-induced mutation screening) was

utilised to screen the *Pik3r6*-targeted TALEN pups. The mutational changes identified for *Pik3r6* TALEN pups #26-32 are depicted by sequence alignments between WT DNA [Query] and *Pik3r6* TALEN pup DNA [Sbjct] (*upper*) with mutations highlighted in red, and associated sequence chromatograms (*lower*) in **Figure 4.6 (A-G)**. The mutations induced within *Pik3r6* by TALEN-targeting were less frequent and less pronounced than those observed for CRISPR-targeting, where only one mutation involved the deletion of more than 2 nucleotides (*Pik3r6* TALEN #32) and many WT alleles were maintained. Therefore, it was concluded that for the present study, CRISPR-targeting of *Pik3r6* was more effective than TALEN-targeting and efforts to generate a p84-deficient mouse using TALEN-targeting were not pursued.

4.2.4 Characterising large CRISPR-induced deletions flanking the target site

It was observed anecdotally at the South Australian Genome-Editing facility (SAGE) that larger deletions to areas outside, but immediately flanking the CRISPR target site could also be introduced as a result of CRISPR component injection (*unpublished observations*). Larger mutations such as these to these areas outside the *Pik3r6* target site would not have been detected by the PCR screening method described in Figure 4.3. Therefore, in order to detect larger deletions within *Pik3r6* of CRISPR-targeted pups #1-25, a supplementary screening PCR was developed to amplify a larger 1.7kb region surrounding exon 1 using p84 CRISPRlong F and p84 CRISPRlong R primers, as shown in **Figure 4.7 (A)**. Genomic DNA samples from *Pik3r6* CRISPR pups #1-25 were then re-screened to reveal further deletions, which were identified by polyacrylamide gel electrophoresis for *Pik3r6* CRISPR pups #1, #5, #7, #16 and #20, as presented in **Figure 4.7 (B)**, where PCR products carrying larger deletions are defined by red arrows. PCR fragments encompassing larger deletions (smaller product bands) were excised, purified and analysed by Big Dye sequencing PCR to identify the deletions. Deletions were found to range between Δ -266bp and Δ -800bp and

were present both 5' and 3' to the CRISPR target region, as depicted in **Figure 4.8**. Of note, *Pik3r6* CRISPR #7 carried a Δ -266bp deletion and was one of the animals used for breeding of the p84-deficient line described in section 4.2.2 (C57Bl/6 *Pik3r6*^{-/-}). However, the desired AAACCC Δ -10bp deletion mutation and the larger undesired Δ -266bp deletion mutation were found to be carried on separate alleles. Therefore, with the thorough screening of female #7 offspring, the desired AAACCC Δ -10bp mutation was maintained and the Δ -266 mutation was eliminated by selective breeding.

Taken together, the data presented in sections 4.2.1 - 4.2.4 describe the successful generation of a novel p84-deficient mouse (C57Bl/6 *Pik3r6*^{-/-}) using CRISPR gene-editing technology. The generation of this genetically-modified strain to a homozygous line was achieved in a total of 9 months following zygote injection with CRISPR *Pik3r6*-targeting components. This represented a significantly reduced time investment relative to the time required for traditional embryonic stem cell mutagenesis techniques for genetic modification. *Pik3r6*^{-/-} pups were found to be born at normal male:female Mendelian ratios and no obvious developmental defects were observed. All *Pik3r6*^{-/-} mice utilised for experiments presented in this study were genotyped to confirm the CRISPR-induced (Δ -10bp) deletion to exon 1 of *Pik3r6*.

4.2.5 PI3K γ subunit expression in *Pik3r6*^{-/-} tissues

The expression of p110 γ , p101 and p84 PI3K γ subunits were assessed in lymphoid tissues of *Pik3r6*^{-/-} mice relative to wildtype C57Bl/6 controls at the transcript and protein levels. The stability of p101 and p84 adaptor proteins has been shown to be affected by the deletion of the p110 γ catalytic subunit^{4, 121}, however the effect of p84 adaptor deletion on endogenous p110 γ and p101 expression has not yet been examined. Quantitative PCR

analyses of p84, p101 and p110 γ levels in lymph node and thymus tissue samples from *Pik3r6*^{-/-} and wildtype mice showed no difference in the transcript expression of p84, p101 or p110 γ , as depicted in **Figure 4.9 (A-C)**. Although *Pik3r6*^{-/-} mice have been generated to lack functional p84 at the protein level, mRNA transcribed from *Pik3r6* was expected to be present, albeit in a modified form (AAACCC Δ -10bp) indistinguishable from the wildtype message as detected by the qPCR primers used for this assay (**Figure 4.9 (A)**). The expression of an *in silico* predicted mRNA transcript for p84, named *Pik3r6* X1, was also assessed in these samples. The *Pik3r6* X1 variant is predicted to have an alternate splice pattern (relative to variant 1) that does not include exon 1, therefore would not be affected by the CRISPR-induced AAACCC Δ -10bp deletion within exon 1 and the transcribed mRNA would thereby result in the translation of the truncated p84 X1 protein. However, as shown in **Figure 4.9 (D)**, negligible expression of the X1 variant transcript was detected.

Protein expression of p84 was assessed in the spleen, lymph nodes, thymus and bone marrow of *Pik3r6*^{-/-} mice compared with wildtype counterparts by targeted Parallel Reaction Monitoring (PRM) mass spectrometry, which was utilised due to the absence of a reliable p84 antibody with which to detect endogenous p84 from tissue samples. PRM is a highly sensitive form of targeted mass spectrometry that allows the relative quantification of selected peptides. During a PRM run, peptides are targeted for fragmentation and detection using their observed precursor ion mass within the mass spectrometer, taking into account the mass and charge of the peptides (known as m/z). During PRM analysis, data is matched back to a spectral library containing previously acquired fragmentation spectra of the peptides of interest ensuring specificity, and area under the curve measurements are calculated for the detected fragment ions. Sensitivity is achieved in the technique by

targeting and fragmenting only specific masses of interest. As expected, selected p84 peptides were not detected (above background noise) in tissue samples from *Pik3r6*^{-/-} mice, whereas p84 peptides were readily identified from wildtype tissue samples (representative PRM plots are shown in **Figure 4.10 (A)**). This confirmed the successful protein knockout of p84 in these mice.

Consistent with comparable mRNA transcript levels, the protein expression of p101 and p110 γ subunits detected in lymph node (**B**) and thymus (**C**) tissue lysates were found to be proportionate, with some variation existing within both wildtype and *Pik3r6*^{-/-} grouped samples, as determined by Western blot analysis in **Figure 4.10**. Collectively, these data suggest that the expression and stability of p101 and p110 γ proteins are not dependent on p84.

4.2.6 Lymphoid organ development in *Pik3r6*^{-/-} mice

The newly-generated *Pik3r6*^{-/-} mice were first characterised in the context of immune cell biology. PI3K γ subunit-deficient mice have previously been established to exhibit defects in immune cell development and activation (refer to Table 1.2)³³. Specifically, functional roles for PI3K γ have been described for mast cell activation downstream of adenosine receptor stimulation^{121, 126}, for the migration of thymocytes during developmental stages in the thymus^{114, 157, 222} and for the trafficking of neutrophils and lymphocytes in models of inflammation^{7-9, 130}. Although PI3K γ as an enzyme complex has been implicated in the above processes, the requirement of p84 for these functions is unknown. Therefore, the role of p84 was investigated in these PI3K γ -dependent systems by comparing *Pik3r6*^{-/-} and wildtype animals (C57Bl/6n; sourced from the Waite Animal Facility) to determine the effect of p84 deletion at homeostasis and during immune responses. Unfortunately,

wildtype littermate controls that would have been the preferred control animals for experiments presented in this study were not available due to the time constraints.

Total animal weight and weights of selected lymphoid organs of 6-8 week-old male mice $\text{Pik3r6}^{-/-}$ mice relative to wildtype control animals were compared at homeostasis. **Figure 4.11** demonstrates that the weights of naïve $\text{Pik3r6}^{-/-}$ mice are comparable to wildtype controls, as determined by the total animal weight (**A**) and weights of the spleen (**B**), inguinal lymph nodes (**C**) and the thymus (**D**). The proportions of immune cell subsets were then assessed in the spleen, lymph nodes and blood of $\text{Pik3r6}^{-/-}$ and wildtype mice by flow cytometry for naïve and activated CD4^+ and CD8^+ T lymphocytes, B lymphocytes and neutrophils. No significant differences were observed in the proportions of any of these cell subsets between $\text{Pik3r6}^{-/-}$ and wildtype animals, as shown in **Figure 4.12** for the spleen (**A-D**), lymph node (**E-H**) and blood (**I-K**), suggesting that $\text{Pik3r6}^{-/-}$ animals maintain normal lymphoid organ development and cell differentiation at homeostasis.

4.2.7 Reduced PI3K γ signal activation in $\text{Pik3r6}^{-/-}$ bone marrow-derived cells

The role of p84 in immune cell development and function was then assessed in a range of cellular contexts. Firstly, the effect of p84 deletion on PI3K γ activation in $\text{Pik3r6}^{-/-}$ bone marrow cells was assessed to determine whether PI3K γ signalling was altered by loss of p84. It has been previously shown that both p84 and p101 adaptors can mediate p110 γ translocation to the membrane and the activation of lipid-kinase signalling^{6, 11, 130}, indicating a degree of functional redundancy between the adaptor proteins. However, deletion of p101 results in reduced but not ablated PI3K γ activation (as determined by the induction of phosphorylated Akt and recruitment of GFP-tagged PH domains)^{5, 87}, which indicates that p84 cannot completely compensate for the loss of p101 expression. In the

present study, in order to investigate the individual requirement of p84 in PI3K γ signal activation, bone marrow cells were isolated and stimulated with IL-8 (CXCL8) to induce PI3K γ signalling downstream of CXCR2. IL-8 was chosen as a stimulant as it is a potent activator of neutrophils and neutrophils were determined to be the predominant immune cell subset present in the bone marrow of 8-10 week old male mice used (*data not shown*). The induction of phosphorylated Akt (p-Akt) in response to IL-8 was determined by Western blot analysis of bone marrow lysates as a measure of PI3K γ activation. Wildtype bone marrow cells were found to exhibit transient p-Akt induction in response to IL-8 stimulation, as demonstrated by strong protein bands present after 1 minute of stimulation (**Figure 4.13 (A) upper panel**). In contrast, bone marrow cells isolated from *Pik3r6*^{-/-} mice showed only very low levels of p-Akt that could not be induced by IL-8 stimulation (**Figure 4.13 (A) lower panel**). This suggests that p84 is crucial for the activation of PI3K γ signalling and the induction of p-Akt in neutrophils, and that the loss of p84 expression cannot be compensated for by p101. The level of total Akt was detected as a control and was shown to be equivalent across all lysate samples (**Figure 4.13 (B) upper and lower panels**).

4.2.8 The effect of p84 deletion on bone marrow-derived mast cell maturation and function

Unlike other immune cells, mast cells are the only haematopoietic cell type reported to express a single adaptor, p84, in conjunction with p110 γ ^{121, 124}. The absence of p101 protein expression in mast cells has been documented following Western blot analysis of mast cell lysates¹²¹ and therefore all characterised PI3K γ -dependent processes in these cells have been presumed to dependent on p84^{28, 29, 121}. Therefore the effect of p84 deletion was assessed in bone marrow-derived mast cells (BMMC) and it was hypothesised that the

phenotype of p84-deficient mice would mimic the mast cell defects observed in the $p110\gamma^{-/-}$ mouse.

Bone marrow cells were harvested from 5 week-old female $Pik3r6^{-/-}$ and wildtype control mice and mast cells were selectively cultured *in vitro* in the presence of IL-3 for 6 weeks. The maturity of cultured mast cells was assessed at 5.5 weeks by May-Grunwald Giemsa staining and flow cytometry for c-kit and FcεRI maturity cell surface markers. As shown in **Figure 4.14**, both wildtype and $Pik3r6^{-/-}$ BMBC displayed mature granular phenotypes as determined by May-Grunwald Giemsa staining (**A**) and were found to be greater than 90% c-kit⁺ FcεRI⁺ mature mast cells as determined by flow cytometric staining (**B, C**). Genomic DNA and total protein was extracted from cultured $Pik3r6^{-/-}$ BMBCs to confirm CRISPR-induced mutation (AAACCCΔ-10bp deletion) within exon 1 of *Pik3r6* and absent p84 protein expression relative to wildtype counterparts, using previously optimised PCR and PRM mass spectrometry screening techniques (described in sections 4.2.2 and 4.2.5). DNA sequencing confirmed that each of the four $Pik3r6^{-/-}$ BMBC cultures carried the AAACCCΔ-10bp deletion within *Pik3r6* exon 1 compared with wildtype cultures that maintained the wildtype genomic sequence, as depicted in representative chromatograms presented in **Figure 4.14 (D)** and protein knockout of p84 expression was confirmed by PRM proteomic analyses of $Pik3r6^{-/-}$ BMBC cultures compared with wildtype BMBC culture samples (*data not shown*).

$Pik3r6^{-/-}$ mice were then assessed in two functional assays to determine the effect of p84 deletion on PI3Kγ-dependent processes in BMBCs; β-hexaminidase release and the secretion of IL-6, in the presence of the GPCR agonist adenosine. These assays measure the degranulation response and cytokine secretion induced by activation, respectively,

where both assays are well-established indicators of mast cell functionality^{29, 121}. Adenosine signalling through the adenosine A3 receptor (A3AR) is known to potentiate the degranulation response in BMDCs²⁹. Since p84 has been reported to be the solely expressed adaptor protein responsible for mediating PI3K γ signalling in BMDC^{121, 124}, it was hypothesised that deletion of p84 would result in the loss of adenosine-mediated potentiation of mast cell degranulation. In the present study, *Pik3r6*^{-/-} and wildtype BMDCs were sensitised overnight with anti-DNP IgE, then incubated in the presence of adenosine prior to DNP antigen-mediated activation to induce degranulation. The extent of BMDC degranulation was measured by the degree of β -hexaminidase release into the culture supernatant. Consistent with previous reports, data produced in the present study confirmed that adenosine stimulation during DNP antigen activation of wildtype BMDC resulted in the potentiation of degranulation, as measured by increased β -hexaminidase release in the presence of DNP and adenosine compared with DNP alone (**Figure 4.15 (A) *third and fourth columns***). This adenosine-induced potentiation of degranulation was confirmed to be PI3K γ -dependent as shown by the ability of AS605240 treatment to prevent this potentiating effect (**Figure 4.15 (A) *fifth column***). Contrary to the hypothesis, the adenosine-mediated potentiation of degranulation was observed to be equivalent in *Pik3r6*^{-/-} BMDC as in wildtype BMDCs, as demonstrated by an equivalent increase in β -hexaminidase release in the presence of DNP and adenosine compared with DNP alone (**Figure 4.15 (A) *eighth and ninth columns***). These data suggest that p84 is not required for the PI3K γ -dependent potentiation of BMDC degranulation induced by adenosine.

A similar phenotype between *Pik3r6*^{-/-} and wildtype BMDCs was observed for the adenosine-mediated potentiation of IL-6 secretion from DNP antigen-stimulated BMDC. Specifically, like β -hexaminidase release, *Pik3r6*^{-/-} BMDCs exhibited indistinguishable

potentiation of IL-6 secretion from wildtype BMMCs in the presence of adenosine, as shown in **Figure 4.15 (B)** by ELISA. Collectively, these data indicate that PI3K γ signalling downstream of adenosine/A3AR stimulation is independent of p84 in $\text{Pik3r6}^{-/-}$ BMMC, which is contrary to hypothesised p84/p110 γ signalling mechanisms described for these cells¹²¹.

The expression of p101 in wildtype and $\text{Pik3r6}^{-/-}$ BMMCs was therefore investigated in the presence of adenosine to determine whether p101 expression had been induced to compensate for the absence of functional p84. Whilst very low, p101 mRNA transcript expression could be detected in wildtype BMMC, which was not affected by the presence of adenosine (**Figure 4.16**). Interestingly, the transcript expression of p101 in $\text{Pik3r6}^{-/-}$ BMMCs was found to be significantly up-regulated upon incubation with adenosine (45 minute stimulation), relative to unstimulated $\text{Pik3r6}^{-/-}$ BMMC and wildtype BMMCs, shown in **Figure 4.16**. This result provides evidence first that BMMCs express low levels of p101 and secondly, that p101 expression is regulated in p84-deficient BMMCs presumably to compensate for the absence of p84. Furthermore, these data represent the first description of PI3K γ adaptor subunit compensation as a mechanism of PI3K γ signal regulation in mast cells. Although not the main goal of these experiments, to extend these findings, the protein expression of p101 in adenosine-stimulated $\text{Pik3r6}^{-/-}$ BMMCs was examined to determine whether the increased mRNA transcript levels were reflected at the protein level. Although p101 could be weakly detected by IP/Western blot of adenosine-stimulated $\text{Pik3r6}^{-/-}$ BMMCs (*data not shown*), insufficient amounts of protein and time constraints prevented experimental replication and therefore, these data will need to be confirmed.

4.2.9 Thymocyte development is unaltered in *Pik3r6*^{-/-} mice

PI3K γ has been shown to be involved in the control of thymocyte survival and development. Previous studies have shown that p110 γ ^{-/-} thymocytes display defects in the number and proportion of double positive (CD4⁺CD8⁺) immature transitional precursors, compared with wildtype littermates, which was determined to be due to an inability of cells to respond to adenosine pro-survival signals¹¹⁴. A separate study revealed that p101 is required for PI3K γ signalling downstream of CXCR4 during β -selection in the thymus using the p101-deficient mouse¹⁵⁷. However, the specific contribution of p84 during thymocyte development, if any, has yet to be determined. Therefore, in the present study, the effect of p84 deletion on the proportion and number of various thymocyte subpopulations was examined by flow cytometry. The thymi of 6-7 week-old male *Pik3r6*^{-/-} and wildtype mice were analysed for CD4⁺ and CD8⁺ mature single-positive (SP), CD4⁺CD8⁺ immature double-positive (DP) and double-negative (DN1-4) intermediaries. Flow cytometric analyses of these cell populations demonstrated that thymocyte development occurred independently of p84, as determined by comparable proportions (**Figure 4.17**) and numbers (*data not shown*) of SP, DP (**A, B**) and DN1-4 (**C, D**) populations between *Pik3r6*^{-/-} and wildtype thymi. This suggests that PI3K γ -dependent signalling during thymocyte development is dependent on p101-mediated PI3K γ activity and that p84 is redundant during this process.

4.2.10 Neutrophil migration is inhibited by the loss of p84 in *Pik3r6*^{-/-} mice

In addition to immune cell development, another major function of PI3K γ signalling is during the induction of leukocyte chemotaxis in response to GPCR agonists. During inflammatory responses, neutrophils require the rapid activation of PI3K γ signalling pathways in order to respond to inflammatory mediators and traffic to sites of infection.

Consistent with this, $p110\gamma^{-/-}$ neutrophils display significantly inhibited migration towards chemokine gradients *in vitro*⁷ and $p110\gamma^{-/-}$ mice exhibit reduced neutrophil accumulation during *in vivo* infection models^{8, 24, 114, 145}. The role of p84 in neutrophil chemotaxis was assessed in the present study in response to IL-8 stimulation of $Pik3r6^{-/-}$ and wildtype neutrophils. The bone marrow of male 6-8 week-old mice was used as a source of neutrophils. It was found that wildtype bone marrow comprised approximately 52% neutrophils, as defined by forward and side scatter parameters and $CD11b^{+} Gr-1^{+}$ staining as presented in **Figure 4.18** (*representative plot in (A) and proportion (B)*). In contrast, $Pik3r6^{-/-}$ mice displayed a modest reduction in the proportion of $CD11b^{+} Gr-1^{+}$ bone marrow neutrophils relative to wildtype controls (**Figure 4.18 (A, B)**). Total bone marrow cells were subjected to a transwell chemotaxis assay, where the migration of cells was assessed in response to the neutrophil agonist IL-8 for 30 minutes. The migrated cell population was analysed by flow cytometry (as gated in **Figure 4.18 (C)**) and normalised using unlabelled flow cytometry beads (shown by the gated population in the upper left of **(C)**). $Pik3r6^{-/-}$ neutrophils showed significantly reduced ability to respond and migrate towards IL-8 gradients in comparison to wildtype cells (**Figure 4.18; gated in lower panel of (C) and presented as normalised chemotactic index in (D)**). These data demonstrate that p84 is required for the effective migration of neutrophils, an effect that could not be compensated for by p101.

4.2.11 $Pik3r6^{-/-}$ mice are protected from EAE disease

Directed cell migration is crucial for the induction of immune responses, both in the activation and differentiation of effector cells within secondary lymphoid organs and their trafficking to inflammatory sites. Experimental autoimmune encephalomyelitis (EAE) is a murine inflammatory autoimmune model that mimics the priming and effector phases of

the human condition, multiple sclerosis^{170, 171}. PI3K γ has been implicated in both the priming of pathogenic Th1 and Th17 cells in the spleen in response to neuropeptide/CFA immunisation and also in the trafficking of these activated cells into the central nervous system during EAE, where they potentiate inflammation, resulting in damage to the neuronal sheaths of oligodendrocytes and symptoms of ascending paralysis^{9, 139}. In the present study, the contribution of p84 to PI3K γ -dependent processes during EAE was assessed in *Pik3r6*^{-/-} mice compared with wildtype counterparts. In response to the induction of MOG₃₅₋₅₅-induced chronic EAE, disease severity was found to be significantly inhibited in *Pik3r6*^{-/-} mice relative to wildtype controls, where *Pik3r6*^{-/-} mice were completely protected from hind limb paralysis, as shown by the measure of clinical disease score in **Figure 4.19** (refer to Table 2.3 for EAE clinical disease scoring). Reduced disease severity in *Pik3r6*^{-/-} mice was coupled with a significant reduction in the number and proportion of Th cells that had infiltrated the CNS, relative to wildtype animals (**Figure 4.20 (A, E)**). The proportion and number of CNS-infiltrating Th1 (CD4⁺ IFN- γ ⁺) cells was significantly reduced (**B, F**), however whilst the number of CNS-infiltrating Th17 (CD4⁺ IL-17⁺) cells was minimal in *Pik3r6*^{-/-} mice (**G**), these data were not statistically significant. Although, it is important to mention that 3 wildtype mice did not respond to immunisation or develop disease, which was reflected by corresponding low numbers of CNS-infiltrating cells (**Figure 4.20**). No significant difference in the proportion or number of regulatory T lymphocytes was observed in the CNS of *Pik3r6*^{-/-} and wildtype mice (**Figure 4.20 (D, H)**). Consistent with ameliorated disease symptoms and reduced infiltration of Th cells into the CNS, *Pik3r6*^{-/-} mice also showed a significant reduction in the number of neutrophils that had accumulated in the inflamed CNS relative to wildtype animals, as shown in **Figure 4.20 (I, J)**. Collectively, the observed reduction of immune cell infiltrate

into the CNS of EAE-diseased $\text{Pik3r6}^{-/-}$ mice is consistent with reduced disease severity and protection from paralysis compared with EAE disease observed in wildtype animals.

The reduction in the number of CNS-infiltrating activated cells was not due to a deficiency in priming of activated Th1 and Th17 cells in secondary lymphoid organs. Although modest differences in the proportion of Th subsets were observed in the spleen between $\text{Pik3r6}^{-/-}$ and wildtype mice, no significant differences in the number of Th1 or Th17 activated cells were identified within the spleen, **Figure 4.20 (K-M, O-Q)**, or lymph nodes (*data not shown*). In comparison to inflammatory Th cells, an increased proportion and number of regulatory T cells were observed in the spleen of $\text{Pik3r6}^{-/-}$ mice relative to wildtype controls, although this was not reflected in the CNS (**Figure 4.20 (N, R) and (H)**).

Considering that $\text{Pik3r6}^{-/-}$ mice were shown to display reduced infiltration of Th cells to the CNS during EAE induction, but their activation in secondary lymphoid organs was unaffected, it was proposed that defective trafficking of activated cells was responsible for reduced accumulation within the CNS. This hypothesis was based on the known role of $\text{PI3K}\gamma$ in lymphocyte migration⁹. Consistent with this hypothesis, activated Th1 and Th17 cells were found to accumulate in the blood of $\text{Pik3r6}^{-/-}$ mice compared with wildtype counterparts, as depicted in **Figure 4.20 (S, T)**. This suggests that whilst $\text{Pik3r6}^{-/-}$ Th1 and Th17 cells are capable of emigrating the spleen and lymph nodes and entering the blood, they are unable to complete their migratory path into the CNS during EAE disease induction, and instead accumulate in the blood. This may be as a result of defective adhesion or chemotaxis of $\text{Pik3r6}^{-/-}$ Th1 and Th17 cells.

In keeping with these findings, the early priming events measured at day 10 post EAE disease induction were also found to be equivalent between $\text{Pik3r6}^{-/-}$ and wildtype mice, as shown by comparable proportion and number of Th1 and Th17 cells detected in the spleen (**Figure 4.21 (A-F)**) and lymph nodes (*data not shown*). No significant differences in the proportion or number CNS-infiltrating Th1, Th17 or neutrophil populations were observed at early disease stages 10 days post disease induction, as shown in **Figure 4.21 (G-L)**.

4.3 Summary

The data presented in Chapter 4 describe the generation of a novel p84-deficient mouse (C57Bl/6 $\text{Pik3r6}^{-/-}$), which was used to demonstrate previously uncharacterised p84-dependent roles within the immune system. Using experimental autoimmune encephalomyelitis as a lymphocyte-dependent model of chronic inflammatory disease, it was shown that the trafficking of activated Th lymphocytes, but not their differentiation, was dependent on p84. Specifically, the infiltration of Th cells into the inflamed CNS was inhibited in $\text{Pik3r6}^{-/-}$ mice relative to wildtype animals, which correlated with reduced EAE disease severity. In addition to lymphocyte trafficking, the accumulation of neutrophils within the inflamed CNS of $\text{Pik3r6}^{-/-}$ mice during EAE disease was also found to be decreased relative to wildtype control mice. Furthermore, the migration of neutrophils *in vitro* was shown to be dependent on p84. The *in vitro* transwell migration of naïve $\text{Pik3r6}^{-/-}$ lymphocytes isolated from the spleen were also assessed; although variable results were observed using chemokine ligands (*data not shown*) and these experiments therefore require confirmation. However, it is expected that the *in vitro* migration of $\text{Pik3r6}^{-/-}$ Th cells will be inhibited relative wildtype cells, consistent with p84-deficient neutrophils and the reduced trafficking of $\text{Pik3r6}^{-/-}$ Th cells during inflammation *in vivo*.

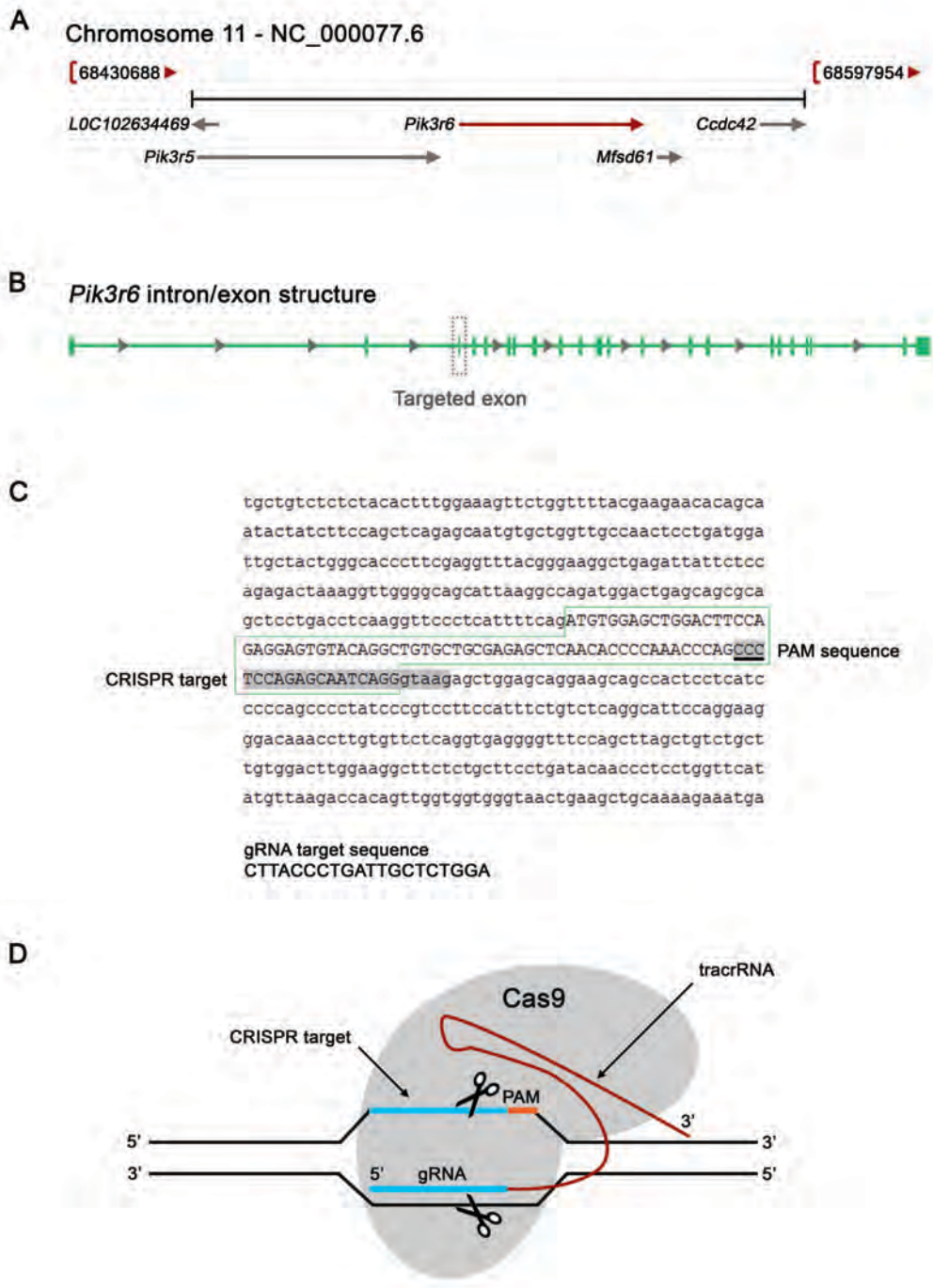
An interesting mechanism of PI3K γ adaptor subunit compensation was observed in mast cells, an inflammatory cell subset that has been previously reported to express only the p84 adaptor protein in association with p110 γ . Data presented in Chapter 4 demonstrate that in the absence of endogenous p84 expression in Pik3r6^{-/-} bone marrow-derived mast cells, the expression of p101 could be up-regulated to compensate for the loss of p84 and maintain PI3K γ -dependent processes.

Collectively, the generation of the p84-deficient mouse in this study represents a valuable tool that can be utilised to elucidate further p84-dependent processes at both homeostasis and during inflammation.

Intentionally blank

Figure 4.1: CRISPR target design for murine *Pik3r6* (p84).

A CRISPR guide RNA (gRNA) was designed to target a region within exon 1 of *Pik3r6*. (A) Position of *Pik3r6* within chromosome 11 (11B3) of the *mus musculus* genome. (B) The intron/exon structure of *Pik3r6*; exons are designated by *vertical green lines* interspersed by intron regions, strand direction is demonstrated by *grey arrows*, scale is relative. (C) The genomic region surrounding the CRISPR target site in *Pik3r6* exon 1; features are defined as follows: intron (*lower case*), exon (*upper case and boxed in green*), PAM sequence (*underlined*), CRISPR gRNA target sequence (*shaded grey*). (D) Schematic of CRISPR-Cas9 targeting induced by homology between the gRNA and the CRISPR target facilitates nuclease activity by associated Cas-9 nuclease towards the target.



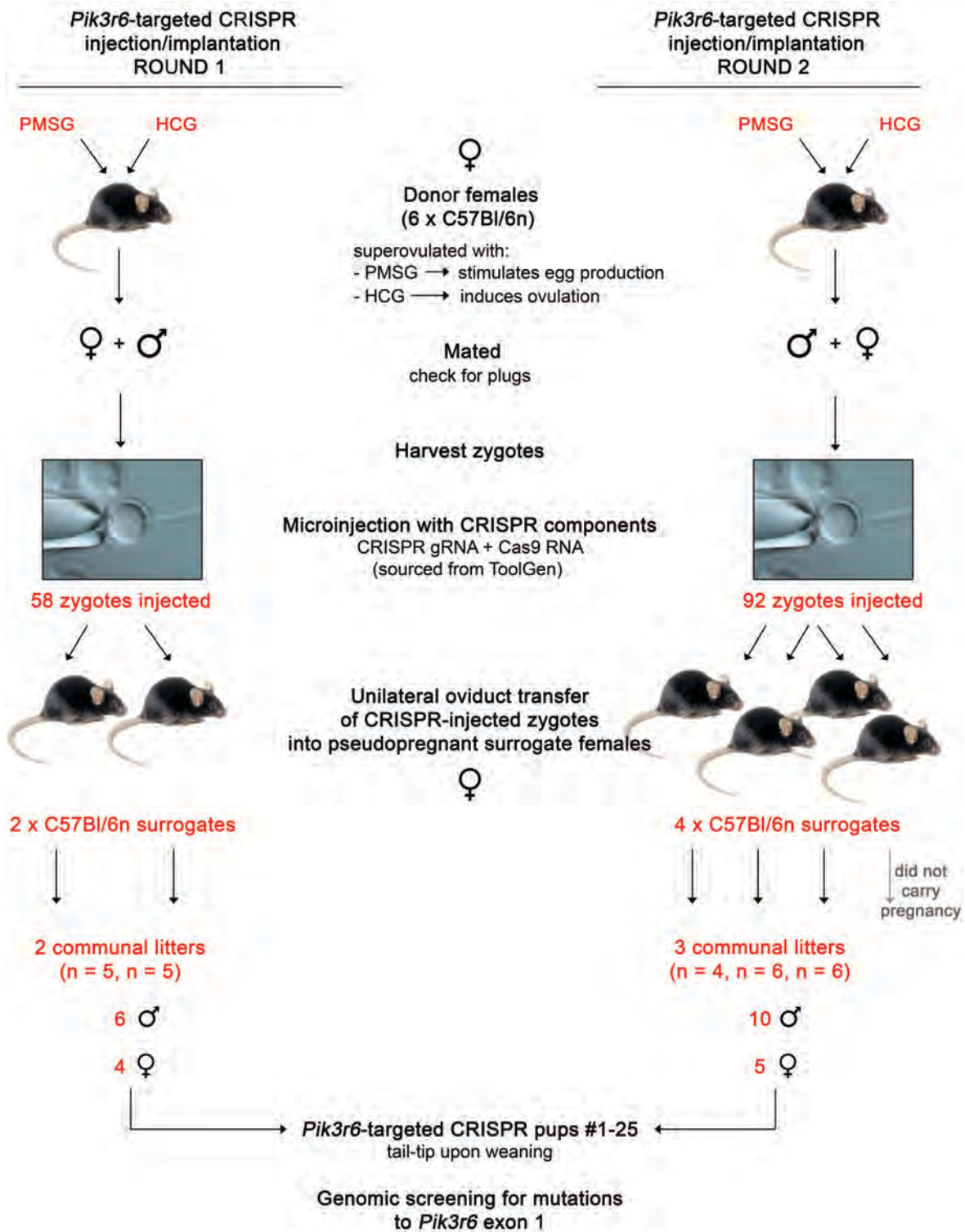


Figure 4.2: Strategy workflow of CRISPR component injection into C57Bl/6n zygotes. Zygotes were harvested from superovulated donor female mice and injected with CRISPR gRNA and Cas9 components to target a sequence within *Pik3r6* exon 1. Modified zygotes were implanted into surrogate female mice by oviduct transfer and embryos were carried to term. Pups were screened for CRISPR-induced mutations to exon 1 of *Pik3r6*.

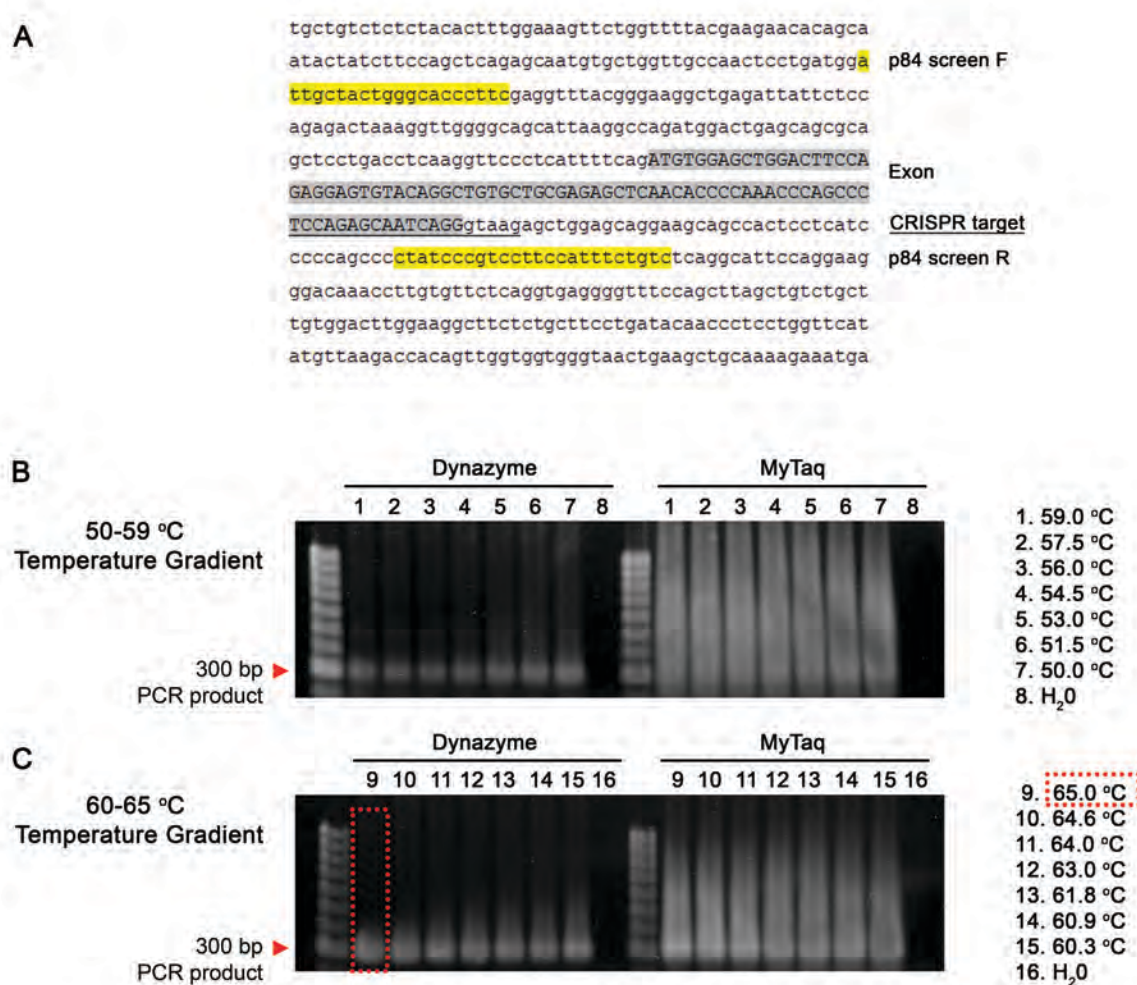


Figure 4.3: Screening for *Pik3r6* CRISPR-induced mutations within exon 1.

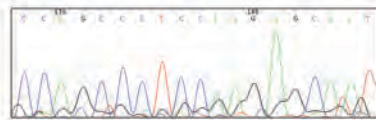
Genomic DNA was isolated from the tail-tips of pups produced from CRISPR-targeted zygotes and a 300bp region within exon 1 of *Pik3r6* flanking the CRISPR target site was screened by PCR and sequencing. (A) Screening PCR primers for the 300bp amplification product, features are defined as follows: exon 1 (highlighted grey), p84 screen forward (F) and reverse (R) screening primers (highlighted yellow), CRISPR target region (underlined). Sequencing PCR was employed using the p84 screen F primer only. (B) Amplification of the 300bp screening PCR product (red arrows) generated by Bioline MyTaq or ThermoScientific Dynazyme polymerase/buffer systems using an annealing temperature gradient covering 50-59°C. (C) Amplification of the 300bp screening PCR product (red arrows) generated by Bioline MyTaq or ThermoScientific Dynazyme polymerase/buffer systems using an annealing temperature gradient covering 60-65°C; optimal conditions of 65°C annealing temperature with Dynazyme polymerase amplification is designated (red dotted box).

A *Pik3r6* CRISPR #1

```

Query 166 CTGTGCTGCGAGAGCTCAACACCCCAACCCAGCCCTCC-AGAGCAATCAGGGTAAGAGC 224
          |||
Sbjct 139 CTGTGCTGCGAGAGCTCAACACCCCAACCCAGCCCTCCAGAGCAATCAGGGTAAGAGC 198

Query 166 CTGTGCTGCGAGAGCTCAACACCCCAACCCAGCCCTCC-AGAGCAATCAGGGTAAGAGC 224
          |||
Sbjct 139 CTGTGCTGCGAGAGCTCAACACCCCAACCCAGCCCTCCAGAGCAATCAGGGTAAGAGC 198
    
```



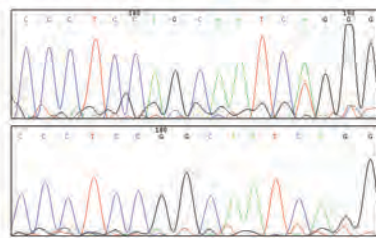
A insertion

B *Pik3r6* CRISPR #2

```

Query 169 TGCTGGAGAGCTCAACACCCCAACCCAGCCCTCCAGAGCAATCAGGGTAAGAGCTGGA 228
          |||
Sbjct 145 TGCTGGAGAGCTCAACACCCCAACCCAGCCCTCCAGCAATCAGGGTAAGAGCTGGA 202

Query 174 CGAGAGCTCAACACCCCAACCCAGCCCTCCAGAGCAATCAGGGTAAGAGCTGGAGCAGG 233
          |||
Sbjct 149 CGAGAGCTCAACACCCCAACCCAGCCCTCCAGCAATCAGGGTAAGAGCTGGAGCAGG 206
    
```



deletion -2

2x single bp deletions

C *Pik3r6* CRISPR #3

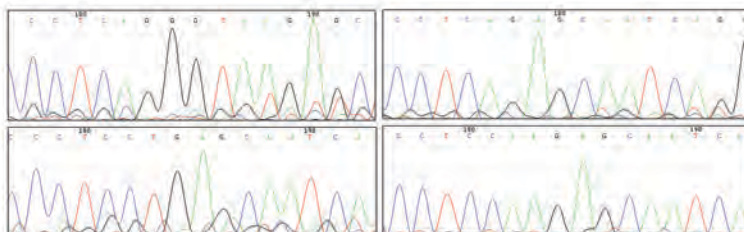
```

Query 174 CGAGAGCTCAACACCCCAACCCAGCCCTCCAGAGCAATCAGGGTAAGAGCTGGAGCAGG 233
          |||
Sbjct 152 CGAGAGCTCAACACCCCAACCCAGCCCTCCAGGGTAAGAGCTGGAGCAGG 201

Query 174 CGAGAGCTCAACACCCCAACCCAGCCCTCCAGAGCAATCAGGGTAAGAGCTGGAGCAGG 233
          |||
Sbjct 152 CGAGAGCTCAACACCCCAACCCAGCCCTCCAGCAATCAGGGTAAGAGCTGGAGCAGG 211

Query 165 GCTGTGCTGCGAGAGCTCAACACCCCAACCCAGCCCTCCAGAGCAATCAGGGTAAGAGC 224
          |||
Sbjct 138 GCTGTGCTGCGAGAGCTCAACACCCCAACCCAGCCCTCCAGAGCAATCAGGGTAAGAGC 196

Query 174 CGAGAGCTCAACACCCCAACCCAGCCCTCC-AGAGCAATCAGGGTAAGAGCTGGAGCAG 232
          |||
Sbjct 151 CGAGAGCTCAACACCCCAACCCAGCCCTCCAGAGCAATCAGGGTAAGAGCTGGAGCAG 210
    
```



deletion -10

single bp deletion

single bp substitution

A insertion

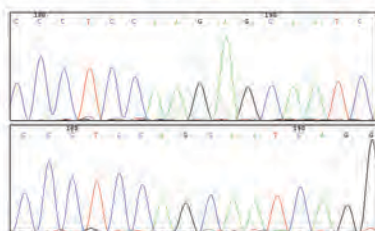
D *Pik3r6* CRISPR #4

```

Query 169 TGCTGCGAGAGCTCAACACCCCAAACCCAGCCCTCC-AGAGCAATCAGGGTAAGAGCTGG 227
          |||
Sbjct 148 TGCTGCGAGAGCTCAACACCCCAAACCCAGCCCTCCAGAGCAATCAGGGTAAGAGCTGG 207

Query 223 CGAGAGCTCAACACCCCAAACCCAGCCCTCCAGAGCAATCAGGGTAAGAGCTGGAGCAGG 282
          |||
Sbjct 153 CGAGAGCTCAACACCCCAAACCCAGCCCTCCAGCAATCAGGGTAAGAGCTGGAGCAGG 210

```

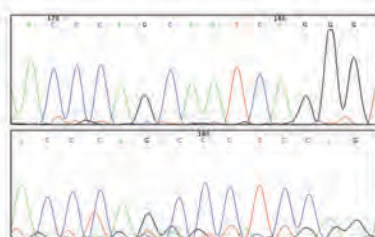
**E** *Pik3r6* CRISPR #5

```

Query 164 GGCTGTGCTGCGAGAGCTCAACACCCCAAACCCAGCCCTCCAGAGCAATCAGGGTAAGAG 223
          |||
Sbjct 140 GGCTGTGCTGCGAGAGCTCAACACCCCAAACCC-----AGCAATCAGGGTAAGAG 189

Query 173 GCGAGAGCTCAACACCCCAAACCCAGCCCTCCAGAGCAATCAGGGTAAGAGCTGGAGCAG 232
          |||
Sbjct 153 GCGAGAGCTCAACACCCCAAACCCAGCCCTCCAGAGCAATCAGGGTAAGAGCTGGAGCAG 212

```

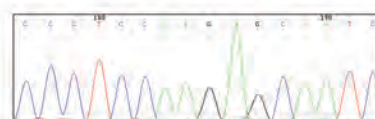
**F** *Pik3r6* CRISPR #6

```

Query 166 CTGTGCTGCGAGAGCTCAACACCCCAAACCCAGCCCTCC-AGAGCAATCAGGGTAAGAGC 224
          |||
Sbjct 144 CTGTGCTGCGAGAGCTCAACACCCCAAACCCAGCCCTCCAGAGCAATCAGGGTAAGAGC 203

Query 166 CTGTGCTGCGAGAGCTCAACACCCCAAACCCAGCCCTCC-AGAGCAATCAGGGTAAGAGC 224
          |||
Sbjct 144 CTGTGCTGCGAGAGCTCAACACCCCAAACCCAGCCCTCCAGAGCAATCAGGGTAAGAGC 203

```

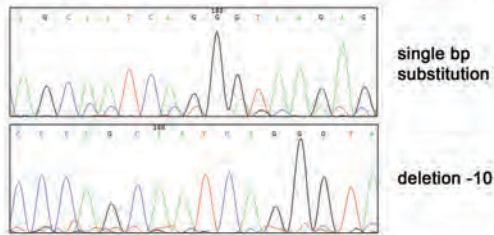


G *Pik3r6* CRISPR #7

```

Query 179 GCGAGGCTCAACACCCCAACCCAGCCCTCCAGCAATCAGGGTAAGAGCTGGAGCAG 232
          |||
Sbjct 153 GCTAGAGCTCAACACCCCAACCCAGCCCTCCAGCAATCAGGGTAAGAGCTGGAGCAG 212

Query 179 GCTCAACACCCCAACCCAGCCCTCCAGCAATCAGGGTAAGAGCTGGAGCAGGAAGCA 238
          |||
Sbjct 159 GCTCAACACCCCAACCC-----AGCAATCAGGGTAAGAGCTGGAGCAGGAAGCA 208
    
```

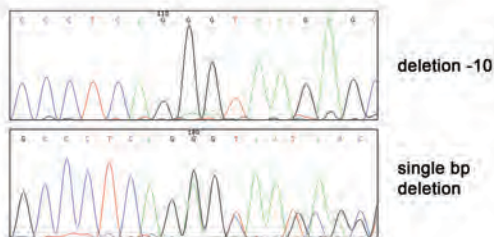


H *Pik3r6* CRISPR #8

```

Query 230 TCAACACCCCAACCCAGCCCTCCAGGCAATCAGGGTAAGAGCTGGAGCAGGAAGCAGC 289
          |||
Sbjct 181 TCAACACCCCAACCCAGCCCT-----TCAGGGTAAGAGCTGGAGCAGGAAGCAGC 230

Query 230 TCAACACCCCAACCCAGCCCTCCAGGCAATCAGGGTAAGAGCTGGAGCAGGAAGCAGC 289
          |||
Sbjct 181 TCAACACCCCAACCCAGCCCTCCAGCAATCAGGGTAAGAGCTGGAGCAGGAAGCAGC 239
    
```

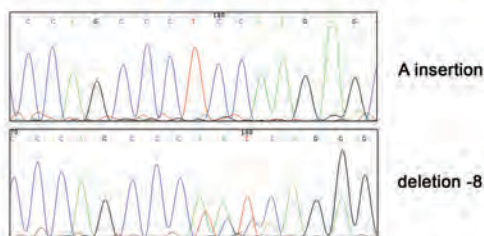


I *Pik3r6* CRISPR #9

```

Query 174 CGAGAGCTCAACACCCCAACCCAGCCCTCCAGAGCAATCAGGGTAAGAGCTGGAGCAG 232
          |||
Sbjct 151 CGAGAGCTCAACACCCCAACCCAGCCCTCCAGAGCAATCAGGGTAAGAGCTGGAGCAG 210

Query 174 CGAGAGCTCAACACCCCAACCCAGCCCTCCAGAGCAATCAGGGTAAGAGCTGGAGCAG 233
          |||
Sbjct 150 CGAGAGCTCAACACCCCAACCCAGCC-----CAATCAGGGTAAGAGCTGGAGCAG 201
    
```



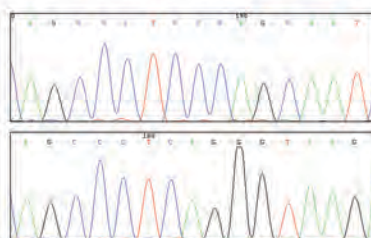
J *Pik3r6* CRISPR #10

```

Query 214 GCTGTGCTGCGAGAGCTCAACACCCCAAAACCAGCCCTCCAGAGCAATCAGGGTAAGAGC 273
          |||
Sbjct 149 GCTGTGCTGCGAGAGCTCAACACCCCAAAACCAGCCCTCCAGAGCAATCAGGGTAAGAGC 207

Query 215 CTGTGCTGCGAGAGCTCAACACCCCAAAACCAGCCCTCCAGAGCAATCAGGGTAAGAGCT 274
          |||
Sbjct 144 CTGTGCTGCGAGAGCTCAACACCCCAAAACCAGCCCTCCAGGGTAAGAGCT 193

```

single bp
substitution,
deletion

deletion -10

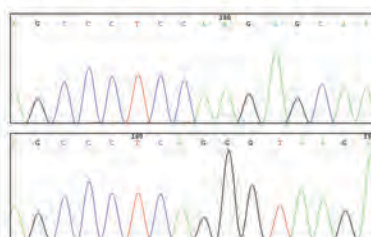
K *Pik3r6* CRISPR #11

```

Query 223 CGAGAGCTCAACACCCCAAAACCAGCCCTCC-AGAGCAATCAGGGTAAGAGCTGGAGCAG 281
          |||
Sbjct 148 CGGGAGCTCAACACCCCAAAACCAGCCCTCCAGAGCAATCAGGGTAAGAGCTGGAGCAG 207

Query 223 CGAGAGCTCAACACCCCAAAACCAGCCCTCCAGAGCAATCAGGGTAAGAGCTGGAGCAGG 282
          |||
Sbjct 152 CGAGAGCTCAACACCCCAAAACCAGCCCTCCAGGGTAAGAGCTGGAGCAGG 201

```



A insertion

deletion -10

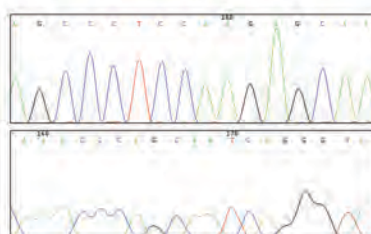
L *Pik3r6* CRISPR #12

```

Query 214 GCTGTGCTGCGAGAGCTCAACACCCCAAAACCAGCCCTCC-AGAGCAATCAGGGTAAGAG 272
          |||
Sbjct 139 GCTGTGCTGCGAGAGCTCAACACCCCAAAACCAGCCCTCCAGAGCAATCAGGGTAAGAG 198

Query 225 AGAGCTCAACACCCCAAAACCAGCCCTCCAGAGCAATCAGGGTAAGAGCTGGAGCAGG-A 283
          |||
Sbjct 144 AGAGCTCAACACCCCAAAACCAGGGTAAGAGCTGGAGCANGAA 193

```



A insertion

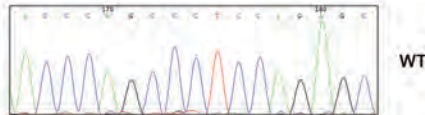
deletion -10

M *Pik3r6* CRISPR #13

```

Query 173 GCGAGAGCTCAACACCCCAAAACCCAGCCCTCCAGAGCAATCAGGGTAAGAGCTGGAGCAG 232
          |||
Sbjct 153 GCGAGAGCTCAACACCCCAAAACCCAGCCCTCCAGAGCAATCAGGGTAAGAGCTGGAGCAG 212

Query 173 GCGAGAGCTCAACACCCCAAAACCCAGCCCTCCAGAGCAATCAGGGTAAGAGCTGGAGCAG 232
          |||
Sbjct 153 GCGAGAGCTCAACACCCCAAAACCCAGCCCTCCAGAGCAATCAGGGTAAGAGCTGGAGCAG 212
    
```

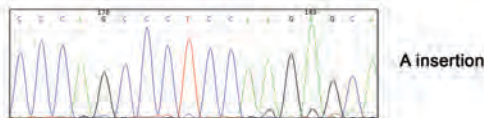


N *Pik3r6* CRISPR #14

```

Query 223 CGAGAGCTCAACACCCCAAAACCCAGCCCTCC-AGA GCAATCAGGGTAAGAGCTGGAGCAG 281
          |||
Sbjct 150 CGAGAGCTCAACACCCCAAAACCCAGCCCTCC-AGA GCAATCAGGGTAAGAGCTGGAGCAG 209

Query 223 CGAGAGCTCAACACCCCAAAACCCAGCCCTCC-AGA GCAATCAGGGTAAGAGCTGGAGCAG 281
          |||
Sbjct 150 CGAGAGCTCAACACCCCAAAACCCAGCCCTCC-AGA GCAATCAGGGTAAGAGCTGGAGCAG 209
    
```

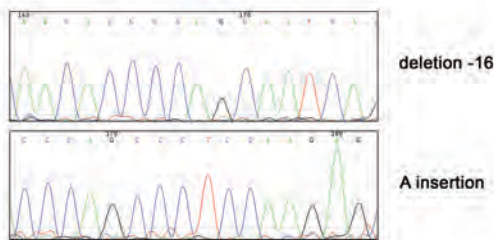


O *Pik3r6* CRISPR #15

```

Query 214 GCTGTGCTGCGAGAGCTCAACACCCCAAAACCCAGCCCTCCAGAGCAATCAGGGTAAGAGC 273
          |||
Sbjct 142 GCTGTGCTGCGAGAGCTCAACACCCCAAAACCCAGCCCTCCAGAGCAATCAGGGTAAGAGC 185

Query 223 CGAGAGCTCAACACCCCAAAACCCAGCCCTCC-AGA GCAATCAGGGTAAGAGCTGGAGCAG 281
          |||
Sbjct 149 CGAGAGCTCAACACCCCAAAACCCAGCCCTCC-AGA GCAATCAGGGTAAGAGCTGGAGCAG 208
    
```



P *Pik3r6* CRISPR #16

```

Query 215 CTGTGCTGCGAGAGCTCAACACCCCAAAACCCAGCCCTCCAGAGCAATCAGGGTAAGAGCT 274
          |||
Sbjct 138 CTGTGCTGCGAGAGCTCAACACCCCAAAACCCAGCCCTCCAGAGCAATCAGGGTAAGAGCT 187

Query 215 CTGTGCTGCGAGAGCTCAACACCCCAAAACCCAGCCCTCCAGAGCAATCAGGGTAAGAGCT 274
          |||
Sbjct 138 CTGTGCTGCGAGAGCTCAACACCCCAAAACCCAGCCCTCCAGAGCAATCAGGGTAAGAGCT 187
    
```



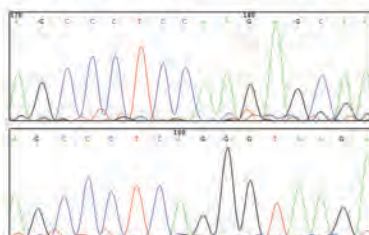
Q *Pik3r6* CRISPR #17

```

Query 223 CGAGAGCTCAACACCCCAAAACCCAGCCCTCC-AGAGCAATCAGGGTAAGAGCTGGAG 281
          |||
Sbjct 147 CGAGAGCTCAACACCCCAAAACCCAGCCCTCCAGAGCAATCAGGGTAAGAGCTGGAG 206

Query 223 CGAGAGCTCAACACCCCAAAACCCAGCCCTCCAGAGCAATCAGGGTAAGAGCTGGAGC 282
          |||
Sbjct 150 CGAGAGCTCAACACCCCAAAACCCAGCCCC-----TCAGGGTAAGAGCTGGAGC 199

```

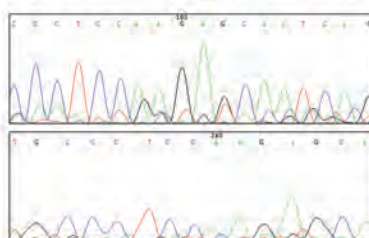
**R** *Pik3r6* CRISPR #18

```

Query 223 CGAGAGCTCAACACCCCAAAACCCAGCCCTCCA-GAGCAATCAGGGTAAGAGCTGGAGCA 281
          |||
Sbjct 149 CGAGAGCTCAACACCCCAAAACCCAGCCCTCCGGAGCANTCAGGGTAAGAGCTGGAAACA 208

Query 224 GAGAGCTCAACACCCCAAAACCCAGCCCTCCA-GAGCAATCAGGGTAAGAGCTGGAGCAG 281
          |||
Sbjct 210 GAGAGCTCAACACCCCAAAACCCAGCCCTCCAAGAGCAATCANGGTAATACCTGGANCA 269

```

**S** *Pik3r6* CRISPR #19

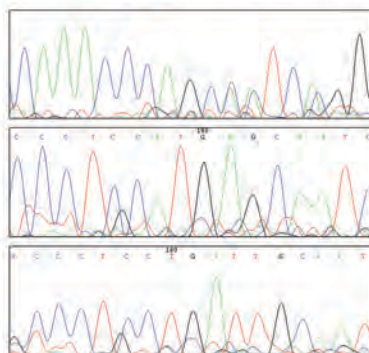
```

Query 61 CAGGCTGTGCTGCGAGAGCTCAACACCCCAAAACCCAGCCCTCCAGAGCAATCAGGGTAAG 120
          |||
Sbjct 61 CAGGCTGTGCTGCGAGAGCTCAACACCCCAAAACCC-----AGCAATCAGGGTAAG 110

Query 234 CACCCCAAAACCCAGCCCTCCA-GAGCAATCAGGGTAAGAGCTGGAGCAGGAAGCAGCCAC 292
          |||
Sbjct 158 CACCCCAAAACCCAGCCCTCCAAGAGCAATCAGGGTAAGAGCTGGAGCAGGAAGCAGCCAC 217

Query 232 AACACCCCAAAACCCAGCCCTCCAGA--GCAATCAGGGTAAGAGCTGGAGCAGGAAGCAGC 289
          |||
Sbjct 158 AACACCCCAAAACCCAGCCCTCCGAGGCAATCAGGGTAAGAGCTGGAGCAGGAAGCAGC 217

```

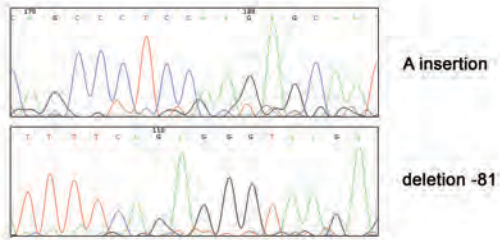


T *Pik3r6* CRISPR #20

```

Query 254 -AGAGCAATCAGGGTAAGAGCTGGAGCAGGAAGCAGCCACTCCTCATCCCCAGCCCCCTA 312
Sbjct 178 AGAGCAATCAGGGTAAGAGCTGGAGCAGGAAGCAGCCACTCCTCATCCCCAGCCCCCTA 237

AAGGTTCCCTCAITTTICAGATGTGGAGCTGGACTTCCAGAGGAGTGTACAGGCTGTGCTGCGAGAGCTCAACA
|||||
AAGGTTCCCTCAITTTICAG-----
|||||
CCCCAACCAGCCCTCCAGAGCAATCAGGGTAAGAGCTGGAGCAGGAAGCAGCCACTCCTCATC
|||||
-----GGTAAGAGCTGGAGCAGGAAGCAGCCACTCCTCATC
    
```

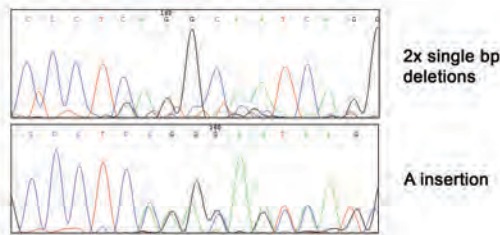


U *Pik3r6* CRISPR #21

```

Query 216 TGTGCTGCGAGAGCTCAACACCCCAACCAGCCCTCCAGAGCAATCAGGGTAAGAGCTG 275
Sbjct 147 TGTGCTGCGAGAGCTCAACACCCCAACCAGCCCTCAGCAATCAGGGTAAGAGCTG 204

Query 61 CAGGCTGTGCTGCGAGAGCTCAACACCCCAACCAGCCCTCC-AGAGCAATCAGGGTAA 119
Sbjct 61 CAGGCTGTGCTGCGAGAGCTCAACACCCCAACCAGCCCTCCAGAGCAATCAGGGTAA 120
    
```

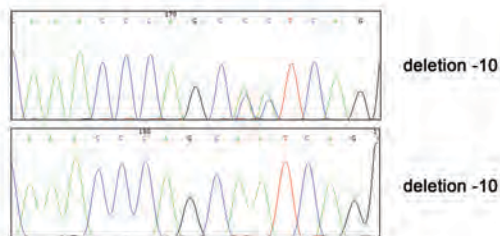


V *Pik3r6* CRISPR #22

```

Query 212 GGCTGTGCTGCGAGAGCTCAACACCCCAACCAGCCCTCCAGAGCAATCAGGGTAAGA 271
Sbjct 136 GGCTGTGCTGCGAGAGCTCAACACCCCAACCAGCC-----TCAGGGTAAGA 185

Query 213 GGCTGTGCTGCGAGAGCTCAACACCCCAACCAGCCCTCCAGAGCAATCAGGGTAAGAG 272
Sbjct 148 GGCTGTGCTGCGAGAGCTCAACACCCCAACC-----AGCAATCAGGGTAAGAG 197
    
```



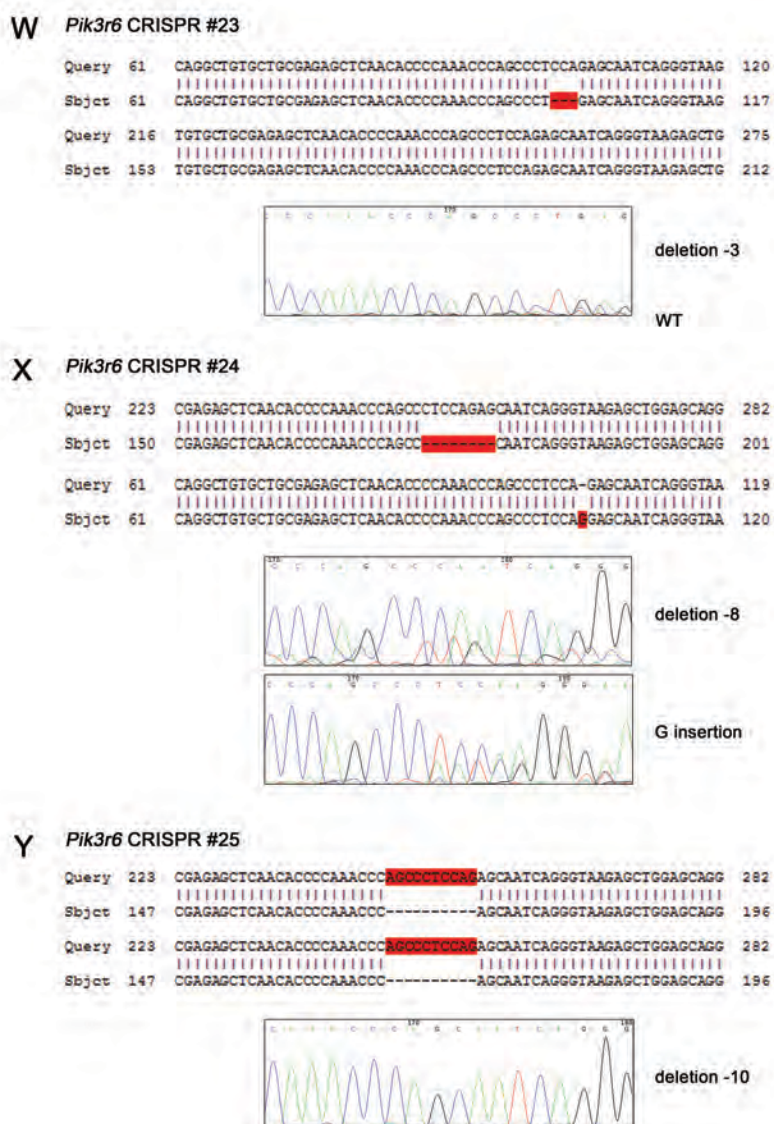


Figure 4.4: Screening CRISPR-induced mutations within exon 1 from *Pik3r6* CRISPR pups.

Genomic DNA was isolated from the tail-tips of *Pik3r6* CRISPR pups #1-25 and the 300bp PCR amplification region flanking the CRISPR target site within exon 1 of *Pik3r6* was screened by PCR and sequencing. (A-Y) CRISPR-induced mutations identified from *Pik3r6* CRISPR pups #1-25 are shown by sequence alignment (upper) and corresponding chromatograms for each allele (lower); mutations (substitution/deletion/insertion) are highlighted in red for Query (represents wildtype *Pik3r6* sequence) and Subject (represents CRISPR pup *Pik3r6* sequence).

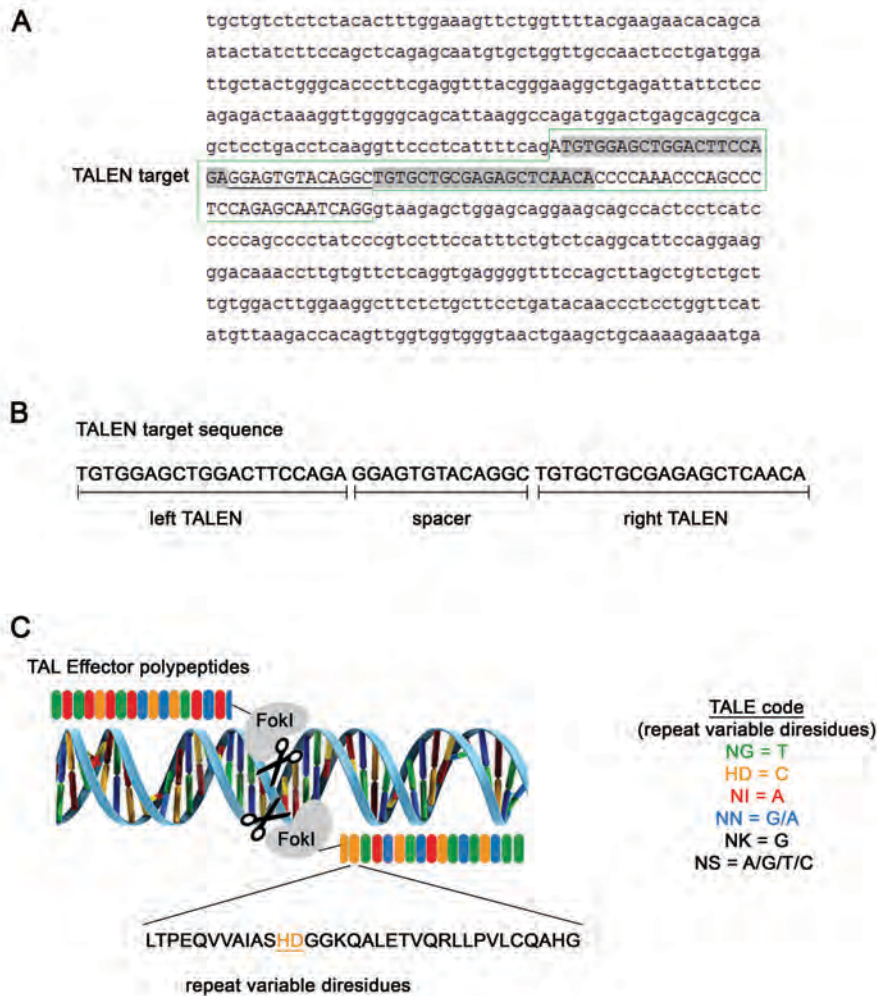


Figure 4.5: TALEN design to target murine *Pik3r6* (p84).

A TALEN sequence was designed to target a region within exon 1 of *Pik3r6*. (A) The region surrounding TALEN target region; features are defined as follows: intron (*lower case*), exon (*upper case and boxed in green*), left and right TALEN sequences (*shaded grey*), TALEN spacer sequence (*underlined*). (B) TALEN target sequence. (C) Schematic of TALEN targeting by FokI nuclease-coupled effector DNA-binding polypeptides and TALE code.

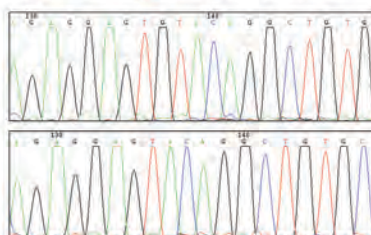
A *Pik3r6* TALEN #26

```

Query 182 ATGTGGAGCTGGACTTCCAGAGGAGTGTACAGGCTGTGCTGCGAGAGCTCAACACCCCAA 241
          |||
Sbjct 1   ATGTGGAGCTGGACTTCCAGAGGAGTGTACAGGCTGTGCTGCGAGAGCTCAACACCCCAA 58

Query 182 ATGTGGAGCTGGACTTCCAGAGGAGTGTACAGGCTGTGCTGCGAGAGCTCAACACCCCAA 241
          |||
Sbjct 1   ATGTGGAGCTGGACTTCCAGAGGA GTACAGGCTGTGCTGCGAGAGCTCAACACCCCAA 58

```

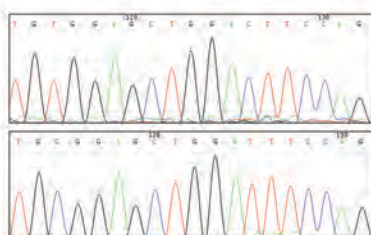
**B** *Pik3r6* TALEN #27

```

Query 155 CTGACCTCAAGGTTCCCTCATTTTCAGATGTGGAGCTGGACTTCCAGAGGAGTGTACAGG 214
          |||
Sbjct 86   CTGACCTCAAGGTTCCCTCATTTTCAGATGTGGAGCTGGACTTCCAGAGGAGTGTACAGG 145

Query 163 AAGGTTCCCTCATTTTCAGATGTGGAGCTGGACTTCCAGAGGAGTGTACAGGCTGTGCTG 222
          |||
Sbjct 93   AAGGTTCCCTCATTTTCAGATG GAGCTGGA TCCAGAGGAGTGTACAGGCTGTGCTG 152

```

**C** *Pik3r6* TALEN #28

```

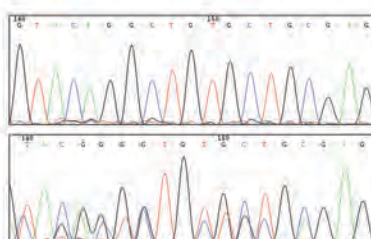
Query 155 CTGACCTCAAGGTTCCCTCATTTTCAGATGTGGAGCTGGACTTCCAGAGGAGTGTACAGG 214
          |||
Sbjct 86   CTGACCTCAAGGTTCCCTCATTTTCAGATGTGGAGCTGGACTTCCAGAGGAGTGTACAGG 145

Query 154 CCTGACCTCAAGGTTCCCTCATTTTCAGATGTGGAGCTGGACTTCCAGAGGAGTGTACAG 213
          |||
Sbjct 85   CCTGACCTCAAGGTTCCCTCATTTTCAGATGTGGAGCTGGACTTCCAGAGGAGTGTACAG 144

Query 214 GCTGTGCTGCGAGAGCTCAACACCCCAAACCCAGCCCTCCAGAGCAATCAGGGTAAGAGC 273
          |||
Sbjct 145 G TGTGCTGCGAGAGCTCAAC CCCCAAACCCAGCCCTCCAGAGCAATC GGGTAAGAGC 204

Query 274 TGGAGCAGGAAGCAGCCACTCCTCATCCCCAGCCCTATCCCGTCCCTCCATTTCTGTC 333
          |||
Sbjct 205 TGG CA GAAGCA CCACTCCTCATCCCCA CCGCTATCCCGTCTTCTTTTGTGTC 264

```

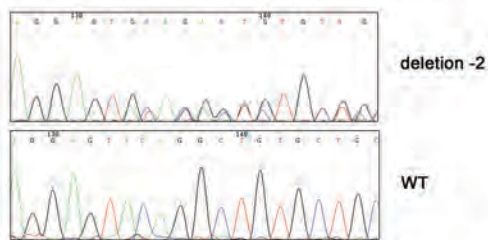


D *Pik3r6* TALEN #29

```

Query 157 GACCTCAAGGTTCCCTCATTTCAGATGTGGAGCTGGACTTCCAGAGGAGTGTACAGGCT 216
          |||
Sbjct  83 GACCTCAAGGTTCCCTCATTTCAGATGTGGAGCTGGACTTCCAGAGGAGTGTACAGGCT 140
          |||

Query 155 CTGACCTCAAGGTTCCCTCATTTCAGATGTGGAGCTGGACTTCCAGAGGAGTGTACAGG 214
          |||
Sbjct  83 CTGACCTCAAGGTTCCCTCATTTCAGATGTGGAGCTGGACTTCCAGAGGAGTGTACAGG 142
          |||
    
```

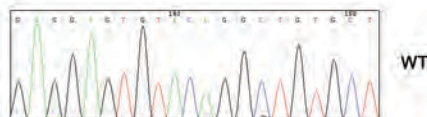


E *Pik3r6* TALEN #30

```

Query 155 CTGACCTCAAGGTTCCCTCATTTCAGATGTGGAGCTGGACTTCCAGAGGAGTGTACAGG 214
          |||
Sbjct  83 CTGACCTCAAGGTTCCCTCATTTCAGATGTGGAGCTGGACTTCCAGAGGAGTGTACAGG 142
          |||

Query 155 CTGACCTCAAGGTTCCCTCATTTCAGATGTGGAGCTGGACTTCCAGAGGAGTGTACAGG 214
          |||
Sbjct  83 CTGACCTCAAGGTTCCCTCATTTCAGATGTGGAGCTGGACTTCCAGAGGAGTGTACAGG 142
          |||
    
```

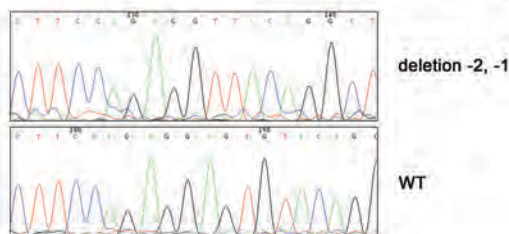


F *Pik3r6* TALEN #31

```

Query 163 AAGGTTCCCTCATTTCAGATGTGGAGCTGGACTTCCAGAGGAGTGTACAGGCTGTGCTG 222
          |||
Sbjct  92 AAGGTTCCCTCATTTCAGATGTGGAGCTGGACTTCCAGAGGAGTGTACAGGCTGTGCTG 148
          |||

Query 171 CTCATTTTCAGATGTGGAGCTGGACTTCCAGAGGAGTGTACAGGCTGTGCTGCGAGAGCT 230
          |||
Sbjct 153 CTCATTTTCAGATGTGGAGCTGGACTTCCAGAGGAGTGTACAGGCTGTGCTGCGAGAGCT 212
          |||
    
```



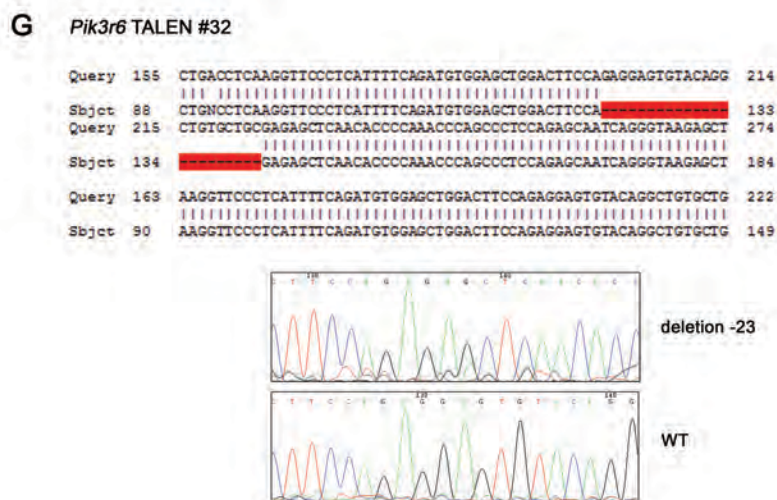


Figure 4.6: Screening TALEN-induced mutations within exon 1 from *Pik3r6* TALEN pups.

Genomic DNA was isolated from the tail-tips of *Pik3r6* TALEN pups #26-32 and the 300bp PCR amplification region flanking the TALEN target site within exon 1 of *Pik3r6* was screened by PCR and sequencing. (A-G) TALEN-induced mutations identified from *Pik3r6* TALEN pups #26-32 are shown by sequence alignment (*upper*) and corresponding chromatograms for each allele (*lower*); mutations (substitution/deletion/insertion) are highlighted in *red* for Query (represents wildtype *Pik3r6* sequence) and Subject (represents TALEN pup *Pik3r6* sequence).

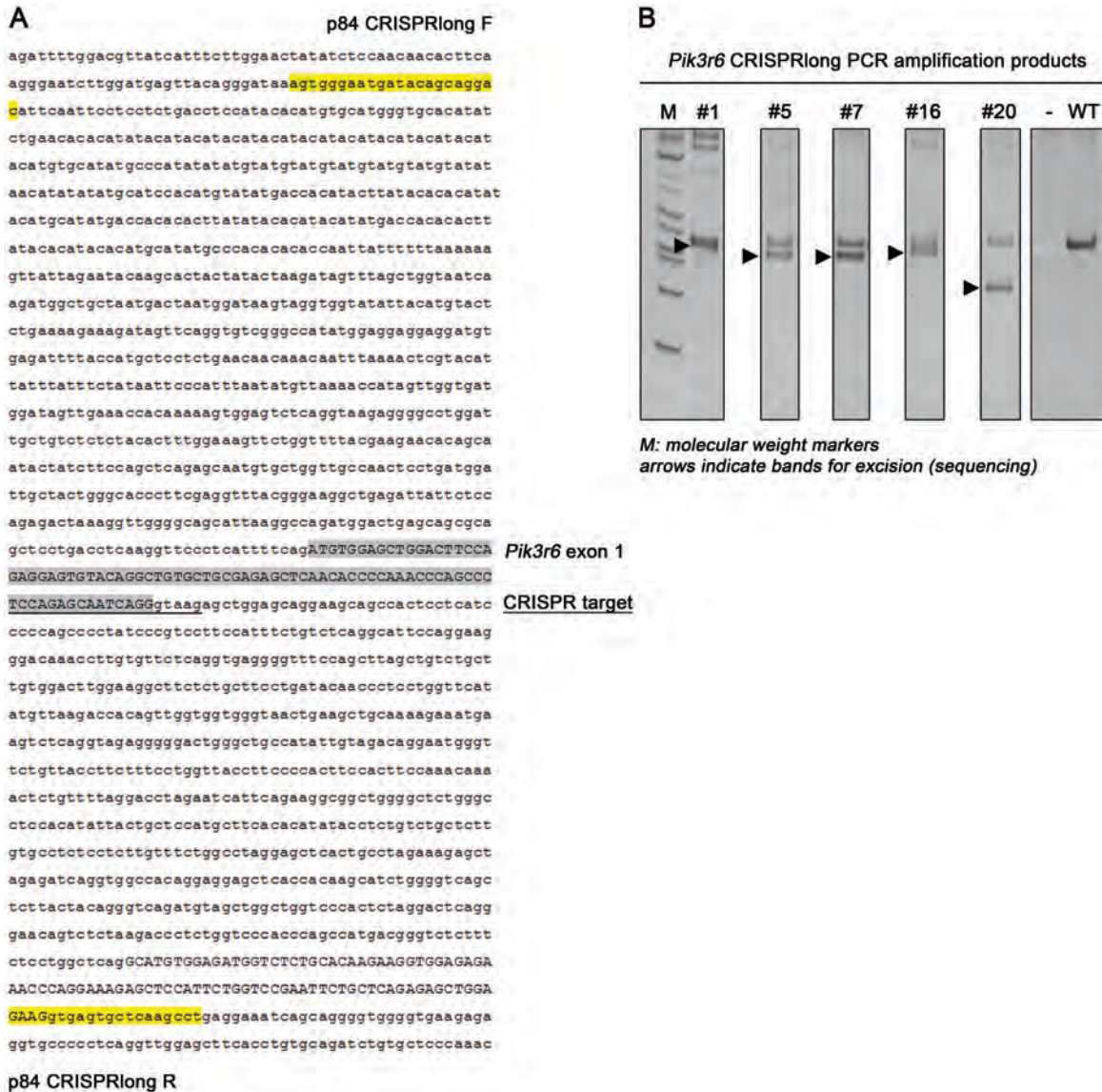


Figure 4.7: CRISPR-based gene-targeting can induce large deletions to regions immediately flanking the CRISPR target site.

Genomic DNA isolated from *Pik3r6* CRISPR pups #1-25 was screened for larger deletions in the regions flanking the CRISPR target. (A) PCR screening primers for a 1.7kb amplification product, features are defined as follows: intron (*lower case*), exon 1 (*highlighted grey*), CRISPR target region (*underlined*) and p84 CRISPRlong forward (F) and reverse (R) primers (*highlighted yellow*). (B) CRISPRlong PCR amplification products were separated by polyacrylamide gel electrophoresis to reveal large deletions, shown are gel separations for *Pik3r6* CRISPR #1, #5, #7, #16 and #20. PCR products containing large deletions are designated (*arrows*) and were excised for sequencing, performed using the p84 CRISPRlong R primer.

A

agtgggaaatgatacagcagga
 gat tcaat tccct cctct gacct cccata cacat gtgcat gggg tgcacat at
 ctgaa cacacat ataca tacat acata cacata cacata cacata cacat
 acatgtgcatatgccccatataatgta tgtatgtatgtatgtatgtat
 aacatataatgcatccacatgtatata gaccacatacttatacacacat at
 acatgcatatgacacacacactatatacacatacacatgaccacacact
 atacacatacacatgcatatgcccacacacaccaattat ttttttaaaaa
 gttat tagaata caagcactactatactaaga tagttagctggtaatca
 agatggctgcta atgactaatggataagtaggtggtatattacatgtact
 ctgaaaaaagaatagttcaggtgtcgggccatgaggaggaggatgt
 gagat tttacca tgcctctctgaa caa caa caa aatt taaa actogt acat
 tatttatttcta taattcccat ttaatatgttaaaacatagttggtgat
 ggtatgtt gaaacacaaaaagtgaggctcaggttaagggggcctggat
 tgctgtctctctacacttggaaagttctgggtttta cgaagaacacagca
 ata ctatcttccagctcagagcaatgtctggttgc caact cctgatgga
 ttgctactgggcaccttcgagggtta cgggaaggctgagattattctcc
 agagactaaaggttggggcagcattaaagccagatggactgagcagcgca
 gctcctgacctcaaggttccctcattttcagA TGTGGAGCTGGACTTCCA
 GAGGAGTGTACAGGCTGTGCTGCGAGAGCTCAACACCCCAAACCCAGCCC
 TCCAGAGCAATCAGGgttaagagctggagcaggaagcagccactcctcatc
 ccccagccccta tcccg tccctccatt tctgtctcaggcat tccaggaag
 ggacaaaacctgtgtttcaggtgaggggtttccagcttagctgtctgtct
 tgtggacttggaaaggcttctctgcttccctgat acaaacctcctgggttcat
 atgttaagacca cagttgggtgggttaactgaa gctgcaaaagaaatga
 agtctcaggttagaggggactgggctgccaata tttgtagacaggaatgggt
 tctgtttaccttcttccctgggttaccttcccaacttccacttccaaaaaa
 actctgttttaggaacctagaatcattcagaagcggctggggctctgggc
 ctccacataatta ctgctccatgcttca cacataacactctgtctgtctctt
 gtgctctctctgtttctggcctaggagctcactgcctagaaagagct
 agagatcaggtggccacaggaggagctcaccacaagcatctggggtcagc
 tcttactacaggtcagatgtagctggctgggtcccactctaggactcagg
 gaa cagctcttaagacctctggtcccacccagccatgacgggtctcttt
 ctctggctcagGCATGTGGAGATGGTCTCTGCACAAGAAGGTGGAGAGA
 AACCCAGGAAAGAGCTCCATTCTGGTCCGAATTCTGCTCAGAGAGCTGGA
 GAAggtgagtgctcaagcct

Pik3r6 CRISPR #1

- 328 bp

B

agtgggaaatgatacagcagga
 gat tcaat tccct cctct gacct cccata cacat gtgcat gggg tgcacat at
 ctgaa cacacat ataca tacat acata cacata cacata cacata cacat
 acatgtgcatatgccccatataatgta tgtatgtatgtatgtatgtatgtat
 aacatataatgcatccacatgtatata gaccacatacttatacacacat at
 acatgcatatgacacacacactatatacacatacacatgaccacacact
 atacacatacacatgcatatgcccacacacaccaattat ttttttaaaaa
 gttat tagaata caagcactactatactaaga tagttagctggtaatca
 agatggctgcta atgactaatggataagtaggtggtatattacatgtact
 ctgaaaaaagaatagttcaggtgtcgggccatgaggaggaggatgt
 gagat tttacca tgcctctctgaa caa caa caa aatt taaa actogt acat
 tatttatttcta taattcccat ttaatatgttaaaacatagttggtgat
 ggtatgtt gaaacacaaaaagtgaggctcaggttaagggggcctggat
 tgctgtctctctacacttggaaagttctgggtttta cgaagaacacagca
 ata ctatcttccagctcagagcaatgtctggttgc caact cctgatgga
 ttgctactgggcaccttcgagggtta cgggaaggctgagattattctcc
 agagactaaaggttggggcagcattaaagccagatggactgagcagcgca
 gctcctgacctcaaggttccctcattttcagA TGTGGAGCTGGACTTCCA
 GAGGAGTGTACAGGCTGTGCTGCGAGAGCTCAACACCCCAAACCCAGCCC
 TCCAGAGCAATCAGGgttaagagctggagcaggaagcagccactcctcatc
 ccccagccccta tcccg tccctccatt tctgtctcaggcat tccaggaag
 ggacaaaacctgtgtttcaggtgaggggtttccagcttagctgtctgtct
 tgtggacttggaaaggcttctctgcttccctgat acaaacctcctgggttcat
 atgttaagacca cagttgggtgggttaactgaa gctgcaaaagaaatga
 agtctcaggttagaggggactgggctgccaata tttgtagacaggaatgggt
 tctgtttaccttcttccctgggttaccttcccaacttccacttccaaaaaa
 actctgttttaggaacctagaatcattcagaagcggctggggctctgggc
 ctccacataatta ctgctccatgcttca cacataacactctgtctgtctctt
 gtgctctctctgtttctggcctaggagctcactgcctagaaagagct
 agagatcaggtggccacaggaggagctcaccacaagcatctggggtcagc
 tcttactacaggtcagatgtagctggctgggtcccactctaggactcagg
 gaa cagctcttaagacctctggtcccacccagccatgacgggtctcttt
 ctctggctcagGCATGTGGAGATGGTCTCTGCACAAGAAGGTGGAGAGA
 AACCCAGGAAAGAGCTCCATTCTGGTCCGAATTCTGCTCAGAGAGCTGGA
 GAAggtgagtgctcaagcct

Pik3r6 CRISPR #5

- 334 bp

C

agtgggaatgat acagcagga

gattcaattcctcctctgacctccatacacatgtgcatgggtgcacatat
 ctgaacacacatatatacatatacatatacatatacatatacatatacat
 acatgtgcatatgccatataatgtatgtatgtatgtatgtatgtat
 aacatataatgcatccacatgtatatagccacatacttatacacacatat
 acatgcatatgaccacacacttatacacatatacatatgaccacacactt
 atacacatacacatgcatatgcccacacacaccaattatTTTTAAAAA
 gttatagaatacaagcactactataactaagatagtttagctggtaatca
 agatggctgctaagactaatggataagtaggtgtatattacatgtact
 ctgaaaagaaagatagttcagggtgctggccatattggaggaggatgt
 gagatTTTaccatgctcctctgaaacaaacaaatTTAAAACTcgtacat
 TTTTatttcta taattccatttaaatatgtTAAAAccatagttggTgat
 ggatagttgaaacacaaaagtgagctcaggttaagggggcctggat
 tgctgtctctctacactttggaaagtctctgtttta cgaagaacacagca
 atactatctccagctcagagcaatgtgctggttgccaact cctgagtgga
 ttgctactgggcaaccttcgagggtta cgggaaggctgagattattctcc
 agagactaaagttggggcagcattaaaggccagatggactgagcagcgca
 gctcctgacctcaaggttccctcattttcagATGTGGAGCTGGACTTCCA
 GAGGAGTGTACAGGCTGTGCTGCGAGAGCTCAACACCCCAACCCAGCCC
 TCCAGAGCAATCAGGgttaagagctggagcaggaagcagcactcctcctc
 cccagccccta tcccg tccctccatttctgtctcaggcat tccaggaag
 ggaacaaacctgtgttctcaggtgaggggtttccagcttagctgtctgct
 tgtggacttggaaggcttctctgctcctgat acaaacctcctggttcat
 atgttaagaccaagttgggtgggttaactgaagctgcaaaagaaatga
 agtctcaggttagaggggactgggtgccaattgttagacaggaatgggt
 tctgttaccttcttctcctggttaccttccccacttccacttccaaacaa
 actctgttttaggacctagaatcattcagaaggoggtgggctctgggc
 ctccacataatta ctgctccatgctca cacatatacctctgtctgtctct
 gtgctctcctcttggttctggcctaggagctcactgcctagaagagct
 agagatcaggtggccacaggaggagctcacca caagcatctggggtcagc
 tcttactacagggctcagatgtagctggctggctccactctaggactcagg
 gaaagctctctaagacctctggtcccacccagccatgaogggctctctt
 ctctggctcagGCATGTGGAGATGGTCTCTGCACAAGAAGGTGGAGAGA
 AACCCAGGAAAGAGCTCCATTCTGGTCCGAATTCTGCTCAGAGAGCTGGA
 GAAGgtgagtgctcaagcct

Pik3r6 CRISPR #7

- 266 bp

D

agtgggaatgat acagcagga

gattcaattcctcctctgacctccatacacatgtgcatgggtgcacatat
 ctgaacacacatatatacatatacatatacatatacatatacatatacat
 acatgtgcatatgccatataatgtatgtatgtatgtatgtatgtat
 aacatataatgcatccacatgtatatagccacatacttatacacacatat
 acatgcatatgaccacacacttatacacatatacatatgaccacacactt
 atacacatacacatgcatatgcccacacacaccaattatTTTTAAAAA
 gttatagaatacaagcactactataactaagatagtttagctggtaatca
 agatggctgctaagactaatggataagtaggtgtatattacatgtact
 ctgaaaagaaagatagttcagggtgctggccatattggaggaggatgt
 gagatTTTaccatgctcctctgaaacaaacaaatTTAAAACTcgtacat
 TTTTatttcta taattccatttaaatatgtTAAAAccatagttggTgat
 ggatagttgaaacacaaaagtgagctcaggttaagggggcctggat
 tgctgtctctctacactttggaaagtctctgtttta cgaagaacacagca
 atactatctccagctcagagcaatgtgctggttgccaact cctgagtgga
 ttgctactgggcaaccttcgagggtta cgggaaggctgagattattctcc
 agagactaaagttggggcagcattaaaggccagatggactgagcagcgca
 gctcctgacctcaaggttccctcattttcagATGTGGAGCTGGACTTCCA
 GAGGAGTGTACAGGCTGTGCTGCGAGAGCTCAACACCCCAACCCAGCCC
 TCCAGAGCAATCAGGgttaagagctggagcaggaagcagcactcctcctc
 cccagccccta tcccg tccctccatttctgtctcaggcat tccaggaag
 ggaacaaacctgtgttctcaggtgaggggtttccagcttagctgtctgct
 tgtggacttggaaggcttctctgctcctgat acaaacctcctggttcat
 atgttaagaccaagttgggtgggttaactgaagctgcaaaagaaatga
 agtctcaggttagaggggactgggtgccaattgttagacaggaatgggt
 tctgttaccttcttctcctggttaccttccccacttccacttccaaacaa
 actctgttttaggacctagaatcattcagaaggoggtgggctctgggc
 ctccacataatta ctgctccatgctca cacatatacctctgtctgtctct
 gtgctctcctcttggttctggcctaggagctcactgcctagaagagct
 agagatcaggtggccacaggaggagctcacca caagcatctggggtcagc
 tcttactacagggctcagatgtagctggctggctccactctaggactcagg
 gaaagctctctaagacctctggtcccacccagccatgacgggtctctt
 ctctggctcagGCATGTGGAGATGGTCTCTGCACAAGAAGGTGGAGAGA
 AACCCAGGAAAGAGCTCCATTCTGGTCCGAATTCTGCTCAGAGAGCTGGA
 GAAGgtgagtgctcaagcct

Pik3r6 CRISPR #16

- 10 bp and - 483 bp

E

```

                                agtgggaaatgatacagcagga
cattcaattcctcctctgacctccatacacatgtgcatgggtgcacatat
ctgaacacacatatacatacatacatacatacatacatacacacacat
acaatgcatatgcccataatataatgtaatgtaatgtaatgtaatgtaat
aacatataatgcatccacatgtaatgacacatacttatacacacacatat
acatgcatatgaccacacacttatacacacacacacacacacacacactt
atacacatacacatgcatatgcccacacacaccaattattttttaaaaaa
gttattagaatacaagcaactactataactaagatagtttagctggtaatca
agatggctgctaataatgactaatggataagtaggtgggtatattacatgtact
ctgaaaaaagaatagttcagggtgtcgggccaatgaggaggaggatgt
gagattttaccatgctcctctgaacaaacaaacaaacttaaaactcgtacat
tatttatttctaataatcccatttaataatgtaaaacacatagttgggtgat
ggatagttgaaacacaaaaagtgaggtctcaggtaagaggggctggat
tgctgtctctctacactttggaagttctgggttttaagaagaacacagca
atactatctccagctcagagcaatgtgctgggtgccaactcctgatgga
ttgctactgggcacccttcgaggtttaagggaaggctgagattattctcc
agagactaaagggtggggcagcattaaggccagatggactgagcagcgca
gctcctgacctcaaggttcctcattttcagATGTGGAGCTGGACTTCCA
GAGGAGTGTACAGGCTGTGCTGCGAGAGCTCAACACCCCAACCCAGCCC
TCCAGAGCAATCAGGgt aagagctggagcaggaagcagccactcctcacc
ccccagccctaaccgctcctccatttctgtctcaggcattccaggaag
ggacaaacctgtgttctcaggtgaggggtttccagcttagctgtctgct
tgtggacttggaggcttctctgcttctgatacaaacctcctgggtcat
atgttaagaccacagttgggtgggttaactgaagctgcaaaagaaatga
agtctcaggttagaggggactgggctgcoatatgtagacaggaatgggt
tctgttaccttcttctcctggttaccttccccacttccacttccaaa caaa
actctgttttaggacctagaatcattcagaaggcggctggggctctgggc
ctccacataattaactgctccatgcttccacacatacctctgtctgtctctt
gtgctctcctctctgttctggcctaggagctcactgcctagaagagct
agagatcaggtggccacaggaggagctcaccacaagcactctggggtcagc
tcttactacaggtcagatgtagctggctgggtccccctctaggactcagg
gaaacagctctcaagaacctctggteccacccagccatgacgggtctcttt
ctcctggctcagGCATGTGGAGATGGTCTCTGCACAGAAGGTGGAGAGA
AACCCAGGAAGAGCTCCATTCTGGTCCGAAATCTGCTCAGAGAGCTGGA
GAAGgtgagtgctcaagcct

```

Pik3r6 CRISPR #20

- 800 bp

Figure 4.8: Sequencing PCR of *Pik3r6* CRISPR pups #1, #5, #7, #16 and #20 confirms large deletions to regions flanking the CRISPR target site.

PCR products amplified from the genomic DNA of *Pik3r6* CRISPR #1, #5, #7, #16 and #20 were sequenced to determine CRISPR-induced large deletions. The regions flanking *Pik3r6* exon 1, the CRISPR target site, the CRISPRlong F and R primers (*highlighted yellow*) and the deletions identified (*highlighted grey*) are summarised for (A) #1, (B) #5, (C) #7, (D) #16 and (E) #20.

Intentionally blank

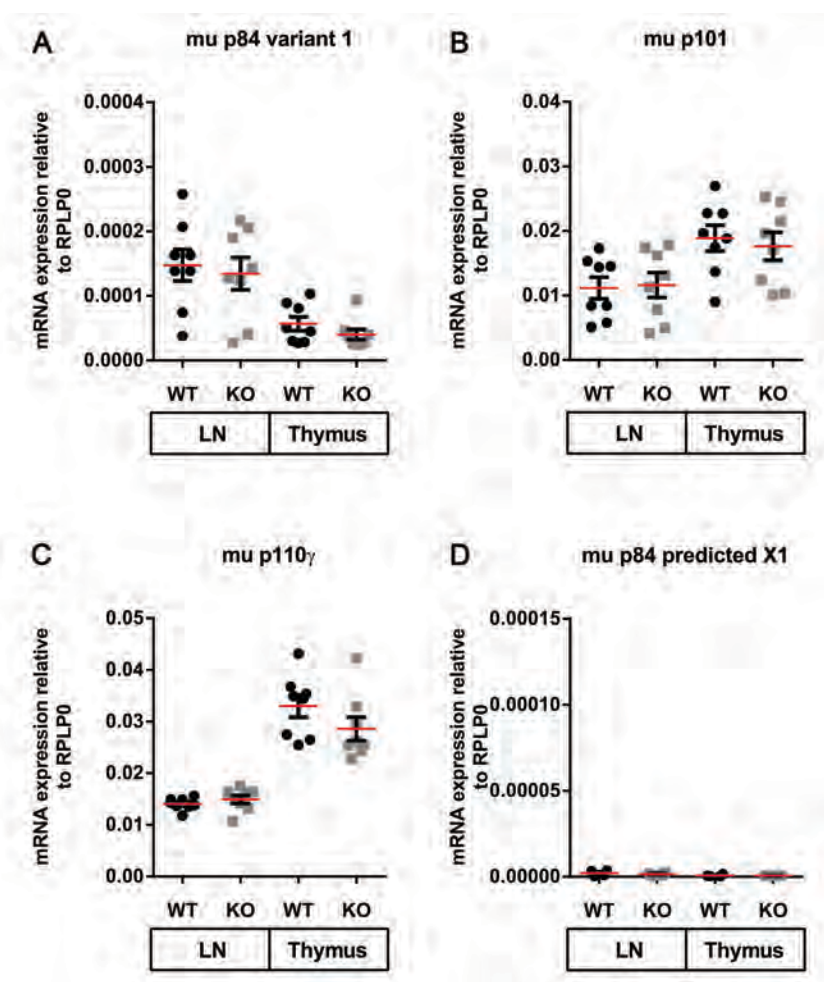
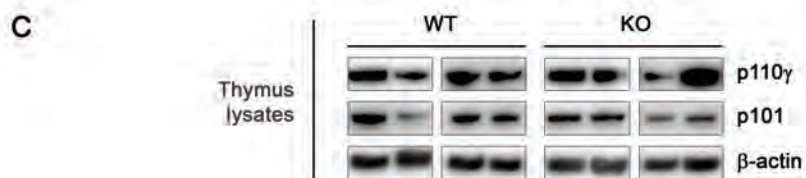
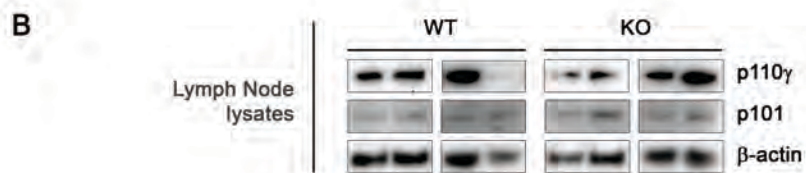
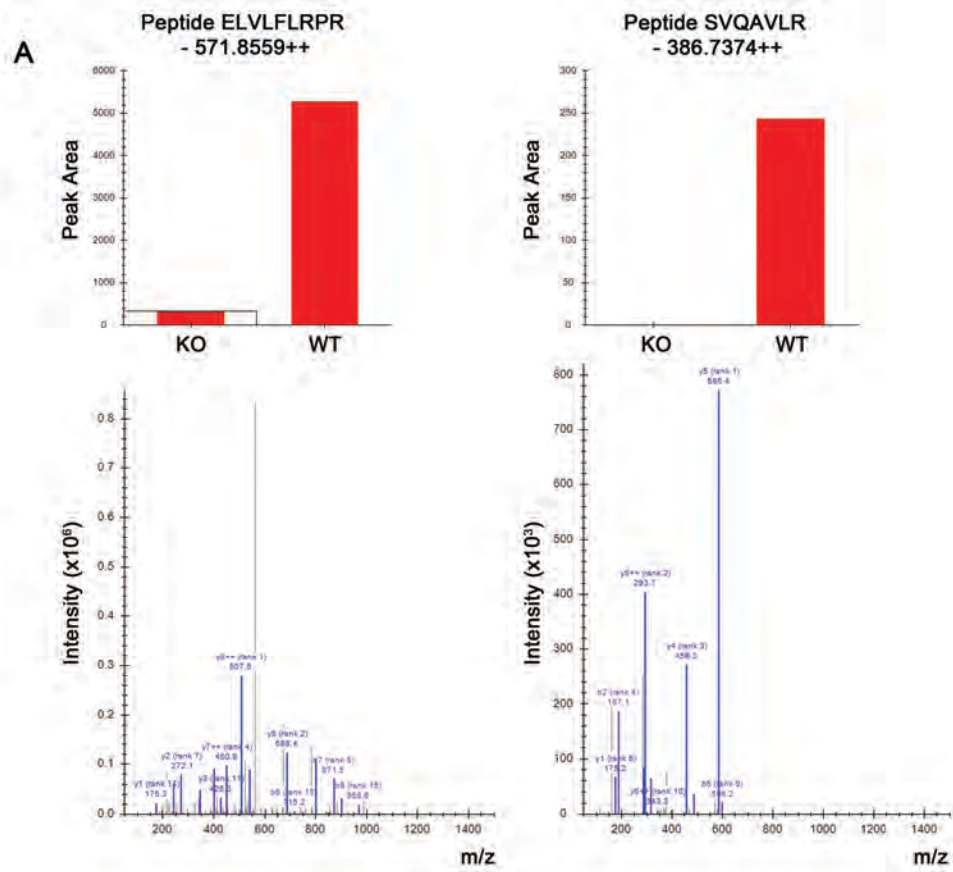


Figure 4.9: Genomic CRISPR-induced deletion (Δ -10bp) within *Pik3r6* does not alter the transcript expression of PI3K γ subunits.

Total RNA from the lymph nodes (2×10^5 cells) and thymus (5×10^5 cells) of wildtype and *Pik3r6*^{-/-} mice were isolated for quantitative PCR analysis. The mRNA transcript expression is shown for (A) *Pik3r6* (p84), (B) *Pik3r5* (p101), (C) *Pik3cg* (p110 γ) and (D) a predicted X1 isoform of *Pik3r6*. Data is presented as expression relative to RPLP0 \pm SEM (n=8).

Figure 4.10: Genetic mutation of *Pik3r6* does not destabilise the protein expression of p101 and p110 γ PI3K γ subunits.

(A) Knockout of p84 protein expression confirmed from spleen, thymus and bone marrow tissues of *Pik3r6*^{-/-} mice relative to wildtype tissues by Parallel Reaction Monitoring using a Dionex nano-flow HPLC coupled to an Impact II QTOF (Bruker Daltonics). Two peptides were targeted; the doubly charged forms of ELVLFLRPR (m/z 571.8559) and SVQAVLR (m/z 386.7374). Peptides were selected based on previous acquisition data for *Pik3r6* (refer to section 3.2.2) as observed precursor ion masses were known and fragmentation spectra were available for use in a spectral library. Representative spectra for *Pik3r6*^{-/-} and wildtype spleen samples are shown. Protein expression of p110 γ and p101 assessed by Western blot analysis of total protein lysates from (B) lymph node (7 μ g lysate per lane) and (C) thymus (10 μ g lysate per lane), relative to the expression of β -actin as a protein loading control; (n=4).



Intentionally blank

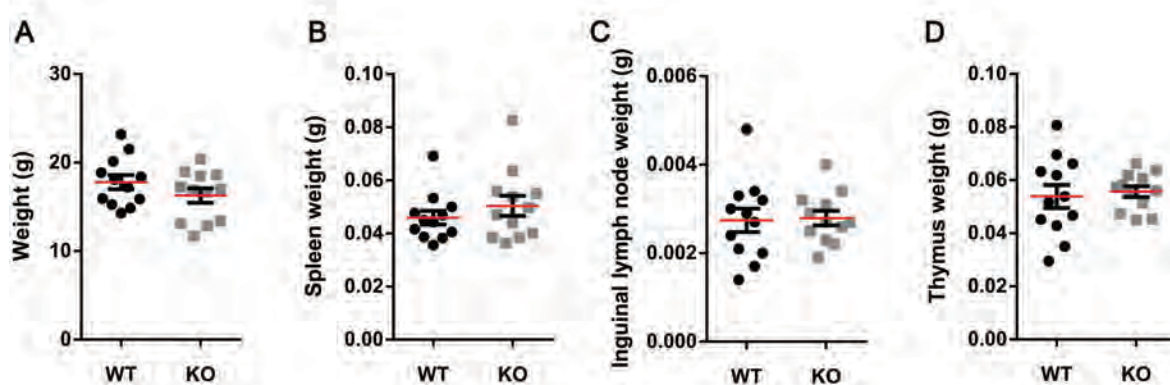


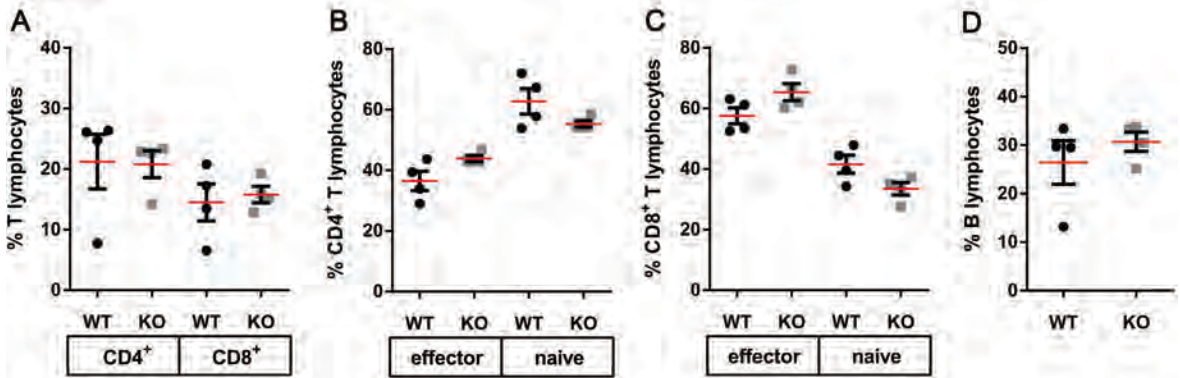
Figure 4.11: The weights of lymphoid organs of $Pik3r6^{-/-}$ mice are comparable to wildtype C57Bl/6n mice.

(A) Total animal weight and the weight of the (B) spleen, (C) inguinal lymph nodes and (D) thymus of 6-8 week-old male mice were assessed. Data are presented as mean \pm SEM (n=12).

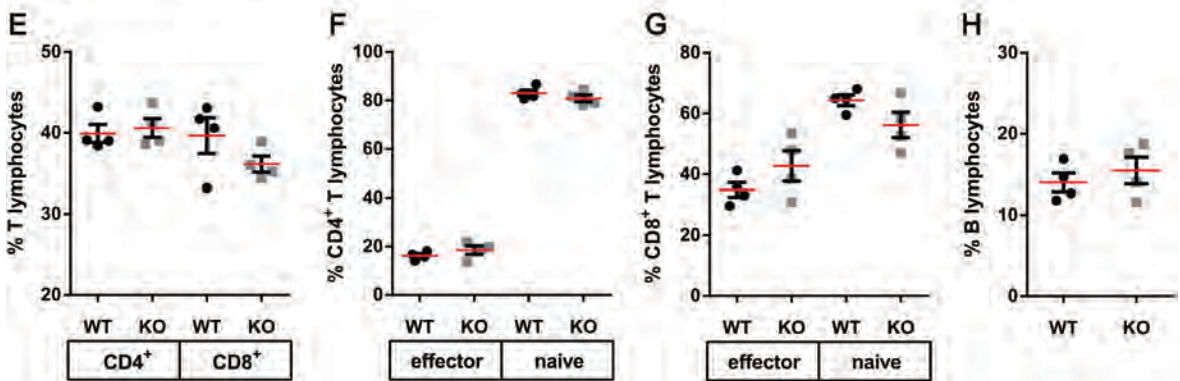
Figure 4.12: Immune cell subsets within lymphoid compartments and the blood of $Pik3r6^{-/-}$ mice are consistent with wildtype mice.

The spleen, lymph nodes and peripheral blood were harvested from 8 week-old wildtype control and $Pik3r6^{-/-}$ mice and analysed by flow cytometry for populating cell subsets. Proportions for cell subsets are shown for **(A-D)** spleen, **(E-H)** lymph nodes and **(I-K)** peripheral blood; subsets are defined as follows: Helper and cytotoxic T lymphocytes ($CD3^+CD4^+$; $CD3^+CD8^+$) were divided into naïve and effector populations based on CD44 expression (naïve, $CD44^-$; activated, $CD44^+$), B lymphocytes ($B220^+$) and neutrophils ($CD11b^+ F4/80^- Gr-1^+$). Data are presented as mean percentage positive \pm SEM (n=4).

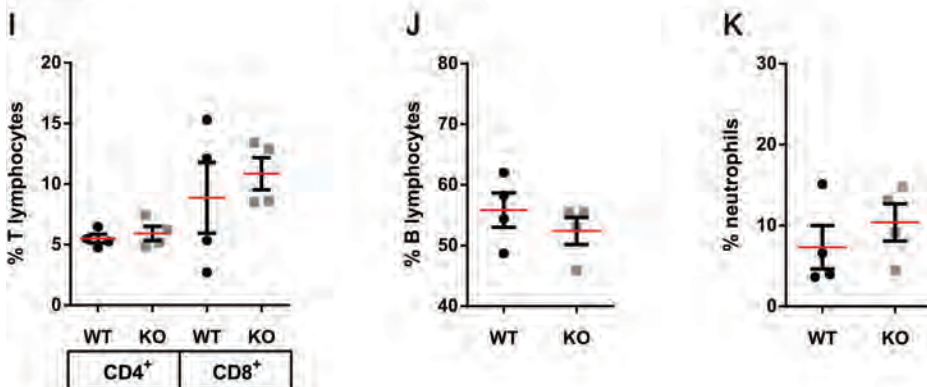
Spleen



Lymph Node



Blood



Intentionally blank

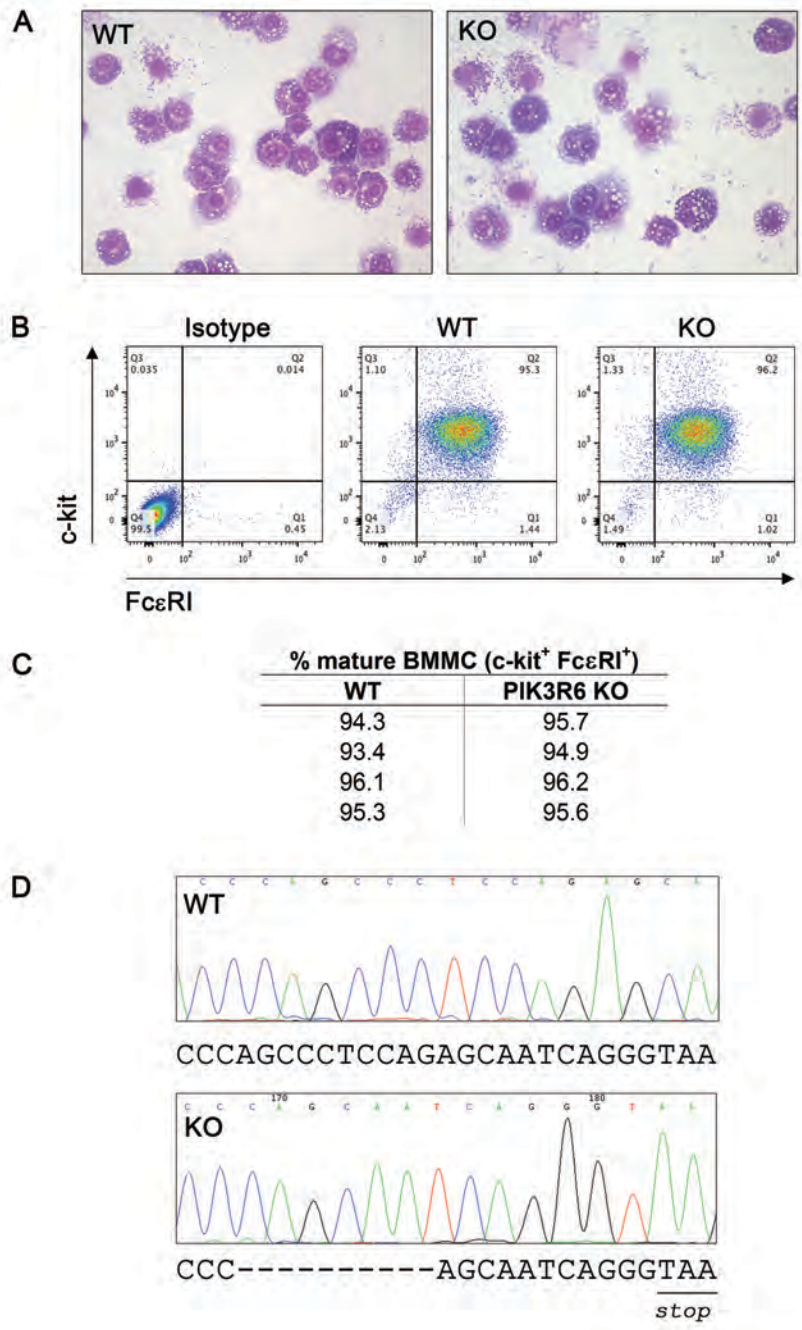


Figure 4.13: $Pik3r6^{-/-}$ bone marrow cells display inhibited induction of phosphorylated Akt in response to GPCR stimulation.

Total bone marrow cells were harvested from the femurs and tibias of $Pik3r6^{-/-}$ and wildtype mice, rested and then stimulated with 10nM IL-8. Western blot analysis of stimulated bone marrow cell lysates was used to detect (A) phosphorylated Akt as a measure of PI3K γ activation, in comparison to the level of (B) total Akt as a loading control. Representative blot shown.

Figure 4.14: p84-deficient bone marrow-derived mast cells are phenotypically similar to wildtype cells and express maturity markers.

Total bone marrow was harvested from the femurs and tibias of $Pik3r6^{-/-}$ and wildtype mice, then mast cells were cultured and expanded for 6 weeks in IL-3 supplemented media. **(A)** May-Grunwald Giemsa staining of 6 week-old bone marrow mast cell (BMMC) cultures revealed a mature phenotype; representative images of WT and $Pik3r6^{-/-}$ BMDCs (n=4). **(B, C)** Maturity of BMMC cultures assessed by flow cytometric analyses based on a mature $c\text{-kit}^+ Fc\epsilon RI^+$ phenotype, shown by representative plots and the percentage of live cells from WT and $Pik3r6^{-/-}$ BMMC cultures; (n=4). **(D)** Genetic CRISPR-induced (Δ -10bp) deletion of $Pik3r6^{-/-}$ BMDCs confirmed by genomic DNA sequencing PCR compared with wildtype BMDCs; representative chromatogram shown (n=4).



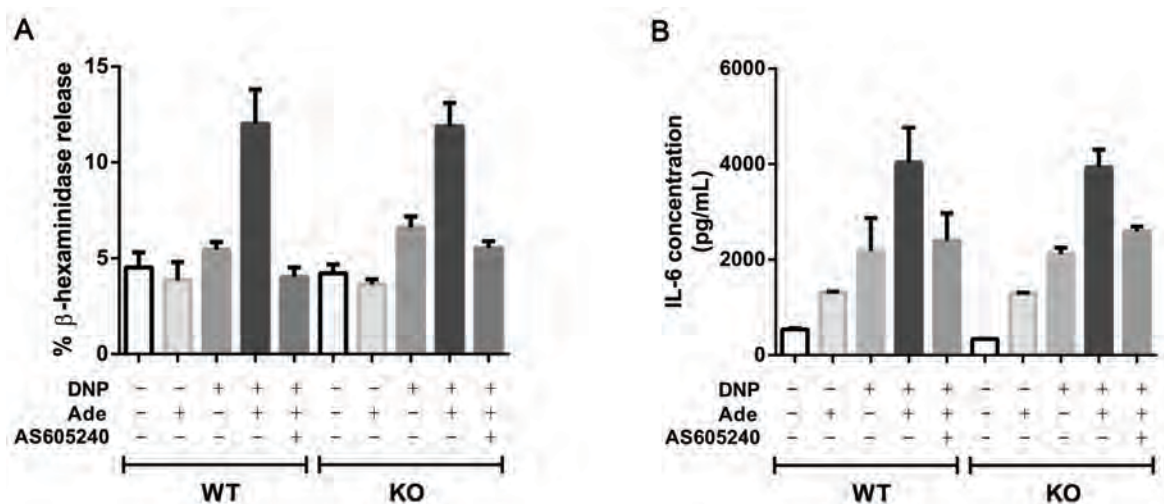


Figure 4.15: $Pik3r6^{-/-}$ BMMCs maintain adenosine-mediated potentiation of degranulation and IL-6 cytokine production.

Functionality of $Pik3r6^{-/-}$ and wildtype bone marrow-derived mast cells (BMMCs) was assessed in the context of degranulation and cytokine release in the presence of adenosine. (A) BMMCs were sensitised overnight with anti-DNP IgE and stimulated with $10\mu\text{g}$ DNP in the presence or absence of $20\mu\text{M}$ adenosine and $1\mu\text{M}$ AS605240; β -hexaminidase release was calculated as a measure of antigen/IgE-mediated degranulation; (n=4). (B) BMMCs were sensitised overnight with anti-DNP IgE and stimulated with $10\mu\text{g}$ DNP in the presence or absence of $20\mu\text{M}$ adenosine and $1\mu\text{M}$ AS605240; IL-6 cytokine release was determined by ELISA of the cell supernatant; (n=4).

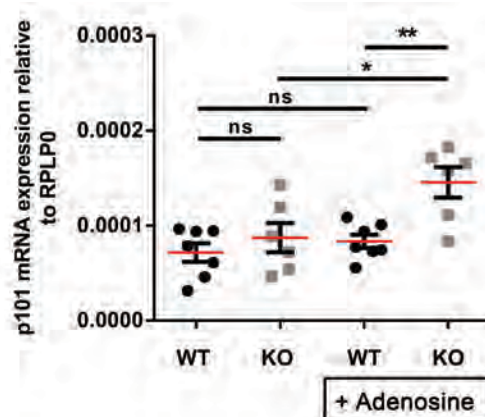


Figure 4.16: *Pik3r6*^{-/-} BMMCs display redundancy between p84 and p101 adaptor subunits.

Pik3r6^{-/-} and wildtype BMMCs were cultured for 45 minutes in the presence or absence of 20 μ M adenosine, lysed and RNA was harvested. qPCR analysis of p101 mRNA transcript expression relative to RPLP0, data are presented as mean \pm SEM, (n=6), t-test *p<0.05, **p<0.01.

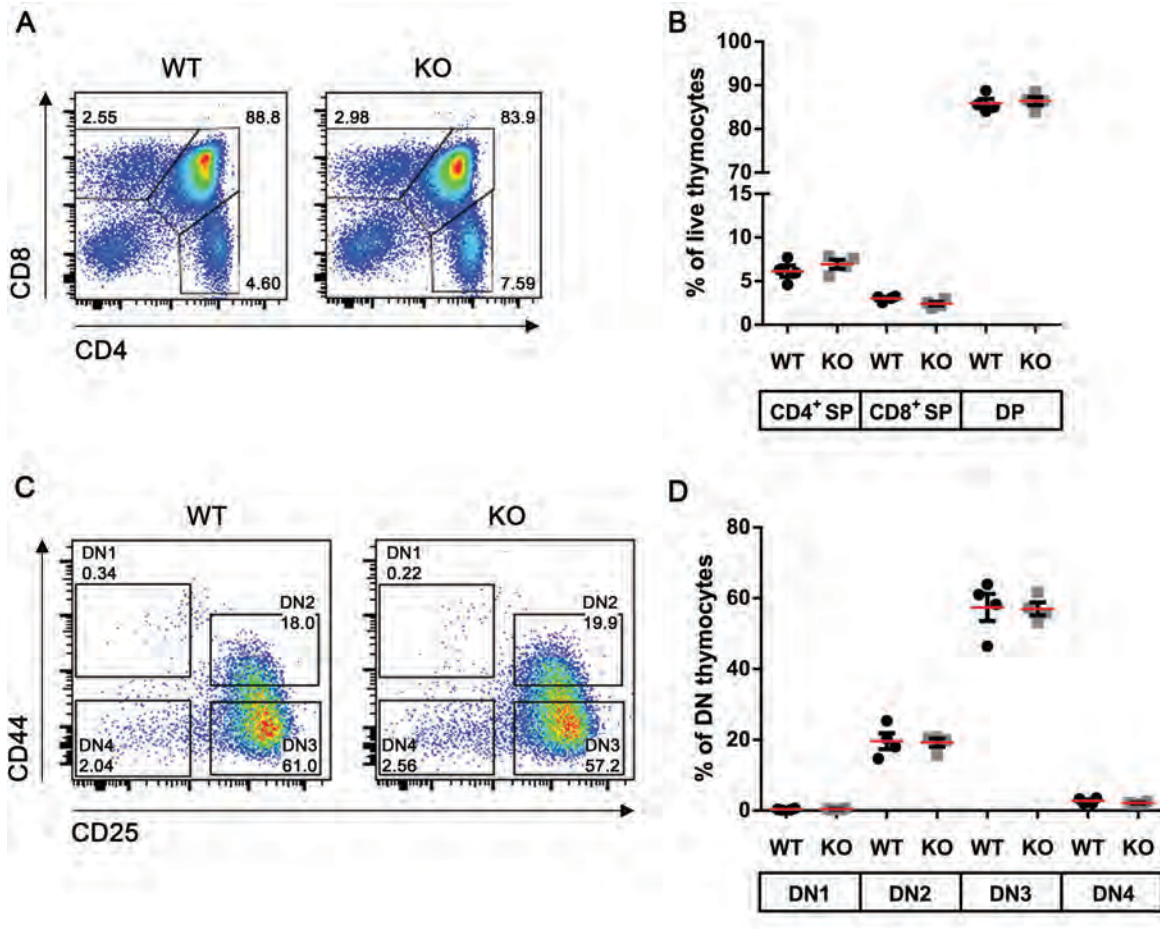


Figure 4.17: Thymocyte development is unaffected in $Pik3r6^{-/-}$ mice.

The proportions of double positive ($CD4^{+}CD8^{+}$) and double negative thymocyte populations (DN1-4) were determined by flow cytometry. (A) Representative dot plots and (B) proportion of wildtype and $Pik3r6^{-/-}$ thymocytes defined as CD4 single positive ($CD4^{+}CD8^{-}$), CD8 single positive ($CD4^{-}CD8^{+}$) or double positive ($CD4^{+}CD8^{+}$). (C) Representative dot plots and (D) proportion of wildtype and $Pik3r6^{-/-}$ double negative thymocyte populations (DN1-4) based on a lineage dump pre-gate (CD3, CD4, CD8, CD11c, Gr-1, CD45R), then $CD44^{+/-}CD25^{+/-}$ phenotype, defined as follows: DN1 ($CD44^{+}CD25^{-}$), DN2 ($CD44^{+}CD25^{+}$), DN3 ($CD44^{-}CD25^{+}$) and DN4 ($CD44^{-}CD25^{-}$). Data are presented as mean percentage positive \pm SEM, (n=4).

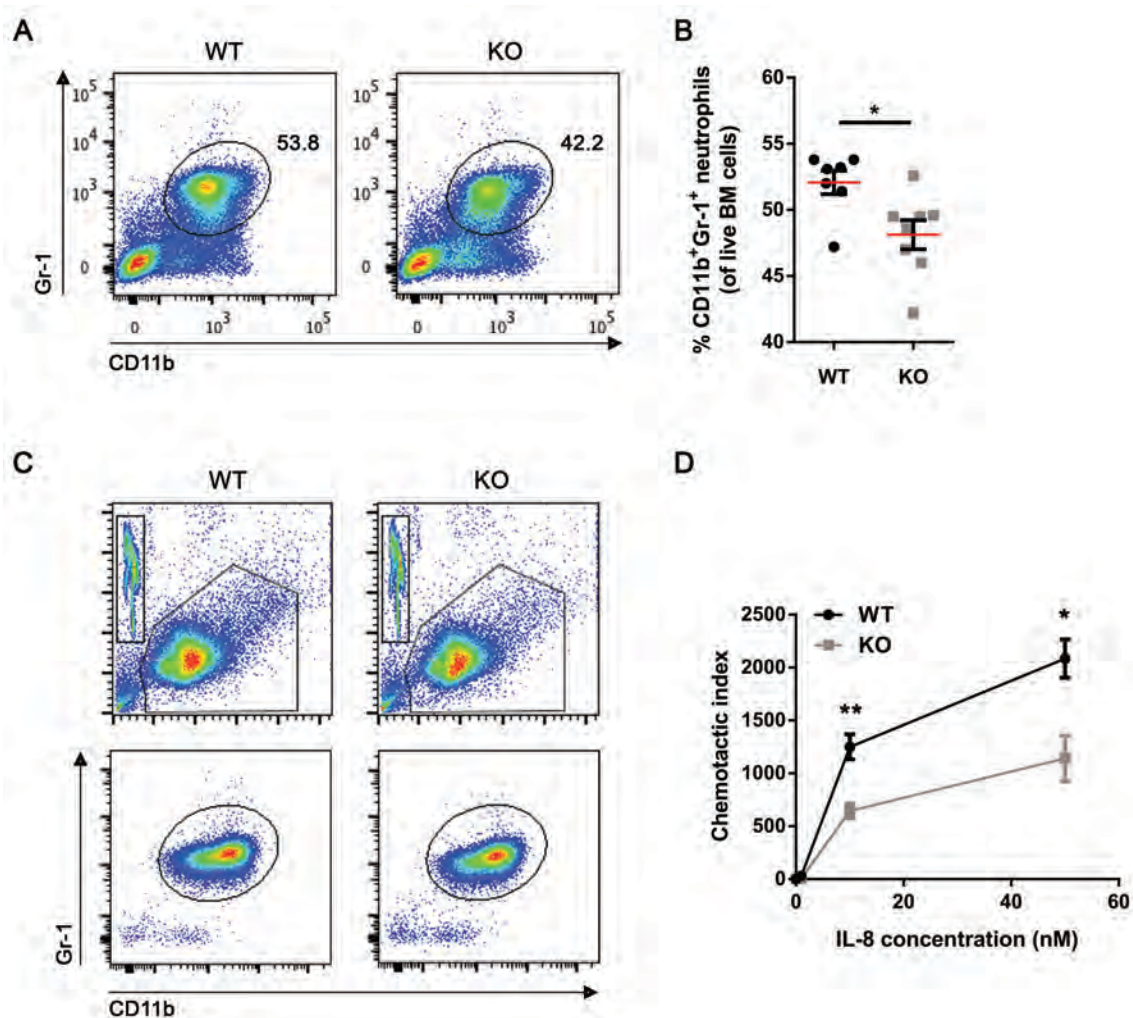


Figure 4.18: $Pik3r6^{-/-}$ bone marrow-derived neutrophils display reduced migration *in vitro*.

Total bone marrow cells were harvested from 8 week-old male wildtype and $Pik3r6^{-/-}$ mice for transwell chemotaxis. (A) Representative plots and (B) proportion of live $CD11b^{+}Gr-1^{+}$ neutrophils within total bone marrow cells for wildtype and $Pik3r6^{-/-}$ mice, as determined by flow cytometry. Total bone marrow cells were induced to migrate in response to 0nM, 1nM, 10nM or 50nM IL-8 gradients in a transwell chemotaxis assay for 30 mins. Neutrophil migration was calculated as chemotactic index as determined flow cytometric analysis relative to the negative control (0 μ M IL-8) and standardised using BD FACS microbeads; shown as (C) representative plots and (D) chemotactic index of $Pik3r6^{-/-}$ and wildtype neutrophils. Data are presented as mean \pm SEM, (n=8), t-test * $p < 0.05$, ** $p < 0.01$.

Intentionally blank

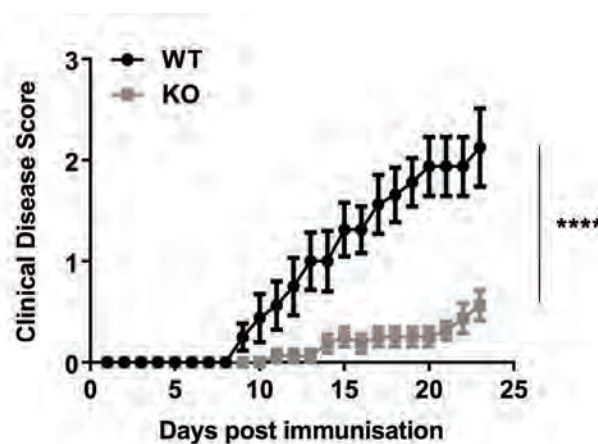
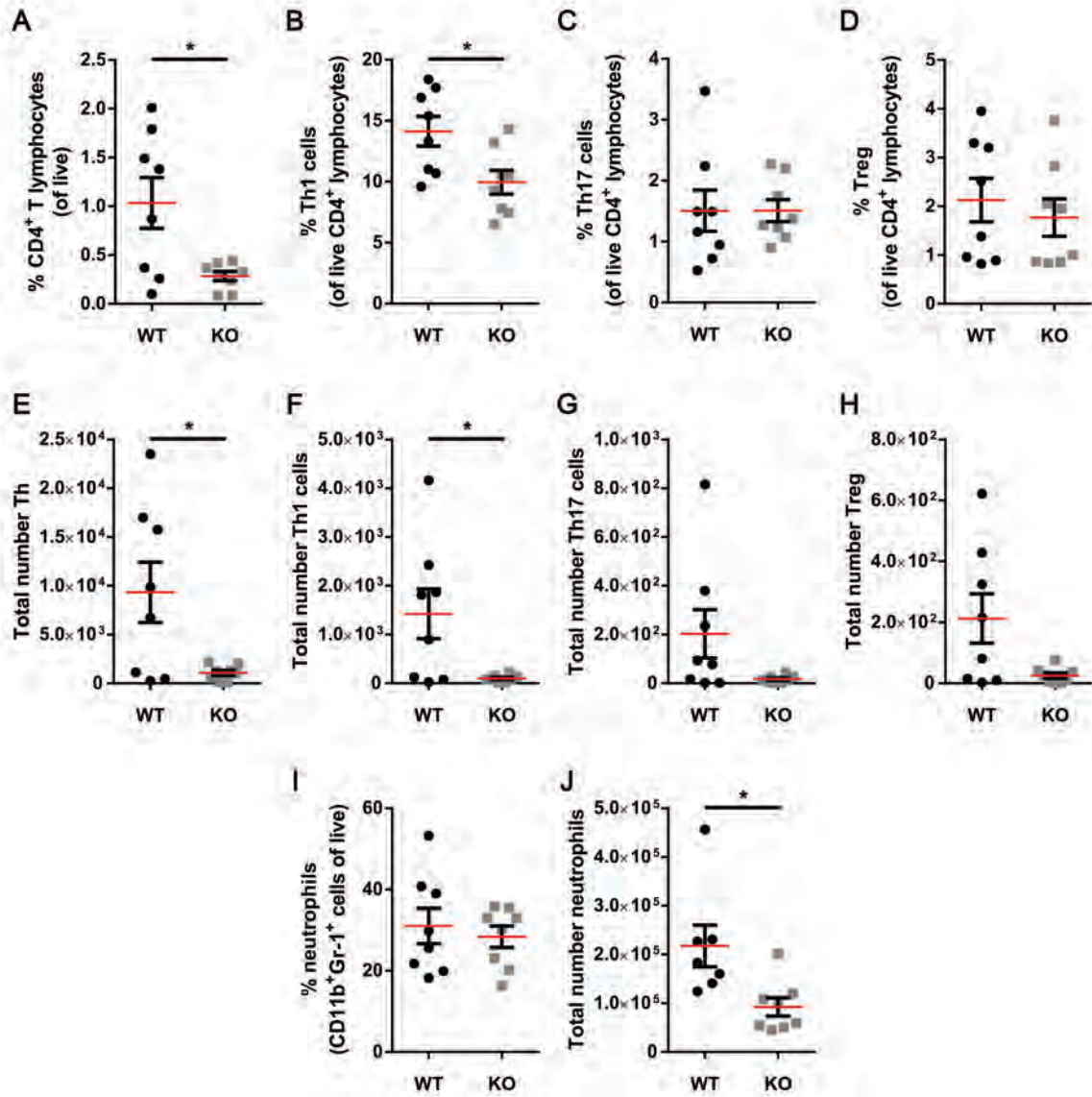


Figure 4.19: $Pik3r6^{-/-}$ mice display attenuated disease upon induction of MOG_{35-55} -induced chronic experimental autoimmune encephalomyelitis.

Chronic experimental autoimmune encephalomyelitis disease was induced with subcutaneous hind flank injection of $50\mu\text{g}$ MOG_{35-55} peptide in a CFA emulsion and dual injections of 300ng pertussis toxin administered intravenously. The clinical disease scores of wildtype and $Pik3r6^{-/-}$ mice were monitored daily post induction, ($n=8$); 2-way ANOVA **** $p<0.0001$.

CNS



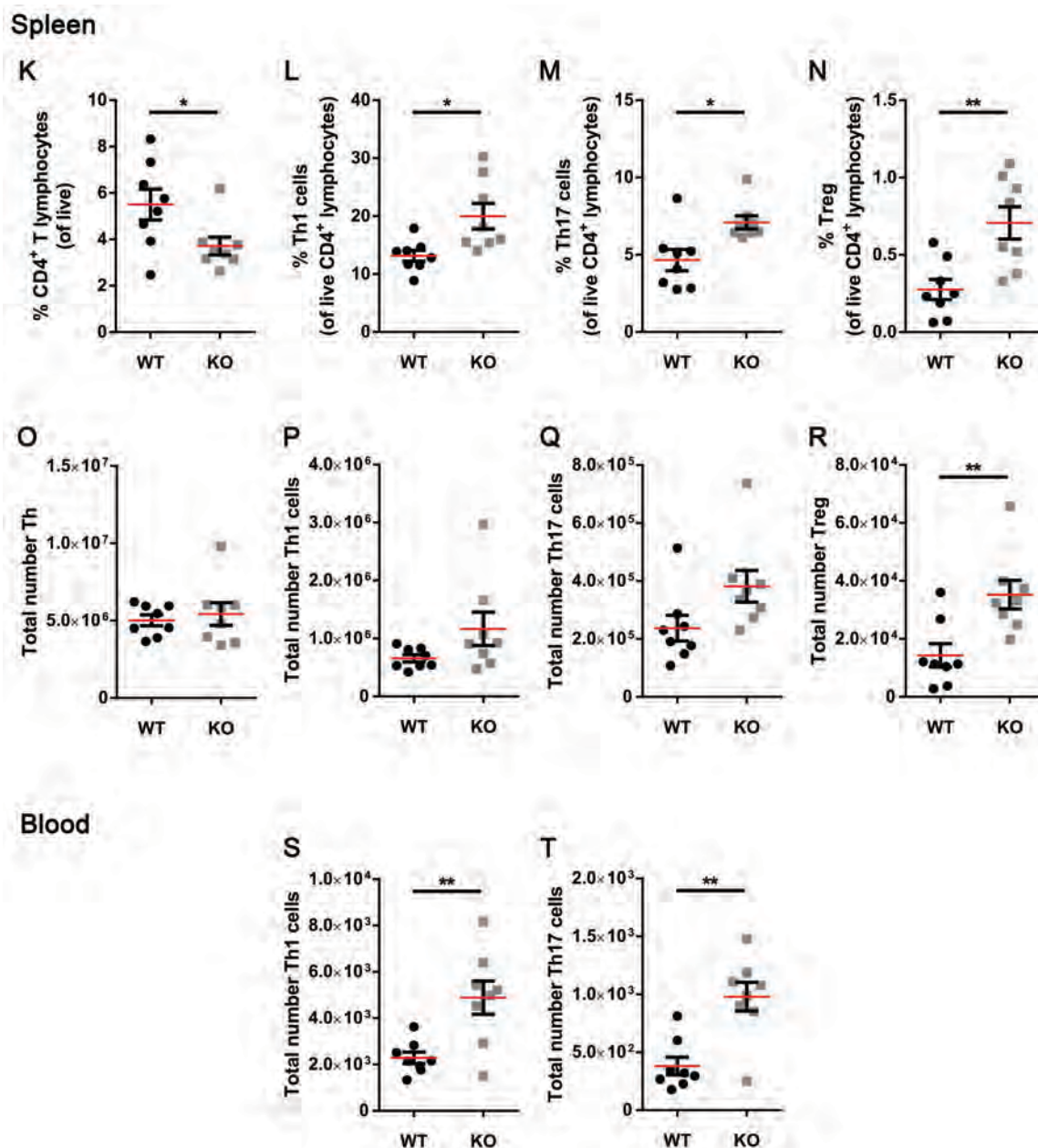


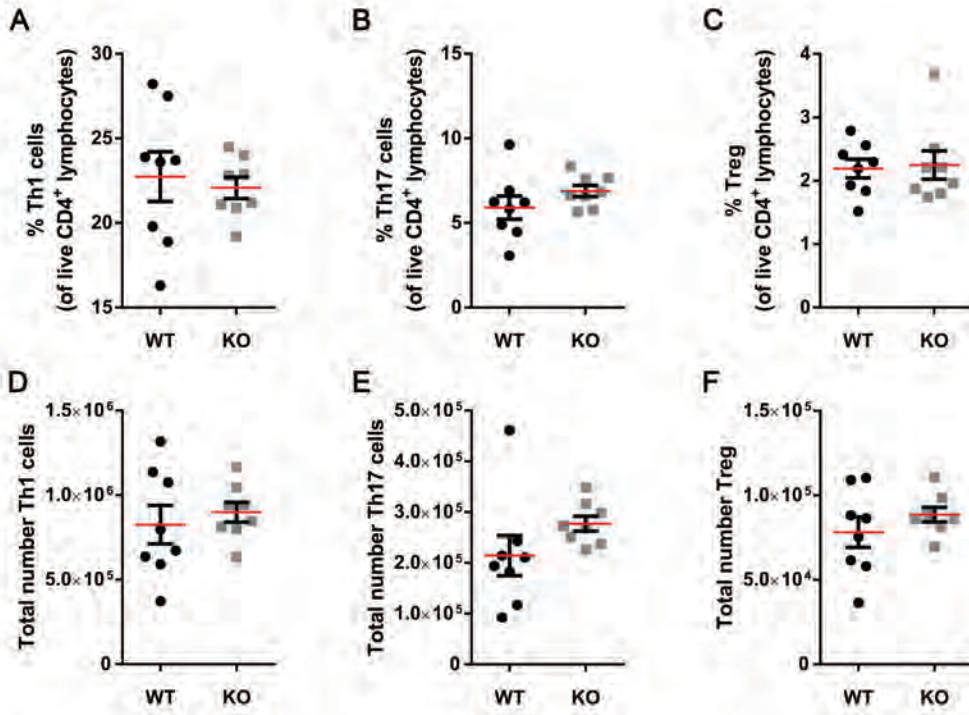
Figure 4.20: Dampened EAE disease severity in $Pik3r6^{-/-}$ mice is coupled with reduced infiltration of Th cells into the CNS.

The spleen, peripheral blood, brain and spinal cord were harvested from diseased wildtype and $Pik3r6^{-/-}$ mice at day 23-post EAE disease induction to assess the generation and trafficking of CD4⁺ T helper subsets and the recruitment of neutrophils to the damaged CNS. The proportion and number of defined immune cell subsets are presented for (A-J) CNS, (K-R) spleen and (S, T) peripheral blood preparations, as determined by flow cytometry. Populations were defined as follows; Th1 (CD4⁺ FoxP3⁻ IFN- γ ⁺ IL-17A⁻), Th17 (CD4⁺ FoxP3⁻ IFN- γ ⁻ IL-17A⁺), Treg (CD4⁺ FoxP3⁺), neutrophils (CD45⁺ CD11b⁺ F4/80⁻ Gr-1⁺). Data are presented as mean \pm SEM, (n=8), t-test *p<0.05, **p<0.01.

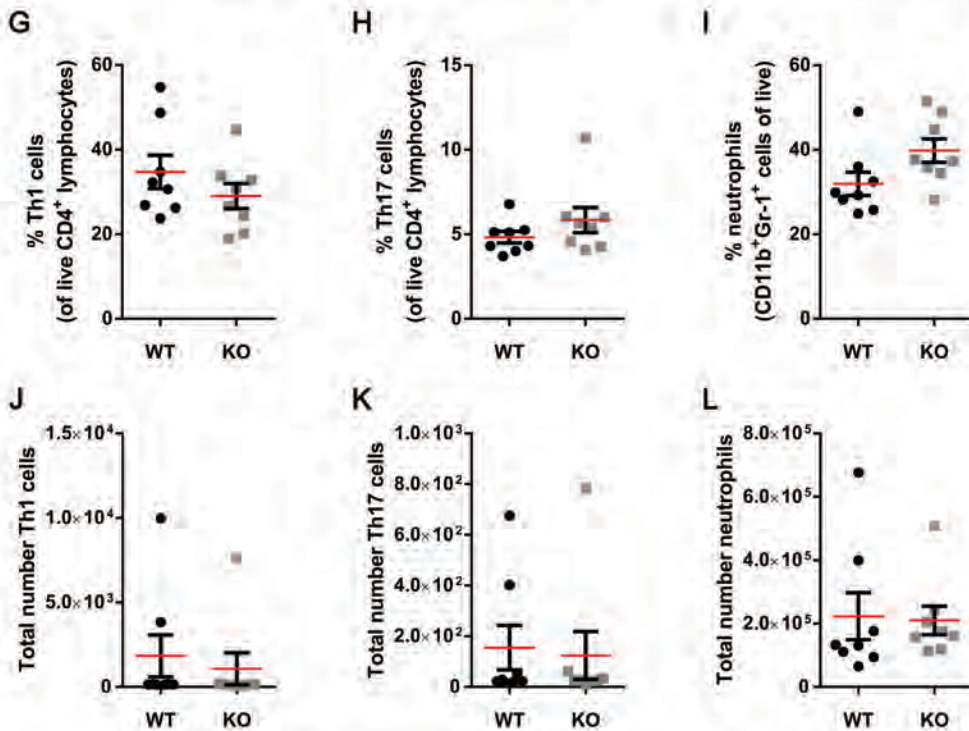
Figure 4.21: Generation of Th1 and Th17 effector cells is unaffected in *Pik3r6*^{-/-} mice during early stage EAE disease compared with wildtype controls.

The spleen, brain and spinal cord were harvested from immunised wildtype and *Pik3r6*^{-/-} mice at day 10 post-EAE disease induction to assess the generation of CD4⁺ T helper subsets and the recruitment of neutrophils to the CNS. The proportion and number of defined immune cell subsets are presented for (*A-F*) spleen and (*G-L*) CNS preparations, as determined by flow cytometry. Populations were defined as follows; Th1 (CD4⁺ FoxP3⁻ IFN- γ ⁺ IL-17A⁻), Th17 (CD4⁺ FoxP3⁻ IFN- γ ⁻ IL-17A⁺), Treg (CD4⁺ FoxP3⁺), neutrophils (CD45⁺ CD11b⁺ F4/80⁻ Gr-1⁺). Data are presented as mean \pm SEM, (n=8).

Spleen



CNS



Chapter 5: Quantitative proteome
profiling of CNS-infiltrating CD4⁺ Th
cells during EAE

Chapter 5: Quantitative proteome profiling of CNS-infiltrating CD4⁺ Th cells reveals selective changes during experimental autoimmune encephalomyelitis

5.1 Introduction

PI3K γ has established roles in the priming of pathogenic Th1 and Th17 cells in secondary lymphoid organs and for their trafficking to the inflamed CNS during EAE disease pathology^{9, 139}. Previous publications from our laboratory have demonstrated that p110 γ -deficient mice (p110 γ ^{-/-}) display reduced EAE disease severity relative to wildtype control animals and that priming of CD4⁺ Th effector cell subsets is impaired as a result of defective dendritic cell migration into secondary lymphoid organs¹³⁹. Others have shown that activated Th cells also exhibit migratory defects during disease induction, which results in significantly reduced accumulation of immune cells within the inflamed CNS, compared with wildtype animals⁹. For these reasons, it was hypothesised that the PI3K γ adaptor protein p84 would be required for PI3K γ -dependent lymphocyte migration during EAE disease induction. To address the requirement of p84 in PI3K γ -dependent processes during EAE, two approaches were undertaken to generate a p84-deficient mouse. The first approach and initial strategy, which was conducted in years 1 and 2 of the project, involved the cloning of a DOX-inducible lentiviral p84 knockdown construct for the transduction of bone marrow-derived stem cells. Transduced stem cells would be used to create reconstituted chimeric mice where p84 expression could be inducibly knocked down in haematopoietic cells using doxycycline. However, while the cloned p84 knockdown constructs were capable of reducing p84 expression in transduced cell lines upon doxycycline treatment, the lentiviral transduction of bone marrow-derived stem cells with these constructs was unreliable and inefficient (*data not shown*). Therefore, when CRISPR and TALEN gene-editing technologies became available at the commencement of year 3 of

the project, these were employed to generate a broad p84 knockout mouse (data presented in Chapter 4). Targeting p84 using CRISPR gene-editing of *Pik3r6* proved the most efficient method to produce a p84-deficient mouse and was therefore pursued and resulted in the generation and characterisation of the *Pik3r6*^{-/-} mouse.

Prior to the generation of the p84-deficient mouse, a proteomic strategy was developed that would be used to compare the proteomes of p84-deficient and wildtype CD4⁺ Th cells during EAE disease progression. The optimisation of an isotope-coded protein-labelling (ICPL) method using wildtype cells isolated during EAE disease was conducted to firstly develop the method of cell isolation, labelling and analysis and secondly, to determine the mechanisms by which CD4⁺ cells promote inflammation in the CNS during EAE. Ultimately, the goals of the devised proteomic analyses were to determine the proteins involved in the activation, differentiation, migration and pathobiology of CD4⁺ cells during EAE disease and elucidate the signalling pathways that are dependent on p84. After the initial study using wildtype cells, this would be achieved by comparing the proteomes of CD4⁺ cells isolated from the spleen, peripheral blood and CNS of *Pik3r6*^{-/-} and wildtype mice during EAE disease progression, in order to examine CD4⁺ cell priming in secondary lymphoid organs through to their migration into the inflamed CNS.

However, extensive proteomic analyses on defined cell populations isolated during EAE disease had not been performed due to the rarity of CD4⁺ cells in the blood and inflamed CNS, particularly during disease induction. Rather, previous studies relating to EAE have utilised whole tissues (such as the brain, spinal cord and cerebrospinal fluid) for proteomic analyses²²³⁻²³⁷. The disadvantage of these approaches is that highly abundant serum proteins dominate whole-tissue analyses and it is not possible to distinguish between

proteins derived from CNS-infiltrating cells and tissue-resident cells. In order to gather information regarding the pathobiology of CD4⁺ cells specifically, these cells would need to be isolated from diseased tissues for proteomic analysis. Therefore, an initial study was performed to determine the feasibility of an extensive quantitative isotope-coded protein labelling (ICPL) approach to investigate the differential proteome profiles of wildtype and p84-deficient CD4⁺ cells isolated during EAE disease. For this initial study, CD4⁺ cells were isolated from the CNS of wildtype mice induced with EAE disease, at different time-points during disease progression, and were compared using quantitative ICPL labelling to determine the validity of ICPL as an approach and optimise the isolation of CD4⁺ cells from tissues. Specifically, CD4⁺ cells were isolated from the CNS of EAE-diseased wildtype mice in two EAE disease models; MOG₃₅₋₅₅-induced chronic EAE and PLP₁₃₉₋₁₅₁-induced relapsing-remitting EAE. For chronic MOG-induced EAE, the proteomes of CD4⁺ cells isolated from the CNS at disease onset and peak-disease were compared with CD4⁺ cells isolated from the spleens of naïve mice as an unactivated cell control (3 data points). For relapsing-remitting PLP-induced EAE, the proteomes of CD4⁺ cells isolated from the CNS at disease onset, peak-disease and remission phases were compared with CD4⁺ cells isolated from the spleens of naïve mice as an unactivated cell control (4 data points).

The data presented in Chapter 5 represent the results of this comprehensive initial study, which demonstrate that ICPL labelling of CD4⁺ cells isolated from tissues at multiple stages during EAE disease progression is a valid approach to assess the proteomes of pathogenic Th cells. Due to time constraints, ICPL analyses of p84-deficient (compared with wildtype) CD4⁺ cells during EAE disease progression could not be completed. Despite this, the results of this initial study described herein provide the platform for future

studies comparing the proteomes of p84-deficient and wildtype CD4⁺ cells during EAE pathogenesis.

5.2 Results

5.2.1 Isolating CD4⁺ cells during EAE disease progression for ICPL labelling

The goal of this initial study was to employ ICPL quadruplex and triplex labelling methods to examine the proteins differentially regulated by activated CD4⁺ Th cells during EAE disease progression compared with naïve CD4⁺ Th cells. This was achieved by comparing CNS-infiltrating CD4⁺ cells isolated at disease onset, peak-disease and remission phases with naïve unactivated CD4⁺ controls from wildtype mice. Two models of EAE were examined; PLP₁₃₉₋₁₅₁-induced relapsing-remitting EAE in SJL/J mice and MOG₃₅₋₅₅-induced chronic EAE in C57Bl/6 mice, in order to determine common mechanisms of cell-mediated pathology¹⁷¹. The proteomic workflow for this feasibility study in wildtype mice is presented in **Figure 5.1**. Briefly, CD4⁺ cells were isolated from the CNS of mice with PLP₁₃₉₋₁₅₁-induced EAE or MOG₃₅₋₅₅-induced EAE at defined disease stages; disease onset, peak-disease +/- remission (remission relevant only to PLP-induced relapsing-remitting EAE disease). As an unactivated cell control, naïve CD4⁺ cells were purified from the spleen of healthy controls. Total protein from each of these control or disease groups were differentially labelled with quadruplex (PLP-EAE analysis; 4 data points) or triplex (MOG-EAE analysis; three data points) ICPL, pooled and separated by LDS-PAGE and HPLC fractionation. MALDI-TOF/TOF analysis was used to determine differentially regulated proteins across disease stages and identified protein candidates were subjected to network/pathway analyses and validation by quantitative PCR of mRNA transcript expression.

CD4⁺ cells were isolated from the brain and spinal cord of mice with PLP₁₃₉₋₁₅₁-induced relapsing-remitting EAE (SJL/J) (*left*) or MOG₃₅₋₅₅-induced chronic EAE (C57Bl/6) (*right*) at designated disease stages, as shown in **Figure 5.2 (A)**, and the purity of isolated cells after positive selection using anti-CD4-coupled Dynabeads from mixed CNS (*data not shown*) and spleen cell populations was confirmed to be >95% CD4⁺, as determined by flow cytometric analysis (**Figure 5.2 (B)**). The disease progression observed for both EAE models was consistent with previous reports by ourselves and others^{139, 238, 239}, and as expected, the number of cells isolated from the CNS throughout disease progression mimicked the clinical disease score based on the severity of clinical symptoms. At disease onset, which varied between days 8 and 12 post-disease induction for individual mice, on average 2×10^4 cells could be isolated from the CNS, compared with approximately 1×10^5 cells that could be isolated at peak-disease and remission stages, as shown in **Figure 5.2 (C)**. Although infiltrating immune cells have been detected in the CNS as early as day 6 post EAE disease-induction^{240, 241}, these were too few at this early disease stage for a comprehensive proteomic analysis. Moreover, since the pathogenic CD4⁺ target cells that infiltrate the CNS to initiate disease are a rare population of cells, the total CD4⁺ cells recovered from numerous mice at each disease stage were required to be pooled to attain sufficient amounts of protein for ICPL labelling procedures.

5.2.2 ICPL labelling and triplex/quadruplex analyses

Total protein lysates extracted from CD4⁺ cells from each disease group (naïve, disease onset, peak-disease +/- remission) were differentially labelled with one of three (triplex) or four (quadruplex) ICPL isotopic labels; light (¹H₄¹²C₆), light-mid (²H₄¹²C₆), mid-heavy (¹H₄¹³C₆), or heavy (²H₄¹³C₆), according to established protocols²⁴² and as shown in **Figure 5.3 (A)**. Labelled samples were pooled, separated by LDS-PAGE, stained with Coomassie Brilliant Blue and excised into 34 distinct gel bands for analysis. Proteins were subjected

to tryptic digestion and HPLC fractionation, then peptides were analysed using either the UltraflexIII MALDI-TOF/TOF instrument for the MOG-EAE triplex analysis or the more sensitive next generation UltrafleXtreme MALDI-TOF/TOF instrument for the PLP-EAE quadruplex analysis, which became available to us after the acquisition of the triplex dataset. Regulated labelled peptides were quantified and identified using WARP LC and MASCOT software (**Figure 5.3 (A)**).

ICPL quadruplex analyses of CNS-infiltrating CD4⁺ cells isolated during PLP₁₃₉₋₁₅₁-induced relapsing-remitting EAE resulted in the identification of 1515 unique proteins, of which 1073 were successfully quantified. Quantification of a peptide requires the detection of that defined peptide at least once with each of the isotopic labels. This allows the calculation of relative expression of the defined peptide across the analysis groups. In comparison to the quadruplex dataset, ICPL triplex analyses of chronic MOG₃₅₋₅₅-induced EAE resulted in the identification of 565 proteins and the quantification of 336 proteins. The discrepancy between the numbers of proteins identified between these two analyses was due to the acquisition of the ICPL quadruplex data on the more sensitive technical platform afforded by the UltrafleXtreme instrument, compared with the Ultraflex III system.

Collectively, 30.8% of the total quantified proteins across the two analyses were found to be differentially regulated by at least 2-fold during EAE disease progression relative to unactivated naïve control CD4⁺ cells, as depicted in **Figure 5.3 (B, C)**. Proteins identified to be commonly up- and down-regulated by at least 2-fold in both relapsing-remitting (PLP-EAE) and chronic (MOG-EAE) models of EAE disease, respectively, relative to naïve control samples are summarised in **Figure 5.3 (C)** and **Tables 5.1-5.3**. Although the

main focus of this study was to determine proteins differentially regulated in both analyses, and hence relevant to disease progression in both relapsing-remitting and chronic disease models, the proteins regulated in each individual analyses are presented in **Appendix A3 and A4**.

The ICPL datasets were further analysed using DAVID Functional Annotation Bioinformatics and STRING protein association network tools, as presented in **Figure 5.4**. The assignment of quantified proteins to the DAVID functional GOTERM_BP_1 annotation revealed that a major percentage of proteins contributed to cellular and metabolic processes (PLP: 77.8%, MOG: 83.7% and PLP: 61.7%, MOG: 64.6%, respectively), in addition to immune system processes (PLP: 6.9%) and the establishment of localisation and cell migration (PLP: 16.0%) (**Figure 5.4 (A)**). Of the quantified proteins determined to be up-regulated in both relapsing-remitting EAE quadruplex and chronic EAE triplex datasets, a proportion of proteins were found to cluster as a functional group when assessed using the protein association network tool, STRING. This evaluation tool builds association networks based on experimental evidence, where the functional groups highlighted in **Figure 5.4 (B)** represent proteins with known roles in immune function during inflammation and disease. Proteins within these clusters were identified as pro-inflammatory factors (Lcn2, S100A4, S100A9, S100A10), anti-inflammatory factors (AnxA1), adhesion molecules involved in trans-endothelial migration (Lgals3), mediators of signal transduction (AnxA2, Calm1, Nfkb1) and regulators of cytoskeletal rearrangement, lymphocyte adhesion and transmigration (Lcp1, Vim). Proteins involved in lymphocyte migration and inflammation were of particular interest since these potentially represent novel CD4⁺ cell-driven mechanisms of EAE disease regulation. Furthermore, since the migration and infiltration of activated CD4⁺ Th cells into the CNS represents a

major step in the development of EAE disease, these proteins may be required for effective infiltration of lymphocytes into the inflamed CNS. As expected for activated cells, other major protein clusters were associated based on functional involvement with protein translation and glycolysis (**Figure 5.4 (B)**).

5.2.3 Validating protein candidates identified to be up-regulated during EAE

Collectively, across PLP₁₃₉₋₁₅₁-induced relapsing-remitting EAE and MOG₃₅₋₅₅-induced chronic EAE analyses, the expression of 13 proteins were determined to be commonly up-regulated and the expression of 10 proteins were determined to be commonly down-regulated by CNS-infiltrating CD4⁺ cells by at least 2-fold during disease progression in both models, relative to their expression by naïve control cells. **Tables 5.1 and 5.2** summarise the degree of regulation of these proteins in each disease model, where the intensity of shading represents the extent fold-increase/decrease of peptide intensity. The associated annotated spectra and extracted ion chromatograms can be accessed online (www.pubs.acs.org/doi/suppl/10.1021/pr500158r) as Supporting Information associated with the published manuscript. Four proteins identified to be up-regulated during EAE disease progression were selected for validation based on their established roles in inflammation (S100A4 and S100A9)²⁴³⁻²⁴⁸, tissue repair (AnxA1)²⁴⁹⁻²⁵¹ or membrane cytoskeletal rearrangement (AnxA2)^{252, 253}. The expression of these four candidate proteins were validated by quantitative PCR analyses of mRNA transcript levels using RNA extracted from CNS-infiltrating CD4⁺ cells isolated from individual mice during PLP₁₃₉₋₁₅₁-induced EAE disease progression. The use of biological replicates for validation experiments was achievable due to the small amount of RNA required for qPCR analyses, therefore the small numbers of CD4⁺ cells that could be isolated from the CNS of a single mouse were sufficient to analyse each mouse individually. In contrast, ICPL required large amounts of protein for comprehensive analyses. Therefore, since CNS-infiltrating CD4⁺

cells were such a rare cell population and large amounts of protein could not be easily attained, it required the pooling of protein isolated from the CD4⁺ cells from multiple mice within a disease group for proteomic ICPL labelling. For candidate validation by qPCR analysis, CD4⁺ cells were isolated at peak-disease and remission disease stages, as shown in **Figure 5.5 (A)**, and the expression of S100A4, S100A9, Annexin A1 and Annexin A2 were assessed relative to unactivated CD4⁺ cells isolated from the spleens of naïve mice, **Figure 5.5 (B-E)**, respectively. Up-regulated expression of S100A4, S100A9 and Annexin A1 proteins during EAE disease were confirmed at the mRNA transcript level and were consistent with regulation observed at the protein level. S100 proteins are known inflammatory mediators that have established roles as chemoattractants for neutrophils²⁴³. The expression of S100 proteins by CNS-infiltrating CD4⁺ cells may therefore contribute to lymphocyte-mediated neutrophil accumulation within the inflamed CNS during EAE progression. In contrast to the protein expression of Annexin A2, transcriptional analysis of AnxA2 mRNA revealed no significant difference between transcript levels within naïve and CNS-infiltrating CD4⁺ cells during EAE, suggesting that translational regulation may account for the observed increase in protein levels of AnxA2 (**Figure 5.5 (E)**).

5.3 Summary

The results of the initial ICPL proteomic study presented in Chapter 5 demonstrate that differentially regulated proteins required for immune system processes could be successfully identified and quantified using ICPL isotopic labelling methods of CNS-infiltrating CD4⁺ cells during EAE disease progression. This work investigating the proteomes of wildtype CD4⁺ lymphocytes during EAE pathogenesis provides the foundation for future works investigating the proteomes of CD4⁺ cells isolated from the CNS of p84-deficient (Pik3r6^{-/-}) mice during EAE disease progression. In order to conduct future analyses of CD4⁺ cells isolated from spleen, blood and CNS of Pik3r6^{-/-} mice during EAE, the colony would need to be expanded, since relative to diseased wildtype animals fewer CD4⁺ cells can be isolated from the CNS of Pik3r6^{-/-} mice (refer to section 4.2.11). For this reason and due to time constraints, ICPL proteomic analyses using Pik3r6^{-/-} mice were outside the scope of this project.

Intentionally blank

Figure 5.1: CD4⁺ cell sample preparation and ICPL proteomic workflow.

The proteomes of CD4⁺ cells isolated from the CNS during experimental autoimmune encephalomyelitis (EAE) disease progression in two disease models were examined relative to unactivated control CD4⁺ cells isolated from healthy naïve mice. PLP₁₃₉₋₁₅₁-induced relapsing-remitting EAE and MOG₃₅₋₅₅-induced chronic EAE disease were induced in SJL/J and C57Bl/6 mice, respectively, and disease was monitored daily. Infiltrating CD4⁺ Th cells were isolated from the diseased CNS at disease onset, peak-disease and remission for PLP₁₃₉₋₁₅₁-induced relapsing-remitting EAE, or disease onset and peak-disease for MOG₃₅₋₅₅-induced chronic EAE, in addition to control CD4⁺ cells isolated from the spleens of naïve mice. Protein samples from naïve control or EAE disease groups were labelled using quadruplex (PLP-induced EAE; 4 data points) or triplex (MOG-induced EAE; 3 data points) isotope-coded protein labelling (ICPL) methods, separated by LDS-PAGE and then tryptic digest was performed. Differentially regulated peptides were identified by LC-MS/MS analyses and proteins identified to be differentially regulated by CD4⁺ cells during EAE disease by >2-fold relative to naïve control cells were subjected to pathway/network analyses using Database for Annotation, Visualisation and Integrated Discovery (DAVID) and Search Tool for the Retrieval of Interacting Genes/Proteins (STRING) evaluation tools. The mRNA transcript expression of selected protein candidates was examined by quantitative PCR analyses of CNS-infiltrating CD4⁺ cells isolated during EAE disease progression from individual diseased mice relative to control CD4⁺ cells isolated from naïve mice.

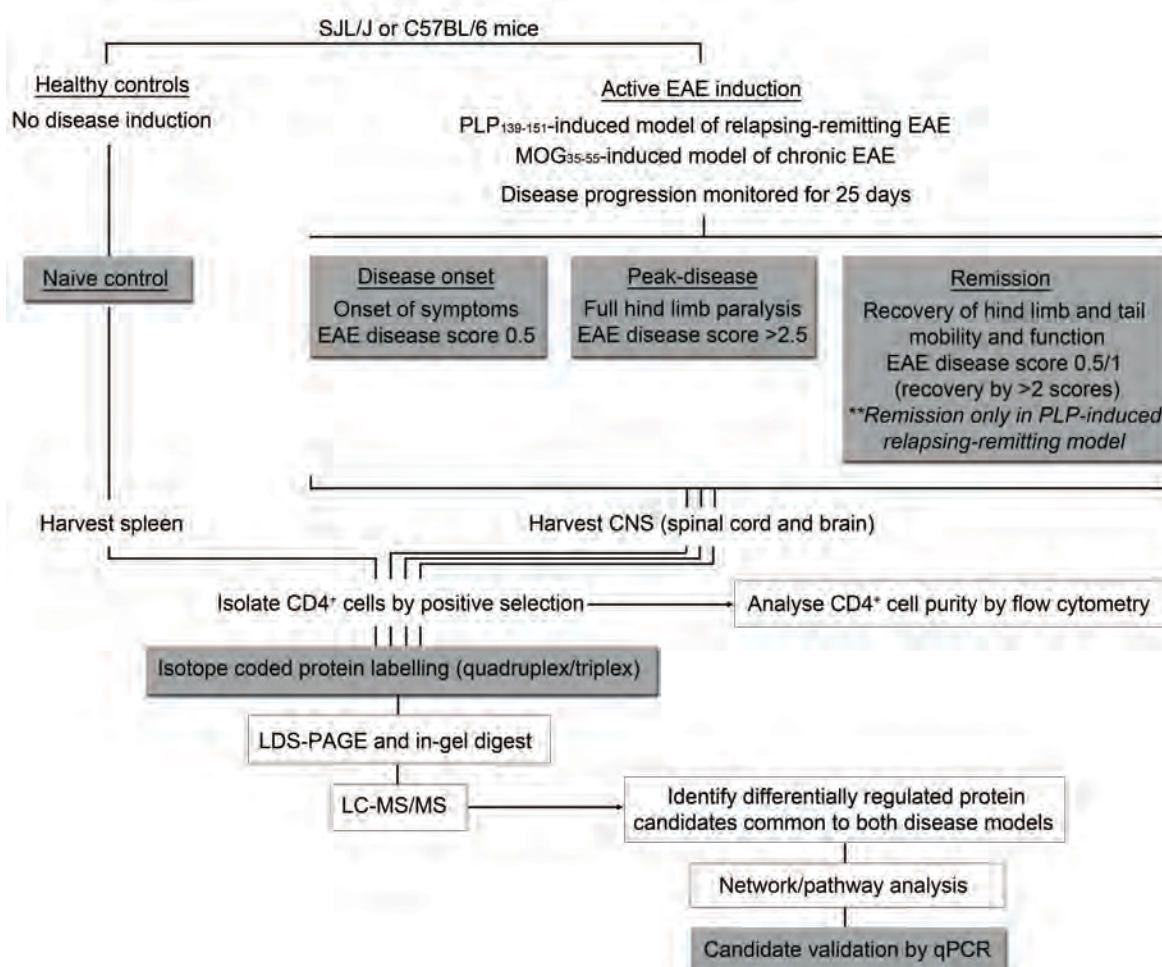


Figure 5.2: CD4⁺ cell isolation from the CNS during EAE disease progression.

CD4⁺ cells were isolated from the CNS of EAE-diseased mice at various disease stages in two models of EAE disease. **(A)** Disease progression for PLP₁₃₉₋₁₅₁-induced relapsing-remitting EAE in SJL/J mice (*left panel*) and MOG₃₅₋₅₅-induced chronic EAE in C57Bl/6 mice (*right panel*); clinical disease score monitored daily, (n=14). Selected disease stages for analysis (disease onset, peak-disease ± remission) are designated (*arrows*) and defined as follows; disease onset (clinical disease score 0.5), peak-disease (clinical disease score >2.5) and remission (clinical disease score 0.5/1, recovery >2 scores; PLP-induced EAE only). **(B)** CD4⁺ cells were isolated from CNS or spleen cell preparations at designated disease stages by positive cell selection using CD4-specific antibody-coupled Dynabeads. Representative flow cytometry plots of CD4⁺ cell purity pre- and post-CD4⁺ cell isolation from a naïve splenocyte suspension is shown. Live lymphocytes were pre-gated (*left panel*) and the percentage of cells stained positive for CD4 surface expression (*black histogram*) relative to the isotype control staining (*grey shaded histogram*) is depicted for pre-isolation (*middle panel*) and post-isolation (*right panel*) samples. **(C)** The number of CD4⁺ cells isolated from pooled CNS samples within each disease stage group was enumerated following positive selection. Each data point represents the average number of cells isolated per mouse from each isolation sample. PLP₁₃₉₋₁₅₁-induced EAE: disease onset (n=53; 11 isolations), peak-disease (n=17; 7 isolations), remission (n=20; 6 isolations); MOG₃₅₋₅₅-induced EAE: disease onset (n=51; 8 isolations), peak-disease (n=22; 6 isolations).

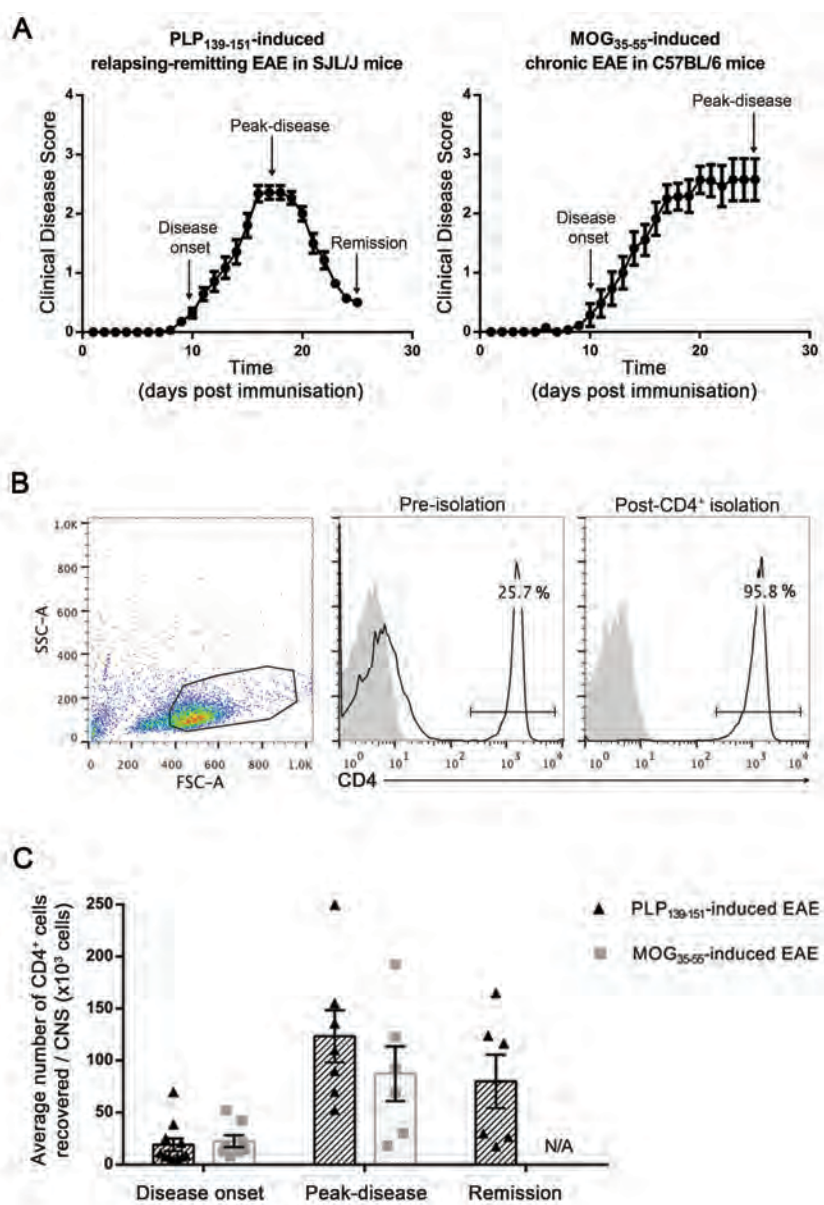


Figure 5.3: Examining two EAE disease models: ICPL analysis of CD4⁺ cells isolated from the CNS during relapsing-remitting and chronic EAE disease progression.

(A) Total protein lysates (15µg) from each disease sample group were differentially labelled with one of four ICPL isotopic labels; light ($^1\text{H}_4^{12}\text{C}_6$), light/mid ($^2\text{H}_4^{12}\text{C}_6$), mid/heavy ($^1\text{H}_4^{13}\text{C}_6$) or heavy ($^2\text{H}_4^{13}\text{C}_6$), then pooled and separated by LDS-PAGE. Gel bands were excised (*annotated by dotted lines*), tryptic digest was performed and resultant peptides were fractionated by HPLC for acquisition on either UltrafleXtreme (PLP-induced EAE) or Ultraflex III (MOG-induced EAE) MALDI-TOF/TOF instruments. The intensity distribution of individual ICPL labels determined for each peptide was quantified and identified using WARP LC 1.2 and MASCOT software tools. Fold-regulation of peptide intensity was calculated relative to naïve CD4⁺ control samples for quadruplex and triplex labelling, where significance was considered to be >2-fold up- or down-regulation. (B) Summary of identified and regulated proteins for PLP₁₃₉₋₁₅₁-induced relapsing-remitting EAE analysis. (C) Summary of identified and regulated proteins for MOG₃₅₋₅₅-induced chronic EAE analysis. (D) Venn diagram depicting the number of proteins identified, quantified and determined to be differentially regulated between two EAE model analyses.

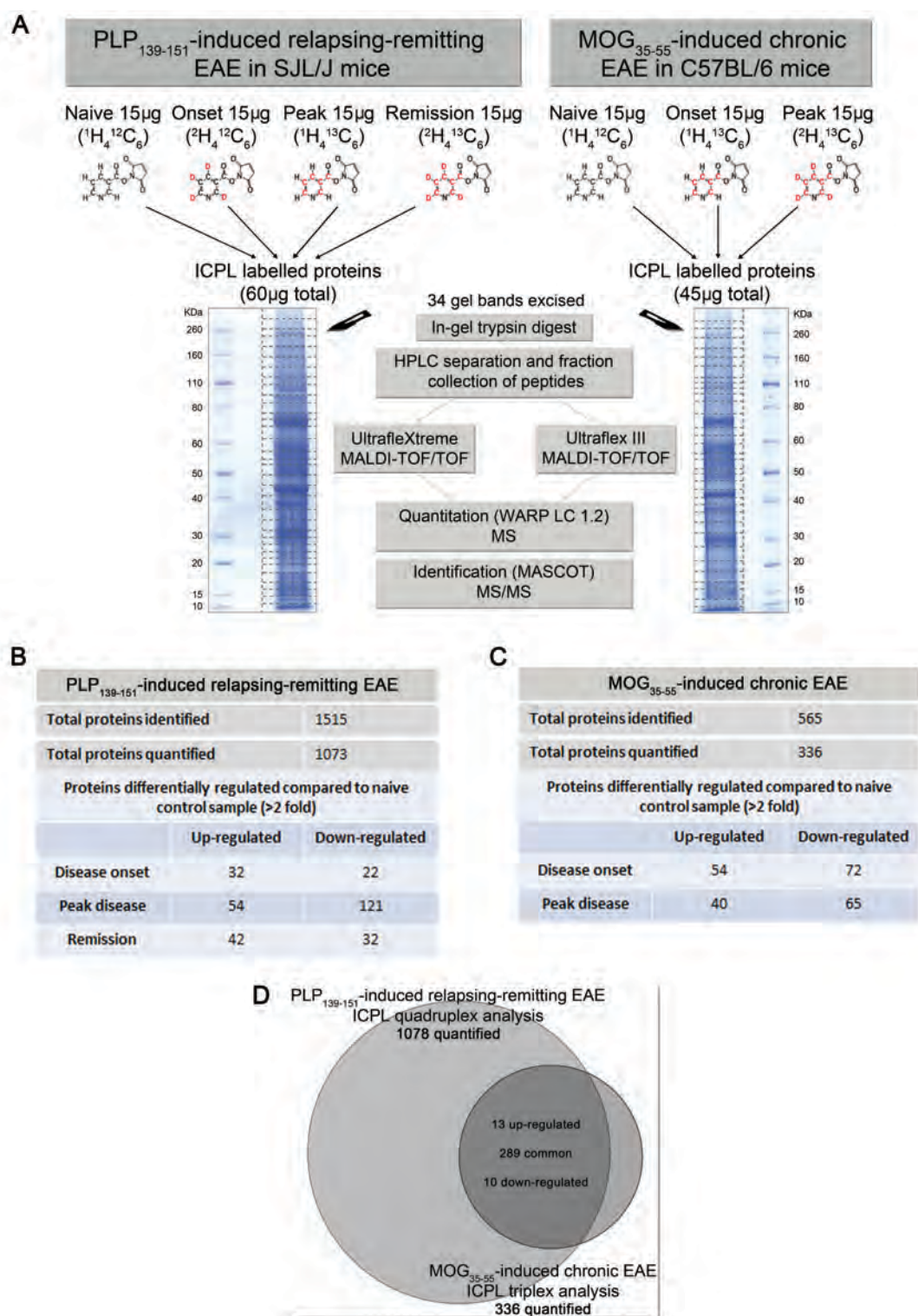


Figure 5.4: Analyses of CNS-infiltrating CD4⁺ cells isolated during relapsing-remitting and chronic EAE disease progression identified a broad coverage of regulated proteins.

(A) Total quantified proteins for PLP₁₃₉₋₁₅₁-induced and MOG₃₅₋₅₅-induced EAE analyses were subjected to Database for Annotation, Visualisation and Integrated Discovery (DAVID) and categorised based on the functional gene ontology annotation, GOTERM_BP_1, which assigned proteins to functional groups. (B) Search Tool for Retrieval of Interacting Genes/Proteins (STRING 9.05) was used to evaluate proteins determined to be up-regulated during PLP₁₃₉₋₁₅₁-induced and MOG₃₅₋₅₅-induced EAE disease progression relative to control samples; association clusters were compiled based on experimentally verified and predicted protein-protein interactions. A sub-network of proteins associated with immune function during inflammation and disease is highlighted (*dashed box*).

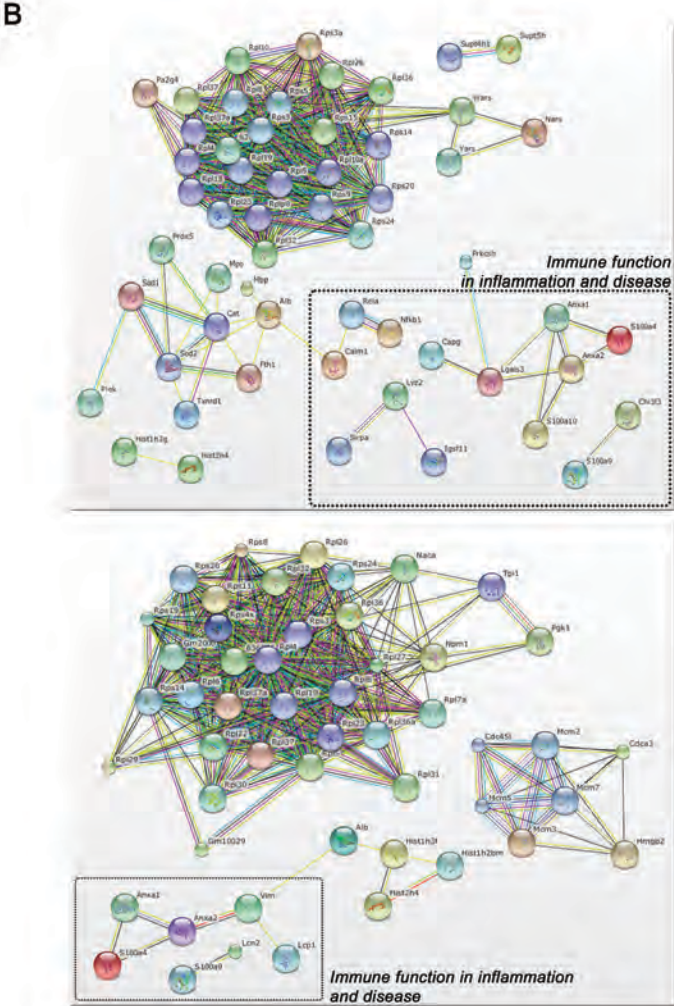
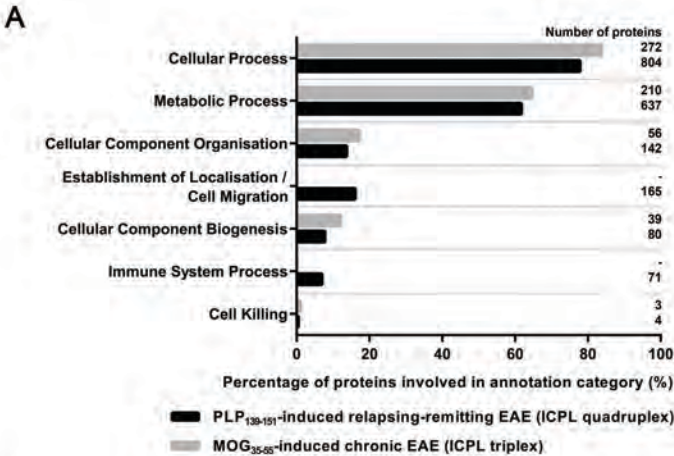


Table 5.1: Proteins up-regulated by CNS-infiltrating CD4⁺ cells during both relapsing-remitting and chronic EAE progression.

Differential regulation defined as >2-fold increase in intensity relative to naïve CD4⁺ control; selected protein candidates for validation are highlighted.

		PLP ₁₃₉₋₁₅₁ -induced relapsing-remitting EAE in SJL/J mice ICPL (quadruplex)										MOG ₃₅₋₅₅ -induced chronic EAE in C57BL/6 mice ICPL (triplex)														
Accession ^a	Protein name ^b	Disease onset					Peak-disease					Remission					Disease onset					Peak-disease				
		Peptides	Multiplets ^c	change ^d	SD	Fold	Peptides	Multiplets ^c	change ^d	SD	Fold	Peptides	Multiplets ^c	change ^d	SD	Fold	Peptides	Multiplets ^c	change ^d	SD	Fold					
ALBU_MOUSE	Serum albumin	8	5/2	3.82	1.22	3.18	1.31	1.49	1.29	1.29	2	1/1	3.05	-	6.01	-	2	1/1	3.05	-	6.01	-				
ANXA1_MOUSE	Annexin A1	4	3/1	3.10	-	3.00	-	2.35	-	-	5	4/4	2.83	1.08	3.27	1.19	5	4/4	2.83	1.08	3.27	1.19				
ANXA2_MOUSE	Annexin A2	12	2/2	2.48	1.15	3.04	1.20	2.15	1.30	1.30	12	6/6	2.79	1.23	3.45	1.29	12	6/6	2.79	1.23	3.45	1.29				
CAPG_MOUSE	Macrophage-capping protein	30	6/4	2.11	1.57	2.80	1.47	3.13	1.89	1.89	7	2/2	1.52	1.07	2.59	1.24	7	2/2	1.52	1.07	2.59	1.24				
EFHD2_MOUSE	EF-hand domain-containing protein D2	5	2/1	1.47	-	2.27	-	2.00	-	-	3	1/1	4.16	-	4.90	-	3	1/1	4.16	-	4.90	-				
H4_MOUSE	Histone H4	26	6/6	3.09	1.21	6.26	1.23	5.69	1.35	1.35	11	5/5	6.46	1.83	2.07	1.63	11	5/5	6.46	1.83	2.07	1.63				
RL26_MOUSE	60S ribosomal protein L26	42	12/11	1.29	1.29	2.12	1.29	1.25	1.25	1.25	29	11/11	2.89	1.35	2.45	1.48	29	11/11	2.89	1.35	2.45	1.48				
RL32_MOUSE	60S ribosomal protein L32	10	3/3	1.20	1.17	2.04	1.26	1.36	1.41	1.41	5	3/3	3.06	1.23	2.26	1.46	5	3/3	3.06	1.23	2.26	1.46				
RL36_MOUSE	60S ribosomal protein L36	8	1/1	1.35	-	2.08	-	1.86	-	-	4	1/1	2.92	-	2.45	-	4	1/1	2.92	-	2.45	-				
RL37_MOUSE	60S ribosomal protein L37	14	4/4	1.75	1.43	2.45	1.52	2.34	1.43	1.43	12	4/4	3.13	1.53	2.75	1.52	12	4/4	3.13	1.53	2.75	1.52				
RS24_MOUSE	40S ribosomal protein S24	11	2/2	1.47	1.07	2.05	1.14	1.71	1.08	1.08	4	2/2	4.07	1.08	3.65	1.07	4	2/2	4.07	1.08	3.65	1.07				
S10A4_MOUSE	Protein S100-A4	7	3/2	2.29	1.10	1.74	1.08	2.16	1.11	1.11	1	1/1	3.39	-	6.30	-	1	1/1	3.39	-	6.30	-				
S10A9_MOUSE	Protein S100-A9	10	2/1	11.76	-	18.37	-	11.12	-	-	4	2/1	10.23	-	2.09	-	4	2/1	10.23	-	2.09	-				

Criteria**-

Proteins enriched in ICPL analysis of both EAE disease models; intensity of green shading depicts degree of up-regulation (between 2 and 5-fold = light green; > 5-fold = dark green)
Protein candidates for validation are highlighted in blue

^a Accession designations are derived from the UniProt database

^b Protein names are derived from the UniProt database

^c Multiplets before/after manual accuracy review of individual spectra (Supplementary Materials 1-4)

^d Fold changes were calculated relative to ICPL peptide intensities of naive CD4⁺ cell control samples

Table 5.2: Proteins down-regulated by CNS-infiltrating CD4⁺ cells during both relapsing-remitting and chronic EAE progression.

Differential regulation defined as >2-fold decrease in intensity relative to naïve CD4⁺ control.

Accession ^a	Protein name ^b	PLP ₁₃₉₋₁₅₁ -induced relapsing-remitting EAE in SJL/J mice ICPL (quadruplex)						MOG ₃₅₋₅₅ -induced chronic EAE in C57BL/6 mice ICPL (triplex)						
		Disease onset		Peak-disease		Remission		Disease onset		Peak-disease		Remission		
		Peptides	Fold change ^c	SD	Fold change ^c	SD	Fold change ^d	Peptides	Fold change ^c	SD	Fold change ^c	SD	Fold change ^d	
ACON_MOUSE	Aconitate hydratase, mitochondrial	17	7 / 4	1.85	0.49	1.85	0.85	1.13	9	2 / 2	0.40	1.15	0.37	1.38
ACTN1_MOUSE	Alpha-actinin-1	19	10 / 2	2.08	0.32	2.08	0.39	1.57	11	5 / 5	0.17	1.26	0.15	1.85
ADRO_MOUSE	NADPH:adenodoxin oxidoreductase, mitochondrial	8	3 / 1	1.71	0.33	1.71	0.73	1.20	2	1 / 1	0.58	-	0.35	-
COR07_MOUSE	Coronin-7	12	5 / 1	1.44	0.36	1.44	0.60	1.38	5	1 / 1	0.35	-	0.57	-
HNRL2_MOUSE	Heterogeneous nuclear ribonucleoprotein U-like protein 2	4	2 / 2	1.75	0.38	1.75	0.54	1.33	4	1 / 1	0.22	-	0.16	-
HNRPF_MOUSE	Heterogeneous nuclear ribonucleoprotein F	26	11 / 2	2.18	0.48	2.18	0.97	1.72	9	3 / 3	0.48	1.10	0.50	1.28
IDHP_MOUSE	Isocitrate dehydrogenase [NADP], mitochondrial	8	4 / 2	1.28	0.47	1.28	0.76	1.28	2	1 / 1	0.29	-	0.23	-
LIMD2_MOUSE	LIM domain-containing protein 2	8	3 / 3	1.21	0.40	1.21	0.42	1.08	1	1 / 1	0.51	-	0.35	-
TIF1B_MOUSE	Transcription intermediary factor 1-beta	18	9 / 7	2.13	0.46	2.13	0.63	1.18	5	4 / 4	0.27	1.81	0.26	2.28
TPSN_MOUSE	Tapasin	18	8 / 5	2.21	0.44	2.21	0.59	1.44	2	1 / 1	0.41	-	0.47	-

Criteria.**

Proteins enriched in ICPL analysis of both EAE disease models; intensity of red shading depicts degree of down-regulation (between 2 and 5-fold = light red; > 5-fold = dark red)

^a Accession designations are derived from the UniProt database

^b Protein names are derived from the UniProt database

^c Multiplets before/after manual accuracy review of individual spectra (Supplementary Materials 1-4)

^d Fold changes were calculated relative to ICPL peptide intensities of naive CD4⁺ cell control samples

Table 5.3: Established cellular functions of identified regulated proteins.

The known functions of proteins identified to be differentially regulated by CD4⁺ cells isolated from the CNS during relapsing-remitting and chronic EAE disease relative to naïve control cells are compiled. Selected protein candidates for validation are highlighted.

Up-regulated proteins	
Accession^a	Known cellular function/s
ALBU_MOUSE	Plasma oncotic pressure regulator
ANXA1_MOUSE	Regulation of inflammation and repair
ANXA2_MOUSE	T cell precursor activation
CAPG_MOUSE	Regulation of actin structures
EFHD2_MOUSE	Modulation of actin bundling / cell migration
H4_MOUSE	Regulation of gene transcription
RL26_MOUSE	Protein Translation
RL32_MOUSE	Protein Translation
RL36_MOUSE	Protein Translation
RL37_MOUSE	Protein Translation
RS24_MOUSE	Protein Translation
S10A4_MOUSE	Inflammation / cell migration / tumour metastasis
S10A9_MOUSE	Inflammation / leukocyte adhesion and migration
Down-regulated proteins	
Accession^a	Known cellular function/s
ACON_MOUSE	Mitochondrial isomerisation of citrate
ACTN1_MOUSE	Cytoskeletal rearrangement / actin-binding
ADRO_MOUSE	Mitochondrial function / electron transport
CORO7_MOUSE	Regulation of golgi morphology and protein export
HNRL2_MOUSE	Pre-mRNA processing, mRNA metabolism and transport
HNRPF_MOUSE	Pre-mRNA processing, mRNA metabolism and transport
IDHP_MOUSE	Mitochondrial function / electron transport
LIMD2_MOUSE	Adaptor for cell-ECM attachments
TIF1B_MOUSE	Regulation of gene transcription
TPSN_MOUSE	Antigen presentation

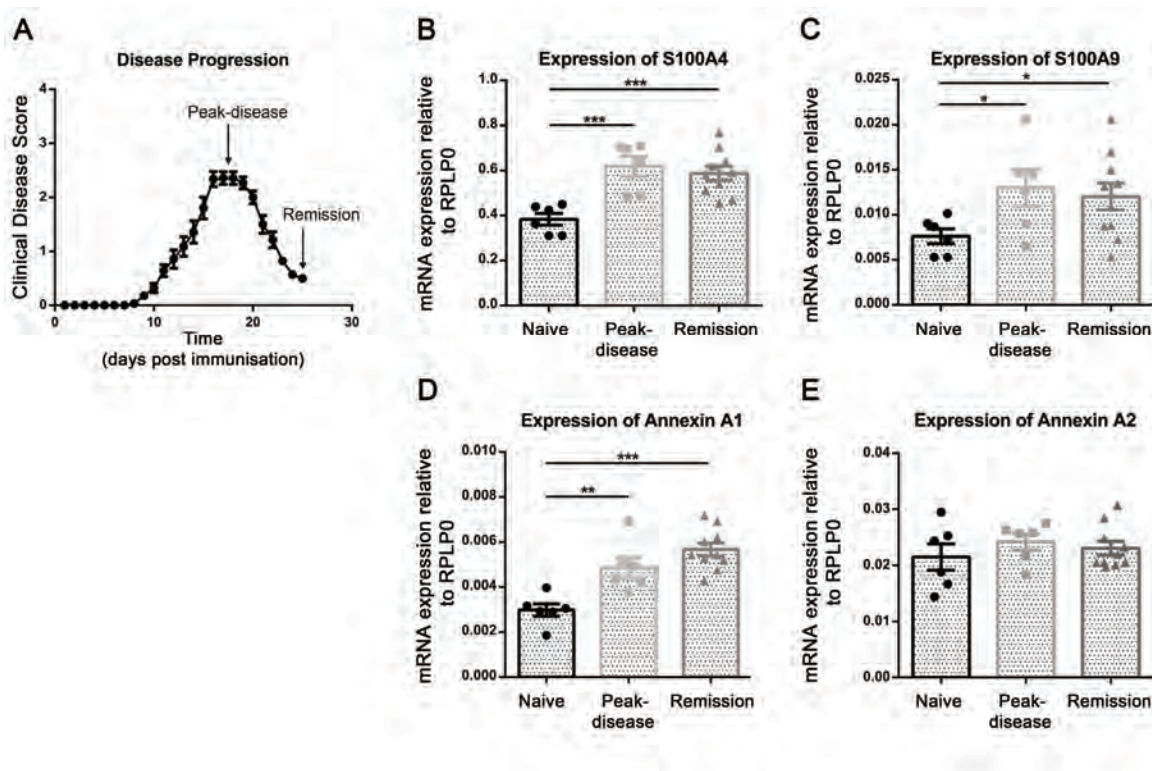


Figure 5.5: Candidate validation by quantitative PCR of mRNA transcript levels.

CD4⁺ cells were isolated from the inflamed CNS of mice induced with PLP₁₃₉₋₁₅₁-EAE at peak-disease and remission stages, in addition to CD4⁺ cells isolated from the spleens of naïve control mice; total RNA was extracted for quantitative PCR of mRNA transcript expression. (A) Disease progression of PLP₁₃₉₋₁₅₁-induced EAE; disease stages for analysis are designated (*arrows*). Transcript expression of (B) S100A4, (C) S100A9, (D) Annexin A1 and (E) Annexin A2 are presented, as determined by quantitative PCR (normalised relative to reference gene RPLP0). Data are presented as mean ± SEM; peak-disease (n=6), remission (n=10), naïve control (n=6); t-test *p<0.05, **p<0.01.

Chapter 6: Discussion

Chapter 6: Discussion

PI3K γ signalling is required for the formation of the leading edge during induction of cell polarisation and migration in response to chemotactic signals transmitted through G protein-coupled receptors (GPCR)^{2, 7, 145, 160, 254}. While the PI3K γ subunits p110 γ , p84 and p101 are expressed by most cells in the organism⁴, they are predominantly expressed by highly motile haematopoietic cells, where PI3K γ signalling is necessary for their coordinated migration during immune responses^{7, 8, 145, 160}. The dependence on PI3K γ complexes for cell migration has been demonstrated primarily through the use of genetically-modified p110 γ -deficient mouse models (p110 $\gamma^{-/-}$ and p110 $\gamma^{KD/KD}$)^{7-9, 121} and the p110 γ -specific inhibitor (AS605240)^{8, 9, 255}. With these tools, the dependence on the catalytic activity of p110 γ for PI3K γ function can be assessed using AS605240 or the p110 $\gamma^{KD/KD}$ mouse, where the kinase activity of p110 γ is inhibited whilst the structure of p110 γ remains intact. In contrast, the p110 $\gamma^{-/-}$ mouse that is deficient in p110 γ protein expression has also been shown to lack expression of p84 and p101 adaptor proteins^{121, 148}. For this reason, in addition to the potential functional redundancy that exists between the regulatory adaptor subunits, elucidating the molecular regulation of p110 γ by p84 and p101 adaptor proteins is a complex task. Upon GPCR engagement, PI3K γ complexes (composed of heterodimeric p84/p110 γ or p101/p110 γ) are transiently recruited to the plasma membrane where they interact with G $\beta\gamma$ and partially integrate into the lipid bilayer, processes that facilitate the activation of p110 γ lipid-kinase activity towards proximal phosphatidylinositol lipid substrates embedded within the membrane^{4-6, 10, 12, 87}. PIP₃ lipids catalysed by PI3K γ propagate phosphorylation cascades involving multiple protein kinase effectors, such as Akt/PKB, which depending on the cell type, ultimately result in transcriptional changes within the cell and/or the induction of chemotaxis^{1, 91, 145, 220}.

Although a number of steps in this signalling pathway are well-characterised, the roles of the p84 and p101 adaptor proteins in PI3K γ signalling are not completely understood. Specifically, the subcellular localisation and kinetics of the interaction between a p110 γ catalytic subunit and an adaptor subunit, and how signal specificity is achieved in relation to the dimerisation of p110 γ with either p84 or p101 are yet to be elucidated. Whilst it has been shown that p110 γ participates in mutually-exclusive binding to a single adaptor protein at any given time^{4, 6, 11, 119, 256}, whether p84 and p101 binding-partners can be

exchanged by the catalytic subunit (depending on the activating signal) or whether p84/p110 γ and p101/p110 γ heterodimeric enzymes exist in different subcellular pools and therefore contribute to distinct signalling cascades¹²¹ remains unclear. Likewise, the molecular mechanisms that drive PI3K γ complex formation and signal activation at the membrane, in addition to those that control the subsequent termination of transient signalling and release of the enzyme from the membrane are yet to be defined.

The importance of PI3K γ signal regulation has been further emphasised by the demonstration that up-regulated expression of p110 γ and/or p101 subunits results in enhanced PIP₃ accumulation and is sufficient to promote cellular transformation^{31, 135, 176}. In comparison to the tumour-promoting potential of p110 γ and p101 described above, data suggesting that p84 maintains a weaker interaction with p110 γ ^{4, 6, 119}, has reduced sensitivity towards G $\beta\gamma$ ^{4, 11} and mediates less robust PI3K γ lipid-kinase activity relative to p101, has led to the proposal that p84 may have an alternative regulatory role within PI3K γ signalling. Divergent roles for p84 and p101 have been previously reported^{119, 120, 122, 123}, for example, p84/p110 γ and p101/p110 γ heterodimers have been shown to differ in their spatio-temporal localisation *in vitro*^{4, 11, 122, 125} and produce distinct intracellular pools of PIP₃ lipid products¹²¹. Furthermore, data from our own laboratory in models of mammary epithelial carcinoma have revealed that unlike p110 γ and p101 that enable growth and facilitate tumour metastasis through heightened and/or prolonged PI3K γ signalling, p84 possesses novel tumour suppressor capacity via an effect on p110 γ membrane localisation¹²³.

While it is clearly important to resolve the molecular regulation of PI3K γ signalling, in particular the distinct contributions of p84 and p101 adaptor proteins, there are significant challenges involved with this research. Firstly, PI3K γ proteins are expressed at low endogenous levels, particularly with respect to the p84 and p101 adaptor proteins, of which there are limited quality reagents to specifically detect their expression and localisation. Secondly, although the highest expression of PI3K γ subunits has been reported in haematopoietic cells, these cells are notoriously difficult to manipulate, which has resulted in many research groups utilising cell lines where PI3K γ subunits can be ectopically expressed in order to study protein complex interactions^{4, 6, 11, 87, 119, 135}. Furthermore, since p84 and p101 adaptor proteins have been shown to mediate PI3K γ signalling through

analogous mechanisms, where signalling is commonly defined and measured by the accumulation of membrane-localised PIP₃ and the induction of phosphorylated Akt, potential redundancy and compensation between these adaptor subunits must be considered.

The aims and experiments of the present study were undertaken to increase our knowledge of the molecular regulation of p84 and the distinct roles for p84 in PI3K γ signalling and PI3K γ -dependent cell functions. This was achieved using three main avenues of research. The first examined the molecular regulation of p84 by investigating the phosphorylation status of p84 in response to GPCR-mediated cell stimulation. Regulatory phosphorylation sites identified within p84 were assessed for their role in p84/p110 γ heterodimer formation, subunit localisation and the tumour suppressor function of p84. This first aspect of the project utilised the MDA.MB.231 mammary carcinoma cell line to examine mechanisms of PI3K γ signal activation in the context of p84-mediated tumour suppression. The second major research aim led to the generation and characterisation of a p84-deficient mouse (C57Bl/6 *Pik3r6*^{-/-}) using CRISPR gene-editing technology, which was utilised to assess the requirement of p84 for haematopoietic cell function during homeostasis and disease. The third and final aspect of this research project was centred on the development and optimisation of an ICPL proteomics method to investigate the proteomes of migratory effector lymphocytes during inflammatory disease, with the ultimate aim of deciphering p84- and PI3K γ -dependent signalling pathways in these cells.

The research presented in this thesis has resulted in the characterisation of a p84-dependent mechanism within PI3K γ signalling to control p110 γ membrane localisation and inhibit the growth and metastasis of breast cancer cells. In addition, the *Pik3r6*^{-/-} mouse strain was used to identify novel p84-dependent roles within immune cell migration *in vivo* and *in vitro*. Finally, the results presented here described the optimisation of an ICPL proteome labelling approach to analyse differentially-regulated proteins expressed by CD4⁺ lymphocytes during the induction of the autoimmune inflammatory condition, EAE. The presented proteomic analyses represent a platform for future investigation of the role of p84 in PI3K γ -dependent signalling and cell migration during inflammatory disease, through comparisons between p84-deficient lymphocytes and wildtype counterparts.

6.1 The induction of Thr607-dependent p84/p110 γ heterodimers represents a regulatory mechanism of PI3K γ signalling that is required for the tumour suppressor function of p84

The ability of p84 to suppress tumour metastasis was previously observed in a model of experimental haematogenous metastasis, where the siRNA-induced knockdown of p84 expression in MDA.MB.231 mammary carcinoma cells was found to enhance their metastatic potential *in vivo*¹²³. In that study, PI3K γ signalling in p84-knockdown cells was dysregulated, as shown by persistent membrane-localisation of p110 γ and constitutive phosphorylation of Akt in the absence of additional GPCR stimulation, indicative of constitutive PI3K γ activity. This phenotype observed for p84-knockdown cells suggests that p84 is required for the termination of PI3K γ signalling. In contrast, p110 γ - and p101-knockdown cells displayed a reduction in metastatic potential, characterised by diminished PI3K γ signalling¹²³, thereby confirming the role of p110 γ and p101 subunits in PI3K γ -dependent metastasis. Collectively, these data suggest that p110 γ and p101 subunits promote tumour metastasis whilst p84 possesses tumour suppressor function in MDA.MB.231 cells through the control of p110 γ localisation and therefore activity. However despite these findings, the molecular mechanisms by which p84 participates in PI3K γ signal activation/termination and influences the localisation of p110 γ in MDA.MB.231 cells remain unclear. Therefore to understand the mechanisms by which p84 functions as a tumour suppressor, information regarding the regulation of the p84 adaptor protein during PI3K γ signalling was sought.

There are three regulatory mechanisms known to control PI3K family interactions that promote or inhibit lipid-kinase activity; these are structural restrictions where heterodimers adopt open or closed conformations that dictate adaptor binding and/or kinase activity^{12, 59, 71, 72}, the phosphorylation of catalytic or adaptor subunits that allow or prevent heterodimerisation^{66, 124} and the phosphorylation of catalytic subunits within PI3K γ complexes that directly inhibits their kinase activity^{74, 108, 120}. Thus, transient phosphorylation of PI3K complexes represents an integral mode of regulation that defines the activity of PI3K heterodimers. Structural analyses of p84 have been limited by the inability to generate crystals of sufficient quality for hydrogen-deuterium exchange mass spectrometry (HDX-MS) and to date the crystal structure of p84 has not been resolved¹²⁴.

At the commencement of the present study, protein expression of codon-optimised human p84 was attempted in mammalian and insect cells using baculovirus expression vectors in order to purify p84 for crystallisation (*data not shown*). However, as per previous reports in the field, the expression of full-length p84 protein was not achieved to sufficient amounts or purity for crystallisation with the technology available and therefore was not further pursued. Had this been a major aim of the project, p84 protein truncation mutants could have been designed and screened in order to crystallise segments of the protein, although this approach is limited since the domain structure of p84 remains unknown.

In the data presented in this thesis, the regulation of PI3K γ signalling was examined in the context of transient regulatory phosphorylation of p84 upon GPCR stimulation. The phosphorylation status of p84 during PI3K γ signalling downstream of CXCL12/CXCR4 stimulation was investigated to identify regulatory phosphorylation sites within p84 that may influence the activity and/or localisation of p84/p110 γ heterodimers. Regulatory phosphorylation events have been previously reported for Class I PI3K isoforms, where phosphorylation of p85 α at Ser608 by p110 α has been shown to inhibit the lipid-kinase activity of PI3K α by 3- to 7-fold¹⁰⁸. This represents a mechanism of intrinsic PI3K regulation and it was therefore proposed that a similar phosphorylation-dependent mechanism of regulation might be relevant to PI3K γ complexes through the phosphorylation of p84. *In silico* analyses, mass spectrometry of p84 immunoprecipitated from stimulated cells and *in vitro* kinase assays using p84 peptides resulted in the identification of two putative phosphorylation sites within p84, Ser358 and Thr607. These regulatory sites were predicted to be phosphorylated by two known downstream kinases of the PI3K γ signalling pathway, namely GSK-3^{33, 219} and Akt^{91, 220}, respectively, indicating that phosphorylation of p84 at these sites may represent feedback signalling within the system. Numerous oxidation modifications to p84 were also identified by mass spectrometry of p84 isolated from stimulated cell lysates. Although the biological relevance of these modifications was not examined, the significance of these novel oxidation events to p84 should be investigated in future studies, particularly Met236, where oxidation was induced upon stimulation. Reversible methionine oxidation is a common post-translational modification that often alters the activity of the protein²⁵⁷. For instance, cofilin is a regulator of actin dynamics during T cell activation and migration that

is sensitive to oxidation modifications, where the oxidation of cofilin results in the inactivation of its actin-depolymerising activity²⁵⁸.

Phosphorylation of Ser358 within p84 has been previously reported in a large-scale kinome study²⁵⁹ and in the present study, phosphorylation of Ser358 was identified to be constitutive, as determined by mass spectrometry of p84 isolated from resting and CXCL12-stimulated MDA.MB.231 cell lysates. In contrast to Ser358 and despite *in silico* prediction data, Thr607 phosphorylation could not be identified within p84 precipitated from cell lysates. Assuming that phosphorylation of p84 by Akt kinase on Thr607 is a true phosphorylation event in response to GPCR stimulation in cells, three explanations as to why p-Thr607 was not detected from cell lysates could be proposed. Firstly, the phosphorylation of Thr607 is a brief transient signalling event and the stimulation conditions and isolation method employed failed to detect phosphorylation of p-Thr607. Secondly, only a small percentage of p84 is transiently phosphorylated on Thr607 and this was below the detection limit of the method. The extent of detectable phosphorylation may also have been reduced by the extensive sample manipulation involved in extracting p84 from total cell lysates, despite the presence of phosphatase inhibitors, which prevented the detection of p-Thr607. Although phosphorylation on Ser358 would be compromised to the same extent within isolated p84, phosphorylation at this site was observed to be constitutive and a strong signal above the detection limit. The third explanation that cannot be ruled out is that p84 is not phosphorylated on Thr607 in cells contrary to *in silico* predictions, although as discussed below, substantial further data suggest this is unlikely.

Since Akt kinase was predicted to phosphorylate p84 on Thr607 (based on Thr607 and surrounding residues forming a defined Akt consensus site), but p-Thr607 was not detected in cell lysates, the phosphorylation of a p84 peptide was assessed *in vitro*. Whilst no antibodies were available to detect phosphorylated p84 directly (discussed later), a commercially-available antibody was utilised that detected the presence of phosphorylation at an Akt kinase-phosphorylation consensus site such as phosphorylation on Thr607 within the p84 peptide. Using this antibody, Akt was found to readily phosphorylate Thr607 within the synthetic p84 peptide and furthermore, Akt co-precipitated with p84-HA in lysates from both resting and stimulated MDA.MB.231 cells. While it is unclear if the basal co-precipitation of Akt with p84-HA is real or as a consequence of *in vitro* culture, the interaction is clearly induced upon GPCR stimulation. These data showing a physical

interaction between p84 and Akt further support an Akt-mediated feedback signal through the phosphorylation of p84 on Thr607, downstream of PI3K γ signal activation. This phosphorylation within p84 represents another instance where transient phosphorylation of single residues within Class I PI3K signalling complexes is a mode of regulation, as has been described for p110 α /p85 interactions with phospho-tyrosine residues of activated RTKs⁶⁶ and the displacement of p84 from p110 γ in mast cells through the phosphorylation of the helical domain of p110 γ ¹²⁴. Phosphorylation of p84 on Thr607 and the numerous oxidation sites identified by mass spectrometry in the present study represent novel post-translational modifications to p84.

The role of identified putative Ser358 and Thr607 phosphorylation sites in the tumour suppressor function of p84 was assessed using the MDA.MB.231 model of mammary carcinoma. As described earlier, one of the major challenges facing PI3K γ research is the lack of quality reagents available to specifically detect endogenous PI3K γ subunit expression, particularly with respect to p84. In the present study, the sole commercially-available antibody (Santa Cruz anti-p87^{PIKAP}), an anti-p84 antibody developed in-house (anti-p84.2) and a newly-developed in-house phospho-specific antibody (against a synthetic Thr607-phosphorylated p84 peptide) to detect p84 phosphorylated on Thr607 were tested for their sensitivity and specificity against MDA.MB.231 cell lysates. Unfortunately, each was found to be ineffective for the detection of p84 or p84-pThr607, respectively. In the literature there is evidence of a polyclonal antibody that specifically recognises p84^(4, 6). Unfortunately, this has not been commercialised and has not been shared by the inventors.

Therefore, to examine the ability of p84 to dimerise with p110 γ , the kinetics of p84/p110 γ recruitment to the plasma membrane and determine the requirement of Ser358 and Thr607 residues for p84 function, an HA-tagged p84 expression system was developed using the retroviral expression vector pMSCV. Engineered constructs were used to transduce MDA.MB.231 cells to express wildtype p84 (p84-HA) or mutant p84 (p84-S358A-HA and p84-T607A-HA) proteins, where Ser358 and Thr607 residues had been mutated to alanine, thereby negating phosphorylation at these sites. This system led to the stable, high level of expression of wildtype and mutant p84-HA proteins in MDA.MB.231 cells and allowed their detection and immunoprecipitation utilising high quality, sensitive anti-HA

commercial antibodies. The control cell line employed for experiments where p84-HA was expressed was MDA.MB.231 cells transduced with the empty pMSCV retroviral expression vector. This control served two purposes; firstly to allow the comparison between endogenous p84 and the effect of enhanced p84 expression on the tumourigenic properties of MDA.MB.231 carcinoma cells; and secondly to provide a negative control for p84 protein interaction studies in which interaction partners were detected using anti-HA precipitations. Collectively, in the absence of quality p84-specific antibodies, the p84-HA expression system was concluded to be a valid method to specifically assess the function of p84 and Ser358/Thr607 regulatory residues through the detection of p84 proteins using the HA tag. Advances in methodology allow for novel approaches, for example another alternative approach that may be considered in the future would be to genetically-modify cells to incorporate the HA fusion tag immediately 5' of the endogenous gene for p84 (*Pik3r6*). This could be achieved using CRISPR technology^{199, 200, 203} and would allow the detection and isolation of endogenously expressed p84 using anti-HA antibodies.

Considering that siRNA-induced knockdown of p84 expression was shown to enhance the metastatic potential of MDA.MB.231 cells¹²³, consistent with a tumour suppressor function of p84, it was hypothesised that the increased expression of p84 would inhibit the metastatic potential of these cells. A major aim of the present study was therefore to determine the mechanism by which p84 mediated tumour suppression of MDA.MB.231 mammary carcinoma cells. In keeping with the above hypothesis, increased expression of wildtype p84 was found to reduce the metastatic capability of MDA.MB.231 cells both *in vivo*, in a model of experimental haematogenous metastasis, and *in vitro* in an attachment-independent growth assay. Collectively, these assays assessed the ability of cancer cells to survive and form tumour masses from single cells. These data support the tumour suppressor function of p84 and suggest that increased expression of p84 is sufficient to inhibit tumour growth properties. Although speculative, it was proposed that increased expression of p84 led to the suppression of MDA.MB.231 cell tumourigenesis through the inhibition of PI3K γ signalling. In this context, p84 may act as a negative regulator of PI3K γ and compete with p101 for p110 γ binding, resulting in reduced PI3K γ signalling. This model assumes that p110 γ is available for either p84- or p101-binding at the same spatial localisation (allowing competition between adaptors) and would be consistent with

the phenotype observed in p84-knockdown cells, where the absence of p84 expression resulted in increased PI3K γ activity and constitutive p110 γ localisation at the membrane (mediated by p101).

In addition to data generated in p84-knockdown MDA.MB.231 cells¹²³ and described above, the tumour suppressor function of p84 documented in the present study is supported by large-scale genomic and expression studies of human invasive primary breast cancer samples¹⁹⁵⁻¹⁹⁷. More specifically, a publication by Curtis *et al.* (2012) in *Nature* documented a high-throughput transcriptomics screen of over 2,000 primary human breast cancer samples, which identified p84 to be commonly down-regulated by invasive breast cancer cells at a number of stages of tumour progression. For instance, within invasive ductal carcinoma that represented a large breast cancer sub-group, p84 was found to be down-regulated in >80% of patient samples¹⁹⁵. Likewise, when interrogating cancer studies in the cBio Cancer Genomic Portal database for genome mutation and copy number alterations (<http://www.cbioportal.org/>)^{196, 197}, it was found that of 98 studies where data was available for *Pik3r6* (p84), alterations were observed in 47 analyses across numerous cancer types. Of these 47 studies, 78% documented only mutation and/or deletion alterations to *Pik3r6* in comparison to 4% that documented solely amplification alterations. Of these, a single analysis included invasive breast cancer samples where cases of mutation and deletion were reported, whilst no amplification events were identified. Together, these two large-scale studies suggest that p84 is commonly deleted or down-regulated in human invasive breast cancer, which is consistent with the data presented in this thesis generated in human breast cancer cell lines describing p84 as a tumour suppressor protein.

Beyond the confirmation of p84 as a novel tumour suppressor protein, further experimentation revealed that the tumour suppressor function of p84 was dependent on Thr607, but not Ser358. Whilst expression of wildtype p84 was shown to suppress the oncogenic potential of MDA.MB.231 cells *in vivo* and *in vitro* relative to the vector control cell line, the suppression conferred by p84 was lost in the absence of Thr607, where cells expressing p84-T607A showed a comparable number of metastases to the vector control cell line. Although it cannot be concluded that the tumour suppressor function of p84 is dependent specifically on phosphorylation at Thr607 (due to the inability to isolate p84-pThr607 from cells), it suggests that Thr607 is an essential residue to the function of p84, whether as a phosphorylation site or as a residue required for the structure or conformation

of the protein. Specifically, p84-T607A may not function in the same manner as wildtype p84 due to an inability to fold as required, an inability to bind with other interaction partners such as ras-GTPase, or an inability to localise near or interact with p110 γ . Indeed, by examining the interactions between p110 γ and wildtype p84 or p84-T607A, it was found that p84-T607A displayed reduced binding with p110 γ in response to GPCR stimulation.

The requirement of Thr607 to the function of p84 was further emphasised by the comparison of MDA.MB.231 cells transduced to express p84-T607A with cells lacking p84 expression (p84-knockdown cells). In a model of *in vitro* PI3K γ -dependent migration, the expression of p84-T607A was found to accelerate the migration of MDA.MB.231 cells in a similar fashion to p84 knockdown, when compared with cells expressing the wildtype protein. Comparable phenotypes observed for p84-T607A-expressing cells and p84-knockdown cells indicate that p84-T607A may represent a non-functional p84 protein, at least in the context of cell migration. Furthermore, it could be speculated based on these data that in the absence of p84-mediated suppression in p84-T607A-expressing cells, enhanced tumorigenicity may be driven by heightened or prolonged PI3K γ signalling as a result of increased availability of the p110 γ catalytic subunit for p101-mediated PI3K γ activation, as has been previously proposed for p84-knockdown cells¹²³. Although it remains unclear whether p84 and p101 adaptor proteins directly compete for p110 γ -binding in an endogenous system, these data and previous data¹²³ suggest that loss of functional p84 results in enhanced PI3K γ signalling driven by p101. The molecular regulation of heterodimeric complexes by two distinct adaptor proteins that possess opposing functions as tumour-suppressive or oncogenic adaptor proteins, has been previously described for tumour suppressor Pbx-regulating protein-1 (Prep1) and myeloid ecotropic viral integration site-1 (Meis1) proteins that competitively bind the same partner, pre-B-cell leukemia homeobox-1 (Pbx1), to regulate protein stability and tumorigenesis²⁶⁰.

In contrast to Thr607, the loss of Ser358 (p84-S358A) was not found to affect the tumour suppressor function of p84, indicating that the constitutive phosphorylation identified on Ser358 is dispensable for p84-mediated suppression. In addition, p84-S358A showed comparable heterodimerisation to p110 γ to wildtype p84 and the expression of p84-S358A

did not alter the kinetics of p110 γ membrane recruitment upon cell stimulation. Collectively, the loss of Ser358 did not impact p84 function in the context of PI3K γ signal regulation or tumour suppression *in vitro* or *in vivo*. Rather, it could be proposed that phosphorylation on Ser358 is required for additional interactions of p84 with other protein binding partners, such as ras-GTPase¹¹, or may play specific roles in other cell types under different stimulation conditions, such as in cardiomyocytes where p84 is required as a structural protein in a multimeric complex involved in the regulation of cardiac contractility^{120, 143}.

In order to determine the molecular mechanism by which p84 exerts tumour suppression in a Thr607-dependent manner in MDA.MB.231 cells, the ability of wildtype and mutant p84 proteins to form heterodimers with p110 γ and translocate to the plasma membrane was investigated. These experiments were designed to determine whether p84-mediated tumour suppression was as a result of p84 participation in PI3K γ enzymatic activity at the plasma membrane. In the present study, basic attachment-independent survival (*data not shown*) and cellular proliferation of MDA.MB.231 cells were not affected by the expression of wildtype or mutant p84 (p84-S358A and p84-T607A) proteins, indicating that the tumour suppression conferred by p84 was not a result of inhibited proliferation from the single carcinoma cell stage. This suggests that these particular tumour cell properties are not governed by p84 expression, which is consistent with the known contributions of PI3K α , PI3K β and PI3K γ to the control of proliferation and survival^{2, 3, 34, 160}. However, these are in contrast to the significant effect of p84 expression on the spherical tumour growth of MDA.MB.231 cells, which may alternatively be regulated via an effect on apoptosis.

Although the expression of wildtype p84 was shown to limit the tumourigenicity of MDA.MB.231 cells in a Thr607-dependent manner *in vitro* and *in vivo*, cell proliferation in these cells was found to be unaltered. The data presented in this thesis suggest that p84 negatively regulates PI3K γ signalling, therefore the ability of wildtype and mutant p84 (p84-S358A and p84-T607A) proteins to dimerise with p110 γ and translocate to the plasma membrane was examined. PI3K γ activity downstream of GPCR stimulation requires the translocation of PI3K γ heterodimers (p84/p110 γ or p101/p110 γ) to the plasma membrane where the lipid-kinase activity of p110 γ is activated by the interaction of the complex with G $\beta\gamma$, partial integration of p110 γ into the lipid membrane and direct

stimulation by the adaptor protein, as has been proven in the case of p101^{4, 12, 129, 130}. In contrast, p84 lacks intrinsic p110 γ -activating ability and requires the auxiliary actions of ras-GTPase to form a catalytically-active PI3K γ complex^{4, 11}. In the present study using co-precipitation assays, wildtype p84 was found to maintain a low basal level of interaction with p110 γ in the absence of cell stimulation, which was further induced upon 10 minutes stimulation with CXCL12. This represents the first description of inducible dimerisation of p84 with p110 γ in response to stimulation. Independent studies in cardiomyocytes and peripheral blood mononuclear cells had previously observed that p101/p110 γ complexes were induced in response to persistent stimulation, but in contrast to the data of the present study, p84/p110 γ dimerisation in those analyses was found to be constant^{4, 120}. The differences observed between p84/p110 γ dimerisation in our study (inducible dimerisation) compared with previous reports in cardiomyocytes and peripheral blood mononuclear cells (stable dimerisation) could be attributed to the temporal context of the stimulation and differences between the cell types examined. Specifically, in the previous studies described above, cardiomyocytes and peripheral blood mononuclear cells were persistently stimulated (from 24 hours to weeks). Whereas in contrast, the stimulation of MDA.MB.231 cells in the present study was limited to 0-20 minutes, as these experiments were designed to assess the immediate activation of PI3K γ signalling.

Next, the formation of induced p84/p110 γ heterodimers in response to cell stimulation was considered in relation to the kinetics of p-Akt induction (as an indication of PI3K γ signal activation) to establish the contribution of p84/p110 γ complexes to p-Akt generation in MDA.MB.231 cells. The phosphorylation of Akt was unaffected by the expression of wildtype or mutant p84, and was found to occur within 5 minutes stimulation with CXCL12 in MDA.MB.231 cells. It should be noted that this assay was not capable of distinguishing between PI3K γ signalling mediated by p84/p110 γ as opposed to p101/p110 γ complexes. However, since the detectable induction of p84/p110 γ heterodimers (at 10 minutes) was found to occur after the induction of p-Akt (peaking at 5 minutes), it suggests that initial PI3K γ -lipid-kinase activity was not mediated by p84/p110 γ complexes. Instead, the observed PI3K γ activation leading to peak p-Akt levels at 5 minutes stimulation was likely to be facilitated by p101 adaptor-mediated PI3K γ , as has been previously proposed, where p101 has been shown to execute more rapid and robust PIP₃ catalysis^{6, 10-12}. Alternatively, these data may reflect a scenario where p84/p110 γ heterodimers contribute

to PI3K γ signalling resulting in Akt phosphorylation, but that an increase in p84 expression does not affect this outcome.

In contrast to wildtype p84, there was no induction of p84-T607A/p110 γ heterodimers upon cell stimulation even though a similar level of basal dimerisation was evident. This suggests that the ability of p84 to form an inducible heterodimer with p110 γ is dependent on Thr607. It should also be noted that although the domain structure for p84 is unknown, it has been proposed that the N-terminal portion of the protein is required for p110 γ -binding (based on a degree of homology with p101)^{5,6}, whereas Thr607 is located closer to the C-terminus of p84. However, crystallisation of the p84/p110 γ complex will be required to resolve and define the p110 γ -binding interface of p84.

A second approach was employed to determine the likely contribution of induced p84/p110 γ heterodimers to active PI3K γ signalling. Subcellular fractionation of stimulated MDA.MB.231 cells allowed the detection of membrane-localised p84 and p110 γ subunits, and was utilised to determine whether the observed Thr607-dependent p84/p110 γ heterodimer induced at 10 minutes stimulation was likely to represent a catalytically-active enzyme at the plasma membrane. At 10 minutes CXCL12 stimulation (when p84/p110 γ dimer formation peaked) neither wildtype p84 nor p110 γ were found to be membrane-localised, as shown by minimal detection of these proteins within the membrane fraction of stimulated cell lysates. This indicated that p84/p110 γ heterodimers were not present at the membrane (plasma or endosomal) near its substrate and were therefore unlikely to constitute an active enzyme complex. Instead, these data suggest that p84/p110 γ heterodimers, formed after initial PI3K γ signal activation, may represent an intrinsic negative regulatory mechanism where p84 sequesters p110 γ from the membrane in order to terminate the transient signal. This is the first description of adaptor-mediated negative PI3K γ signal regulation. However, as discussed in previous sections, it remains unclear whether a given p110 γ subunit exchanges between p101 and p84 adaptor subunits in order to actively terminate signalling or whether the inducible heterodimerisation of p84 with p110 γ after initial PI3K γ signal activation is a separate mechanism to sequester p110 γ from interactions with p101 that is independent of pre-existing p101/p110 γ complexes.

Furthermore, the inability of p84-T607A to form induced heterodimers with p110 γ and the failure of p84-T607A to mediate tumour suppression (compared with wildtype p84), suggests firstly, that Thr607 is required for the negative regulation of p110 γ activity by p84 and secondly, that the tumour suppressor function of p84 is dependent on the formation of induced p84/p110 γ dimers. Together, these data identify a novel mechanism by which p84 limits the tumorigenicity of MDA.MB.231 cells by controlling PI3K γ signalling.

In vector control MDA.MB.231 cells, endogenous p110 γ was not detected in the membrane fraction prior to stimulation, but was recruited to the membrane in response to CXCL12 stimulation where peak levels were observed transiently at 1 minute stimulation, then decreased levels were observed by 10 minutes. In contrast, the membrane localisation of wildtype p84 did not mimic the kinetics observed for p110 γ and instead was found to be minimal under both resting and stimulation conditions. This further supports the proposed model that the membrane recruitment of p110 γ and initial activation of PI3K γ signalling resulting in p-Akt induction is mediated by p101 in these cells (p101/p110 γ PI3K γ heterodimers). However, in order to fully comprehend PI3K γ signal activation by p101 and p84 adaptors, the precise kinetics and localisation of p-Akt induction in cells, in addition to the dimerisation and membrane recruitment of p101/p110 γ and p84/p110 γ heterodimers should be confirmed in future studies by tracking tagged endogenous proteins in real-time by immunofluorescence to visualise the formation of distinct PI3K γ heterodimers and their subcellular localisation.

Whilst the expression of p84-T607A (or wildtype p84) were not shown to alter the induction of phosphorylated Akt in stimulated MDA.MB.231 cells, it was found that expression of p84-T607A resulted in delayed and increased membrane recruitment of p110 γ . Specifically, in cells expressing p84-T607A, p110 γ was shown to translocate to the membrane at 5 minutes and persisted at the membrane through to 10 minutes stimulation. This is in contrast to cells expressing wildtype p84 that showed transient translocation of p110 γ to the membrane that peaked at 1 minute. Since p110 γ must be at the membrane to mediate PI3K γ lipid-kinase activity, and peak p-Akt levels were similarly observed at 5 minutes stimulation in both of these cell lines (expressing wildtype p84 or p84-T607A), it suggests that the delayed recruitment of p110 γ in p84-T607A-expressing cells was sufficient to facilitate p-Akt production within the time-frames assessed. It was postulated

that the increased level of membrane-localised p110 γ observed at 5 minutes was sufficient to compensate for the delayed recruitment of p110 γ and thereby maintain p-Akt induction (similarly observed at 5 minutes stimulation). p84-T607A showed increased membrane localisation relative to wildtype p84, and although the loss of Thr607 clearly changes the behaviour of p84, the consequence and biological relevance of this spatial difference remains unclear. However, it could be speculated that due to aberrant localisation and inhibited dimerisation with p110 γ (compared with wildtype p84), p84-T607A is a non-functional p84 protein and that endogenous p84 protein expression is not sufficient to compensate and mediate the effects observed for the expression of p84-HA.

Together, the data obtained in MDA.MB.231 cells investigating the role of p84 in PI3K γ signal activation and the function of p84 as a tumour suppressor have led to the characterisation of a novel regulatory function for p84 in the control of PI3K γ signalling and the suppression of tumourigenesis. Unlike established PI3K γ adaptor functions related to the activation of lipid-kinase signalling, the data indicate that p84 forms a negative PI3K γ heterodimer with p110 γ that is dependent on Thr607 and that does not localise to the membrane. As discussed previously, although phosphorylation on Thr607 could not be identified within stimulated cell lysates, Thr607 is predicted to be phosphorylated by Akt. Phosphorylation of p84 by Akt on Thr607 (downstream of initial PI3K γ activation mediated by p101/p110 γ heterodimers) and the subsequent induction of inhibitory p84/p110 γ heterodimers would represent the first description of negative feedback signalling within the PI3K γ pathway. This proposed model of PI3K γ signal regulation is presented in **Figure 6.1**.

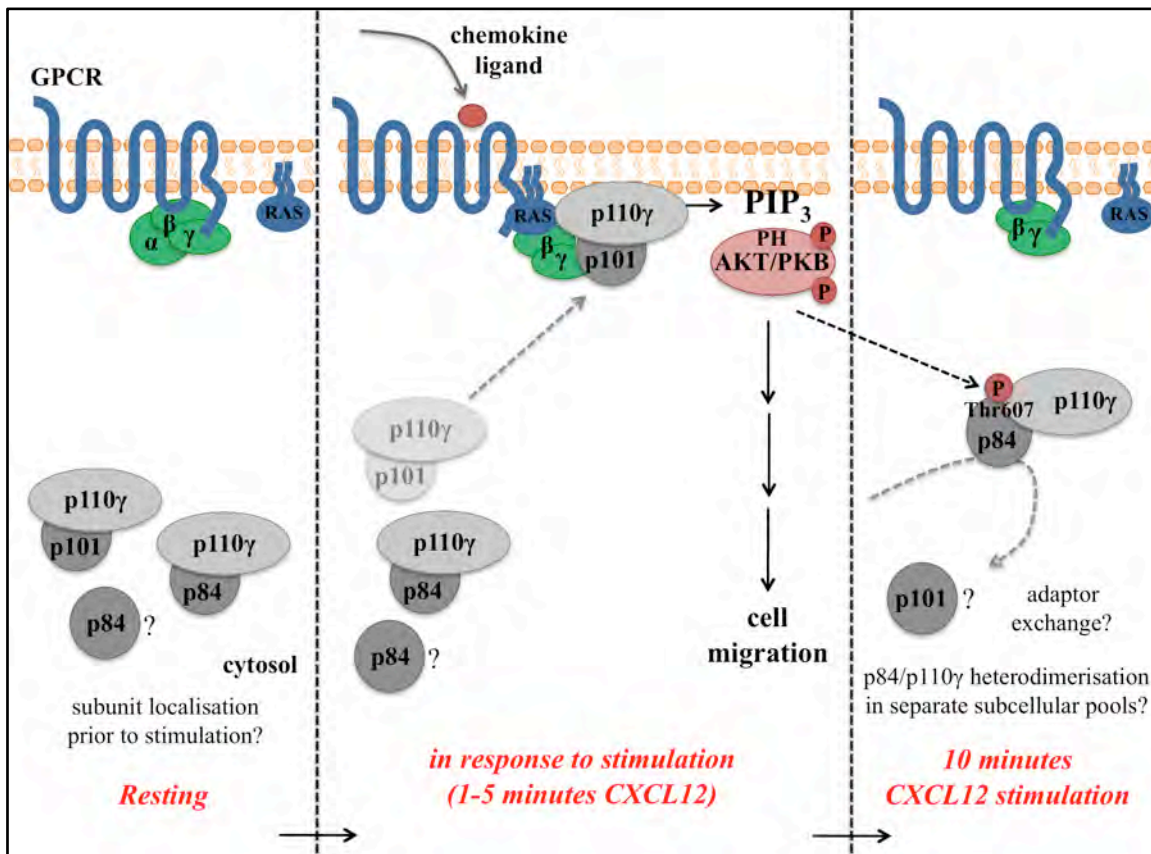


Figure 6.1: Proposed mechanism of PI3K γ signalling in MDA.MB.231 cells in response to CXCL12 stimulation.

Upon GPCR engagement with the cognate chemokine ligand, p101/p110 γ heterodimers are recruited to the plasma membrane where they become activated through interactions with G $\beta\gamma$, ras-GTPase and membrane phospholipids. Catalysis of PIP₃ lipids at the leading edge membrane by p101/p110 γ leads to the recruitment of PH domain-containing effector proteins such as Akt/PKB that become activated (p-Akt induced after 5 minutes CXCL12 stimulation) and propagate phosphorylation-dependent signalling cascades resulting in cell responses such as migration. After 10 minutes CXCL12 stimulation, p84 forms an inducible heterodimer with p110 γ in a complex that is dependent on Thr607 (p84) and is not localised at the membrane. p84 is predicted to be phosphorylated by Akt on Thr607. The induced p84/p110 γ heterodimer is proposed to represent a negative regulatory mechanism of PI3K γ signalling through the control of p110 γ localisation.

6.2 Generation of a *Pik3r6*^{-/-} mouse and characterisation of p84-dependent processes in haematopoietic cell function

Much of the functional data pertaining the roles of PI3K γ signalling with respect to the p110 γ catalytic and p101 adaptor subunits has been determined through the characterisation of PI3K γ subunit-deficient or kinase-dead mutant mice^{7, 8, 157, 160, 254, 255} (refer to Introduction section 1.3.3 and Table 1.2). However, the lack of a p84-deficient genetically-modified mouse strain has limited the exploration of distinct p84-dependent functions within PI3K γ -dependent processes. Therefore, two approaches were undertaken in order to generate a p84-deficient mouse system. Firstly, a DOX-inducible lentiviral p84 knockdown construct was engineered in order to transduce bone marrow-derived stem cells, which would allow the inducible knockdown of p84 expression in the haematopoietic cells of reconstituted bone marrow chimeric mice. However, the inefficient transduction of bone marrow-derived stem cells with the lentiviral inducible p84 knockdown construct limited this approach. Fortunately, CRISPR gene-editing technology became available in the final year of the project and was subsequently employed to generate a p84 knockout (*Pik3r6*^{-/-}) mouse strain through the mutation of *Pik3r6* exon 1, resulting in the early termination of translation and the production of a nonsense p84 protein that would likely be degraded. However, during the final stages of thesis preparation, a manuscript was published describing the generation of another p84-deficient mouse by the Stephens/Hawkins laboratories of Cambridge University, UK. Unlike the *Pik3r6*^{-/-} mouse generated in this study using CRISPR technology, Deladeriere *et al.* (2015) generated their knockout mouse (named p84^{-/-} by the authors, and herein) by traditional embryonic stem cell homologous recombination techniques in conjunction with the European Conditional Mouse Mutagenesis Program (EUCOMM), which provided the targeting vector¹⁴⁸. Whilst the publication by Deladeriere *et al.* (2015) characterised the effect of p84 deletion on PI3K γ signalling in neutrophils¹⁴⁸ (discussed further in later sections), the data presented in this thesis provide more broad and detailed analyses regarding the role of p84 in immune cell function.

The primary advantage of CRISPR technology relative to other genome-editing techniques, such as traditional embryonic stem cell mutagenesis methods, is the reduced time by which genetically-modified organisms can be made and screened¹⁹⁸⁻²⁰⁰. The

Pik3r6^{-/-} mouse generated in the present study demanded a total of 9 months from the injection of zygotes with CRISPR components to the availability of homozygous knockout animals ready for experimentation. More specifically, following the design, synthesis and injection of synthetic CRISPR guide RNA and Cas9 transcript components into zygotes, gene-modified pups were born after a 3-week gestation period and were available for genetic screening a further 3 weeks later after weaning. PCR screening of genomic DNA from these pups was performed and selected animals with desired CRISPR-induced mutations were mated in breeding trios once sexual maturity was reached at 6 weeks of age. The breeding process to screen, select and maintain the desired CRISPR-induced AAACCCA-10bp deletion modification to homozygosity required a further 7 months. This time-frame (9 months total) represents considerably less time investment than that required for traditional embryonic stem (ES) cell mutagenesis methods, which typically demand 18-24 months to generate the desired strain^{210, 261, 262}. A TALEN based gene-editing approach was also designed to mutate *Pik3r6* in the present study, and like CRISPR-induced mutagenesis, was rapid in comparison to traditional ES cell methods. However, screening of TALEN-modified pups revealed that this approach was not successful in producing the desired frame-shift mutations and was therefore not pursued.

Despite obvious time advantages, it is also worth noting that CRISPR technology, conceived *in vitro* in June 2012⁽²⁰¹⁾ and first published in two competing manuscripts in the February 2013 edition of *Science*^{204, 205}, is a relatively new technological advance that will require optimisation and improvement as potential complications are identified. For instance, the characterisation of CRISPR-induced off-target mutation events has been the focus of a number of publications in recent years and has placed minor doubt over the validity of the method²⁶³⁻²⁶⁵. The concern, such as for any targeted genome-modification technology, is that additional off-target mutations may occur undetected and contribute to a phenotype, where resultant effects are incorrectly attributed to the desired gene-modification. An awareness of this potential risk and thorough screening design is therefore necessary to ensure effective genome-modification using CRISPR technologies. Additional precautions including the generation of multiple independent lines and the use of backcrossing can also be undertaken.

Consistent with this, the CRISPR gRNA construct utilised in the present study was shown (in a proportion of CRISPR-injected zygotes) to elicit large deletions to the regions

outside, but immediately flanking the CRISPR target site within exon 1 of *Pik3r6*. Although these deletion mutations appeared to be specific to the designed gRNA and corresponding target site, as determined by the close proximity to the target region for each of the deletions described, they represented unanticipated modifications. The majority of non-target region deletions observed (*Pik3r6* CRISPR pups #1, #5, #7, #20) existed on separate alleles to desired mutations within the exon 1 target site and could therefore be eliminated by selective breeding, whereby only the desired allele is selected and maintained. This was the case for *Pik3r6* CRISPR female #7 that was selected for breeding due to the identification of one allele carrying the desired CRISPR-induced AAACCC Δ -10bp deletion within exon 1, in addition to a second allele that carried a non-target Δ -266bp deletion immediately downstream of exon 1. Selective out-breeding allowed the maintenance of the AAACCC Δ -10bp allele to homozygosity and the loss of the undesired non-target deletion allele. *Pik3r6* CRISPR mouse #16 was determined to possess two distinct mutations on a single allele; a Δ -10bp deletion within the exon 1 CRISPR target site and a non-target Δ -483bp deletion to the region immediately downstream of the target. Due to this, *Pik3r6* CRISPR #16 was completely discounted for breeding purposes.

Although not identified by the extensive screening performed, other non-target mutations to the selected alleles outside the PCR screened region cannot be ruled out. Therefore, in order to verify that the current *Pik3r6*^{-/-} breeding strain possesses the *Pik3r6* AAACCC Δ -10bp deletion as the sole mutation, whole genome sequencing of the homozygous line should ultimately be undertaken in order to confirm that any phenotypes observed in the *Pik3r6*^{-/-} mouse are a result of p84 deletion alone. Due to time constraints, this was not possible in the present study, however could be conducted in the future in conjunction with the Mouse Engineering at Garvan /ABR (MEGA) facility based at Australian BioResources and the Australian Genome Research Facility (AGRF). In spite of this, with the resources available and within the time constraints of the current project, it was concluded that CRISPR gene-editing technology was successfully employed to generate a p84-deficient mouse strain.

At the time of writing, this study represented the generation and characterisation of the first and only p84 knockout (*Pik3r6*^{-/-}) mouse strain, however as mentioned above, upon final thesis preparation, a new manuscript was published in Science Signalling by the Stephens

and Hawkins laboratories of Cambridge University, UK. The published manuscript describes a brief characterisation of the p84^{-/-} phenotype at homeostasis and demonstrates both p84-dependent and -independent functions within PI3K γ signalling in neutrophils¹⁴⁸. Consistent with the observations presented in this thesis, Deladeriere *et al.* (2015) found that the p84^{-/-} mouse was viable, fertile, of comparable size to wildtype littermates and possessed no obvious phenotype¹⁴⁸. It was demonstrated that neutrophils isolated from p84^{-/-} mice displayed a 50% reduction in PIP₃ production, compared with p101- and p110 γ -deficient neutrophils that exhibited reductions of 50% and 95%, respectively¹⁴⁸. This suggested that both p84 and p101 adaptor proteins contribute to PI3K γ signalling and PIP₃ accumulation in neutrophils. However, despite reduced ability to stimulate PIP₃ production, p84^{-/-} neutrophils displayed only modest reductions in p-Akt induction in response to fMLP and C5a stimulation¹⁴⁸.

Neutrophil migration in response to chemoattractant signalling through GPCRs is well established as a PI3K γ -dependent process involving cytoskeletal rearrangement and cell polarisation⁷. Consistent with this, Deladeriere *et al.* (2015) showed that neutrophils from p101^{-/-} and p110 γ ^{-/-} mice displayed significant migratory defects *in vitro* and *in vivo*, which was coupled with reduced ability to polarise F-actin at the leading edge of the cell¹⁴⁸. In contrast to this, p84^{-/-} neutrophils showed indistinguishable F-actin polarisation and migration from wildtype littermates in both an *in vitro* transwell migration assay to fMLP and in an *in vivo* model of neutrophil accumulation after the intraperitoneal injection of thioglycollate. These data indicate that p84 is completely redundant in these processes, and suggest that PI3K γ signalling for the induction of neutrophil migration is dependent on p101/p110 γ complexes¹⁴⁸. Conversely, the opposite dependency of PI3K γ adaptor subunits was found for the production of reactive oxygen species (ROS) in neutrophils, a process that is required for the killing and degradation of pathogens. As previously published by the same authors, Stephens *et al.* (2015) showed that ROS production was ablated in p110 γ ^{-/-} neutrophils whilst unaffected in p101^{-/-} neutrophils¹⁴⁸. The authors therefore predicted that ROS production was dependent on p84-mediated adaptor function. This hypothesis was supported whereby p84^{-/-} neutrophils displayed approximately 50% reduction in ROS production relative to wildtype controls in response to GPCR engagement with chemoattractants¹⁴⁸.

In comparison the published work of Deladeriere *et al.* (2015) detailed in the previous two paragraphs, which focused on the function of p84 adaptor-mediated PI3K γ signalling in neutrophils alone, the data presented in this thesis using the *Pik3r6*^{-/-} mouse strain depict a broad and more detailed characterisation of roles for p84 in immune organ development, haematopoietic cell activation and migration during homeostasis and during the induction of immune responses. The findings and implications of the present study are discussed hereafter.

PI3K γ functions predominantly within the immune system, where the subunits are expressed at highest levels⁴ and where lipid-kinase-dependent functions of PI3K γ enzymes have been identified within the innate and adaptive arms of immunity. For instance, PI3K γ has been shown to be required for functions in neutrophils^{7, 114}, mast cells^{29, 121, 124}, developing thymocytes during education^{114, 157, 222, 266} and mature T lymphocyte activation and migration during immune responses^{8, 114, 254}. Although roles for PI3K γ as an enzymatic entity have been well established, the relative contributions and/or redundancy of the individual adaptor subunits, p84 and p101, within these functions remained largely unknown, particularly regarding distinct roles for p84. The p84-deficient *Pik3r6*^{-/-} mouse generated in this study was developed to address this and was therefore assessed for haematopoietic cell genesis, differentiation, activation and effector function both at homeostasis and during immune responses using a number of experimental models. *Pik3r6*^{-/-} mice generated in the present study were viable, fertile, of comparable size to wildtype animals of the same age and had no obvious developmental defects. This was expected, based on the prior characterisation of the p110 γ -deficient mouse¹⁴⁵, which does not display an outward developmental phenotype, and the assumption that dependence on p84 would be in the context of PI3K γ activity. Collectively, these observations are consistent with those recently published by Deladeriere *et al.* (2015)¹⁴⁸.

Lymphoid organs of the *Pik3r6*^{-/-} mouse including the spleen, lymph nodes and thymus were found to develop normally in terms of weight and cell subset proportions at homeostasis. Though not required for splenic or lymph node architecture, both p110 γ and p101 have been previously shown to be involved in the progression of immature thymocytes through double negative stages of development in the thymus^{114, 157}. This requirement for PI3K γ signalling in thymocytes was shown to be downstream of CXCR4

and adenosine GPCR receptors, where thymocytes from p110 γ - and p101-deficient mice lacked the ability to respond to survival and migratory signals, respectively^{114, 157}. In the present study, examination of thymocyte developmental stages revealed that mature and immature thymocyte populations were equivalent between the thymi of wildtype and Pik3r6^{-/-} mice. This demonstrates that p84 is dispensable in PI3K γ signalling during thymocyte development and indicates that signalling through p101 adaptor-mediated PI3K γ complexes drives this process. This is consistent with expression data generated by Shymanets *et al.* (2013) that indicated higher expression of p101 relative to p84 in the thymus (refer to Table 1.3)⁴. Alternatively, these data could indicate that p101 is sufficient to compensate for the loss of p84 expression in Pik3r6^{-/-} thymocytes.

The proportions of circulating leukocytes were also assessed in Pik3r6^{-/-} mice and were determined to be comparable to wildtype controls. Although this comparison comprised only four replicates in each group, the data are conflicting with the observations of Deladeriere *et al.* (2015) that suggested the numbers of circulating blood leukocytes are reduced in p84^{-/-} mice relative to wildtype littermates¹⁴⁸. However, these findings that were described in-text by Deladeriere *et al.* (2015) were not presented as manuscript figures nor were available as supplementary manuscript files and are therefore difficult to discuss further.

Through an unknown mechanism, the stability of PI3K γ adaptor proteins has been shown to be altered by the loss of p110 γ catalytic subunit expression, where decreased protein expression of both p84 and p101 adaptors has been reported in p110 γ ^{-/-} neutrophils and mast cells^{6, 121, 148}. In the present study, the stability of p101 and p110 γ subunits at homeostasis was assessed at the mRNA transcript and protein levels in the Pik3r6^{-/-} mouse and was found to be independent of p84 expression. This confirms that the stability of the catalytic p110 γ subunit does not require the presence of either adaptor, consistent with the stable expression of p110 γ and p84 in the p101^{-/-} mouse¹³⁰. In a previous study, the absence of p84 had been proposed to result in slightly elevated p101 protein expression in resting neutrophils¹⁴⁸, suggesting a degree of compensation between the PI3K γ subunits. However, the data presented to support this hypothesis was neither statistically significant nor conclusive due to experimental variation¹⁴⁸. In contrast, in the present study, the expression of p101 in resting cells of the lymph node and thymus of Pik3r6^{-/-} mice was determined to

be equivalent to wildtype counterparts at both transcript and protein levels. As expected, p84 protein was undetectable by mass spectrometry analyses of lymphoid tissues derived from *Pik3r6*^{-/-} mice, thereby confirming the successful deletion of p84 through CRISPR genome-targeting.

Mast cells are innate inflammatory cells involved in the propagation of allergic responses and represent a unique cell type in the context of PI3K γ signalling, as they are the only haematopoietic cell subset reported to express p84 as the lone adaptor protein^{121, 124}. Hence, p84/p110 γ complexes have been previously assumed to mediate all characterised PI3K γ -dependent processes within mast cells²⁹. One such process is the potentiation of IgE/antigen-induced mast cell degranulation in the presence of adenosine, where PI3K γ signalling downstream of the adenosine A3 receptor (A3AR) leads to a heightened and sustained degranulation response^{29, 121}. It was therefore hypothesised that potentiation of the degranulation response downstream of adenosine stimulation would be abolished in the absence of p84; as previously shown for p110 γ -deficient mast cells²⁹. Contrary to this, the adenosine-mediated potentiating effect observed for both IgE/antigen-induced β -hexaminidase release and IL-6 secretion in wildtype bone marrow-derived mast cells (BMMCs) was maintained to equal levels in *Pik3r6*^{-/-} BMMCs. The observed potentiation was confirmed to be PI3K γ -dependent, as determined by AS605240-induced inhibition of the response, thereby suggesting that PI3K γ activation downstream of adenosine in these assays in *Pik3r6*^{-/-} mast cells does not require p84. The ability of p84-deficient mast cells to maintain PI3K γ -dependent processes was reconciled by the up-regulation of p101 adaptor expression in the presence of adenosine, which was shown in *Pik3r6*^{-/-} BMMCs but not wildtype control BMMCs. This not only suggests that p101 can compensate for the loss of p84 in mast cells upon adenosine stimulation; it is also the first evidence of complete functional compensation between PI3K γ adaptor proteins.

Up-regulation of p101 expression in response to persistent stimulation or stress has been reported in peripheral blood mononuclear cells and cardiomyocytes, respectively^{4, 120}. However the mechanisms that facilitate transcriptional regulation of p101 in p84-deficient mast cells and other aforementioned cell types is not known. To date, the only report of post-transcriptional control of p101 expression is the suppression of p101 translation by micro RNA miR-155 described in BMMCs¹²⁷. Whilst microRNAs are capable of

mediating both repression and activation of protein translation²⁶⁷, such has been described for the synthetic microRNA miRcxcr4, any microRNAs that up-regulate p101 expression are yet to be identified. Therefore, the signalling events necessary to induce the compensatory up-regulation of p101 in p84-deficient BMDCs requires further investigation and should include a screen of microRNAs present in these cells in response to adenosine stimulation by microRNA sequencing.

The rapid migration of neutrophils towards chemoattractant gradients during inflammatory responses relies on transient activating bursts of PI3K γ signalling. Consistent with this, neutrophils from p101^{-/-} and p110 γ ^{-/-} mice have been shown to display significant migratory defects *in vitro* and *in vivo*, in addition to a reduced ability to polarise F-actin at the leading edge of the cell^{7, 130, 148}. In the present study, it was determined firstly that p84-deficient mice exhibit a modest reduction in the proportion of CD11b⁺Gr-1⁺ neutrophils isolated from the bone marrow at homeostasis, and secondly, that these neutrophils displayed reduced migration to IL-8 gradients *in vitro* relative to wildtype neutrophils. These data, in conjunction with previous reports in the p101^{-/-} mouse¹³⁰ suggest that the two PI3K γ adaptors have non-redundant roles in neutrophil migration. Whether p84 and p101 act in synergy to mediate maximal migratory capacity of neutrophils or whether each adaptor is required individually for PI3K γ signalling in response to different stimuli is still to be determined.

In conflict with the data presented in the current study, recent data published by Deladeriere *et al.* (2015) using the independently generated p84^{-/-} mouse found no distinguishable difference between the *in vitro* migration of p84^{-/-} and wildtype neutrophils in a transwell chemotaxis assay towards the GPCR agonist, fMLP¹⁴⁸. However, the transwell conditions employed by Deladeriere *et al.* (2015) appeared to be designed to facilitate maximum migration of neutrophils and may therefore have potentially masked a relatively subtle effect elicited by loss of p84. More specifically, a high concentration of fMLP (1 μ M) was used, far exceeding that necessary to induce migration of highly motile neutrophils and excessive in comparison to nanomolar concentrations used routinely in the literature; and a migration time-frame of one hour, which represented more than double the migratory time-frame assessed in the present study (as is also generally used in the literature). Furthermore, the migration of p110 γ ^{-/-} neutrophils assessed in parallel was

determined to be reduced by only 30-40%⁽¹⁴⁸⁾ compared with previous reports by the same authors of up to 90% reduction in migration of p110 γ -deficient neutrophils when conducted under lower chemoattractant concentrations and shorter times¹³⁰. Collectively, it could be concluded that the differences in conditions between the present study and that of Deladeriere *et al.* (2015) account for the discrepancy between results, and that p84 and p101 have non-redundant functions in neutrophil migration.

Like in neutrophils, PI3K γ signalling has been heavily implicated in the differentiation and migration of lymphocytes, where p110 γ ^{-/-} mice are protected from the CD4⁺ lymphocyte-mediated inflammatory autoimmune condition, experimental autoimmune encephalomyelitis (EAE)^{9, 139}. EAE is an experimental murine model for human multiple sclerosis (MS) that mimics both the priming and effector phases of MS aetiology driven by autoreactive Th1 and Th17 cells, which ultimately results in symptoms of ascending paralysis^{9, 170, 171, 240}. Previous work conducted in the laboratory demonstrated that p110 γ -deficient animals display impaired Th1 and Th17 cell priming in secondary lymphoid organs as a result of defective dendritic cell migration to these sites¹³⁹. Whilst active PI3K γ complexes are required for the migration of Th1 and Th17 cells into the damaged CNS⁹, the dependence on either or both PI3K γ adaptors to this process was previously unexplored.

In the present study, it was demonstrated that MOG₃₅₋₅₅-induced chronic EAE disease in Pik3r6^{-/-} animals was inhibited to a similar extent as in p110 γ -deficient mice^{9, 139}, thus implicating p84 as the major adaptor protein for PI3K γ signalling during disease induction and demonstrating that loss of p84 could not be compensated for by the endogenous expression of p101 in Pik3r6^{-/-} mice. Cellular analyses revealed that reduced disease severity observed in Pik3r6^{-/-} mice was as a result of defective migration and infiltration of pathogenic Th1 and Th17 cells into the CNS, as determined by the reduction in total CD4⁺ Th cells that had infiltrated the CNS in Pik3r6^{-/-} mice relative to wildtype controls. Rather, Th1 and Th17 cells accumulated in the blood of Pik3r6^{-/-} mice, indicative of an inability to traverse the blood brain barrier and enter the CNS. This suggests that p84 is required for PI3K γ -dependent trafficking of activated CD4⁺ Th cells during inflammatory disease. Furthermore, the decreased presence of inflammatory Th1 and Th17 cells correlated with a reduction in neutrophils within the CNS of Pik3r6^{-/-} mice, compared with wildtype

controls. Although not delineated by the present data, the cause of reduced neutrophil migration to the CNS may be two-fold. Firstly, reduced neutrophil accumulation within the CNS may be as a direct result of impaired neutrophil migration, as was observed *in vitro*. Additionally, reduced neutrophil accumulation may be indirectly influenced by the absence of Th1 and Th17 cells within the CNS of $\text{Pik3r6}^{-/-}$ mice, and subsequently reduced levels of lymphocyte-derived inflammatory mediators present in the CNS milieu required for neutrophil migration.

The priming and differentiation of pathogenic Th1 and Th17 cells in the spleen and lymph nodes were determined to be comparable between $\text{Pik3r6}^{-/-}$ and wildtype mice, as shown by equivalent total numbers of Th1 and Th17 cells during both early disease (at day 10 post-disease induction) and at the experimental end-point (day 23). $\text{Pik3r6}^{-/-}$ mice were also found to display an increased proportion and number of regulatory T cells relative to wildtype controls. However, whilst consistent with reduced disease, the mechanism which regulatory T cells were expanded in $\text{Pik3r6}^{-/-}$ mice is not apparent. Moreover, although p84- and p110 γ -deficient animals are similarly protected from EAE disease symptoms, the priming and activation of pathogenic cells in the spleens of p110 $\gamma^{-/-}$ mice has been previously shown to be deficient as a result of reduced dendritic cell migration to secondary lymphoid organs¹³⁹. Since p84 was shown to be dispensable for effector cell priming, together these data suggest that the migration of dendritic cells and PI3K γ -dependent priming of CD4⁺ Th cells in secondary lymphoid organs may be mediated by p101 rather than p84, whereas the PI3K γ -dependent migration of activated cells to the CNS is dependent on signalling through p84/p110 γ heterodimers. This supports the notion that p84 and p101 possess distinct adaptor-mediated functions during adaptive immune responses that are non-redundant. Detailed characterisation of these unique adaptor functions will require further investigation using the p84-deficient ($\text{Pik3r6}^{-/-}$) and p101-deficient mouse models.

6.3 Proteomic analyses of CNS-infiltrating CD4⁺ cells during EAE disease

The signalling and cellular processes required for CD4⁺ Th cells to infiltrate the CNS and initiate inflammation and tissue damage during EAE disease progression were further investigated by examining the proteomes of CNS-infiltrating CD4⁺ cells relative to unactivated CD4⁺ control cells by quantitative ICPL proteomic analyses. The proteomic analyses presented in this thesis constituted an initial study using CD4⁺ cells isolated from the CNS of wildtype mice during EAE disease, in order to determine the feasibility of employing ICPL quantitation methods to assess the differences between the proteomes of wildtype and p84-deficient CD4⁺ Th cells in this disease model. This aspect of the project was commenced long before the generation and screening of the *Pik3r6*^{-/-} mouse strain, in order to optimise the sample preparation, proteomic analyses and data processing involved with the chosen methods that would require extensive time investment. Experimental autoimmune encephalomyelitis (EAE) was chosen as the model of lymphocyte-dependent inflammatory disease for proteomic studies as it had been shown previously in the laboratory that *p110γ*^{-/-} mice displayed reduced EAE disease severity as a result of defective dendritic cell migration and impaired Th cell priming in secondary lymphoid organs^{9, 139, 170}. It was therefore hypothesised that the p84 adaptor protein would be required for the PI3Kγ-dependent migration of lymphocytes in this model.

The presented proteomic analyses demonstrated quadruplex and triplex ICPL quantitative labelling methods to be an effective approach to compare the proteomes of CD4⁺ cells isolated from the CNS of EAE-diseased mice at multiple disease stages relative to unactivated control CD4⁺ cells. To ensure biological relevance, two different models of EAE were investigated; PLP₁₃₉₋₁₅₁-induced relapsing-remitting EAE in SJL/J mice and MOG₃₅₋₅₅-induced chronic EAE in C57Bl/6 mice¹⁷¹. Of the 1622 unique proteins identified within CD4⁺ cell lysates across both analyses (relapsing-remitting and chronic EAE models), the number of differentially regulated candidate proteins was condensed to 13 up-regulated and 10 down-regulated proteins that were common to both analyses and therefore relevant to disease progression in dual models of EAE, where differential regulation was considered to be at least 2-fold relative to naïve control cells.

Included in this preliminary candidate list were the known pro-inflammatory S100A4 and S100A9 proteins, that were found to be significantly up-regulated by activated CNS-

infiltrating CD4⁺ cells relative to naïve controls. S100A4 and S100A9 act as potent chemoattractant proteins for neutrophils and have been implicated in the pathogenesis of multiple inflammatory disorders such as rheumatoid arthritis, transplant rejection, sarcoidosis and EAE^{244-247, 268}. Whilst S100 proteins have already been associated with inflammation during EAE, the present study is the first proteomic analysis to show that S100A4 and S100A9 production is intrinsic to pathogenic CNS-infiltrating CD4⁺ lymphocytes. Therefore, CD4⁺ cell-derived S100A4 and S100A9 proteins are likely to represent important factors within the inflammatory milieu within the CNS that contribute to the recruitment of neutrophils and the promotion of tissue damage during EAE. Furthermore, S100 proteins including S100A4 have been shown to mediate the activation of PI3K signalling for the induction of cell migration^{248, 269-271}. Considering that p84-deficient mice display minimal numbers of CD4⁺ Th cells and reduced neutrophil recruitment to the inflamed CNS during EAE disease relative to wildtype animals, it could be speculated that the reduction in CNS-infiltrating neutrophils in *Pik3r6*^{-/-} mice is caused by decreased presence of CD4⁺ lymphocyte-derived S100 proteins in the inflammatory milieu to trigger their recruitment. In addition, neutrophil migration and recruitment to the CNS may also be limited by the inability of *Pik3r6*^{-/-} neutrophils to respond to S100 proteins in the absence of p84-mediated PI3K γ activity downstream of cell activation.

Another protein identified to be up-regulated by activated CNS-infiltrating CD4⁺ cells relative to naïve controls at both the mRNA transcript and protein levels during EAE progression in wildtype mice was annexin A1. Unlike the S100 proteins, the transcript expression of annexin A1 was found to peak during the remission phase of relapsing-remitting EAE disease. Annexin A1 has been previously associated with the resolution of inflammation and tissue repair in disease models characterised by the activation of the adaptive immune system, primarily through the restriction of lymphocyte transmigration at the microvasculature^{250, 251, 272-275}. This is the first description of CD4⁺ cell-derived annexin A1 and represents the successful identification and quantitation of a protein/process involved in the regulation of lymphocyte migration into the CNS during EAE.

In summary, the data of this initial feasibility study confirm that the optimised cell isolation procedures and ICPL data processing and analysis methods are a valid approach to investigate the proteomes of antigen-activated wildtype and p84-deficient CD4⁺ T cells. However, since p84-deficient CD4⁺ cells display defective migration into the CNS during

EAE compared with wildtype cells, CD4⁺ cells will be isolated from the spleen, blood and CNS of wildtype and *Pik3r6*^{-/-} mice and analysed in order to investigate p84-dependent signal transduction processes required for their pathobiology. This will assess CD4⁺ cell priming in secondary lymphoid organs and trafficking to the CNS where they promote inflammation causing tissue damage. Another method that could be utilised is an antigen-specific system, which would involve crossing the *Pik3r6*^{-/-} mouse with the TCR transgenic (2D2) mouse specific for the MOG₃₅₋₅₅ EAE immunising peptide, allowing the analysis of MOG-specific CD4⁺ T cells.

6.4 Summary and outlook

In summary, the data presented in this thesis highlight distinct roles for p84 both in the regulation of PI3K γ signalling and to PI3K γ -dependent processes in the context of immune cell function and migration. Firstly, a novel regulatory mechanism was identified in mammary carcinoma cells where p84 forms an inducible heterodimer with p110 γ in response to GPCR stimulation that is dependent on Thr607. This induced p84/p110 γ heterodimer was shown to form after initial PI3K γ signal activation (measured by the induction of p-Akt), in a complex sequestered from active signalling at the plasma membrane. Evidence was provided to indicate that p84 was phosphorylated on Thr607 by feedback signalling facilitated by Akt, the major kinase effector of PI3K γ signalling. The formation of the inducible p84/p110 γ heterodimer was found to be required for the tumour suppressor function of p84 in MDA.MB.231 cells and the control of migration and metastasis.

Whilst carcinoma cells (such as MDA.MB.231 cells) are a useful model to study the regulation of PI3K γ signalling, as shown by the differential roles of the adaptor proteins during tumourigenesis¹²³, it would be interesting to determine whether the described p84-mediated regulatory mechanisms exist within other cell types. Expression data generated by Shymanet *et al.* (2013) showed that whilst p110 γ is always expressed with at least one PI3K γ adaptor protein, compared with p101, p84 is more widely expressed⁴. The data presented in that study provide evidence that less-motile cells predominantly express p84 as the major adaptor protein and that p84 expression is maintained at low levels. In contrast, highly motile cells such as those of the haematopoietic system, express both p84 and p101 adaptors at relatively high levels in conjunction with p110 γ ⁴. Those data, in

extension with the findings in the present study, suggest that p84 may possess different roles in PI3K γ signalling depending on the cellular context.

To demonstrate specific roles for p84 in PI3K γ -dependent processes within immune system function, a novel p84-deficient (*Pik3r6*^{-/-}) mouse was generated using CRISPR gene-editing technology. Haematopoietic compartments were found to develop normally in terms of leukocyte subset proportions and numbers at homeostasis, however upon stimulation, it was determined that neutrophils and activated CD4⁺ Th lymphocytes exhibited reduced migration *in vitro* in a transwell chemotaxis assay and *in vivo* in a model of inflammatory autoimmunity, respectively. However, it remains unclear what implications the loss of p84 has on PI3K γ signalling at the molecular level in *Pik3r6*^{-/-} lymphocytes and neutrophils that results in their impaired migratory responses *in vivo*. The molecular regulation of PI3K γ signalling in *Pik3r6*^{-/-} cells stimulated *ex-vivo* should therefore be examined in future studies. A novel mechanism of PI3K γ subunit compensation was also identified in mast cells where p101 expression could be up-regulated to compensate for the loss of p84 expression in *Pik3r6*^{-/-} mice. Collectively, these data suggest that some functional redundancy exists between p84 and p101 adaptor subunits, whilst in other contexts, p84 has unique function that cannot be compensated for by p101. Based on the results observed in BMDCs, the compensation between p84 and p101 adaptor proteins should also be assessed in more detail in other haematopoietic cell types to determine if the up-regulation of p101 expression in *Pik3r6*^{-/-} cells is a common mechanism.

To extend the work of the current project, the next major avenue of investigation should be to determine the effect of loss of the p84 adaptor protein on PI3K γ signalling at the molecular level. The molecular regulation of PI3K γ signalling is more complex than initially anticipated and although functions of p84 within the immune system have been characterised in this study using *Pik3r6*^{-/-} mice, the effect at the molecular level is still unclear. Specifically, examining the spatial localisation of PIP₃ production in *Pik3r6*^{-/-} cells at different time-points, including during prolonged activation, would be important to ascertain whether p84 is acting as a suppressor protein that controls PI3K γ -dependent PIP₃ accumulation. This would elucidate whether the loss of p84 leads to reduced migration as a result of an inability to form a defined leading edge; or whether p84 is instead required to

mediate active PI3K γ signalling to facilitate migration in response to specific stimuli, where loss of p84 cannot be compensated for by p101. Furthermore, the roles of Ser358 and Thr607 regulatory sites within p84 could be further examined during PI3K γ signalling using embryonic fibroblasts isolated from *Pik3r6*^{-/-} mice. These cells lack endogenous p84 expression and could be transduced to express mutant p84-S348A-HA and p84-T607A-HA proteins, in order to assess the activity and subcellular localisation of these p84 mutants during PI3K γ signalling.

Increased PI3K γ signalling driven by dysregulated activity of p110 γ and p101 subunits has also been shown to promote tumourigenesis^{31, 135, 176}. Therefore, consistent with the observed role of p84 as a tumour suppressor in MDA.MB.231 cells, it would be of interest to determine whether *Pik3r6*^{-/-} mice spontaneously develop cancers in the absence of p84-mediated suppression of PI3K γ signalling. A chemical carcinogenesis model such as methylcholanthrene-induced fibrosarcoma²⁷⁶⁻²⁷⁸ could be examined in *Pik3r6*^{-/-} and wildtype mice in order to address this and could be further extended to include comparisons with p101- and p110 γ -deficient mice.

Within the current project, different immune cell processes were shown to have different requirements for the individual PI3K γ adaptor subunits and the functions of p84 were shown to be, at least in part, cell type-specific. For instance, thymocyte development through immature double-negative transitional stages was found to be entirely independent of p84 expression and instead relied completely on signalling through p101/p110 γ ¹⁵⁷, whereas the activation and migration of Th cells during inflammation was found to require the contributions of both p84 and p101 at different temporal stages of the immune response¹³⁹. In contrast, in mast cells that had previously been reported to solely express the p84 adaptor (and lack p101 expression), PI3K γ -dependent functions were maintained in *Pik3r6*^{-/-} cells via the up-regulation of p101 expression in response to adenosine stimulation, to compensate for the loss of p84. This was not the case in bone marrow cells, where the loss of p84 expression in *Pik3r6*^{-/-} cells was shown to inhibit the activation of PI3K γ lipid-kinase activity, as measured by reduced p-Akt induction relative to wildtype cells. This phenotype in bone marrow cells suggests that p84 is required as an adaptor protein to activate PI3K γ activity in response to IL-8, a role that cannot be compensated for by p101. Each of these scenarios describes signal specificity within the PI3K γ system,

where either of the distinct adaptor proteins are mobilised to activate and regulate PI3K γ signalling in response to specific cues. However, mechanisms that determine which adaptor protein (p84 or p101) binds to p110 γ in a given scenario, thereby controlling PI3K γ signal specificity, are yet to be identified. To address this, the activation of p84 and p101 adaptors in response to varied GPCR agonists and in different cell types should be examined to determine whether signal specificity is achieved through differential coupling of individual heterodimers to specific receptors, whether p84/p110 γ and p101/p110 γ complexes display varied localisation within distinct signalling hubs, or whether the activation of specific receptors leads to the promotion/inhibition of one adaptor protein or the other. These questions should be addressed through the generation of genetically-modified mice that have the coding sequences for different protein tags incorporated immediately upstream of the genes for p110 γ (*Pik3cg*), p101 (*Pik3r5*) and p84 (*Pik3r6*). This would allow the detection and tracking of endogenously expressed PI3K γ subunits, where the protein interactions and subcellular localisations of PI3K γ heterodimers in response to GPCR stimulation could be resolved.

In addition, the p84-deficient *Pik3r6*^{-/-} mouse should be used to further characterise cell type-specific roles for p84, not just within the immune system, but also in cardiac function where PI3K γ has been shown to serve both kinase-dependent and kinase-independent roles. The other major extension of the work presented in this thesis is to complete the ICPL proteomic analyses comparing the proteomes of *Pik3r6*^{-/-} and wildtype CD4⁺ Th lymphocytes during EAE disease progression, from their priming and activation in secondary lymphoid organs to their migration into the inflamed CNS. This analysis would be used to determine the p84-dependent signal transduction pathways employed by activated lymphocytes in their migration during adaptive immune responses. The proposed experiments could also be further extended to include comparisons with p101- and p110 γ -deficient CD4⁺ Th cells.

This study has highlighted the complexity and flexibility of the PI3K γ system, signal regulation at the molecular level and provides further evidence for the unique roles of the p84 adaptor protein in the PI3K γ kinase system. The generation and characterisation of a p84-deficient genetically-modified mouse strain represents a valuable tool for the perpetuation of research regarding p84 and PI3K γ signalling in the future.

Chapter 7: Appendices

Appendix A1:

Turvey ME, Klingler-Hoffmann M, Hoffmann P, McColl SR. p84 forms a negative regulatory complex with p110 γ to control PI3K γ signalling during cell migration. *Immunol Cell Biol.* 2015 Mar. doi; 10.1038/icb.2015.35. (Epub ahead of print).

Turvey, M.E., Klingler-Hoffmann, M., Hoffmann, P. & McColl, S.R. (2015). p84 forms a negative regulatory complex with p110 γ to control PI3K γ signalling during cell migration.
Immunology and Cell Biology, 93, 735-743.

NOTE:

This publication is included between pages 272-273 in the print copy of the thesis held in the University of Adelaide Library.

It is also available online to authorised users at:

<http://dx.doi.org/10.1038/icb.2015.35>

Appendix A2:

Turvey ME, Koudelka T, Comerford I, Greer JM, Carroll W, Bernard CC, Hoffmann P, McColl SR. Quantitative proteome profiling of CNS-infiltrating autoreactive CD4⁺ cells reveals selective changes during experimental autoimmune encephalomyelitis. *J Proteome Res.* 2014 Aug 1;13(8):3655-70.

Turvey, M.E., Koudelka, T., Comerford, I., Greer, J.M., Carroll, W., Bernard, C.C., Hoffmann, P. & McColl, S.R. (2014). Quantitative proteome profiling of CNS-infiltrating autoreactive CD4+ cells reveals selective changes during experimental autoimmune encephalomyelitis.
Journal of Proteome Research, 13(8), 3655-3670.

NOTE:

This publication is included between pages 274-275 in the print copy of the thesis held in the University of Adelaide Library.

It is also available online to authorised users at:

<http://dx.doi.org/10.1021/pr500158r>

Appendix A3:

ICPL Quadruplex: Regulated Proteins

Proteins up-regulated in PLP-induced relapsing-remitting EAE analysis

Fold changes were calculated relative to ICPL peptide intensities of naive CD4⁺ cell control samples;

Green shading indicates up-regulation by at least 2-fold; Grey shading indicates co-regulation between EAE disease models.

Accession designations and protein names are derived from the UniProt database.

QUADRUPLEX UP-REGULATED					
UniProt Accession	Protein name	Multiplets	Fold change		
			ICPL_4	ICPL_6	ICPL_10
AASS_MOUSE	Alpha-aminoadipic semialdehyde synthase	5	1.18	2.17	1.40
AGAP2_MOUSE	Arf-GAP with GTPase, ANK repeat	1	1.18	4.66	3.77
ALBU_MOUSE	Serum albumin	5	2.60	2.24	1.57
ALDOC_MOUSE	Fructose-bisphosphate aldolase C	3	1.62	1.85	2.04
ANXA1_MOUSE	Annexin A1	3	2.39	2.45	1.82
ANXA2_MOUSE	Annexin A2	5	2.00	2.60	1.69
ANXA7_MOUSE	Annexin A7	1	3.32	1.34	1.47
BLMH_MOUSE	Bleomycin hydrolase	1	1.12	3.27	1.31
CALM_MOUSE	Calmodulin	1	1.54	2.15	1.29
CAPG_MOUSE	Macrophage-capping protein	6	1.88	2.74	2.51
CH3L3_MOUSE	Chitinase-3-like protein 3	1	2.69	4.29	2.78
CK065_MOUSE	Uncharacterized protein C11orf65 homolog	1	1.15	53.19	0.94
CNDP2_MOUSE	Cytosolic non-specific dipeptidase	3	1.55	1.70	2.81
CRIP1_MOUSE	Cysteine-rich protein 1	1	1.48	2.44	1.65
CS010_MOUSE	UPF0556 protein C19orf10 homolog	1	2.97	0.70	1.10
DRG1_MOUSE	Developmentally-regulated GTP-binding protein	1	18.92	7.16	1.84
EFHD2_MOUSE	EF-hand domain-containing protein D2	2	1.44	2.03	2.05
EHD1_MOUSE	EH domain-containing protein 1	4	1.76	2.69	1.72
FRIH_MOUSE	Ferritin heavy chain	1	1.62	3.93	3.23
GIT2_MOUSE	ARF GTPase-activating protein GIT2	1	1.40	2.34	1.37
GLU2B_MOUSE	Glucosidase 2 subunit beta	2	1.07	2.09	1.70
GSTO1_MOUSE	Glutathione S-transferase omega-1	1	2.12	2.21	2.19
H10_MOUSE	Histone H1.0	2	1.11	1.99	2.25
H13_MOUSE	Histone H1.3	2	1.23	2.00	1.12
H1T_MOUSE	Histone H1t	1	3.56	1.02	1.21
H2A1H_MOUSE	Histone H2A type 1-H	1	2.90	1.99	2.38
H2A3_MOUSE	Histone H2A type 3	2	2.52	4.63	5.24
H2AZ_MOUSE	Histone H2A.Z	1	1.50	3.85	3.37
H2B1C_MOUSE	Histone H2B type 1-C/E/G	2	2.14	7.43	5.99
H31_MOUSE	Histone H3.1	8	3.59	7.66	8.24
H3C_MOUSE	Histone H3.3C	20	2.75	4.22	3.72
H4_MOUSE	Histone H4	7	2.72	5.78	5.04
K2C1B_MOUSE	Keratin, type II cytoskeletal 1b	3	2.20	1.15	2.24
KCRB_MOUSE	Creatine kinase B-type	1	2.07	6.89	2.43
KINH_MOUSE	Kinesin-1 heavy chain	1	1.87	2.16	1.73
LEG3_MOUSE	Galectin-3	2	7.14	9.96	5.94
LYZ2_MOUSE	Lysozyme C-2	2	4.29	5.45	9.47
MBP_MOUSE	Myelin basic protein	3	7.89	3.09	7.90
MTCH2_MOUSE	Mitochondrial carrier homolog 2	1	0.72	0.92	2.87
NFKB1_MOUSE	Nuclear factor NF-kappa-B p105 subunit	1	2.06	0.72	1.05
NH2L1_MOUSE	NHP2-like protein 1	1	2.15	1.57	0.74
OAT_MOUSE	Ornithine aminotransferase, mitochondrial	1	1.16	1.87	2.52
PA2G4_MOUSE	Proliferation-associated protein 2G4	2	1.67	2.02	1.83
PERM_MOUSE	Myeloperoxidase	2	3.14	3.71	2.03
PLEK_MOUSE	Pleckstrin	1	1.50	1.52	2.11
PLST_MOUSE	Plastin-3	1	5.38	2.06	5.35
PRDX5_MOUSE	Peroxisiredoxin-5, mitochondrial	1	2.32	28.18	1.73
RBM24_MOUSE	RNA-binding protein 24	1	0.83	1.06	2.74
RCC1_MOUSE	Regulator of chromosome condensation	1	1.21	1.18	2.25
RL10L_MOUSE	60S ribosomal protein L10-like	2	2.30	3.95	2.01
RL26_MOUSE	60S ribosomal protein L26	12	1.32	2.13	1.29
RL32_MOUSE	60S ribosomal protein L32	3	1.20	2.04	1.36
RL36_MOUSE	60S ribosomal protein L36	1	1.28	2.12	1.75
RL37_MOUSE	60S ribosomal protein L37	4	1.75	2.45	2.34
RS15_MOUSE	40S ribosomal protein S15	1	1.39	2.18	1.86
RS24_MOUSE	40S ribosomal protein S24	2	1.47	2.05	1.71
RS3A_MOUSE	40S ribosomal protein S3a	8	1.63	2.20	1.39
RT18A_MOUSE	28S ribosomal protein S18a, mitochondrial	1	1.14	3.17	1.37
S10A4_MOUSE	Protein S100-A4	3	2.61	1.92	2.23
S10A9_MOUSE	Protein S100-A9	2	5.13	9.21	5.31
S10AA_MOUSE	Protein S100-A10	2	2.54	3.05	2.26
SODC_MOUSE	Superoxide dismutase [Cu-Zn]	1	1.35	2.15	1.97
SPRE_MOUSE	Sepiapterin reductase	2	1.15	0.59	2.33
SPT5H_MOUSE	Transcription elongation factor SPT5	1	0.91	2.39	0.90
SYNC_MOUSE	Asparagine--tRNA ligase, cytoplasmic	1	1.10	1.33	2.61
SYWC_MOUSE	Tryptophan--tRNA ligase, cytoplasmic	1	1.10	1.95	4.31
SYYC_MOUSE	Tyrosine--tRNA ligase, cytoplasmic	1	1.32	2.19	1.47
TI17B_MOUSE	Mitochondrial import inner membrane translocase	1	47.27	0.72	1.91
TMM43_MOUSE	Transmembrane protein 43	2	3.01	2.09	0.95
TMP55_MOUSE	Transmembrane protease serine 5	1	0.96	1.29	13.18
TNR18_MOUSE	Tumor necrosis factor receptor 18	1	1.54	2.58	2.09
TPP1_MOUSE	Tripeptidyl-peptidase 1	1	1.11	1.35	24.37
TRXR1_MOUSE	Thioredoxin reductase 1, cytoplasmic	3	1.64	2.10	1.20
TSPO_MOUSE	Translocator protein	1	0.40	0.44	2.04
TXND5_MOUSE	Thioredoxin domain-containing protein 5	2	1.41	2.38	2.09
UBXN1_MOUSE	UBX domain-containing protein 1	1	1.10	5.39	5.12
UTP23_MOUSE	rRNA-processing protein UTP23 homolog	1	0.55	2.51	0.79
YTHD1_MOUSE	YTH domain family protein 1	1	2.32	0.83	0.96
ZYX_MOUSE	Zyxin	1	2.20	1.56	1.61

Proteins down-regulated in PLP-induced relapsing-remitting EAE analysis

Fold changes were calculated relative to ICPL peptide intensities of naive CD4⁺ cell control samples;

Red shading depicts down-regulation by at least 2-fold; Grey shading indicates co-regulation between EAE disease models.

Accession designations and protein names are derived from the UniProt database.

QUADRUPLEX DOWN-REGULATED					
UniProt Accession	Protein name	Multiplets	Fold change		
			ICPL 4	ICPL 6	ICPL 10
2A5A_MOUSE	Serine/threonine-protein phosphatase 2A	1	0.90	0.45	1.17
ACADV_MOUSE	Very long-chain specific acyl-CoA dehydrogenas	1	1.26	0.37	1.58
ACON_MOUSE	Aconitate hydratase, mitochondrial	7	0.86	0.49	0.85
ACTN1_MOUSE	Alpha-actinin-1	10	0.51	0.32	0.39
ADRO_MOUSE	NADPH:adrenodoxin oxidoreductase	3	0.88	0.33	0.73
AL4A1_MOUSE	Delta-1-pyrroline-5-carboxylate dehydrogenase	3	0.68	0.39	0.69
ARRB1_MOUSE	Beta-arrestin-1	1	1.22	0.44	1.24
AT5F1_MOUSE	ATP synthase subunit b, mitochondrial	1	0.46	0.80	1.02
ATP5L_MOUSE	ATP synthase subunit g, mitochondrial	1	1.07	0.49	0.43
ATPD_MOUSE	ATP synthase subunit delta, mitochondrial	2	1.02	0.48	0.88
AUP1_MOUSE	Ancient ubiquitous protein 1	1	0.99	0.49	0.83
BCAT2_MOUSE	Branched-chain-amino-acid aminotransferase	1	0.49	0.40	0.47
BDH_MOUSE	D-beta-hydroxybutyrate dehydrogenase	3	0.72	0.40	0.56
BPHL_MOUSE	Valacyclovir hydrolase	3	0.90	0.48	1.01
BRE1A_MOUSE	E3 ubiquitin-protein ligase BRE1A	1	1.56	0.34	0.80
BRI3B_MOUSE	BRI3-binding protein	1	1.10	0.38	0.90
BZW1_MOUSE	Basic leucine zipper and W2 domain-containing	1	0.35	0.55	0.32
CD11B_MOUSE	Cyclin-dependent kinase 11B	1	0.89	0.43	0.67
CD3E_MOUSE	T-cell surface glycoprotein CD3 epsilon chain	2	0.77	0.49	0.75
CD3G_MOUSE	T-cell surface glycoprotein CD3 gamma chain	2	0.95	0.34	0.87
CECR5_MOUSE	Cat eye syndrome critical region protein 5	1	0.99	0.33	0.49
CISY_MOUSE	Citrate synthase, mitochondrial	1	0.72	0.47	0.81
CLIP1_MOUSE	CAP-Gly domain-containing linker protein 1	1	0.75	0.38	0.64
CMC1_MOUSE	Calcium-binding mitochondrial carrier protein	7	0.70	0.48	0.71
COMT_MOUSE	Catechol O-methyltransferase	1	1.18	0.43	1.16
CORO7_MOUSE	Coronin-7	5	0.68	0.36	0.60
COX2_MOUSE	Cytochrome c oxidase subunit 2	1	1.31	0.32	1.23
COX4I_MOUSE	Cytochrome c oxidase subunit 4 isoform 1	2	0.74	0.21	0.48
COX5A_MOUSE	Cytochrome c oxidase subunit 5A	1	0.80	0.44	0.75
CPSF7_MOUSE	Cleavage and polyadenylation specificity factor	1	0.83	0.48	0.83
CSN2_MOUSE	COP9 signalosome complex subunit 2	2	0.76	0.95	0.47
DAZP1_MOUSE	DAZ-associated protein 1	3	0.57	0.43	0.55
DBR1_MOUSE	Lariat debranching enzyme	1	1.39	0.16	0.81
DCPS_MOUSE	m7GpppX diphosphatase	3	0.86	0.48	0.84
DDI2_MOUSE	Protein DDI1 homolog 2	3	1.53	0.49	1.03
DDX58_MOUSE	Probable ATP-dependent RNA helicase DDX58	1	0.76	0.49	0.98
DHB8_MOUSE	Estradiol 17-beta-dehydrogenase 8	1	1.24	0.33	0.65
DHRS4_MOUSE	Dehydrogenase/reductase SDR family member 4	2	0.87	0.37	0.76
DKC1_MOUSE	H/ACA ribonucleoprotein complex subunit 4	3	0.39	0.38	0.44
DNJA1_MOUSE	DnaJ homolog subfamily A member 1	1	0.39	0.50	0.48
ELOB_MOUSE	Transcription elongation factor B polypeptide 2	2	0.53	0.71	0.33
EVL_MOUSE	Ena/VASP-like protein	6	0.49	0.35	0.64
FMNL_MOUSE	Formin-like protein 1	1	0.91	0.49	0.78
FNBP4_MOUSE	Formin-binding protein 4	1	0.50	0.72	0.48
GIMA4_MOUSE	GTPase IMAP family member 4	2	0.65	0.46	0.68
GPX1_MOUSE	Glutathione peroxidase 1	1	0.96	0.39	0.83
GUA_A_MOUSE	GMP synthase [glutamine-hydrolyzing]	1	1.12	0.46	1.02
HCD2_MOUSE	3-hydroxyacyl-CoA dehydrogenase type-2	2	0.70	0.36	0.44
HIBCH_MOUSE	3-hydroxyisobutyryl-CoA hydrolase	1	0.60	0.48	0.75
HNRL2_MOUSE	Heterogeneous nuclear ribonucleoprotein U-like	2	0.66	0.38	0.54
HNRPC_MOUSE	Heterogeneous nuclear ribonucleoproteins C1/C2	1	0.82	0.38	0.76
HNRPF_MOUSE	Heterogeneous nuclear ribonucleoprotein F	11	1.11	0.48	0.97
HP1B3_MOUSE	Heterochromatin protein 1-binding protein 3	5	0.45	0.51	0.53
HYEP_MOUSE	Epoxide hydrolase 1	2	0.71	0.28	0.57
IDHP_MOUSE	Isocitrate dehydrogenase [NADP]	4	0.72	0.47	0.76
IL16_MOUSE	Pro-interleukin-16	4	0.65	0.48	0.53
IMDH1_MOUSE	Inosine-5'-monophosphate dehydrogenase 1	1	0.81	0.43	0.81
K1C15_MOUSE	Keratin, type I cytoskeletal 15	1	0.49	0.52	0.53
KBTBB_MOUSE	Kelch repeat and BTB domain-containing protein	3	0.92	0.36	0.68
LAGE3_MOUSE	L antigen family member 3	1	0.73	0.35	0.65
LCK_MOUSE	Proto-oncogene tyrosine-protein kinase LCK	1	0.59	0.34	0.56
LIMD2_MOUSE	LIM domain-containing protein 2	3	0.31	0.40	0.42
LMNB2_MOUSE	Lamin-B2	6	0.78	0.49	0.65
LYP2_MOUSE	Acyl-protein thioesterase 2	1	0.40	0.33	0.35
MGN2_MOUSE	Protein mago nashi homolog 2	1	0.73	0.25	0.66
MSH2_MOUSE	DNA mismatch repair protein Msh2	2	1.19	0.42	0.84
MY18A_MOUSE	Unconventional myosin-XVIIIa	2	0.73	0.49	0.52
MYH10_MOUSE	Myosin-10	2	0.96	0.45	0.50
NCEH1_MOUSE	Neutral cholesterol ester hydrolase 1	1	0.57	0.42	0.54
NDUAB_MOUSE	NADH dehydrogenase [ubiquinone] 1 alpha	1	0.85	0.31	0.76

QUADRUPLEX DOWN-REGULATED cont.					
UniProt Accession	Protein name	Multiplets	Fold change		
			ICPL_4	ICPL_6	ICPL_10
NDUBB_MOUSE	NADH dehydrogenase [ubiquinone] 1 beta	1	0.31	0.42	0.33
NIPS1_MOUSE	Protein NipSnap homolog 1	1	0.73	0.39	0.64
NRF1_MOUSE	Nuclear respiratory factor 1	1	0.69	0.40	0.56
NSUN5_MOUSE	Putative methyltransferase NSUN5	1	0.79	0.42	0.75
NTSD1_MOUSE	5'-nucleotidase domain-containing protein 1	1	1.10	0.37	0.73
NUPL1_MOUSE	Nucleoporin p58/p45	1	0.83	0.25	0.60
ODBA_MOUSE	2-oxoisovalerate dehydrogenase subunit alpha	1	1.04	0.32	0.68
ODPX_MOUSE	Pyruvate dehydrogenase protein X component	1	0.73	0.49	0.58
PEPL_MOUSE	Periplakin	1	0.38	0.07	0.19
PGAM5_MOUSE	Serine/threonine-protein phosphatase PGAM5	1	1.13	0.48	0.97
PIGS_MOUSE	GPI transamidase component PIG-S	1	0.75	0.38	0.68
PPIL4_MOUSE	Peptidyl-prolyl cis-trans isomerase-like 4	1	0.96	0.35	0.59
PPP5_MOUSE	Serine/threonine-protein phosphatase 5	1	0.21	0.21	0.25
PRDX3_MOUSE	Thioredoxin-dependent peroxide reductase	2	0.81	0.34	0.71
PSB10_MOUSE	Proteasome subunit beta type-10	1	0.72	0.30	0.64
PSD13_MOUSE	26S proteasome non-ATPase regulatory 13	1	0.84	0.47	0.85
PSDE_MOUSE	26S proteasome non-ATPase regulatory 14	1	0.97	0.47	0.95
PSMD5_MOUSE	26S proteasome non-ATPase regulatory 5	2	0.50	0.52	0.48
PSME1_MOUSE	Proteasome activator complex subunit 1	2	0.56	0.88	0.47
PSMG1_MOUSE	Proteasome assembly chaperone 1	1	1.14	0.37	1.07
PTPRO_MOUSE	Receptor-type tyrosine-protein phosphatase O	1	0.19	0.21	0.16
PUF60_MOUSE	Poly(U)-binding-splicing factor PUF60	2	0.99	0.50	0.77
QCR1_MOUSE	Cytochrome b-c1 complex subunit 1	2	1.32	0.22	0.96
RALY_MOUSE	RNA-binding protein Raly	1	1.47	0.19	0.69
RALS3_MOUSE	RAS protein activator like-3	2	0.92	0.26	0.76
RBM25_MOUSE	RNA-binding protein 25	2	0.56	0.55	0.47
RHOG_MOUSE	Rho-related GTP-binding protein RhoG	2	0.64	0.37	0.67
RM09_MOUSE	39S ribosomal protein L9, mitochondrial	2	0.70	0.44	0.55
RM19_MOUSE	39S ribosomal protein L19, mitochondrial	1	0.61	0.68	0.42
RM21_MOUSE	39S ribosomal protein L21, mitochondrial	1	0.46	1.14	0.44
RMXL1_MOUSE	RNA binding motif protein, X-linked-like-1	1	0.75	0.19	0.87
ROMO1_MOUSE	Reactive oxygen species modulator 1	1	1.59	0.30	0.77
RPN2_MOUSE	Dolichyl-diphosphooligosaccharide glycosyltransf	2	1.49	0.42	1.28
SDS3_MOUSE	Sin3 histone deacetylase corepressor SDS3	1	0.86	0.37	0.55
SELB_MOUSE	Selenocysteine-specific elongation factor	2	0.78	0.31	0.62
SELW_MOUSE	Selenoprotein W	1	0.65	0.45	0.52
SEM4D_MOUSE	Semaphorin-4D	1	0.69	0.88	0.44
SERB_MOUSE	Phosphoserine phosphatase	2	1.07	0.34	0.57
SNX12_MOUSE	Sorting nexin-12	1	0.45	0.88	0.48
SP1_MOUSE	Transcription factor Sp1	1	0.69	0.39	0.65
SP3_MOUSE	Transcription factor Sp3	1	1.14	0.45	1.20
SPCS2_MOUSE	Signal peptidase complex subunit 2	1	0.29	0.37	0.34
SPT4A_MOUSE	Transcription elongation factor SPT4-A	1	0.49	0.43	0.44
SPTB2_MOUSE	Spectrin beta chain, non-erythrocytic 1	1	0.47	0.60	0.41
SPTN1_MOUSE	Spectrin alpha chain, non-erythrocytic 1	5	0.52	0.45	0.38
SR140_MOUSE	U2 snRNP-associated SURP motif-protein	1	0.74	0.42	0.51
SRSF4_MOUSE	Serine/arginine-rich splicing factor 4	1	0.87	0.40	0.72
SSRD_MOUSE	Translocon-associated protein subunit delta	1	0.85	0.40	0.96
STALP_MOUSE	AMSH-like protease	1	0.81	0.44	0.56
STK4_MOUSE	Serine/threonine-protein kinase 4	1	0.59	1.00	0.42
SUN2_MOUSE	SUN domain-containing protein 2	1	0.87	0.19	0.65
TADBP_MOUSE	TAR DNA-binding protein 43	3	0.50	0.75	0.58
TAP1_MOUSE	Antigen peptide transporter 1	5	0.64	0.44	0.64
THIM_MOUSE	3-ketoacyl-CoA thiolase, mitochondrial	2	0.83	0.28	0.69
THMS1_MOUSE	Protein THEMIS	1	0.65	0.47	0.51
THOC4_MOUSE	THO complex subunit 4	2	0.85	0.36	0.63
TIF1B_MOUSE	Transcription intermediary factor 1-beta	9	0.68	0.46	0.63
TMED4_MOUSE	Transmembrane emp24 domain protein 4	1	0.77	0.34	0.75
TMED9_MOUSE	Transmembrane emp24 domain protein 9	2	0.62	0.35	0.61
TPSN_MOUSE	Tapasin	8	1.00	0.44	0.59
TR150_MOUSE	Thyroid hormone receptor-associated protein 3	1	0.60	1.08	0.39
TS101_MOUSE	Tumor susceptibility gene 101 protein	1	0.70	0.44	0.60
TSNAX_MOUSE	Translin-associated protein X	2	1.11	0.40	1.06
TSPO_MOUSE	Translocator protein	1	0.40	0.44	2.04
U2AF2_MOUSE	Splicing factor U2AF 65 kDa subunit	4	0.86	0.42	0.77
US20_MOUSE	U5 small nuclear ribonucleoprotein helicase	1	0.82	0.41	0.71
UBA5_MOUSE	Ubiquitin-like modifier-activating enzyme 5	1	0.92	0.36	0.71
UBP7_MOUSE	Ubiquitin carboxyl-terminal hydrolase 7	1	0.90	0.34	0.83
VMA21_MOUSE	Vacuolar ATPase assembly protein VMA21	1	0.24	0.28	0.29
VTA1_MOUSE	Vacuolar sorting-associated protein VTA1	1	1.17	0.25	0.91

Appendix A4:

ICPL Triplex: Regulated Proteins

Proteins up-regulated in MOG-induced chronic EAE analysis

Fold changes were calculated relative to ICPL peptide intensities of naive CD4⁺ cell control samples;

Green shading depicts up-regulation by at least 2-fold; Grey shading indicates co-regulation between EAE disease models.

Accession designations and protein names are derived from the UniProt database.

TRIPLEX UP-REGULATED					
UniProt Accession	Protein name	Multiplets	Fold change		
			ICPL_4	ICPL_6	
ABCD4_MOUSE	ATP-binding cassette sub-family D member 4	1	0.48	9.62	
ALBU_MOUSE	Serum albumin	1	3.05	6.01	
ANXA1_MOUSE	Annexin A1	4	2.83	3.27	
ANXA2_MOUSE	Annexin A2	6	2.79	3.45	
ARMC2_MOUSE	Armadillo repeat-containing protein 2	1	1.19	3.39	
BHA09_MOUSE	Class A basic helix-loop-helix protein 9	1	32.21	0.92	
BRI3B_MOUSE	BRI3-binding protein	1	2.71	0.47	
CALR_MOUSE	Calreticulin	1	3.57	2.09	
CAPG_MOUSE	Macrophage-capping protein	2	1.52	2.59	
CDCA3_MOUSE	Cell division cycle-associated protein 3	1	2.81	0.20	
CEL2_MOUSE	Cadherin EGF LAG seven-pass G-type 2	1	3.25	0.74	
COF1_MOUSE	Cofilin-1	2	2.35	2.14	
DDX6_MOUSE	Probable ATP-dependent RNA helicase DDX6	1	0.65	7.70	
EFHD2_MOUSE	EF-hand domain-containing protein D2	1	4.16	4.90	
FKBP2_MOUSE	Peptidyl-prolyl cis-trans isomerase FKBP2	1	2.11	1.16	
FMOS_MOUSE	Dimethylaniline monooxygenase 5	1	1.25	23.01	
H11_MOUSE	Histone H1.1	1	2.78	0.92	
H12_MOUSE	Histone H1.2	4	6.41	3.48	
H14_MOUSE	Histone H1.4	3	3.17	1.47	
H2A1H_MOUSE	Histone H2A type 1-H	4	3.31	1.05	
H2A1_MOUSE	Histone H2A.J	3	2.59	0.78	
H2B1M_MOUSE	Histone H2B type 1-M	1	3.03	1.33	
H32_MOUSE	Histone H3.2	16	5.89	1.98	
H4_MOUSE	Histone H4	5	6.46	2.07	
HMGB2_MOUSE	High mobility group protein B2	2	3.32	2.03	
KBTBB_MOUSE	Kelch repeat and BTB domain-containing 11	1	3.01	0.74	
LBR_MOUSE	Lamin-B receptor	2	2.58	1.15	
MCM3_MOUSE	DNA replication licensing factor MCM3	2	2.34	2.60	
MRCKG_MOUSE	Serine/threonine-protein kinase MRCK gamma	1	0.96	152.39	
NACA_MOUSE	Nascent polypeptide-associated complex alpha	1	2.30	1.23	
NGAL_MOUSE	Neutrophil gelatinase-associated lipocalin	1	7.95	1.33	
NPM_MOUSE	Nucleophosmin	1	2.84	3.51	
PGK1_MOUSE	Phosphoglycerate kinase 1	1	1.03	2.45	
PLSL_MOUSE	Plastin-2	1	1.50	2.27	
RL21_MOUSE	60S ribosomal protein L21	8	2.28	2.47	
RL22_MOUSE	60S ribosomal protein L22	3	2.04	2.08	
RL26_MOUSE	60S ribosomal protein L26	11	2.89	2.45	
RL27_MOUSE	60S ribosomal protein L27	4	2.32	1.91	
RL29_MOUSE	60S ribosomal protein L29	4	3.13	2.59	
RL30_MOUSE	60S ribosomal protein L30	1	2.89	3.33	
RL31_MOUSE	60S ribosomal protein L31	5	2.61	1.86	
RL32_MOUSE	60S ribosomal protein L32	3	3.06	2.26	
RL35_MOUSE	60S ribosomal protein L35	4	3.51	2.80	
RL35A_MOUSE	60S ribosomal protein L35a	5	2.15	1.99	
RL36_MOUSE	60S ribosomal protein L36	1	2.92	2.45	
RL36A_MOUSE	60S ribosomal protein L36a	4	2.88	2.59	
RL37_MOUSE	60S ribosomal protein L37	4	3.13	2.75	
RL37A_MOUSE	60S ribosomal protein L37a	1	3.51	2.81	
RL5_MOUSE	60S ribosomal protein L5	10	2.84	2.73	
RL6_MOUSE	60S ribosomal protein L6	3	2.21	2.43	
RL7A_MOUSE	60S ribosomal protein L7a	3	2.02	1.93	
RS11_MOUSE	40S ribosomal protein S11	5	1.94	2.14	
RS14_MOUSE	40S ribosomal protein S14	4	2.02	1.39	
RS19_MOUSE	40S ribosomal protein S19	5	2.26	1.88	
RS20_MOUSE	40S ribosomal protein S20	1	2.87	2.56	
RS24_MOUSE	40S ribosomal protein S24	2	4.07	3.65	
RS4X_MOUSE	40S ribosomal protein S4, X isoform	6	1.73	2.23	
RS8_MOUSE	40S ribosomal protein S8	7	2.33	2.56	
RSMB_MOUSE	Small nuclear ribonucleoprotein-associated p8	1	3.43	2.04	
S10A4_MOUSE	Protein S100-A4	1	3.39	6.30	
S10A9_MOUSE	Protein S100-A9	2	7.83	1.94	
SRSF1_MOUSE	Serine/arginine-rich splicing factor 1	1	2.25	1.81	
TCF4_MOUSE	Activated RNA polymerase II coactivator p15	4	2.88	2.18	
VIME_MOUSE	Vimentin	7	2.62	1.07	

Proteins down-regulated in MOG-induced chronic EAE analysis

Fold changes were calculated relative to ICPL peptide intensities of naive CD4⁺ cell control samples;

Red shading depicts down-regulation by at least 2-fold; Grey shading indicates co-regulation between EAE disease models.

Accession designations and protein names are derived from the UniProt database.

TRIPLEX DOWN-REGULATED				
UniProt Accession	Protein name	Multiplets	Fold change	
			ICPL_4	ICPL_6
I433G_MOUSE	14-3-3 protein gamma	2	0.53	0.49
ABCD4_MOUSE	ATP-binding cassette sub-family D member 4	1	0.48	9.62
ACON_MOUSE	Aconitate hydratase, mitochondrial	2	0.40	0.37
ACTBL_MOUSE	Beta-actin-like protein 2	2	0.43	0.72
ACTN1_MOUSE	Alpha-actinin-1	5	0.17	0.15
ACTN4_MOUSE	Alpha-actinin-4	2	0.38	0.44
ADRO_MOUSE	NADPH:adrenodoxin oxidoreductase	1	0.58	0.35
ADT1_MOUSE	ADP/ATP translocase 1	1	0.54	0.46
ADT2_MOUSE	ADP/ATP translocase 2	2	0.39	0.58
AL9A1_MOUSE	4-trimethylaminobutyraldehyde dehydrogenase	1	0.46	0.54
AP1B1_MOUSE	AP-1 complex subunit beta-1	1	0.54	0.50
ARHG1_MOUSE	Rho guanine nucleotide exchange factor 1	1	0.25	0.45
ARPC4_MOUSE	Actin-related protein 2/3 complex subunit 4	4	0.37	0.71
ATP5E_MOUSE	ATP synthase subunit epsilon, mitochondrial	1	0.42	0.34
ATP5I_MOUSE	ATP synthase subunit e, mitochondrial	2	0.62	0.35
ATPA_MOUSE	ATP synthase subunit alpha, mitochondrial	13	0.56	0.47
ATPG_MOUSE	ATP synthase subunit gamma, mitochondrial	2	0.55	0.43
ATPK_MOUSE	ATP synthase subunit f, mitochondrial	1	0.30	0.28
BRI3B_MOUSE	BRI3-binding protein	1	2.71	0.47
CAC1E_MOUSE	Voltage-dep R-type calcium channel alpha-1E	1	0.18	0.10
CBR1_MOUSE	Carbonyl reductase [NADPH] 1	2	0.31	0.23
CD3E_MOUSE	T-cell surface glycoprotein CD3 epsilon chain	1	0.44	0.44
CDCA3_MOUSE	Cell division cycle-associated protein 3	1	2.81	0.20
CLAP2_MOUSE	CLIP-associating protein 2	1	0.18	0.04
COPA_MOUSE	Coatomer subunit alpha	1	0.50	0.92
CORO7_MOUSE	Coronin-7	1	0.35	0.57
DDX5_MOUSE	Probable ATP-dependent RNA helicase DDX5	2	0.64	0.49
DHE3_MOUSE	Glutamate dehydrogenase 1, mitochondrial	4	0.47	0.38
DHX15_MOUSE	pre-mRNA-splicing factor ATP-dep RNA helicase	2	0.42	0.56
DHX9_MOUSE	ATP-dependent RNA helicase A	1	0.52	0.23
DOCK2_MOUSE	Dedicator of cytokinesis protein 2	1	0.37	1.00
EF1G_MOUSE	Elongation factor 1-gamma	1	0.44	0.56
EFTU_MOUSE	Elongation factor Tu, mitochondrial	1	0.38	0.34
ETF8_MOUSE	Electron transfer flavoprotein subunit beta	1	0.57	0.38
FA49B_MOUSE	Protein FAM49B	1	0.43	0.85
GSTP1_MOUSE	Glutathione S-transferase P 1	1	0.42	0.50
HMHA1_MOUSE	Minor histocompatibility protein HA-1	3	0.37	0.54
HNRL2_MOUSE	Heterogeneous nuclear ribonucleoprotein U-like	1	0.22	0.16
HNRPC_MOUSE	Heterogeneous nuclear ribonucleoproteins C1/C2	3	0.40	0.18
HNRPF_MOUSE	Heterogeneous nuclear ribonucleoprotein F	3	0.48	0.50
HNRPL_MOUSE	Heterogeneous nuclear ribonucleoprotein L	1	0.26	0.23
HNRPM_MOUSE	Heterogeneous nuclear ribonucleoprotein M	1	0.18	0.15
HNRPU_MOUSE	Heterogeneous nuclear ribonucleoprotein U	3	0.19	0.16
HXK1_MOUSE	Hexokinase-1	2	0.18	0.28
IDHP_MOUSE	Isocitrate dehydrogenase [NADP]	1	0.29	0.23
IZUM3_MOUSE	Izumo sperm-egg fusion protein 3	1	0.26	0.57
JIP4_MOUSE	C-Jun-amino-terminal kinase-interacting protein	1	0.01	0.00
KAPO_MOUSE	cAMP-dependent protein kinase type I-alpha	1	0.47	0.40
KI21B_MOUSE	Kinesin-like protein KIF21B	1	0.14	0.38
LEUK_MOUSE	Leukosialin	1	0.39	0.34
LIMD2_MOUSE	LIM domain-containing protein 2	1	0.51	0.35
LSM6_MOUSE	U6 snRNA-associated Sm-like protein LSM6	1	0.49	0.33
MDHC_MOUSE	Malate dehydrogenase, cytoplasmic	1	0.22	0.25
MDHM_MOUSE	Malate dehydrogenase, mitochondrial	2	0.80	0.44
MYH10_MOUSE	Myosin-10	3	0.25	0.56
MYH9_MOUSE	Myosin-9	34	0.34	0.94
NDUA9_MOUSE	NADH dehydrogenase 1 alpha subcomplex 9	1	0.38	0.79
NDUS1_MOUSE	NADH-ubiquinone oxidoreductase subunit	1	0.53	0.40
NDUV1_MOUSE	NADH dehydrogenase flavoprotein 1	1	0.68	0.50
NONO_MOUSE	Non-POU domain-containing octamer-binding	3	0.51	0.43
PCBP2_MOUSE	Poly(rC)-binding protein 2	1	0.44	0.33
PDC6I_MOUSE	Programmed cell death 6-interacting protein	3	0.42	0.69
PHB_MOUSE	Prohibitin	3	0.56	0.47
PRP19_MOUSE	Pre-mRNA-processing factor 19	1	0.38	0.72
PSME2_MOUSE	Proteasome activator complex subunit 2	1	0.38	0.50
PTBP3_MOUSE	Polypyrimidine tract-binding protein 3	1	0.48	0.43
PTN6_MOUSE	Tyrosine-protein phosphatase non-receptor 6	3	0.35	0.44
PTPRC_MOUSE	Receptor-type tyrosine-protein phosphatase C	6	0.39	0.51
PUR4_MOUSE	Phosphoribosylformylglycinamide synthase	1	0.40	0.49
PUR6_MOUSE	Multifunctional protein ADE2	1	0.49	0.67
PUR9_MOUSE	Bifunctional purine biosynthesis protein PURH	1	0.37	0.42
QCR8_MOUSE	Cytochrome b-c1 complex subunit 8	2	0.53	0.36
RAC3_MOUSE	Ras-related C3 botulinum toxin substrate 3	1	0.33	0.52
RALY_MOUSE	RNA-binding protein Raly	1	0.38	0.33
RAP1B_MOUSE	Ras-related protein Rap-1b	2	0.48	0.46
RLA0_MOUSE	60S acidic ribosomal protein P0	2	0.49	0.62
ROA2_MOUSE	Heterogeneous nuclear ribonucleoproteins A2/B1	5	0.75	0.48
ROA3_MOUSE	Heterogeneous nuclear ribonucleoprotein A3	1	0.62	0.44
RU2B_MOUSE	U2 small nuclear ribonucleoprotein B''	1	0.46	0.43
SAMH1_MOUSE	SAM domain and HD domain-containing protein 1	3	0.48	0.43
SNRPA_MOUSE	U1 small nuclear ribonucleoprotein A	1	0.48	0.38
SORCN_MOUSE	Sorcin	1	0.29	0.21
SSRB_MOUSE	Translocon-associated protein subunit beta	1	0.87	0.49
SYEP_MOUSE	Bifunctional glutamate/proline--tRNA ligase	1	0.47	0.53
TCPA_MOUSE	T-complex protein 1 subunit alpha	1	0.38	0.49
TCPD_MOUSE	T-complex protein 1 subunit delta	4	0.26	0.29
TDIF1_MOUSE	Deoxynucleotidyltransferase terminal-interacting	1	0.09	0.02
THIM_MOUSE	3-ketoacyl-CoA thiolase, mitochondrial	1	0.21	0.15
THY1_MOUSE	Thy-1 membrane glycoprotein	1	0.43	0.80
TIF1B_MOUSE	Transcription intermediary factor 1-beta	4	0.27	0.26
TLN1_MOUSE	Talin-1	7	0.39	0.51
TPSN_MOUSE	Tapasin	1	0.41	0.47
UBA1_MOUSE	Ubiquitin-like modifier-activating enzyme 1	3	0.39	0.81
URP2_MOUSE	Fermitin family homolog 3	1	0.41	0.90
ZO3_MOUSE	Tight junction protein ZO-3	1	0.25	0.18

Chapter 8: References

References:

1. Vanhaesebroeck B, Leevers SJ, Ahmadi K, Timms J, Katso R, Driscoll PC *et al.* Synthesis and function of 3-phosphorylated inositol lipids. *Annu Rev Biochem* 2001. **70**: 535-602.
2. Vanhaesebroeck B, Stephens L, Hawkins P. PI3K signalling: the path to discovery and understanding. *Nat Rev Mol Cell Biol* 2012. **13**: 195-203.
3. Cantley LC. The phosphoinositide 3-kinase pathway. *Science* 2002. **296**: 1655-1657.
4. Shymanets A, Prajwal, Bucher K, Beer-Hammer S, Harteneck C, Nurnberg B. p87 and p101 subunits are distinct regulators determining class IB phosphoinositide 3-kinase (PI3K) specificity. *J Biol Chem* 2013. **288**: 31059-31068.
5. Voigt P, Brock C, Nurnberg B, Schaefer M. Assigning functional domains within the p101 regulatory subunit of phosphoinositide 3-kinase gamma. *J Biol Chem* 2005. **280**: 5121-5127.
6. Suire S, Coadwell J, Ferguson GJ, Davidson K, Hawkins P, Stephens L. p84, a new Gbetagamma-activated regulatory subunit of the type IB phosphoinositide 3-kinase p110gamma. *Curr Biol* 2005. **15**: 566-570.
7. Hannigan M, Zhan L, Li Z, Ai Y, Wu D, Huang CK. Neutrophils lacking phosphoinositide 3-kinase gamma show loss of directionality during N-formyl-Met-Leu-Phe-induced chemotaxis. *Proc Natl Acad Sci U S A* 2002. **99**: 3603-3608.
8. Camps M, Ruckle T, Ji H, Ardisson V, Rintelen F, Shaw J *et al.* Blockade of PI3Kgamma suppresses joint inflammation and damage in mouse models of rheumatoid arthritis. *Nat Med* 2005. **11**: 936-943.
9. Berod L, Heinemann C, Heink S, Escher A, Stadelmann C, Drube S *et al.* PI3Kgamma deficiency delays the onset of experimental autoimmune encephalomyelitis and ameliorates its clinical outcome. *Eur J Immunol* 2011. **41**: 833-844.
10. Shymanets A, Ahmadian MR, Kossmeier KT, Wetzker R, Harteneck C, Nurnberg B. The p101 subunit of PI3Kgamma restores activation by Gbeta mutants deficient in stimulating p110gamma. *Biochem J* 2012. **441**: 851-858.
11. Kurig B, Shymanets A, Bohnacker T, Prajwal, Brock C, Ahmadian MR *et al.* Ras is an indispensable coregulator of the class IB phosphoinositide 3-kinase p87/p110gamma. *Proc Natl Acad Sci U S A* 2009. **106**: 20312-20317.
12. Vadas O, Dbouk HA, Shymanets A, Perisic O, Burke JE, Abi Saab WF *et al.* Molecular determinants of PI3Kgamma-mediated activation downstream of G-protein-coupled receptors (GPCRs). *Proc Natl Acad Sci U S A* 2013. **110**: 18862-18867.
13. Wymann MP, Schneider R. Lipid signalling in disease. *Nat Rev Mol Cell Biol* 2008. **9**: 162-176.

14. Sigal YJ, McDermott MI, Morris AJ. Integral membrane lipid phosphatases/phosphotransferases: common structure and diverse functions. *Biochem J* 2005. **387**: 281-293.
15. Brindley DN. Lipid phosphate phosphatases and related proteins: signaling functions in development, cell division, and cancer. *J Cell Biochem* 2004. **92**: 900-912.
16. Dobrowsky RT. Sphingolipid signalling domains floating on rafts or buried in caves? *Cell Signal* 2000. **12**: 81-90.
17. Pyne S, Pyne NJ. Sphingosine 1-phosphate signalling in mammalian cells. *Biochem J* 2000. **349**: 385-402.
18. Sheng X, Yung YC, Chen A, Chun J. Lysophosphatidic acid signalling in development. *Development* 2015. **142**: 1390-1395.
19. Meyer zu Heringdorf D, Jakobs KH. Lysophospholipid receptors: signalling, pharmacology and regulation by lysophospholipid metabolism. *Biochim Biophys Acta* 2007. **1768**: 923-940.
20. Gao X, Lowry PR, Zhou X, Depry C, Wei Z, Wong GW *et al*. PI3K/Akt signaling requires spatial compartmentalization in plasma membrane microdomains. *Proc Natl Acad Sci U S A* 2011. **108**: 14509-14514.
21. Lasserre R, Guo XJ, Conchonaud F, Hamon Y, Hawchar O, Bernard AM *et al*. Raft nanodomains contribute to Akt/PKB plasma membrane recruitment and activation. *Nat Chem Biol* 2008. **4**: 538-547.
22. Nishio M, Watanabe K, Sasaki J, Taya C, Takasuga S, Iizuka R *et al*. Control of cell polarity and motility by the PtdIns(3,4,5)P₃ phosphatase SHIP1. *Nat Cell Biol* 2007. **9**: 36-44.
23. Mondal S, Subramanian KK, Sakai J, Bajrami B, Luo HR. Phosphoinositide lipid phosphatase SHIP1 and PTEN coordinate to regulate cell migration and adhesion. *Mol Biol Cell* 2012. **23**: 1219-1230.
24. Ferguson GJ, Milne L, Kulkarni S, Sasaki T, Walker S, Andrews S *et al*. PI(3)Kgamma has an important context-dependent role in neutrophil chemokinesis. *Nat Cell Biol* 2007. **9**: 86-91.
25. Vanhaesebroeck B, Guillermet-Guibert J, Graupera M, Bilanges B. The emerging mechanisms of isoform-specific PI3K signalling. *Nat Rev Mol Cell Biol* 2010. **11**: 329-341.
26. Hawkins PT, Stephens LR. PI3K signalling in inflammation. *Biochim Biophys Acta* 2015. **1851**: 882-897.

27. Barber DF, Bartolome A, Hernandez C, Flores JM, Redondo C, Fernandez-Arias C *et al.* PI3Kgamma inhibition blocks glomerulonephritis and extends lifespan in a mouse model of systemic lupus. *Nat Med* 2005. **11**: 933-935.
28. Collmann E, Bohnacker T, Marone R, Dawson J, Rehberg M, Stringer R *et al.* Transient targeting of phosphoinositide 3-kinase acts as a roadblock in mast cells' route to allergy. *J Allergy Clin Immunol* 2013. **132**: 959-968.
29. Laffargue M, Calvez R, Finan P, Trifilieff A, Barbier M, Altruda F *et al.* Phosphoinositide 3-kinase gamma is an essential amplifier of mast cell function. *Immunity* 2002. **16**: 441-451.
30. Rivera J, Olivera A. Src family kinases and lipid mediators in control of allergic inflammation. *Immunol Rev* 2007. **217**: 255-268.
31. Kang S, Denley A, Vanhaesebroeck B, Vogt PK. Oncogenic transformation induced by the p110beta, -gamma, and -delta isoforms of class I phosphoinositide 3-kinase. *Proc Natl Acad Sci U S A* 2006. **103**: 1289-1294.
32. Hirsch E, Ciruolo E, Franco I, Ghigo A, Martini M. PI3K in cancer-stroma interactions: bad in seed and ugly in soil. *Oncogene* 2014. **33**: 3083-3090.
33. Liu P, Cheng H, Roberts TM, Zhao JJ. Targeting the phosphoinositide 3-kinase pathway in cancer. *Nat Rev Drug Discov* 2009. **8**: 627-644.
34. Wang X, Li JP, Yang Y, Ding J, Meng LH. A pharmacological model reveals biased dependency on PI3K isoforms for tumor cell growth. *Acta Pharmacol Sin* 2013. **34**: 1201-1207.
35. Zhao L, Vogt PK. Class I PI3K in oncogenic cellular transformation. *Oncogene* 2008. **27**: 5486-5496.
36. Back M, Hansson GK. Anti-inflammatory therapies for atherosclerosis. *Nat Rev Cardiol* 2015. **12**: 199-211.
37. Furuhashi M, Tuncman G, Gorgun CZ, Makowski L, Atsumi G, Vaillancourt E *et al.* Treatment of diabetes and atherosclerosis by inhibiting fatty-acid-binding protein aP2. *Nature* 2007. **447**: 959-965.
38. Madeddu P, Kraenkel N, Barcelos LS, Siragusa M, Campagnolo P, Oikawa A *et al.* Phosphoinositide 3-kinase gamma gene knockout impairs postischemic neovascularization and endothelial progenitor cell functions. *Arterioscler Thromb Vasc Biol* 2008. **28**: 68-76.
39. Callera GE, Montezano AC, Yogi A, Tostes RC, Touyz RM. Vascular signaling through cholesterol-rich domains: implications in hypertension. *Curr Opin Nephrol Hypertens* 2007. **16**: 90-104.
40. Ohanian J, Ohanian V. Lipid second messenger regulation: the role of diacylglycerol kinases and their relevance to hypertension. *J Hum Hypertens* 2001. **15**: 93-98.

41. Hunter JJ, Chien KR. Signaling pathways for cardiac hypertrophy and failure. *N Engl J Med* 1999. **341**: 1276-1283.
42. Frey N, Olson EN. Cardiac hypertrophy: the good, the bad, and the ugly. *Annu Rev Physiol* 2003. **65**: 45-79.
43. Hotamisligil GS. Inflammation and metabolic disorders. *Nature* 2006. **444**: 860-867.
44. Whitman M, Downes CP, Keeler M, Keller T, Cantley L. Type I phosphatidylinositol kinase makes a novel inositol phospholipid, phosphatidylinositol-3-phosphate. *Nature* 1988. **332**: 644-646.
45. Domin J, Pages F, Volinia S, Rittenhouse SE, Zvelebil MJ, Stein RC *et al*. Cloning of a human phosphoinositide 3-kinase with a C2 domain that displays reduced sensitivity to the inhibitor wortmannin. *Biochem J* 1997. **326 (Pt 1)**: 139-147.
46. Virbasius JV, Guilherme A, Czech MP. Mouse p170 is a novel phosphatidylinositol 3-kinase containing a C2 domain. *J Biol Chem* 1996. **271**: 13304-13307.
47. Arcaro A, Volinia S, Zvelebil MJ, Stein R, Watton SJ, Layton MJ *et al*. Human phosphoinositide 3-kinase C2beta, the role of calcium and the C2 domain in enzyme activity. *J Biol Chem* 1998. **273**: 33082-33090.
48. Misawa H, Ohtsubo M, Copeland NG, Gilbert DJ, Jenkins NA, Yoshimura A. Cloning and characterization of a novel class II phosphoinositide 3-kinase containing C2 domain. *Biochem Biophys Res Commun* 1998. **244**: 531-539.
49. Maffucci T, Brancaccio A, Piccolo E, Stein RC, Falasca M. Insulin induces phosphatidylinositol-3-phosphate formation through TC10 activation. *Embo j* 2003. **22**: 4178-4189.
50. Arcaro A, Zvelebil MJ, Wallasch C, Ullrich A, Waterfield MD, Domin J. Class II phosphoinositide 3-kinases are downstream targets of activated polypeptide growth factor receptors. *Mol Cell Biol* 2000. **20**: 3817-3830.
51. Biswas K, Yoshioka K, Asanuma K, Okamoto Y, Takuwa N, Sasaki T *et al*. Essential role of class II phosphatidylinositol-3-kinase-C2alpha in sphingosine 1-phosphate receptor-1-mediated signaling and migration in endothelial cells. *J Biol Chem* 2013. **288**: 2325-2339.
52. Aki S, Yoshioka K, Okamoto Y, Takuwa N, Takuwa Y. Phosphatidylinositol 3-kinase class II alpha-isoform PI3K-C2alpha is required for transforming growth factor beta-induced Smad signaling in endothelial cells. *J Biol Chem* 2015. **290**: 6086-6105.
53. Franco I, Gulluni F, Campa CC, Costa C, Margaria JP, Ciruolo E *et al*. PI3K class II alpha controls spatially restricted endosomal PtdIns3P and Rab11 activation to promote primary cilium function. *Dev Cell* 2014. **28**: 647-658.

-
54. Yoshioka K, Yoshida K, Cui H, Wakayama T, Takuwa N, Okamoto Y *et al.* Endothelial PI3K-C2alpha, a class II PI3K, has an essential role in angiogenesis and vascular barrier function. *Nat Med* 2012. **18**: 1560-1569.
 55. Stephens L, Cooke FT, Walters R, Jackson T, Volinia S, Gout I *et al.* Characterization of a phosphatidylinositol-specific phosphoinositide 3-kinase from mammalian cells. *Curr Biol* 1994. **4**: 203-214.
 56. Schu PV, Takegawa K, Fry MJ, Stack JH, Waterfield MD, Emr SD. Phosphatidylinositol 3-kinase encoded by yeast VPS34 gene essential for protein sorting. *Science* 1993. **260**: 88-91.
 57. Ronan B, Flamand O, Vescovi L, Dureuil C, Durand L, Fassy F *et al.* A highly potent and selective Vps34 inhibitor alters vesicle trafficking and autophagy. *Nat Chem Biol* 2014. **10**: 1013-1019.
 58. Juhasz G, Hill JH, Yan Y, Sass M, Baehrecke EH, Backer JM *et al.* The class III PI(3)K Vps34 promotes autophagy and endocytosis but not TOR signaling in *Drosophila*. *J Cell Biol* 2008. **181**: 655-666.
 59. Miller S, Tavshanjian B, Oleksy A, Perisic O, Houseman BT, Shokat KM *et al.* Shaping development of autophagy inhibitors with the structure of the lipid kinase Vps34. *Science* 2010. **327**: 1638-1642.
 60. Bago R, Malik N, Munson MJ, Prescott AR, Davies P, Sommer E *et al.* Characterization of VPS34-IN1, a selective inhibitor of Vps34, reveals that the phosphatidylinositol 3-phosphate-binding SGK3 protein kinase is a downstream target of class III phosphoinositide 3-kinase. *Biochem J* 2014. **463**: 413-427.
 61. Herman PK, Emr SD. Characterization of VPS34, a gene required for vacuolar protein sorting and vacuole segregation in *Saccharomyces cerevisiae*. *Mol Cell Biol* 1990. **10**: 6742-6754.
 62. Stack JH, Herman PK, Schu PV, Emr SD. A membrane-associated complex containing the Vps15 protein kinase and the Vps34 PI 3-kinase is essential for protein sorting to the yeast lysosome-like vacuole. *Embo j* 1993. **12**: 2195-2204.
 63. Geering B, Cutillas PR, Nock G, Gharbi SI, Vanhaesebroeck B. Class IA phosphoinositide 3-kinases are obligate p85-p110 heterodimers. *Proc Natl Acad Sci U S A* 2007. **104**: 7809-7814.
 64. Cuevas BD, Lu Y, Mao M, Zhang J, LaPushin R, Siminovitch K *et al.* Tyrosine phosphorylation of p85 relieves its inhibitory activity on phosphatidylinositol 3-kinase. *J Biol Chem* 2001. **276**: 27455-27461.
 65. Knight ZA, Shokat KM. Chemically targeting the PI3K family. *Biochem Soc Trans* 2007. **35**: 245-249.

66. Lee JY, Chiu YH, Asara J, Cantley LC. Inhibition of PI3K binding to activators by serine phosphorylation of PI3K regulatory subunit p85alpha Src homology-2 domains. *Proc Natl Acad Sci U S A* 2011. **108**: 14157-14162.
67. Backer JM. The regulation of class IA PI 3-kinases by inter-subunit interactions. *Curr Top Microbiol Immunol* 2010. **346**: 87-114.
68. Hofmann BT, Jucker M. Activation of PI3K/Akt signaling by n-terminal SH2 domain mutants of the p85alpha regulatory subunit of PI3K is enhanced by deletion of its c-terminal SH2 domain. *Cell Signal* 2012. **24**: 1950-1954.
69. Berndt A, Miller S, Williams O, Le DD, Houseman BT, Pacold JI *et al*. The p110 delta structure: mechanisms for selectivity and potency of new PI(3)K inhibitors. *Nat Chem Biol* 2010. **6**: 117-124.
70. Frazzetto M, Suphioglu C, Zhu J, Schmidt-Kittler O, Jennings IG, Cranmer SL *et al*. Dissecting isoform selectivity of PI3K inhibitors: the role of non-conserved residues in the catalytic pocket. *Biochem J* 2008. **414**: 383-390.
71. Burke JE, Williams RL. Dynamic steps in receptor tyrosine kinase mediated activation of class IA phosphoinositide 3-kinases (PI3K) captured by H/D exchange (HDX-MS). *Adv Biol Regul* 2013. **53**: 97-110.
72. Burke JE, Vadas O, Berndt A, Finegan T, Perisic O, Williams RL. Dynamics of the phosphoinositide 3-kinase p110delta interaction with p85alpha and membranes reveals aspects of regulation distinct from p110alpha. *Structure* 2011. **19**: 1127-1137.
73. Wu H, Shekar SC, Flinn RJ, El-Sibai M, Jaiswal BS, Sen KI *et al*. Regulation of Class IA PI 3-kinases: C2 domain-iSH2 domain contacts inhibit p85/p110alpha and are disrupted in oncogenic p85 mutants. *Proc Natl Acad Sci U S A* 2009. **106**: 20258-20263.
74. Vadas O, Burke JE, Zhang X, Berndt A, Williams RL. Structural basis for activation and inhibition of class I phosphoinositide 3-kinases. *Sci Signal* 2011. **4**: re2.
75. Wymann MP, Bulgarelli-Leva G, Zvelebil MJ, Pirola L, Vanhaesebroeck B, Waterfield MD *et al*. Wortmannin inactivates phosphoinositide 3-kinase by covalent modification of Lys-802, a residue involved in the phosphate transfer reaction. *Mol Cell Biol* 1996. **16**: 1722-1733.
76. Ciruolo E, Morello F, Hirsch E. Present and future of PI3K pathway inhibition in cancer: perspectives and limitations. *Curr Med Chem* 2011. **18**: 2674-2685.
77. Jeong Y, Kwon D, Hong S. Selective and potent small-molecule inhibitors of PI3Ks. *Future Med Chem* 2014. **6**: 737-756.
78. Walker EH, Perisic O, Ried C, Stephens L, Williams RL. Structural insights into phosphoinositide 3-kinase catalysis and signalling. *Nature* 1999. **402**: 313-320.

-
79. Stoyanova S, Bulgarelli-Leva G, Kirsch C, Hanck T, Klinger R, Wetzker R *et al.* Lipid kinase and protein kinase activities of G-protein-coupled phosphoinositide 3-kinase gamma: structure-activity analysis and interactions with wortmannin. *Biochem J* 1997. **324 (Pt 2)**: 489-495.
80. Zhang X, Vadas O, Perisic O, Anderson KE, Clark J, Hawkins PT *et al.* Structure of lipid kinase p110beta/p85beta elucidates an unusual SH2-domain-mediated inhibitory mechanism. *Mol Cell* 2011. **41**: 567-578.
81. Nolte RT, Eck MJ, Schlessinger J, Shoelson SE, Harrison SC. Crystal structure of the PI 3-kinase p85 amino-terminal SH2 domain and its phosphopeptide complexes. *Nat Struct Biol* 1996. **3**: 364-374.
82. Xia X, Cheng A, Akinmade D, Hamburger AW. The N-terminal 24 amino acids of the p55 gamma regulatory subunit of phosphoinositide 3-kinase binds Rb and induces cell cycle arrest. *Mol Cell Biol* 2003. **23**: 1717-1725.
83. Vanhaesebroeck B, Leever SJ, Panayotou G, Waterfield MD. Phosphoinositide 3-kinases: a conserved family of signal transducers. *Trends Biochem Sci* 1997. **22**: 267-272.
84. Inukai K, Anai M, Van Breda E, Hosaka T, Katagiri H, Funaki M *et al.* A novel 55-kDa regulatory subunit for phosphatidylinositol 3-kinase structurally similar to p55PIK Is generated by alternative splicing of the p85alpha gene. *J Biol Chem* 1996. **271**: 5317-5320.
85. Pons S, Asano T, Glasheen E, Miralpeix M, Zhang Y, Fisher TL *et al.* The structure and function of p55PIK reveal a new regulatory subunit for phosphatidylinositol 3-kinase. *Mol Cell Biol* 1995. **15**: 4453-4465.
86. Inukai K, Funaki M, Ogihara T, Katagiri H, Kanda A, Anai M *et al.* p85alpha gene generates three isoforms of regulatory subunit for phosphatidylinositol 3-kinase (PI 3-Kinase), p50alpha, p55alpha, and p85alpha, with different PI 3-kinase activity elevating responses to insulin. *J Biol Chem* 1997. **272**: 7873-7882.
87. Brock C, Schaefer M, Reusch HP, Czupalla C, Michalke M, Spicher K *et al.* Roles of G beta gamma in membrane recruitment and activation of p110 gamma/p101 phosphoinositide 3-kinase gamma. *J Cell Biol* 2003. **160**: 89-99.
88. Traynor-Kaplan AE, Thompson BL, Harris AL, Taylor P, Omann GM, Sklar LA. Transient increase in phosphatidylinositol 3,4-bisphosphate and phosphatidylinositol trisphosphate during activation of human neutrophils. *J Biol Chem* 1989. **264**: 15668-15673.
89. Ruderman NB, Kapeller R, White MF, Cantley LC. Activation of phosphatidylinositol 3-kinase by insulin. *Proc Natl Acad Sci U S A* 1990. **87**: 1411-1415.
90. Stephens LR, Hughes KT, Irvine RF. Pathway of phosphatidylinositol(3,4,5)-trisphosphate synthesis in activated neutrophils. *Nature* 1991. **351**: 33-39.

91. Bellacosa A, Chan TO, Ahmed NN, Datta K, Malstrom S, Stokoe D *et al.* Akt activation by growth factors is a multiple-step process: the role of the PH domain. *Oncogene* 1998. **17**: 313-325.
92. Bayascas JR, Alessi DR. Regulation of Akt/PKB Ser473 phosphorylation. *Mol Cell* 2005. **18**: 143-145.
93. Nicholson KM, Anderson NG. The protein kinase B/Akt signalling pathway in human malignancy. *Cell Signal* 2002. **14**: 381-395.
94. Chin YR, Toker A. Function of Akt/PKB signaling to cell motility, invasion and the tumor stroma in cancer. *Cell Signal* 2009. **21**: 470-476.
95. Testa JR, Tschlis PN. AKT signaling in normal and malignant cells. *Oncogene* 2005. **24**: 7391-7393.
96. Kong D, Yamori T. Phosphatidylinositol 3-kinase inhibitors: promising drug candidates for cancer therapy. *Cancer Sci* 2008. **99**: 1734-1740.
97. Song MS, Salmena L, Pandolfi PP. The functions and regulation of the PTEN tumour suppressor. *Nat Rev Mol Cell Biol* 2012. **13**: 283-296.
98. Yin Y, Shen WH. PTEN: a new guardian of the genome. *Oncogene* 2008. **27**: 5443-5453.
99. Wang SI, Puc J, Li J, Bruce JN, Cairns P, Sidransky D *et al.* Somatic mutations of PTEN in glioblastoma multiforme. *Cancer Res* 1997. **57**: 4183-4186.
100. Cantley LC, Neel BG. New insights into tumor suppression: PTEN suppresses tumor formation by restraining the phosphoinositide 3-kinase/AKT pathway. *Proc Natl Acad Sci U S A* 1999. **96**: 4240-4245.
101. Juric D, Castel P, Griffith M, Griffith OL, Won HH, Ellis H *et al.* Convergent loss of PTEN leads to clinical resistance to a PI(3)Kalpha inhibitor. *Nature* 2015. **518**: 240-244.
102. Gil A, Rodriguez-Escudero I, Stumpf M, Molina M, Cid VJ, Pulido R. A Functional Dissection of PTEN N-Terminus: Implications in PTEN Subcellular Targeting and Tumor Suppressor Activity. *PLoS One* 2015. **10**: e0119287.
103. Jacoby M, Cox JJ, Gayral S, Hampshire DJ, Ayub M, Blockmans M *et al.* INPP5E mutations cause primary cilium signaling defects, ciliary instability and ciliopathies in human and mouse. *Nat Genet* 2009. **41**: 1027-1031.
104. Bielas SL, Silhavy JL, Brancati F, Kisseleva MV, Al-Gazali L, Sztriha L *et al.* Mutations in INPP5E, encoding inositol polyphosphate-5-phosphatase E, link phosphatidyl inositol signaling to the ciliopathies. *Nat Genet* 2009. **41**: 1032-1036.

105. Seshacharyulu P, Pandey P, Datta K, Batra SK. Phosphatase: PP2A structural importance, regulation and its aberrant expression in cancer. *Cancer Lett* 2013. **335**: 9-18.
106. Saraf A, Oberg EA, Strack S. Molecular determinants for PP2A substrate specificity: charged residues mediate dephosphorylation of tyrosine hydroxylase by the PP2A/B' regulatory subunit. *Biochemistry* 2010. **49**: 986-995.
107. Kuo YC, Huang KY, Yang CH, Yang YS, Lee WY, Chiang CW. Regulation of phosphorylation of Thr-308 of Akt, cell proliferation, and survival by the B55alpha regulatory subunit targeting of the protein phosphatase 2A holoenzyme to Akt. *J Biol Chem* 2008. **283**: 1882-1892.
108. Foukas LC, Beeton CA, Jensen J, Phillips WA, Shepherd PR. Regulation of phosphoinositide 3-kinase by its intrinsic serine kinase activity in vivo. *Mol Cell Biol* 2004. **24**: 966-975.
109. Huang CH, Mandelker D, Schmidt-Kittler O, Samuels Y, Velculescu VE, Kinzler KW *et al*. The structure of a human p110alpha/p85alpha complex elucidates the effects of oncogenic PI3Kalpha mutations. *Science* 2007. **318**: 1744-1748.
110. Arcaro A, Wymann MP. Wortmannin is a potent phosphatidylinositol 3-kinase inhibitor: the role of phosphatidylinositol 3,4,5-trisphosphate in neutrophil responses. *Biochem J* 1993. **296 (Pt 2)**: 297-301.
111. Vlahos CJ, Matter WF, Hui KY, Brown RF. A specific inhibitor of phosphatidylinositol 3-kinase, 2-(4-morpholinyl)-8-phenyl-4H-1-benzopyran-4-one (LY294002). *J Biol Chem* 1994. **269**: 5241-5248.
112. Bi L, Okabe I, Bernard DJ, Wynshaw-Boris A, Nussbaum RL. Proliferative defect and embryonic lethality in mice homozygous for a deletion in the p110alpha subunit of phosphoinositide 3-kinase. *J Biol Chem* 1999. **274**: 10963-10968.
113. Bi L, Okabe I, Bernard DJ, Nussbaum RL. Early embryonic lethality in mice deficient in the p110beta catalytic subunit of PI 3-kinase. *Mamm Genome* 2002. **13**: 169-172.
114. Sasaki T, Irie-Sasaki J, Jones RG, Oliveira-dos-Santos AJ, Stanford WL, Bolon B *et al*. Function of PI3Kgamma in thymocyte development, T cell activation, and neutrophil migration. *Science* 2000. **287**: 1040-1046.
115. Foukas LC, Claret M, Pearce W, Okkenhaug K, Meek S, Peskett E *et al*. Critical role for the p110alpha phosphoinositide-3-OH kinase in growth and metabolic regulation. *Nature* 2006. **441**: 366-370.
116. Knight ZA, Gonzalez B, Feldman ME, Zunder ER, Goldenberg DD, Williams O *et al*. A pharmacological map of the PI3-K family defines a role for p110alpha in insulin signaling. *Cell* 2006. **125**: 733-747.

117. Cosemans JM, Munnix IC, Wetzker R, Heller R, Jackson SP, Heemskerk JW. Continuous signaling via PI3K isoforms beta and gamma is required for platelet ADP receptor function in dynamic thrombus stabilization. *Blood* 2006. **108**: 3045-3052.
118. Canobbio I, Stefanini L, Cipolla L, Ciruolo E, Gruppi C, Balduini C *et al.* Genetic evidence for a predominant role of PI3Kbeta catalytic activity in ITAM- and integrin-mediated signaling in platelets. *Blood* 2009. **114**: 2193-2196.
119. Voigt P, Dorner MB, Schaefer M. Characterization of p87PIKAP, a novel regulatory subunit of phosphoinositide 3-kinase gamma that is highly expressed in heart and interacts with PDE3B. *J Biol Chem* 2006. **281**: 9977-9986.
120. Perino A, Ghigo A, Ferrero E, Morello F, Santulli G, Baillie GS *et al.* Integrating cardiac PIP3 and cAMP signaling through a PKA anchoring function of p110gamma. *Mol Cell* 2011. **42**: 84-95.
121. Bohnacker T, Marone R, Collmann E, Calvez R, Hirsch E, Wymann MP. PI3Kgamma adaptor subunits define coupling to degranulation and cell motility by distinct PtdIns(3,4,5)P3 pools in mast cells. *Sci Signal* 2009. **2**: ra27.
122. Schmid MC, Avraamides CJ, Dippold HC, Franco I, Foubert P, Ellies LG *et al.* Receptor tyrosine kinases and TLR/IL1Rs unexpectedly activate myeloid cell PI3kgamma, a single convergent point promoting tumor inflammation and progression. *Cancer Cell* 2011. **19**: 715-727.
123. Brazzatti JA, Klingler-Hoffmann M, Haylock-Jacobs S, Harata-Lee Y, Niu M, Higgins MD *et al.* Differential roles for the p101 and p84 regulatory subunits of PI3Kgamma in tumor growth and metastasis. *Oncogene* 2012. **31**: 2350-2361.
124. Walser R, Burke JE, Gogvadze E, Bohnacker T, Zhang X, Hess D *et al.* PKCbeta phosphorylates PI3Kgamma to activate it and release it from GPCR control. *PLoS Biol* 2013. **11**: e1001587.
125. Patrucco E, Notte A, Barberis L, Selvetella G, Maffei A, Brancaccio M *et al.* PI3Kgamma modulates the cardiac response to chronic pressure overload by distinct kinase-dependent and -independent effects. *Cell* 2004. **118**: 375-387.
126. Endo D, Gon Y, Nunomura S, Yamashita K, Hashimoto S, Ra C. PI3Kgamma differentially regulates FcepsilonRI-mediated degranulation and migration of mast cells by and toward antigen. *Int Arch Allergy Immunol* 2009. **149 Suppl 1**: 66-72.
127. Biethahn K, Orinska Z, Vigorito E, Goyeneche-Patino DA, Mirghomizadeh F, Foger N *et al.* miRNA-155 controls mast cell activation by regulating the PI3Kgamma pathway and anaphylaxis in a mouse model. *Allergy* 2014.
128. Huang X, Shen Y, Liu M, Bi C, Jiang C, Iqbal J *et al.* Quantitative proteomics reveals that miR-155 regulates the PI3K-AKT pathway in diffuse large B-cell lymphoma. *Am J Pathol* 2012. **181**: 26-33.

129. Dbouk HA, Vadas O, Shymanets A, Burke JE, Salamon RS, Khalil BD *et al.* G protein-coupled receptor-mediated activation of p110beta by Gbetagamma is required for cellular transformation and invasiveness. *Sci Signal* 2012. **5**: ra89.
130. Suire S, Condliffe AM, Ferguson GJ, Ellson CD, Guillou H, Davidson K *et al.* Gbetagammias and the Ras binding domain of p110gamma are both important regulators of PI(3)Kgamma signalling in neutrophils. *Nat Cell Biol* 2006. **8**: 1303-1309.
131. Akekawatchai C, Holland JD, Kochetkova M, Wallace JC, McColl SR. Transactivation of CXCR4 by the insulin-like growth factor-1 receptor (IGF-1R) in human MDA-MB-231 breast cancer epithelial cells. *J Biol Chem* 2005. **280**: 39701-39708.
132. Guillermet-Guibert J, Bjorklof K, Salpekar A, Gonella C, Ramadani F, Bilancio A *et al.* The p110beta isoform of phosphoinositide 3-kinase signals downstream of G protein-coupled receptors and is functionally redundant with p110gamma. *Proc Natl Acad Sci U S A* 2008. **105**: 8292-8297.
133. Nigorikawa K, Hazeki K, Kumazawa T, Itoh Y, Hoshi M, Hazeki O. Class-IA phosphoinositide 3-kinase p110beta Triggers GPCR-induced superoxide production in p110gamma-deficient murine neutrophils. *J Pharmacol Sci* 2012. **120**: 270-279.
134. Miller S, Oleksy A, Perisic O, Williams RL. Finding a fitting shoe for Cinderella: searching for an autophagy inhibitor. *Autophagy* 2010. **6**: 805-807.
135. Johnson C, Marriott SJ, Levy LS. Overexpression of p101 activates PI3Kgamma signaling in T cells and contributes to cell survival. *Oncogene* 2007. **26**: 7049-7057.
136. Lehmann K, Muller JP, Schlott B, Skroblin P, Barz D, Norgauer J *et al.* PI3Kgamma controls oxidative bursts in neutrophils via interactions with PKCalpha and p47phox. *Biochem J* 2009. **419**: 603-610.
137. Del Prete A, Vermi W, Dander E, Otero K, Barberis L, Luini W *et al.* Defective dendritic cell migration and activation of adaptive immunity in PI3Kgamma-deficient mice. *Embo j* 2004. **23**: 3505-3515.
138. Sallusto F, Schaerli P, Loetscher P, Schaniel C, Lenig D, Mackay CR *et al.* Rapid and coordinated switch in chemokine receptor expression during dendritic cell maturation. *Eur J Immunol* 1998. **28**: 2760-2769.
139. Comerford I, Litchfield W, Kara E, McColl SR. PI3Kgamma drives priming and survival of autoreactive CD4(+) T cells during experimental autoimmune encephalomyelitis. *PLoS One* **7**: e45095.
140. Perrino C, Schroder JN, Lima B, Villamizar N, Nienaber JJ, Milano CA *et al.* Dynamic regulation of phosphoinositide 3-kinase-gamma activity and beta-adrenergic receptor trafficking in end-stage human heart failure. *Circulation* 2007. **116**: 2571-2579.

141. Naga Prasad SV, Barak LS, Rapacciuolo A, Caron MG, Rockman HA. Agonist-dependent recruitment of phosphoinositide 3-kinase to the membrane by beta-adrenergic receptor kinase 1. A role in receptor sequestration. *J Biol Chem* 2001. **276**: 18953-18959.
142. Mohan ML, Jha BK, Gupta MK, Vasudevan NT, Martelli EE, Mosinski JD *et al.* Phosphoinositide 3-kinase gamma inhibits cardiac GSK-3 independently of Akt. *Sci Signal* 2013. **6**: ra4.
143. Perino A, Ghigo A, Damilano F, Hirsch E. Identification of the macromolecular complex responsible for PI3Kgamma-dependent regulation of cAMP levels. *Biochem Soc Trans* 2006. **34**: 502-503.
144. Fumagalli L, Campa CC, Germena G, Lowell CA, Hirsch E, Berton G. Class I phosphoinositide-3-kinases and SRC kinases play a nonredundant role in regulation of adhesion-independent and -dependent neutrophil reactive oxygen species generation. *J Immunol* 2013. **190**: 3648-3660.
145. Hirsch E, Katanaev VL, Garlanda C, Azzolino O, Pirola L, Silengo L *et al.* Central role for G protein-coupled phosphoinositide 3-kinase gamma in inflammation. *Science* 2000. **287**: 1049-1053.
146. Yum HK, Arcaroli J, Kupfner J, Shenkar R, Penninger JM, Sasaki T *et al.* Involvement of phosphoinositide 3-kinases in neutrophil activation and the development of acute lung injury. *J Immunol* 2001. **167**: 6601-6608.
147. Strassheim D, Asehnoune K, Park JS, Kim JY, He Q, Richter D *et al.* Phosphoinositide 3-kinase and Akt occupy central roles in inflammatory responses of Toll-like receptor 2-stimulated neutrophils. *J Immunol* 2004. **172**: 5727-5733.
148. Deladeriere A, Gambardella L, Pan D, Anderson KE, Hawkins PT, Stephens LR. The regulatory subunits of PI3Kgamma control distinct neutrophil responses. *Sci Signal* 2015. **8**: ra8.
149. Ramadani F, Bolland DJ, Garcon F, Emery JL, Vanhaesebroeck B, Corcoran AE *et al.* The PI3K isoforms p110alpha and p110delta are essential for pre-B cell receptor signaling and B cell development. *Sci Signal* 2010. **3**: ra60.
150. Durand CA, Hartvigsen K, Fogelstrand L, Kim S, Iritani S, Vanhaesebroeck B *et al.* Phosphoinositide 3-kinase p110 delta regulates natural antibody production, marginal zone and B-1 B cell function, and autoantibody responses. *J Immunol* 2009. **183**: 5673-5684.
151. Bilancio A, Okkenhaug K, Camps M, Emery JL, Ruckle T, Rommel C *et al.* Key role of the p110delta isoform of PI3K in B-cell antigen and IL-4 receptor signaling: comparative analysis of genetic and pharmacologic interference with p110delta function in B cells. *Blood* 2006. **107**: 642-650.

152. Puri KD, Gold MR. Selective inhibitors of phosphoinositide 3-kinase delta: modulators of B-cell function with potential for treating autoimmune inflammatory diseases and B-cell malignancies. *Front Immunol* 2012. **3**: 256.
153. Jou ST, Carpino N, Takahashi Y, Piekorz R, Chao JR, Carpino N *et al.* Essential, nonredundant role for the phosphoinositide 3-kinase p110delta in signaling by the B-cell receptor complex. *Mol Cell Biol* 2002. **22**: 8580-8591.
154. Okkenhaug K, Bilancio A, Farjot G, Priddle H, Sancho S, Peskett E *et al.* Impaired B and T cell antigen receptor signaling in p110delta PI 3-kinase mutant mice. *Science* 2002. **297**: 1031-1034.
155. Ji H, Rintelen F, Waltzinger C, Bertschy Meier D, Bilancio A, Pearce W *et al.* Inactivation of PI3Kgamma and PI3Kdelta distorts T-cell development and causes multiple organ inflammation. *Blood* 2007. **110**: 2940-2947.
156. Liu D, Uzonna JE. The p110 delta isoform of phosphatidylinositol 3-kinase controls the quality of secondary anti-Leishmania immunity by regulating expansion and effector function of memory T cell subsets. *J Immunol* 2010. **184**: 3098-3105.
157. Janas ML, Varano G, Gudmundsson K, Noda M, Nagasawa T, Turner M. Thymic development beyond beta-selection requires phosphatidylinositol 3-kinase activation by CXCR4. *J Exp Med* 2010. **207**: 247-261.
158. Cekic C, Sag D, Day YJ, Linden J. Extracellular adenosine regulates naive T cell development and peripheral maintenance. *J Exp Med* 2013. **210**: 2693-2706.
159. Fung-Leung WP, Kundig TM, Zinkernagel RM, Mak TW. Immune response against lymphocytic choriomeningitis virus infection in mice without CD8 expression. *J Exp Med* 1991. **174**: 1425-1429.
160. Ladygina N, Gottipati S, Ngo K, Castro G, Ma JY, Banie H *et al.* PI3Kgamma kinase activity is required for optimal T-cell activation and differentiation. *Eur J Immunol* 2013. **43**: 3183-3196.
161. Tsokos GC. Systemic lupus erythematosus. *N Engl J Med* 2011. **365**: 2110-2121.
162. Barber DF, Bartolome A, Hernandez C, Flores JM, Fernandez-Arias C, Rodriguez-Borlado L *et al.* Class IB-phosphatidylinositol 3-kinase (PI3K) deficiency ameliorates IA-PI3K-induced systemic lupus but not T cell invasion. *J Immunol* 2006. **176**: 589-593.
163. Smolen JS, Steiner G. Therapeutic strategies for rheumatoid arthritis. *Nat Rev Drug Discov* 2003. **2**: 473-488.
164. Trentham DE. Collagen arthritis as a relevant model for rheumatoid arthritis. *Arthritis Rheum* 1982. **25**: 911-916.
165. Stuart JM, Townes AS, Kang AH. Collagen autoimmune arthritis. *Annu Rev Immunol* 1984. **2**: 199-218.

166. Terato K, Hasty KA, Reife RA, Cremer MA, Kang AH, Stuart JM. Induction of arthritis with monoclonal antibodies to collagen. *J Immunol* 1992. **148**: 2103-2108.
167. Madsen LS, Andersson EC, Jansson L, krogsgaard M, Andersen CB, Engberg J *et al.* A humanized model for multiple sclerosis using HLA-DR2 and a human T-cell receptor. *Nat Genet* 1999. **23**: 343-347.
168. Dai KZ, Harbo HF, Celius EG, Oturai A, Sorensen PS, Ryder LP *et al.* The T cell regulator gene SH2D2A contributes to the genetic susceptibility of multiple sclerosis. *Genes Immun* 2001. **2**: 263-268.
169. Hong J, Zang YC, Li S, Rivera VM, Zhang JZ. Ex vivo detection of myelin basic protein-reactive T cells in multiple sclerosis and controls using specific TCR oligonucleotide probes. *Eur J Immunol* 2004. **34**: 870-881.
170. Skundric DS, Kim C, Tse HY, Raine CS. Homing of T cells to the central nervous system throughout the course of relapsing experimental autoimmune encephalomyelitis in Thy-1 congenic mice. *J Neuroimmunol* 1993. **46**: 113-121.
171. Baxter AG. The origin and application of experimental autoimmune encephalomyelitis. *Nat Rev Immunol* 2007. **7**: 904-912.
172. MartIn-Fontecha A, Sebastiani S, Hopken UE, Ugucioni M, Lipp M, Lanzavecchia A *et al.* Regulation of dendritic cell migration to the draining lymph node: impact on T lymphocyte traffic and priming. *J Exp Med* 2003. **198**: 615-621.
173. Rommel C, Camps M, Ji H. PI3K delta and PI3K gamma: partners in crime in inflammation in rheumatoid arthritis and beyond? *Nat Rev Immunol* 2007. **7**: 191-201.
174. Doukas J, Wrasidlo W, Noronha G, Dneprovskaja E, Fine R, Weis S *et al.* Phosphoinositide 3-kinase gamma/delta inhibition limits infarct size after myocardial ischemia/reperfusion injury. *Proc Natl Acad Sci U S A* 2006. **103**: 19866-19871.
175. Doukas J, Eide L, Stebbins K, Racanelli-Layton A, Dellamary L, Martin M *et al.* Aerosolized phosphoinositide 3-kinase gamma/delta inhibitor TG100-115 [3-[2,4-diamino-6-(3-hydroxyphenyl)pteridin-7-yl]phenol] as a therapeutic candidate for asthma and chronic obstructive pulmonary disease. *J Pharmacol Exp Ther* 2009. **328**: 758-765.
176. Subramaniam PS, Whye DW, Efimenko E, Chen J, Tosello V, De Keersmaecker K *et al.* Targeting nonclassical oncogenes for therapy in T-ALL. *Cancer Cell* 2012. **21**: 459-472.
177. Samuels Y, Wang Z, Bardelli A, Silliman N, Ptak J, Szabo S *et al.* High frequency of mutations of the PIK3CA gene in human cancers. *Science* 2004. **304**: 554.

-
178. Bachman KE, Argani P, Samuels Y, Silliman N, Ptak J, Szabo S *et al.* The PIK3CA gene is mutated with high frequency in human breast cancers. *Cancer Biol Ther* 2004. **3**: 772-775.
179. Broderick DK, Di C, Parrett TJ, Samuels YR, Cummins JM, McLendon RE *et al.* Mutations of PIK3CA in anaplastic oligodendrogliomas, high-grade astrocytomas, and medulloblastomas. *Cancer Res* 2004. **64**: 5048-5050.
180. Campbell IG, Russell SE, Choong DY, Montgomery KG, Ciavarella ML, Hooi CS *et al.* Mutation of the PIK3CA gene in ovarian and breast cancer. *Cancer Res* 2004. **64**: 7678-7681.
181. Shayesteh L, Lu Y, Kuo WL, Baldocchi R, Godfrey T, Collins C *et al.* PIK3CA is implicated as an oncogene in ovarian cancer. *Nat Genet* 1999. **21**: 99-102.
182. Denley A, Kang S, Karst U, Vogt PK. Oncogenic signaling of class I PI3K isoforms. *Oncogene* 2008. **27**: 2561-2574.
183. Dbouk HA, Pang H, Fiser A, Backer JM. A biochemical mechanism for the oncogenic potential of the p110beta catalytic subunit of phosphoinositide 3-kinase. *Proc Natl Acad Sci U S A* 2010. **107**: 19897-19902.
184. Cleary JM, Shapiro GI. Development of phosphoinositide-3 kinase pathway inhibitors for advanced cancer. *Curr Oncol Rep* 2010. **12**: 87-94.
185. Edling CE, Selvaggi F, Buus R, Maffucci T, Di Sebastiano P, Friess H *et al.* Key role of phosphoinositide 3-kinase class IB in pancreatic cancer. *Clin Cancer Res* 2010. **16**: 4928-4937.
186. El Haibi CP, Sharma PK, Singh R, Johnson PR, Suttles J, Singh S *et al.* PI3Kp110-, Src-, FAK-dependent and DOCK2-independent migration and invasion of CXCL13-stimulated prostate cancer cells. *Mol Cancer* 2010. **9**: 85.
187. Johnson C, Lobelle-Rich PA, Puetter A, Levy LS. Substitution of feline leukemia virus long terminal repeat sequences into murine leukemia virus alters the pattern of insertional activation and identifies new common insertion sites. *J Virol* 2005. **79**: 57-66.
188. Du R, Lu KV, Petritsch C, Liu P, Ganss R, Passegue E *et al.* HIF1alpha induces the recruitment of bone marrow-derived vascular modulatory cells to regulate tumor angiogenesis and invasion. *Cancer Cell* 2008. **13**: 206-220.
189. Lin EY, Li JF, Gnatovskiy L, Deng Y, Zhu L, Grzesik DA *et al.* Macrophages regulate the angiogenic switch in a mouse model of breast cancer. *Cancer Res* 2006. **66**: 11238-11246.
190. Shojaei F, Wu X, Zhong C, Yu L, Liang XH, Yao J *et al.* Bv8 regulates myeloid-cell-dependent tumour angiogenesis. *Nature* 2007. **450**: 825-831.

191. Bronte V, Apolloni E, Cabrelle A, Ronca R, Serafini P, Zamboni P *et al.* Identification of a CD11b(+)/Gr-1(+)/CD31(+) myeloid progenitor capable of activating or suppressing CD8(+) T cells. *Blood* 2000. **96**: 3838-3846.
192. Bunt SK, Sinha P, Clements VK, Leips J, Ostrand-Rosenberg S. Inflammation induces myeloid-derived suppressor cells that facilitate tumor progression. *J Immunol* 2006. **176**: 284-290.
193. Gabrilovich DI, Nagaraj S. Myeloid-derived suppressor cells as regulators of the immune system. *Nat Rev Immunol* 2009. **9**: 162-174.
194. Schmid MC, Franco I, Kang SW, Hirsch E, Quilliam LA, Varner JA. PI3-kinase gamma promotes Rap1a-mediated activation of myeloid cell integrin alpha4beta1, leading to tumor inflammation and growth. *PLoS One* 2013. **8**: e60226.
195. Curtis C, Shah SP, Chin SF, Turashvili G, Rueda OM, Dunning MJ *et al.* The genomic and transcriptomic architecture of 2,000 breast tumours reveals novel subgroups. *Nature* 2012. **486**: 346-352.
196. Cerami E, Gao J, Dogrusoz U, Gross BE, Sumer SO, Aksoy BA *et al.* The cBio cancer genomics portal: an open platform for exploring multidimensional cancer genomics data. *Cancer Discov* 2012. **2**: 401-404.
197. Gao J, Aksoy BA, Dogrusoz U, Dresdner G, Gross B, Sumer SO *et al.* Integrative analysis of complex cancer genomics and clinical profiles using the cBioPortal. *Sci Signal* 2013. **6**: p11.
198. Doudna JA, Charpentier E. Genome editing. The new frontier of genome engineering with CRISPR-Cas9. *Science* 2014. **346**: 1258096.
199. Yang H, Wang H, Shivalila CS, Cheng AW, Shi L, Jaenisch R. One-step generation of mice carrying reporter and conditional alleles by CRISPR/Cas-mediated genome engineering. *Cell* 2013. **154**: 1370-1379.
200. Ma Y, Ma J, Zhang X, Chen W, Yu L, Lu Y *et al.* Generation of eGFP and Cre knockin rats by CRISPR/Cas9. *Febs j* 2014. **281**: 3779-3790.
201. Jinek M, Chylinski K, Fonfara I, Hauer M, Doudna JA, Charpentier E. A programmable dual-RNA-guided DNA endonuclease in adaptive bacterial immunity. *Science* 2012. **337**: 816-821.
202. Kim H, Kim JS. A guide to genome engineering with programmable nucleases. *Nat Rev Genet* 2014. **15**: 321-334.
203. Yu Z, Chen H, Liu J, Zhang H, Yan Y, Zhu N *et al.* Various applications of TALEN- and CRISPR/Cas9-mediated homologous recombination to modify the *Drosophila* genome. *Biol Open* 2014. **3**: 271-280.
204. Mali P, Yang L, Esvelt KM, Aach J, Guell M, DiCarlo JE *et al.* RNA-guided human genome engineering via Cas9. *Science* 2013. **339**: 823-826.

-
205. Cong L, Ran FA, Cox D, Lin S, Barretto R, Habib N *et al.* Multiplex genome engineering using CRISPR/Cas systems. *Science* 2013. **339**: 819-823.
206. Sung YH, Kim JM, Kim HT, Lee J, Jeon J, Jin Y *et al.* Highly efficient gene knockout in mice and zebrafish with RNA-guided endonucleases. *Genome Res* 2014. **24**: 125-131.
207. Jiang W, Zhou H, Bi H, Fromm M, Yang B, Weeks DP. Demonstration of CRISPR/Cas9/sgRNA-mediated targeted gene modification in Arabidopsis, tobacco, sorghum and rice. *Nucleic Acids Res* 2013. **41**: e188.
208. Gilbert LA, Larson MH, Morsut L, Liu Z, Brar GA, Torres SE *et al.* CRISPR-mediated modular RNA-guided regulation of transcription in eukaryotes. *Cell* 2013. **154**: 442-451.
209. DiCarlo JE, Norville JE, Mali P, Rios X, Aach J, Church GM. Genome engineering in *Saccharomyces cerevisiae* using CRISPR-Cas systems. *Nucleic Acids Res* 2013. **41**: 4336-4343.
210. Pelletier S, Gingras S, Green DR. Mouse genome engineering via CRISPR-Cas9 for study of immune function. *Immunity* 2015. **42**: 18-27.
211. Sommer D, Peters A, Wirtz T, Mai M, Ackermann J, Thabet Y *et al.* Efficient genome engineering by targeted homologous recombination in mouse embryos using transcription activator-like effector nucleases. *Nat Commun* 2014. **5**: 3045.
212. Gaj T, Gersbach CA, Barbas CF, 3rd. ZFN, TALEN, and CRISPR/Cas-based methods for genome engineering. *Trends Biotechnol* 2013. **31**: 397-405.
213. Yip KH, Kolesnikoff N, Yu C, Hauschild N, Taing H, Biggs L *et al.* Mechanisms of vitamin D(3) metabolite repression of IgE-dependent mast cell activation. *J Allergy Clin Immunol* 2014. **133**: 1356-1364, 1364.e1351-1314.
214. Zhang X, Shi L, Shu S, Wang Y, Zhao K, Xu N *et al.* An improved method of sample preparation on AnchorChip targets for MALDI-MS and MS/MS and its application in the liver proteome project. *Proteomics* 2007. **7**: 2340-2349.
215. Penno MA, Ernst M, Hoffmann P. Optimal preparation methods for automated matrix-assisted laser desorption/ionization time-of-flight mass spectrometry profiling of low molecular weight proteins and peptides. *Rapid Commun Mass Spectrom* 2009. **23**: 2656-2662.
216. Gustafsson JO, Eddes JS, Meding S, Koudelka T, Oehler MK, McColl SR *et al.* Internal calibrants allow high accuracy peptide matching between MALDI imaging MS and LC-MS/MS. *J Proteomics* 2012. **75**: 5093-5105.
217. Pedrioli PG, Eng JK, Hubley R, Vogelzang M, Deutsch EW, Raught B *et al.* A common open representation of mass spectrometry data and its application to proteomics research. *Nat Biotechnol* 2004. **22**: 1459-1466.

218. Gibb S, Strimmer K. MALDIquant: a versatile R package for the analysis of mass spectrometry data. *Bioinformatics* 2012. **28**: 2270-2271.
219. Cross DA, Alessi DR, Cohen P, Andjelkovich M, Hemmings BA. Inhibition of glycogen synthase kinase-3 by insulin mediated by protein kinase B. *Nature* 1995. **378**: 785-789.
220. Burgering BM, Coffey PJ. Protein kinase B (c-Akt) in phosphatidylinositol-3-OH kinase signal transduction. *Nature* 1995. **376**: 599-602.
221. Fantozzi A, Christofori G. Mouse models of breast cancer metastasis. *Breast Cancer Res* 2006. **8**: 212.
222. Swat W, Montgrain V, Doggett TA, Douangpanya J, Puri K, Vermi W *et al.* Essential role of PI3Kdelta and PI3Kgamma in thymocyte survival. *Blood* 2006. **107**: 2415-2422.
223. Farias AS, Pradella F, Schmitt A, Santos LM, Martins-de-Souza D. Ten years of proteomics in multiple sclerosis. *Proteomics* 2014. **14**: 467-480.
224. Farias AS, Martins-de-Souza D, Guimaraes L, Pradella F, Moraes AS, Facchini G *et al.* Proteome analysis of spinal cord during the clinical course of monophasic experimental autoimmune encephalomyelitis. *Proteomics* **12**: 2656-2662.
225. Liu T, Donahue KC, Hu J, Kurnellas MP, Grant JE, Li H *et al.* Identification of differentially expressed proteins in experimental autoimmune encephalomyelitis (EAE) by proteomic analysis of the spinal cord. *J Proteome Res* 2007. **6**: 2565-2575.
226. Jain MR, Li Q, Liu T, Rinaggio J, Ketkar A, Tournier V *et al.* Proteomic identification of immunoproteasome accumulation in formalin-fixed rodent spinal cords with experimental autoimmune encephalomyelitis. *J Proteome Res* **11**: 1791-1803.
227. Fazeli AS, Nasrabadi D, Sanati MH, Pouya A, Ibrahim SM, Baharvand H *et al.* Proteome analysis of brain in murine experimental autoimmune encephalomyelitis. *Proteomics* **10**: 2822-2832.
228. Vanheel A, Daniels R, Plaisance S, Baeten K, Hendriks JJ, Leprince P *et al.* Identification of protein networks involved in the disease course of experimental autoimmune encephalomyelitis, an animal model of multiple sclerosis. *PLoS One* **7**: e35544.
229. Linker RA, Brechlin P, Jesse S, Steinacker P, Lee DH, Asif AR *et al.* Proteome profiling in murine models of multiple sclerosis: identification of stage specific markers and culprits for tissue damage. *PLoS One* 2009. **4**: e7624.

-
230. Dumont D, Noben JP, Raus J, Stinissen P, Robben J. Proteomic analysis of cerebrospinal fluid from multiple sclerosis patients. *Proteomics* 2004. **4**: 2117-2124.
231. Liu S, Bai S, Qin Z, Yang Y, Cui Y, Qin Y. Quantitative proteomic analysis of the cerebrospinal fluid of patients with multiple sclerosis. *J Cell Mol Med* 2009. **13**: 1586-1603.
232. Lourenco AS, Baldeiras I, Graos M, Duarte CB. Proteomics-based technologies in the discovery of biomarkers for multiple sclerosis in the cerebrospinal fluid. *Curr Mol Med* **11**: 326-349.
233. Rosenling T, Stoop MP, Attali A, van Aken H, Suidgeest E, Christin C *et al.* Profiling and identification of cerebrospinal fluid proteins in a rat EAE model of multiple sclerosis. *J Proteome Res* **11**: 2048-2060.
234. Stoop MP, Singh V, Dekker LJ, Titulaer MK, Stingl C, Burgers PC *et al.* Proteomics comparison of cerebrospinal fluid of relapsing remitting and primary progressive multiple sclerosis. *PLoS One* **5**: e12442.
235. Avasarala JR, Wall MR, Wolfe GM. A distinctive molecular signature of multiple sclerosis derived from MALDI-TOF/MS and serum proteomic pattern analysis: detection of three biomarkers. *J Mol Neurosci* 2005. **25**: 119-125.
236. Sawai S, Umemura H, Mori M, Satoh M, Hayakawa S, Kodera Y *et al.* Serum levels of complement C4 fragments correlate with disease activity in multiple sclerosis: proteomic analysis. *J Neuroimmunol* **218**: 112-115.
237. Alt C, Duvefelt K, Franzen B, Yang Y, Engelhardt B. Gene and protein expression profiling of the microvascular compartment in experimental autoimmune encephalomyelitis in C57Bl/6 and SJL mice. *Brain Pathol* 2005. **15**: 1-16.
238. Kohler RE, Caon AC, Willenborg DO, Clark-Lewis I, McColl SR. A role for macrophage inflammatory protein-3 alpha/CC chemokine ligand 20 in immune priming during T cell-mediated inflammation of the central nervous system. *J Immunol* 2003. **170**: 6298-6306.
239. Cayrol R, Wosik K, Berard JL, Dodelet-Devillers A, Ifergan I, Kebir H *et al.* Activated leukocyte cell adhesion molecule promotes leukocyte trafficking into the central nervous system. *Nat Immunol* 2008. **9**: 137-145.
240. Wohler JE, Smith SS, Zinn KR, Bullard DC, Barnum SR. Gammadelta T cells in EAE: early trafficking events and cytokine requirements. *Eur J Immunol* 2009. **39**: 1516-1526.
241. Smith SS, Barnum SR. Differential expression of beta 2-integrins and cytokine production between gammadelta and alphabeta T cells in experimental autoimmune encephalomyelitis. *J Leukoc Biol* 2008. **83**: 71-79.

242. Schmidt A, Kellermann J, Lottspeich F. A novel strategy for quantitative proteomics using isotope-coded protein labels. *Proteomics* 2005. **5**: 4-15.
243. Donato R, Cannon BR, Sorci G, Riuzzi F, Hsu K, Weber DJ *et al.* Functions of s100 proteins. *Curr Mol Med* **13**: 24-57.
244. Klingelhofer J, Senolt L, Baslund B, Nielsen GH, Skibshoj I, Pavelka K *et al.* Up-regulation of metastasis-promoting S100A4 (Mts-1) in rheumatoid arthritis: putative involvement in the pathogenesis of rheumatoid arthritis. *Arthritis Rheum* 2007. **56**: 779-789.
245. van Lent PL, Grevers L, Blom AB, Sloetjes A, Mort JS, Vogl T *et al.* Myeloid-related proteins S100A8/S100A9 regulate joint inflammation and cartilage destruction during antigen-induced arthritis. *Ann Rheum Dis* 2008. **67**: 1750-1758.
246. Korthagen NM, Nagtegaal MM, van Moorsel CH, Kazemier KM, van den Bosch JM, Grutters JC. MRP14 is elevated in the bronchoalveolar lavage fluid of fibrosing interstitial lung diseases. *Clin Exp Immunol* 2010. **161**: 342-347.
247. Burkhardt K, Radespiel-Troger M, Rupperecht HD, Goppelt-Struebe M, Riess R, Renders L *et al.* An increase in myeloid-related protein serum levels precedes acute renal allograft rejection. *J Am Soc Nephrol* 2001. **12**: 1947-1957.
248. Mishra SK, Siddique HR, Saleem M. S100A4 calcium-binding protein is key player in tumor progression and metastasis: preclinical and clinical evidence. *Cancer Metastasis Rev* **31**: 163-172.
249. McArthur S, Cristante E, Paterno M, Christian H, Roncaroli F, Gillies GE *et al.* Annexin A1: a central player in the anti-inflammatory and neuroprotective role of microglia. *J Immunol* **185**: 6317-6328.
250. Yang YH, Song W, Deane JA, Kao W, Ooi JD, Ngo D *et al.* Deficiency of Annexin A1 in CD4+ T Cells Exacerbates T Cell-Dependent Inflammation. *J Immunol* **190**: 997-1007.
251. Pederzoli-Ribeil M, Maione F, Cooper D, Al-Kashi A, Dalli J, Perretti M *et al.* Design and characterization of a cleavage-resistant Annexin A1 mutant to control inflammation in the microvasculature. *Blood* 2010. **116**: 4288-4296.
252. Rescher U, Ludwig C, Konietzko V, Kharitononkov A, Gerke V. Tyrosine phosphorylation of annexin A2 regulates Rho-mediated actin rearrangement and cell adhesion. *J Cell Sci* 2008. **121**: 2177-2185.
253. Madureira PA, Surette AP, Phipps KD, Taboski MA, Miller VA, Waisman DM. The role of the annexin A2 heterotetramer in vascular fibrinolysis. *Blood* 2011. **118**: 4789-4797.
254. Liu L, Puri KD, Penninger JM, Kubes P. Leukocyte PI3Kgamma and PI3Kdelta have temporally distinct roles for leukocyte recruitment in vivo. *Blood* 2007. **110**: 1191-1198.

-
255. Fougerat A, Gayral S, Gourdy P, Schambourg A, Ruckle T, Schwarz MK *et al.* Genetic and pharmacological targeting of phosphoinositide 3-kinase-gamma reduces atherosclerosis and favors plaque stability by modulating inflammatory processes. *Circulation* 2008. **117**: 1310-1317.
256. Stephens LR, Eguinoa A, Erdjument-Bromage H, Lui M, Cooke F, Coadwell J *et al.* The G beta gamma sensitivity of a PI3K is dependent upon a tightly associated adaptor, p101. *Cell* 1997. **89**: 105-114.
257. Drazic A, Winter J. The physiological role of reversible methionine oxidation. *Biochim Biophys Acta* 2014. **1844**: 1367-1382.
258. Samstag Y, John I, Wabnitz GH. Cofilin: a redox sensitive mediator of actin dynamics during T-cell activation and migration. *Immunol Rev* 2013. **256**: 30-47.
259. Oppermann FS, Gnad F, Olsen JV, Hornberger R, Greff Z, Keri G *et al.* Large-scale proteomics analysis of the human kinome. *Mol Cell Proteomics* 2009. **8**: 1751-1764.
260. Dardaei L, Longobardi E, Blasi F. Prep1 and Meis1 competition for Pbx1 binding regulates protein stability and tumorigenesis. *Proc Natl Acad Sci U S A* 2014. **111**: E896-905.
261. Williams DA. Embryonic stem cells as targets for gene transfer: a new approach to molecular manipulation of the murine hematopoietic system. *Bone Marrow Transplant* 1990. **5**: 141-144.
262. Hall B, Limaye A, Kulkarni AB. Overview: generation of gene knockout mice. *Curr Protoc Cell Biol* 2009. **Chapter 19**: Unit 19.12 19.12.11-17.
263. Fu Y, Foden JA, Khayter C, Maeder ML, Reyon D, Joung JK *et al.* High-frequency off-target mutagenesis induced by CRISPR-Cas nucleases in human cells. *Nat Biotechnol* 2013. **31**: 822-826.
264. Fu Y, Sander JD, Reyon D, Cascio VM, Joung JK. Improving CRISPR-Cas nuclease specificity using truncated guide RNAs. *Nat Biotechnol* 2014. **32**: 279-284.
265. Cho SW, Kim S, Kim Y, Kweon J, Kim HS, Bae S *et al.* Analysis of off-target effects of CRISPR/Cas-derived RNA-guided endonucleases and nickases. *Genome Res* 2014. **24**: 132-141.
266. Janas ML, Turner M. Interaction of Ras with p110gamma is required for thymic beta-selection in the mouse. *J Immunol* 2011. **187**: 4667-4675.
267. Vasudevan S, Tong Y, Steitz JA. Switching from repression to activation: microRNAs can up-regulate translation. *Science* 2007. **318**: 1931-1934.
268. Oslejskova L, Grigorian M, Gay S, Neidhart M, Senolt L. The metastasis associated protein S100A4: a potential novel link to inflammation and consequent aggressive

- behaviour of rheumatoid arthritis synovial fibroblasts. *Ann Rheum Dis* 2008. **67**: 1499-1504.
269. Leclerc E, Fritz G, Vetter SW, Heizmann CW. Binding of S100 proteins to RAGE: an update. *Biochim Biophys Acta* 2009. **1793**: 993-1007.
270. Wang H, Duan L, Zou Z, Li H, Yuan S, Chen X *et al.* Activation of the PI3K/Akt/mTOR/p70S6K pathway is involved in S100A4-induced viability and migration in colorectal cancer cells. *Int J Med Sci* 2014. **11**: 841-849.
271. Klingelhofer J, Grum-Schwensen B, Beck MK, Knudsen RS, Grigorian M, Lukanidin E *et al.* Anti-S100A4 antibody suppresses metastasis formation by blocking stroma cell invasion. *Neoplasia* **14**: 1260-1268.
272. Gavins FN, Hickey MJ. Annexin A1 and the regulation of innate and adaptive immunity. *Front Immunol* **3**: 354.
273. D'Acquisto F. On the adaptive nature of annexin-A1. *Curr Opin Pharmacol* 2009. **9**: 521-528.
274. Paschalidis N, Iqbal AJ, Maione F, Wood EG, Perretti M, Flower RJ *et al.* Modulation of experimental autoimmune encephalomyelitis by endogenous annexin A1. *J Neuroinflammation* 2009. **6**: 33.
275. D'Acquisto F, Merghani A, Lecona E, Rosignoli G, Raza K, Buckley CD *et al.* Annexin-1 modulates T-cell activation and differentiation. *Blood* 2007. **109**: 1095-1102.
276. DiGiovanni J. Multistage carcinogenesis in mouse skin. *Pharmacol Ther* 1992. **54**: 63-128.
277. Halevy O, Rodel J, Peled A, Oren M. Frequent p53 mutations in chemically induced murine fibrosarcoma. *Oncogene* 1991. **6**: 1593-1600.
278. Watanabe H, Shimokado K, Asahara T, Dohi K, Niwa O. Analysis of the c-myc, K-ras and p53 genes in methylcholanthrene-induced mouse sarcomas. *Jpn J Cancer Res* 1999. **90**: 40-47.